

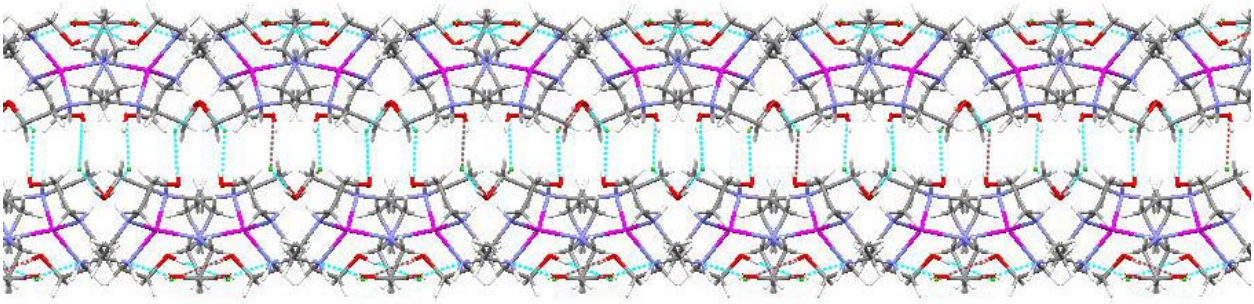
https://dspace.org/

The solid state structures of metallo-beta-amino alcohol complexes

Reisinger, Sandra Ann

2009-05-25T11:50:06Z
http://hdl.handle.net/10539/6979

Downloaded from a DSpace repository. https://dspace.org/



THE SOLID STATE STRUCTURES OF METALLO-BETA-AMINO ALCOHOL COMPLEXES

Dissertation submitted to the Faculty of Science, University of the Witwatersrand, South Africa, for the Degree of **Master of Science**

By

Sandra Ann Reisinger

Supervised by:

Dr. Alvaro S. de Sousa

Prof. Helder M. Marques

SCHOOL OF CHEMISTRY
UNIVERSITY OF THE WITWATERSRAND
JOHANNESBURG
SOUTH AFRICA

September 2008

Declaration

I hereby declare that this dissertation is my own work. It is submitted for the fulfillment of the degree of Master of Science in the Faculty of Science of the University of the Witwatersrand. This dissertation has never been submitted before for any degree or examination in any other university.



…….

S. A. Reisinger

20th of October 2008

Abstract

The ligands N,N'-bis(2-hydroxycyclohexyl)ethylenediamine (Cy_2-en), and 2,2'-[(hydroxypropane-1,3-diyl)diimino]dicyclohexanol (Cy_2-Otn) are synthesised and their solid state structures determined by X-ray diffraction experiments. Complexes are formed with the metal ions Pb^{2+}, Cd^{2+}, Ni^{2+}, and Zn^{2+}. The solid state structures of the lead(II) complex of Cy_2-en and the cadmium(II) complex of Cy_2-en are determined by X-ray diffraction experiments. Further complexations of the Pb^{2+} and Cd^{2+} ions are attempted with N,N'-bis(2-hydroxycyclohexyl)-1,3-propanediamine (Cy_2-tn), and N,N'-bis(2-hydroxycyclohexyl) diethylenetriamine (Cy_2-dien). The reactions are not successful. The ligand N,N'-bis(2-hydroxyethyl)ethylenediamine (BHEEN) is reacted with the metal ions Pb^{2+}, Cd^{2+}, Ni^{2+}, and Zn^{2+}, and the solid state structures of the cadmium(II) complex of BHEEN and the zinc(II) complex of BHEEN are determined by X-ray diffraction experiments. The solid state structures of both the ligands as well as the complexes indicate the presence of hydrogen-hydrogen bonds. The complexes contain more interactions than the uncoordinated ligands. Attempts are made to relate the interactions to the observed log *K* values for the complexes. Molecular mechanics calculations are performed to ascertain if a simple MM approach can suitably predict the conformations of the free ligands as well as the cadmium(II) complex of Cy_2-en. The conformations of the free ligands are predicted well but the cadmium(II) complex of Cy_2-en cannot be predicted without the addition of cadmium parameters to the GAFF force field.

Acknowledgements

I would like to thank my supervisors Dr Alvaro de Sousa and Prof Helder Marques for their advice and guidance. I would also like to thank every member of the Bioinorganic laboratory for their unwavering support and friendship.

My heartfelt gratitude must also be extended to my family who have put up with my erratic working hours as well as my insistence that the proof-read my work. Thank you.

I would also like to thank Dr. Manuel Fernandes for collecting the XRD data for me; Mr. Richard Mampa and Miss Jenny-Lee Panayides for running NMR samples for me; Mr Martin Brits for performing the mass spectrometry analyses.

I would also like to thank the National Research Foundation (NRF) as well as the University of the Witwatersrand (Wits) for funding my research.

List of Figures

Figure 1.1: Diagrams of Lewisite, BAL, and DMSA respectively 2

Figure 1.2: Ethylenediaminetetraacetic acid, EDTA 8

Figure 1.3: Selected chelating drugs 9

Figure 1.4: The four ligands synthesised in the study: Cy_2-en, Cy_2-tn, Cy_2-dien and Cy_2-Otn 17

Figure 1.5: The Bragg scattering angles 25

Figure 1.6: Representation of the unit cell and lattice points 26

Figure 1.7: The various unit cell types 27

Figure 1.8: The ligand BHEEN 35

Figure 2.1: General Setup of the Ligand Reactions 42

Figure 3.1: Superimposed images of the XRD structure (Yellow) of Cy_2-en and the lowest energy structure predicted by MM methods (Purple) 76

Figure 3.2: Superimposed images of the XRD structure (Yellow) of Cy_2-Otn and the lowest energy structure predicted by MM methods (Blue) 77

Figure 3.3: Superimposed images of the XRD structure (Yellow) of BHEEN and the lowest energy structure predicted by MM methods (Red) 79

Figure 3.4: Plot of epsilon versus the third ionisation energy for all metals listed in the MM2 force field 85

Figure 3.5: Plot of epsilon versus the third ionisation energy for all metals listed in the MM2 force field not having an epsilon value of 0.0200 86

Figure 3.6: Plot of epsilon versus the third ionisation energy for selected metals listed in the MM2 force field 86

Figure 3.7: Atom labelling scheme for the MM calculations with selected atom types specified 90

Figure 3.8: Superimposed images of the XRD structure (Yellow) of the Cy_2-en/Cd complex and the lowest energy structure predicted by MM methods (Blue) 93

Figure 3.9: Superimposed images of the lowest energy structure predicted by MM methods (Yellow) of the Cy_2-en/Cd Complex and an

approximation after removal of one set of close contact hydrogen atoms (Purple) 94
Figure 3.10: Superimposed images of the lowest energy structure predicted by MM methods (Yellow) of the Cy_2-en/Cd Complex and an approximation after removal of one set of close contact hydrogen atoms (Blue) 94
Figure 3.11: The three-dimensional plot of the energy minimised M—N and M—O bond lengths with their respective energy values 97
Figure 3.12: The three-dimensional plot of the energy minimised M—N and M—O bond lengths with their respective energy values using a cubic polynomial to interpolate and smooth the data 98
Figure 3.13: The three-dimensional plot of the energy minimised M—N and M—O bond lengths with their respective energy values using a cubic spline to interpolate and smooth the data 99
Figure 3.14: The three-dimensional plots of the energy minimised M—N and M—O bond lengths with their respective energy values, unaltered (bottom), using a cubic spline to interpolate and smooth the data (centre), using a cubic polynomial to interpolate and smooth the data (top) 100
Figure 4.1: The molecular structure of Cy_2-en, showing the atom-labelling scheme and 50% probability displacement ellipsoids 104
Figure 4.2: The molecular structure of Cy_2-en with its labelling scheme (hydrogen atoms included) 104
Figure 4.3: Hydrogen-bonding network of Cy_2-en indicating the four hydrogen bonds emanating from the central Cy_2-en molecule to four further molecules (two above and two below) 106
Figure 4.4: Crystal packing of Cy_2-en viewed along the *b*-axis (H atoms omitted for clarity) 107
Figure 4.5: The 2D packing arrangement of Cy_2-en viewed along the *c*-axis (H atoms omitted for clarity) 107
Figure 4.6: The H-H bonds in Cy_2-en 108

Figure 4.7: The close contact distance between the alcohol oxygen and the amine hydrogen in Cy_2-en 110
Figure 4.8: The AIM analysis of Cy_2-en in the gas phase 111
Figure 4.9: The molecular structure of the chloride salt of Cy_2-en, showing the labelling scheme and 50% probability displacement ellipsoids 113
Figure 4.10: The molecular structure of the chloride salt of Cy_2-en with its labelling scheme (hydrogen atoms included) 113
Figure 4.11: The 2D packing arrangement of the Cy_2-en chloride salt viewed along the *b*-axis (H atoms omitted for clarity) 114
Figure 4.12: Hydrogen-bonding network of the Cy_2-en chloride salt 115
Figure 4.13: The H-H bonds in the chloride salt of Cy_2-en 116
Figure 4.14: The plane defined by the four elements in the ethylene bridge in Cy_2-en 116
Figure 4.15: The plane defined by the four elements in the ethylene bridge in the Cy_2-en chloride salt 117
Figure 4.16: The close contact distances between the alcohol oxygen and an amine hydrogen in the chloride salt of Cy_2-en 118
Figure 4.17: The molecular structure of Cy_2-Otn, showing the atom-labelling scheme and 50% probability displacement ellipsoids 120
Figure 4.18: The molecular structure of Cy_2-Otn with its labelling scheme (hydrogen atoms included) 121
Figure 4.19: The planes defined by the five elements in the propyl bridge in each of the two Cy_2-Otn molecules in the asymmetric unit (hydrogen atoms omitted for clarity) 122
Figure 4.20: Hydrogen-bonding network of Cy_2-Otn, viewed along the *b*-axis 123
Figure 4.21: Crystal packing of Cy_2-Otn, viewed along the *b*-axis (hydrogen atoms omitted for clarity) 123
Figure 4.22: The H-H bonds Cy_2-Otn 125
Figure 4.23: Close contacts involving hydrogen and non-hydrogen atoms in Cy_2-Otn 126
Figure 4.24: The molecular structure of the nitrate salt of BHEEN, showing the

atom-labelling scheme and 50% probability displacement ellipsoids 127
Figure 4.25: The molecular structure of Cy_2-Otn with its labelling scheme (hydrogen atoms included) 127
Figure 4.26: The plane defined by the two amine nitrogen atoms and the two carbon atoms in their midst in the nitrate salt of BHEEN 128
Figure 4.27: Hydrogen-bonding network of the nitrate salt of BHEEN 129
Figure 4.28: The 2D packing arrangement of the nitrate salt of BHEEN (H atoms omitted for clarity) showing the herring-bone type arrangement of the molecules 129
Figure 4.29: Close contacts involving hydrogen and non-hydrogen atoms in BHEEN 130
Figure 4.30: Plot of change in complex stability relating to metal ion size when passing from BHEEN (or DHEEN) to Cy_2-en 132
Figure 4.31: The molecular structure of the lead(II) complex of Cy_2-en, showing the atom-labelling scheme and 50% probability displacement ellipsoids 135
Figure 4.32: The molecular structure of the lead(II) complex of Cy_2-en with its labelling scheme (hydrogen atoms included) 135
Figure 4.33: The ideal bond lengths for chelate rings with en and tn respectively 136
Figure 4.34: The plane defined by the four donor moieties in the ligand Cy_2-en upon complexation to lead(II) 137
Figure 4.35: The plane defined by the two coordinated oxygen moieties on the nitrate ion and one of the alcoholic oxygen moieties on the ligand Cy_2-en upon complexation to lead(II) 138
Figure 4.36: The possible hydrogen-bonding network of the complex of lead(II) with Cy_2-en 139
Figure 4.37: The layered arrangement of the complex of lead(II) with Cy_2-en showing the parallel arrangement of the cyclohexenyl rings as well as the metal ions in layers 139
Figure 4.38: The packing of the lead(II) complex with Cy_2-en viewed along the *b*-axis 140
Figure 4.39: The H-H close contacts of selected hydrogen atoms in the lead(II) complex of Cy_2-en 141

Figure 4.40: The molecular structure of the cadmium(II) complex of Cy_2-en, showing the atom-labelling scheme and 50% probability displacement ellipsoids 146
Figure 4.41: The molecular structure of the cadmium(II) complex of Cy_2-en with its labelling scheme (hydrogen atoms included) 146
Figure 4.42: The plane defined by the two nitrogen atoms, the one coordinated oxygen atom, and one of the chloride ions in the cadmium(II) complex of Cy_2-en 147
Figure 4.43: The hydrogen-bonding network of the cadmium(II) complex of Cy_2-en 148
Figure 4.44: The packing of the cadmium(II) complex of Cy_2-en viewed along the *c*-axis 149
Figure 4.45: The layered arrangement of the complex of cadmium(II) with Cy_2-en showing the parallel arrangement of the cyclohexenyl rings as well as the metal ion centres 149
Figure 4.46: The H-H close contacts of selected hydrogen atoms in the cadmium(II) complex of Cy_2-en 150
Figure 4.47: Close contacts involving hydrogen and non-hydrogen atoms in the cadmium(II) complex of Cy_2-en 151
Figure 4.48: The molecular structure of the cadmium(II) complex of BHEEN, showing the atom-labelling scheme and 50% probability displacement ellipsoids 154
Figure 4.49: The molecular structure of the cadmium(II) complex of BHEEN with its labelling scheme (hydrogen atoms included) 154
Figure 4.50: The plane defined by the two nitrogen atoms, the one coordinated oxygen atom, and one of the chloride ions in the cadmium(II) complex of BHEEN 155
Figure 4.51: The hydrogen-bonding network of the cadmium(II) complex of BHEEN 156
Figure 4.52: The layered arrangement of the complex of cadmium(II) with BHEEN showing the parallel arrangement of the two layers 157
Figure 4.53: The helical arrangement of the complex of cadmium(II) with BHEEN 157

Figure 4.54: The H-H close contacts of selected hydrogen atoms in the cadmium(II) complex of BHEEN 158
Figure 4.55: The molecular structure of the zinc(II) complex of BHEEN, showing the atom-labelling scheme and 50% probability displacement ellipsoids 164
Figure 4.56: The molecular structure of the zinc(II) complex of BHEEN with its labelling scheme (hydrogen atoms included) 165
Figure 4.57: The two planes each defined by two nitrogen atoms as well as the central zinc(II) ion in the zinc(II) complex of BHEEN 166
Figure 4.58: The hydrogen-bonding network of the zinc(II) complex of BHEEN 166
Figure 4.59: The two dimensional hydrogen bonding network of the zinc(II) complex of BHEEN viewed along the *c*-axis 167
Figure 4.60: The packing arrangement of the zinc(II) complex of BHEEN 167
Figure 4.61: The H-H close contacts of selected hydrogen atoms in the zinc(II) complex of BHEEN 168
Figure 4.62: Close contacts involving hydrogen and non-hydrogen atoms in the zinc(II) complex of BHEEN 169
Figure 6.1: The imidazolinium cation produced, **1** 175
Figure 6.2: Imidazole (2) and its derivatives, the imidazolium cation (1), imidazoline (3), and the imidazolinium cation (4) 176
Figure 6.3: General scheme of imidazolinium cations studied in the literature 176
Figure 6.4: Reaction scheme leading to the formation of **1** 177
Figure 6.5: The molecular structure of **1**, showing the atom-labelling scheme and 50% probability ellipsoids 178
Figure 6.6: The molecular structure of **1** with its labelling scheme (hydrogen atoms included) 179
Figure 6.7: The crystal structure of **1** indicating the close contact and its magnitude 181
Figure 6.8: The hydrogen-bonding network of **1** 182
Figure 6.9: The equilibrium between the neutral amino acid and its zwitterions 185
Figure 6.10: The molecular structure of **2**, showing the atom-labelling scheme and 50% probability ellipsoids 186
Figure 6.11: The zwitterion, **2**, formed during the synthesis of Cy_2-Otn 187

Figure 6.12: The unit cell packing of **2** viewed along the *b*-axis 187
Figure 6.13: The 16-membered ring formed by the hydrogen bonds of two zwitterions 188
Figure 6.14: The packing arrangement of the zwitterion viewed along the *b*-axis 188

List of Tables

Table 1.1: Several common Lewis acids and bases and their classes 4

Table 1.2: Essential elements in the body of an average 70 kg person 7

Table 1.3: Selected log *K* values for a five-membered ring system, a six-membered ring system, and the acyclic equivalent in complexations with metal ions 11

Table 2.1: List of Chemicals Used with Suppliers 38

Table 2.2: Masses and Volumes Used to Synthesise Cy_2-en 43

Table 2.3: Crystal Data and Structure Refinement for Cy_2-en 45

Table 2.4: Crystal Data and Structure Refinement for the chloride salt of Cy_2-en 46

Table 2.5: Masses and Volumes Used to Synthesise Cy_2-tn 47

Table 2.6: Masses and Volumes Used to Synthesise Cy_2-dien 49

Table 2.7: Masses and Volumes Used to Synthesise Cy_2-Otn 51

Table 2.8: Crystal Data and Structure Refinement for Cy_2-Otn 53

Table 2.9: Crystal Data and Structure Refinement for Cy_2-en/Pb Complex 57

Table 2.10: Crystal Data and Structure Refinement for Cy_2-en/Cd Complex 62

Table 2.11: Crystal Data and Structure Refinement for BHEEN/Cd Complex 65

Table 2.12: Crystal Data and Structure Refinement for BHEEN/Zn Complex 71

Table 3.1: Charges on Cy_2-en Calculated by Semi-empirical Methods Using PM3 and ZINDO/1 73

Table 3.2: Average Bond Lengths and Angles of Cy_2-en Calculated Using Different Dielectric Constants 74

Table 3.3: Energies of Cy_2-en after Simulated Annealing Runs with Various Run Times Compared to the Energy of the XRD Structure 75

Table 3.4: Average Bond Lengths Found in the CSD and Sorted by VISTA 81

Table 3.5: Nonbonded Parameters for All Metals Found in the MM2 Force Field 84

Table 3.6: Third Ionisation Energies of Selected Metals Found in the MM2 Force Field 84

Table 3.7: Hydrogen Close Contacts Found in the XRD Structure and the Corresponding Values from the Geometry Optimisations as well

as the Removal of Several Close Contact Hydrogen Atoms 95
Table 3.8: Selected Bond Angles in the XRD Structure and the Corresponding Values from the Geometry Optimisations as well as the Removal of Several Close Contact Hydrogen Atoms 96
Table 3.9: Selected Bond Lengths in the XRD Structure and the Corresponding Values from the Geometry Optimisations as well as the Removal of Several Close Contact Hydrogen Atoms 96
Table 4.1: H-H Bonds for the Ligand Cy_2-en 109
Table 4.2: H-H Bonds for the Ligand Cy_2-Otn 124
Table 4.3: Close Contacts for the Nitrate Salt of BHEEN 130
Table 4.4: H-H Bonds for the Lead(II) Complex of Cy_2-en 140
Table 4.5: H-H Bonds for the Cadmium(II) Complex of Cy_2-en 150
Table 4.6: H-H Bonds for the Cadmium(II) Complex of BHEEN 158
Table 4.7: H-H Bonds for the Zinc(II) Complex of BHEEN 168
Table 6.1: Excerpt from the Validation Window for **1** (Using Platon Validate) 180
Table 6.2: Crystal data and structure refinement for **1** 184
Table 6.3: Crystal Data and Structure Refinement for the Zwitterion 189

Abbreviations

APCI	Atmospheric Pressure Chemical Ionisation Mass Spectrometry
BHEEN	N,N'-bis(2-hydroxyethyl)ethylenediamine
Cy_2-dien	N,N'-bis(2-hydroxycyclohexyl)diethylenetriamine
Cy_2-en	N,N'-bis(2-hydroxycyclohexyl)ethylenediamine
Cy_2-Otn	2,2'-[(hydroxypropane-1,3-diyl)diimino]dicyclohexanol
Cy_2-tn	N,N'-bis(2-hydroxycyclohexyl)-1,3-propanediamine
DFT	density functional theory
DMF	Dimethylformamide
en	Ethylenediamine
ESI	Electrospray Ionisation Mass Spectrometry
H-H bond	hydrogen-hydrogen bond
IR	Infra-Red
NMR	Nuclear Magnetic Resonance
r.m.s	root-mean-square
TEA	triethanolamine
XRD	X-Ray Diffraction

Table of Contents

Preliminaries

Abstract **i**

Acknowledgements **ii**

List of Figures **iii**

List of Tables **x**

Abbreviations **xii**

Chapter 1 Introduction **1**

1.1 Chelation Therapy **1**

1.1.1 General Overview 1

1.1.2 Metal Ions in the Human Body 6

1.1.3 Current Drugs 8

1.2 The Element Lead **13**

1.2.1 General Historical Overview 13

1.2.2 The Chemistry of Lead 14

1.2.3 Some Previous Work Done on Lead 15

1.3 The Element Cadmium **17**

1.3.1 General Historical Overview 17

1.3.2 The Chemistry of Cadmium 18

1.3.3 Some Previous Work Done on Cadmium 19

1.4 The Element Nickel **20**

1.4.1 General Historical Overview 20

1.4.2 The Chemistry of Nickel 21

1.4.3 Some Previous Work Done on Nickel 22

1.5 The Element Zinc **22**

1.5.1 General Historical Overview 22

1.5.2 The Chemistry of Zinc 23

1.5.3 Some Previous Work Done on Zinc 23

1.6 X-Ray Diffraction **24**

1.7 Molecular Modelling **27**

1.7.1 General Overview 27
1.7.2 Models 31
1.8 Hydrogen Bonds and Close Contacts 32
1.8.1 Bonded Interactions 33
1.8.2 Non-Bonded Interactions 33
1.9 Objectives and Scope of the Research Project 33
1.10 References 35

Chapter 2 Materials and Methods 37
2.1 Materials 37
2.2 Physical Techniques of Characterisation 39
2.2.1 Nuclear Magnetic Resonance Spectroscopy (NMR) 39
2.2.2 Infra-Red Spectroscopy (IR) 39
2.2.3 Electrospray Ionization (ESI) or Atmospheric Pressure Chemical Ionization (APCI) – Mass Spectrometry 40
2.2.4 Single Crystal X-Ray Diffraction (XRD) 40
2.3 Synthesis of the Free Ligands 41
2.3.1 Synthesis of Cy_2-en 42
2.3.2 Synthesis of Cy_2-tn 46
2.3.3 Synthesis of Cy_2-dien 48
2.3.4 Synthesis of Cy_2-Otn 50
2.4 Synthesis of the Lead Complexes 53
2.4.1 Synthesis of the Cy_2-en/Pb complex 53
2.4.2 Attempted Synthesis of the Cy_2-tn/Pb complex 57
2.4.3 Synthesis of the Cy_2-dien/Pb complex 58
2.4.4 Synthesis of the Cy_2-Otn/Pb complex 58
2.4.5 Synthesis of the BHEEN/Pb complex 59
2.5 Synthesis of the Cadmium Complexes 60
2.5.1 Synthesis of the Cy_2-en/Cd complex 60
2.5.2 Synthesis of the Cy_2-tn/Cd complex 61
2.5.3 Attempted Synthesis of the Cy_2-dien/Cd complex 62

2.5.4 Synthesis of the Cy_2-Otn/Cd complex 63
2.5.5 Synthesis of the BHEEN/Cd complex 63
2.6 Synthesis of the Nickel Complexes 65
2.6.1 Synthesis of the Cy_2-en/Ni complex 65
2.6.2 Synthesis of the Cy_2-Otn/Ni complex 66
2.6.3 Synthesis of the BHEEN/Ni complex 66
2.7 Synthesis of the Zinc Complexes 67
2.7.1 Synthesis of the Cy_2-en/Zn complex 67
2.7.2 Synthesis of the Cy_2-Otn/Zn complex 68
2.7.3 Synthesis of the BHEEN/Zn complex 69
2.8 References 70

Chapter 3 Molecular Mechanics 71
3.1 Modelling of the Free Ligands 71
3.1.1 MM Calculations on Cy_2-en 71
3.1.2 MM Calculations on Cy_2-Otn 75
3.1.3 MM Calculations on BHEEN 77
3.2 Modelling of the Cadmium Complex of Cy_2-en 79
3.3 Conclusions 100
3.4 References 101

Chapter 4 Results and Discussion 101
4.1 Synthesis and Characterisation of the Free Ligands 101
4.1.1 Synthesis of Cy_2-en 101
4.1.2 Synthesis of Cy_2-tn 116
4.1.3 Synthesis of Cy_2-dien 117
4.1.4 Synthesis of Cy_2-Otn 117
4.1.5 Crystallisation of BHEEN 124
4.1.6 Comparison of the Ligands 129
4.2 Synthesis and Characterisation of the Lead Complexes 131
4.2.1 Synthesis of the Cy_2-en/Pb complex 131

4.2.2 Attempted Synthesis of the Cy_2-tn/Pb complex 139
4.2.3 Synthesis of the Cy_2-dien/Pb complex 140
4.2.4 Synthesis of the Cy_2-Otn/Pb complex 141
4.2.5 Synthesis of the BHEEN/Pb complex 141
4.2.6 Comparison of the Lead Complexes 142
4.3 Synthesis and Characterisation of the Cadmium Complexes 143
4.3.1 Synthesis of the Cy_2-en/Cd complex 143
4.3.2 Synthesis of the Cy_2-tn/Cd complex 150
4.3.3 Attempted Synthesis of the Cy_2-dien/Cd complex 150
4.3.4 Synthesis of the Cy_2-Otn/Cd complex 151
4.3.5 Synthesis of the BHEEN/Cd complex 151
4.3.6 Comparison of the Cadmium Complexes 157
4.4 Synthesis and Characterisation of the Nickel Complexes 159
4.4.1 Synthesis of the Cy_2-en/Ni complex 159
4.4.2 Synthesis of the Cy_2-Otn/Ni complex 160
4.4.3 Synthesis of the Cy_2-BHEEN/Ni complex 160
4.4.4 Comparison of the Nickel Complexes 161
4.5 Synthesis and Characterisation of the Zinc Complexes 161
4.5.1 Synthesis of the Cy_2-en/Zn complex 161
4.5.2 Synthesis of the Cy_2-Otn/Zn complex 161
4.5.3 Synthesis of the BHEEN/Zn complex 162
4.5.4 Comparison of the Zinc Complexes 167
4.6 Comparison of All Solid State Structures of the Complexes 168
4.7 References 170

Chapter 5 Conclusions and Future Work 171

Chapter 6 Unexpected Reactions 173
6.1 The Imidazolinium Salt 2,2'-Bis(2-hydroxycyclohexyl)imidazoline Nitrate 173
6.2 The Zwitterion

(3-ammonio-2-hydroxypropyl)carbamate monohydrate **183**

6.3 References **188**

Appendices **189**

Appendix A: MM Data 189

Appendix B: NMR Data 234

Appendix C: IR Data 246

Appendix D: MS Data 262

Appendix E: XRD Data 278

Chapter 1

Introduction

1.1 Chelation Therapy

1.1.1 General Overview

Chelation therapy refers to the use of drugs, called chelation agents, to bind metals in the human body that are present in excess due to poisoning or illness. This excess can be due to exposure to heavy metals or possibly an inability by the human body to remove excess metal ions from itself. There are several illnesses that lead to heavy metal intoxication and they are easily treatable once diagnosed. One of these illnesses is thalassaemia. It is a genetic disorder that leads to a reduced level of the protein haemoglobin. This, in turn, leads to a build-up of iron in the blood stream and impairs the heart, the liver, and the endocrine system.[1]

The chelation agent selectively binds to the metal ion that is to be removed, and transports it from the body. The term chelation stems from the Greek word *chele,* meaning a lobster's claw.

Chelation therapy originated after World War I. The necessity came about for compounds that could bind the chemical weapon Lewisite, Figure 1.1, named after the chemist and soldier Winford Lee Lewis. It is an arsine compound, i.e. it contains the metal arsenic. This is a liquid that was developed in the US after World War I. When combined with mustard gas it forms a lethal combination that causes blistering of the lungs and, if enough of the agent is inhaled, death. The first chelating agent developed to bind Lewisite was called British Anti-Lewisite or BAL, Figure 1.1. This drug has the unpleasant side-effect of being toxic to the human body and was soon replaced by dimercaptosuccinic acid, or DMSA, Figure 1.1.

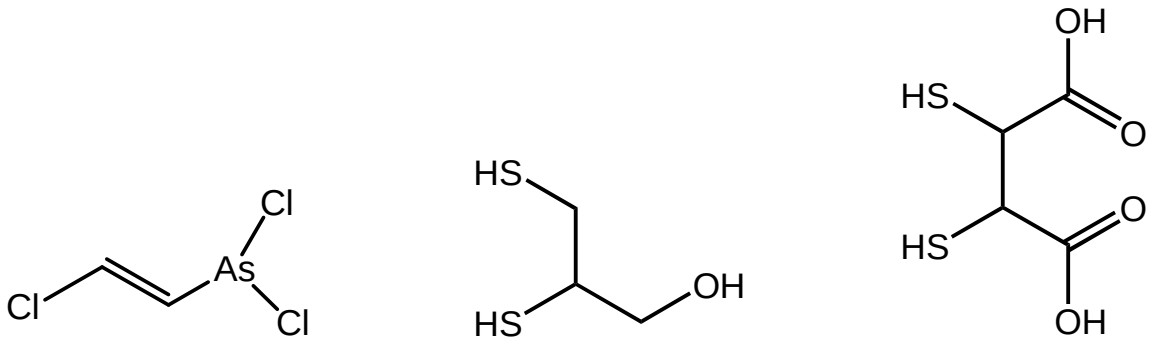


Figure 1.1: Diagrams of Lewisite, BAL, and DMSA respectively

The chelating agent (the compound used to bind to the metal) has electron-rich groups on it which attach to the electron-poor metal and bind it to themselves by forming a ring that includes the metal ion, hence the claw analogy. The compound is then referred to as a metal chelate.

The chelating agent is usually a compound of organic character. In chemical terminology it is also referred to as the ligand as it is a compound that binds to a metal. The ligand must fulfil at least two criteria to be classified as a chelating agent.

Firstly, it must have an electron-rich group such as a nitrogen atom, an oxygen atom or a sulphur atom. In the above Figure 1.1, the electron-rich groups on the ligands BAL and DMSA are the sulfur and oxygen moieties. The binding ability of the various donor moieties and the metal ions is classified according to their hardness or softness. This is done via hard/soft acid/base theory or HSAB proposed by Pearson.[2-4] The general equation to describe the behaviour of Lewis acids and bases, A and :B, and the resulting complex, A:B, is:

$$A+ : B \rightarrow A : B \qquad \textbf{(1)}$$

The atoms that fall into class *a* are classified as hard acids or bases. Hard acids are classified as acceptor atom or ion is highly positively charges, has a small ionic radius, and has rather stable or unexcitable valence electrons. Hard bases are classified as atoms or ions with the following properties: they are not easily polarised or oxidised; they have a high electronegativity; and they most frequently also have empty orbitals of high

energy that are inaccessible to the valence electrons because of the great energy required to occupy them. Soft acids are classified as atoms or ions with low positive charges large radii, and electrons that are easily excited. Soft bases are classified as atoms or ions where the donor atom has a high polarisability and oxidisability, low electronegativity, and has available low-energy orbitals that are vacant.

As is apparent from the above definitions, the classification as hard or soft depends on the energy differences between the highest occupied molecular orbital or HOMO and the lowest unoccupied molecular orbital or LUMO. For species that are classified as hard, there is a large gap between the HOMO and LUMO orbitals. This makes them hard to polarise. Soft species have much smaller HOMO-LUMO gaps.[5] Some common Lewis acid and bases and their respective classes are given in Table 1.1. The rule of thumb that was determined by Pearson is: hard acids prefer to bond to hard bases, and soft acids to soft bases.

The general measure of the stability of acids and bases in solution is via the analysis of their equilibrium constants, *K*. The general form of the constant comes from **(2)** and is determined by evaluating the equation **(3)**.

$$M^{n+}(aq) + xL^{m-}(aq) \rightleftharpoons [ML_x]^{(n-xm)+}(aq) \qquad \textbf{(2)}$$

$$\log K = \log\left[\frac{[ML_x]}{[M^{n+}][L^{m-}]x}\right] \qquad \textbf{(3)}$$

Table 1.1: Several common Lewis acids and bases and their classes[4,5]

Acids	
Class *a* / Hard Acids	Class *b* / Soft Acids
H^+, Li^+, Na^+, K^+	Cu^+, Ag^+, Au^+, Tl^+, Hg^+, Cs^+
Be^{2+}, Mg^{2+}, Ca^{2+}, Sr^{2+}, Sn^{2+}	Pd^{2+}, Cd^{2+}, Pt^{2+}, Hg^{2+}
Al^{3+}, La^{3+}, Cr^{3+}, Co^{3+}, Fe^{3+}, As^{3+}	I^+, Br^+, HO^+, RO^+
$BeMe_2$, BF_3, BCl_3, $B(OR)_3$	I_2, Br_2, INC, etc.
$Al(CH_3)_3$, $Ga(CH_3)_3$, $In(CH_3)_3$	O, Cl, Br, I, R_3C
SO_3, R_3C^+, RCO^+, CO_2, NC^+	M^0 (neutral metals), Bulk metals
Borderline Acids	
Fe^{2+}, Co^{2+}, Ni^{2+}, Cu^{2+}, Zn^{2+}, Pb^{2+}, $B(CH_3)_3$, SO_2, NO^+	
Bases	
Class *a* / Hard Bases	Class *b* / Soft Bases
H_2O, OH^-, F^-	R_2S, RSH, RS^-, H^-, R^-
$CH_3CO_2^-$, PO_4^{3-}, SO_4^{2-}	I^-, SCN^-, $S_2O_3^{2-}$
Cl^-, CO_3^-, ClO_4^-, NO_3^-	R_3P, R_3As, $(RO)_3P$
ROH, RO^-, R_2O, NH_3, RNH_2, N_2H_4	CN^-, RNC, CO, C_2H_4, C_6H_6
Borderline Bases	
$C_6H_5NH_2$, C_5H_5N, N_3^-, Br^-, NO_2^-, SO_3^{2-}, N_2	

The donor groups on the ligands donate some of their electron density to the electron-poor metal creating a simple bond between the metal and the ligand. This bond stabilises the metal making it less reactive and hence less toxic to the system by binding the metal and hence deactivating its reactivity towards biological molecules such as

enzymes. It is also possible to have a multiple bond system such as a π-bond in the ligand that acts as the electron-donor.

Secondly, the ligand must have at least two electron-donating groups. When these groups attach to the metal ion a chelate ring is formed and this ring-formation leads to a strong decrease in the reactivity of the metal ion and leads to a stable and non-intrusive complex that can be safely removed from the human body. This formation of a chelate ring is referred to as the chelate effect and is of particular importance in chemistry. The chelate effect stems mainly from entropy effects but also, to a lesser degree, from enthalpy effects. The simplest manner in which to explain the observed stability is to look at the ease with which a complex is formed when compared to its acyclic analogue. A good example of this is ammonia and ethylenediamine. In the equilibrium, $[Ni(NH_3)_6]^{2+} + 3en \rightleftharpoons [Ni(en)_3]^{2+} + 6NH_3$, there is a drive by entropic effects that pushes the equilibrium towards the right. An increase in the total number of particles is desired, hence the favoured formation of the chelate. Also, once the chelating agent has bonded to the metal centre, it is less likely to be removed from the metal completely when compared to the acyclic analogue. This is due to the fact that even if one of the chelating bonds is broken, there is a second bond that keeps the ligand connected to the metal. The free arm only has limited mobility due to the remaining bonds and so has a much higher statistical probability of being involved in reforming a bond to the metal ion.

Chelation therapy is also used in the treatment of cancer. It has been shown that chelating agents are a likely cause of cancer but at the same time it has been shown that other chelating agents have anti-tumour activity. It appears that certain chelating agents act in anti-tumour manner in one part of the environment and as a carcinogen in another part.[6] A further use of chelation therapy has been advocated by alternative medicine practitioners. They claim that chelating ligands can also be used to treat heart disease and autism.[7]

1.1.2 Metal Ions in the Human Body

There are many elements present in the human body and several of them are metals. The key to the presence of these metals is their relative concentrations, oxidation state and location in the body. What may be good for one part of the body is bad for another.

Table 1.2 gives a summary of some of the essential elements that can be found in the human body. It clearly shows that most of the essential metals are used in enzymatic processes. It is also possible that the metal ion is present as a coenzyme and performs transport or storage functions. This is the case with iron in haemoglobin, a component of blood.[6] It is also common to find metal ions in the body that have been introduced by humans or taken up from the environment. Examples of metals being introduced to the human body are dental fillings made of mercury, vitamin supplements, inhalation of vehicle exhaust fumes, and leaded paint, amongst others.

Table 1.2: Essential elements in the body of an average 70 kg person[8]

Element	Present as	Total amount in body
Oxygen	Mainly as water[a] and present everywhere	43 kg
Carbon	Almost everything but water	12kg
Hydrogen	Mainly as water[a] and present everywhere	6.3 kg
Nitrogen	Protein, DNA, etc	2 kg
Calcium	Bone,[b] teeth, cell messenger	1.1 kg
Phosphorous	Bone,[b] teeth, DNA, ATP[c]	750 g
Potassium	Electrolyte, mainly inside cells	225 g
Sulfur	Amino acids, particularly in hair and skin	150 g
Chlorine	Electrolyte balance	100 g
Sodium	Electrolyte, mainly outside cells	90 g
Magnesium	Metabolic electrolyte	35 g
Silicon	Connective tissue	30 g
Iron	Haemoglobin	4200 mg
Fluorine	Bones and teeth	2600 mg
Zinc	Enzyme cofactor	2400 mg
Copper	Enzyme cofactor	90 mg
Iodine	Thyroid hormones	14 mg
Tin	Not known	14 mg
Selenium	Enzyme, antioxidant	14 mg
Manganese	Enzyme component	14 mg
Nickel	Enzyme component	7 mg
Molybdenum	Enzyme cofactor	7 mg
Vanadium	Lipid metabolism	7 mg
Chromium	Glucose tolerance factor	2 mg
Cobalt	Part of vitamin B_{12}	1.5 mg

[a] Water accounts for around 60% of the body's weight.

[b] Bone accounts for around 13% of the body's weight.

[c] Adenosine triphosphate.

1.1.3 Current Drugs

There are a myriad of drugs available for chelation therapy today. The most commonly used drug to date has been the chelating agent EDTA or ethylenediaminetetraacetic acid, Figure 1.2. In recent years, other drugs have been developed to be more specific for one metal ion rather than almost all, such as EDTA. This has led to a dramatic increase in the investigation of chelating ligands as potential chelating drugs for human use.

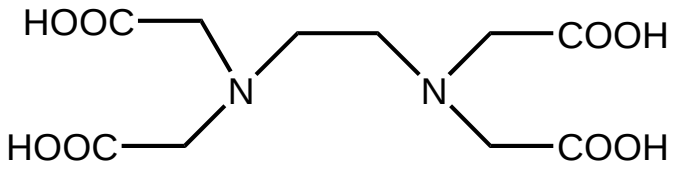


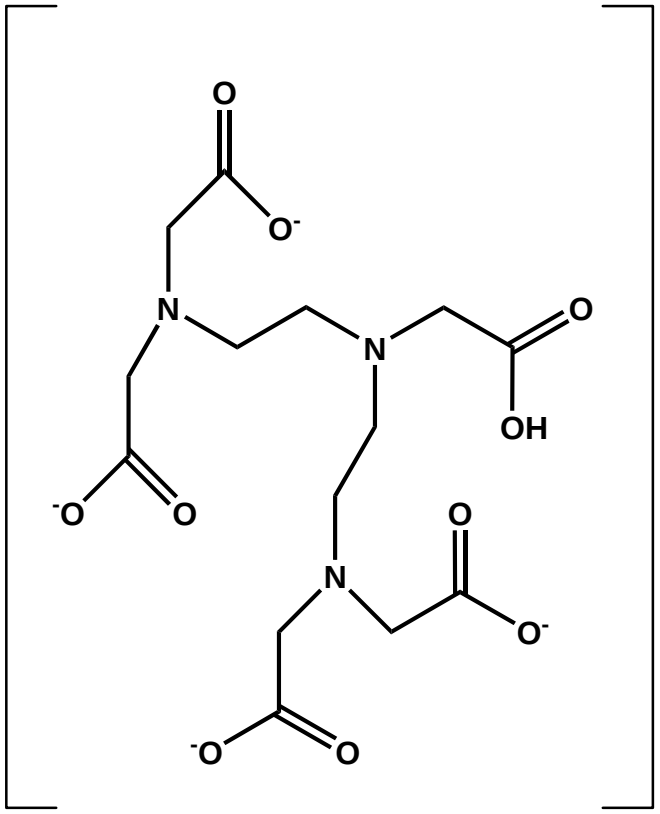
Figure 1.2: Ethylenediaminetetraacetic acid, EDTA

The suggested approach for the chelation of cadmium in intoxication cases is the oral ingestion of DMSA, Figure 1.1, in combination with parenteral $CaNa_3dtpa$, Figure 1.3.[1]

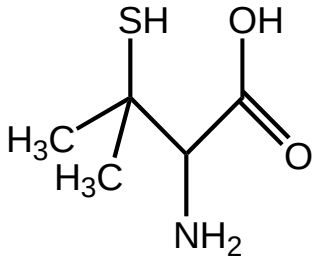
There are several methods to treat lead poisoning. Some of them have toxic side-effects. It is suggested that the best drug to use in chelation therapy for lead poisoning is DMSA. It has been shown in animal studies that the use of other chelating agents such as $dmpaH_2$, $dpaH_2$, and EDTA, which have previously been used as an antidote in lead poisoning, may form toxic complexes with iron in the body.[1]

The most common chelating agents for nickel intoxication are EDTA, diethyldithiocarbamate (edt^-), Figure 1.3, or dimethylglyoxime ($dmgH_2$), Figure 1.3.[1]

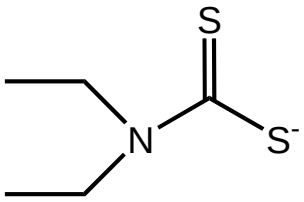
There are many drugs that are used on the treatment of zinc poisoning. Cases are reported of treatment with EDTA as well as $dmpaH_2$, Figure 1.3. Further studies on rodents have shown that EDTA, $cdtaH_4$, and $dtpaH_4$, Figure 1.3, are the best chelating agents for zinc intoxication, but it has also been shown that there is a significant drop in the mortality rate if $dmpsH_3$, Figure 1.3, is used as the drug of choice.[1]



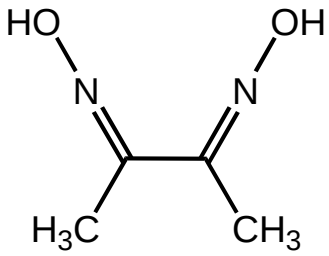
CaNa$_3$dtpa



dpaH$_2$



edt$^-$



dmgH$_2$

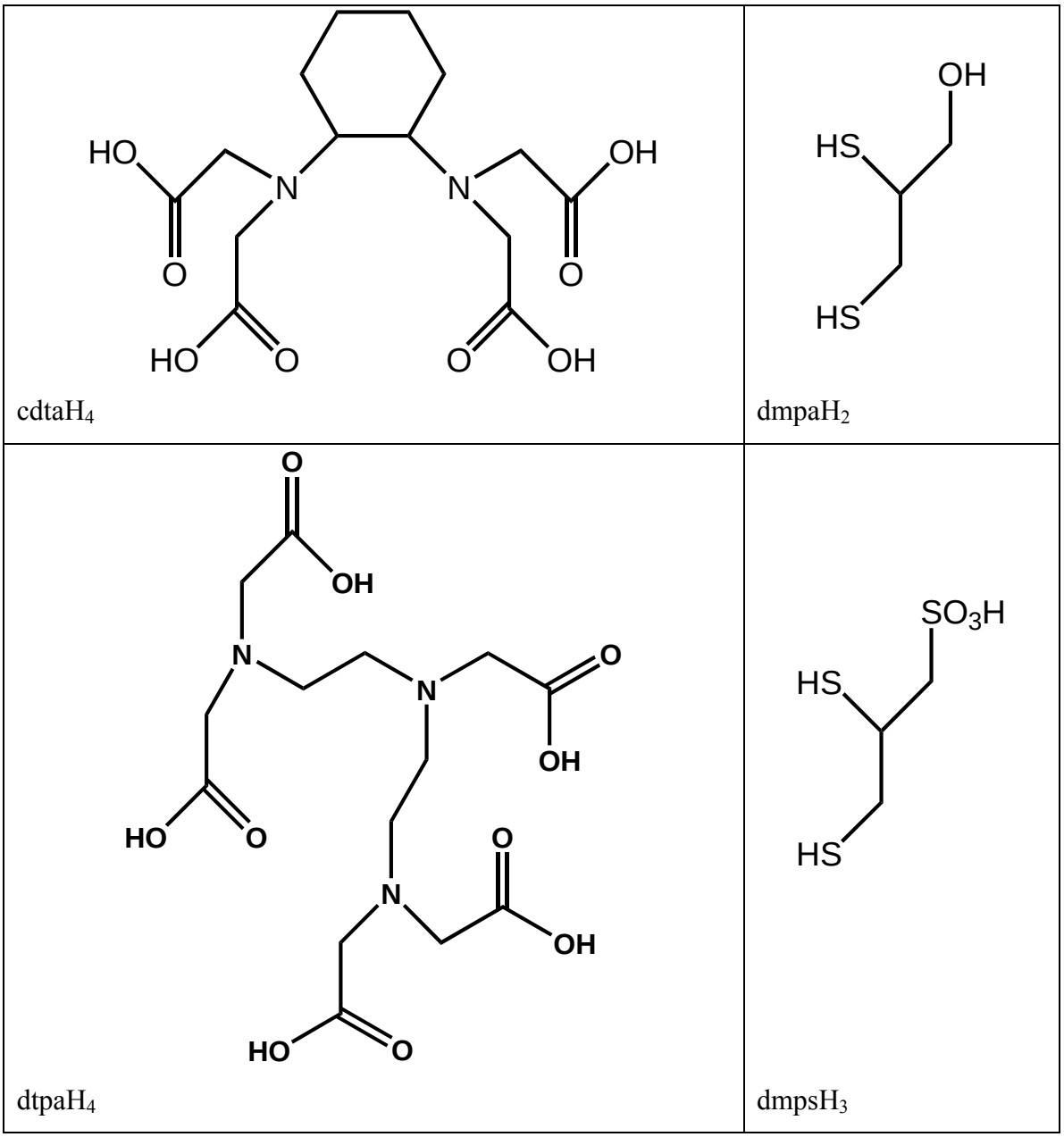


Figure 1.3: Selected chelating drugs

The chelating ability of a ligand can be quantified by log *K* values for the reaction, **(2)**, in going from the free ligand to the complexed ligand in aqueous solution.

$$M^{n+}(aq) + xL^{m-}(aq) \rightleftharpoons [ML_x]^{(n-xm)+}(aq) \qquad \textbf{(2)}$$

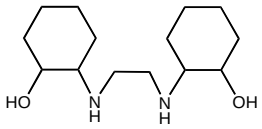
It is found experimentally that the larger metal ions such as lead and cadmium favour forming complexes with ligands that contain five-membered rings compared to ligands with six-membered rings.[9] Selected examples of log *K* values for five-membered and six-membered ring systems with metal ions are given in Table 1.2. Two of the ligands in this study contain six-membered hydroxycyclohexyl rings.

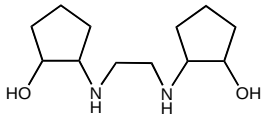
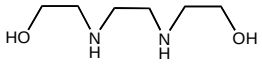
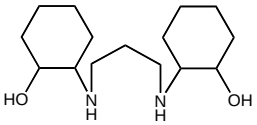
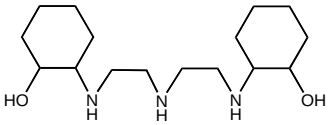
Larger metal ions prefer to form five-membered rings upon complexation due to the fact that the formation of the five-membered ring causes less steric strain on the entire system as compared to the formation of a six-membered ring system. [10] This is indicated by the data in Table 1.3.

The four metal ions listed are all in the +2 oxidation state and sorted in order of increasing ionic radius. Nickel is the smallest of the metal ions with an ionic radius of 0.69 Å. The tabulated data clearly indicates that it favours complex formation with Cy_2-en and BHEEN when compared to Cyp_2-en. The same pattern is observed for the zinc ion with an ionic radius of 0.74 Å, the cadmium ion with an ionic radius of 0.95 Å, and the lead ion with an ionic radius of 1.18 Å.

It is also of interest to note that the addition of a cyclohexenyl ring system to the ligand, as in Cy_2-en when compared to BHEEN, favours the formation of the Cy_2-en complexes. The opposite trend is noted when BHEEN and Cyp_2-en are compared.

Table 1.3: Selected log *K* values for a five-membered ring system, a six-membered ring system, and the acyclic equivalent in complexations with metal ions

Equilibrium	log *K*	Reference
L = Cy_2-en = 		
$Ni^{2+} + L \rightleftharpoons NiL^{2+}$	7.75	9
$Zn^{2+} + L \rightleftharpoons ZnL^{2+}$	6.27	9
$Cd^{2+} + L \rightleftharpoons CdL^{2+}$	6.15	9
$Pb^{2+} + L \rightleftharpoons PbL^{2+}$	6.78	9

L = Cyp_2-en =		
$Ni^{2+} + L \rightleftharpoons NiL^{2+}$	3.79	9
$Zn^{2+} + L \rightleftharpoons ZnL^{2+}$	4.52	9
$Cd^{2+} + L \rightleftharpoons CdL^{2+}$	3.98	9
$Pb^{2+} + L \rightleftharpoons PbL^{2+}$	4.85	9
L = BHEEN =		
$Ni^{2+} + L \rightleftharpoons NiL^{2+}$	6.67	9
$Zn^{2+} + L \rightleftharpoons ZnL^{2+}$	4.79	9
$Cd^{2+} + L \rightleftharpoons CdL^{2+}$	5.07	9
$Pb^{2+} + L \rightleftharpoons PbL^{2+}$	6.12	9
L = Cy_2-tn =		
$L + H^+ \rightleftharpoons LH^+$	10.12	10
$Zn^{2+} + L \rightleftharpoons ZnL^{2+}$	5.04	10
$Cd^{2+} + L \rightleftharpoons CdL^{2+}$	4.15	10
L = Cy_2-dien =		
$L + H^+ \rightleftharpoons LH^+$	9.85	10
$Zn^{2+} + L \rightleftharpoons ZnL^{2+}$	9.57	10
$Cd^{2+} + L \rightleftharpoons CdL^{2+}$	9.34	10
$Pb^{2+} + L \rightleftharpoons PbL^{2+}$	9.01	10

1.2 The Element Lead

1.2.1 General Historical Overview

Lead is seen as one of the most common causes of heavy metal poisoning as it has found uses in almost every facet of human existence over the centuries. It has been used for piping in ancient Roman times, batteries, cable coverings, ammunition, paint, fuel, fine crystal glass, cosmetics, roofing, canned food cans and shielding of nuclear reactors and vessels. It is a common belief that lead may have led to the downfall of ancient empires due to cumulative poisoning. As the riches of the empires increased, so did the contact of the upper classes with leaded products.[8]

Many of the uses of lead have been discontinued over the last fifty years or so as the public awareness of the cumulative effects of lead have been highlighted. The use of tetraethyl lead as an additive in petrol as an anti-knock agent has been phased out since the mid 1980's. The use of leaded paint has also decreased in developing countries. Leaded paint was used to paint houses, bridges, walls, and artworks. The lead in the paint kept the colour bright and dried quickly. When removing the paint it was often pulverised and inhaled leading to poisoning. This has been documented in welders working on bridges and steel structures.[11] During 2007, several recalls of children's toys had to be made by the manufacturers as the products had been painted with leaded paints in China.

The myriad of uses that lead has clearly indicates that it is easy to come into contact with this metal and gather it as a cumulative poison. There are documented cases of lead poisoning reported by the Roman architect and engineer Marcus Vitruvius, although the cause of the poisoning was not known then.[8]

It is also quite ironic that two of the greatest causes of global warming can in part be attributed to one man, Thomas Midgley, Junior. He investigated the compound tetraethyl lead and found it to be a particularly effective anti-knock agent in fuel. He went on to invent CFCs or chlorofluorocarbons that acted as coolants in refrigeration units.[12] In the 1940's a man by the name of Clair Patterson was investigating the age of the earth and found that there was an abnormally high concentration of lead in the

atmosphere. When he investigated the matter further, he found that there had been an exponential growth in lead(II) levels since 1923, the year tetraethyl lead became commercially available. His tireless pursuit to remove lead from fuels finally came to fruition in the 1980's when lead was removed from fuels in the Western world. It is estimated that Americans today still have 625 times more lead in their bodies compared to Americans a century ago.[12]

The general symptoms of lead poisoning are headaches, indigestion, constipation, irritability, lack of concentration, anaemia, depression, insomnia, tingling in the hands and feet, and finally death. The lead ion interferes with the body's ability to make the *haem* molecule which is a part of haemoglobin, the oxygen carrier in the blood stream.

1.2.2 The Chemistry of Lead

Lead can be found in two oxidation states, +2 and +4, with the +2 oxidation state being the more common. It also has several isotopes of which three are stable, namely ^{206}Pb, ^{207}Pb, and ^{208}Pb. They have natural abundances of 24.1%, 22.1%, and 52.4% respectively. The remaining 1.4% of lead comes from ^{204}Pb.[13] Lead is most frequently mined in conjunction with other metals such as zinc, silver, and copper. It is most commonly found as galena (PbS) in nature.

The neutral atom has four valence electrons that are available for bonding. In the +2 oxidation state, there is one lone pair of electrons left. There is a question surrounding the lone pair of electrons on the lead(II) ion when it has formed a complex with the ligands of interest in this study. If it is indeed stereochemically active, i.e. it acts as a domain of electron density in the three-dimensional arrangement and structure, then the metal ion will effectively be seen as a metal ion with a smaller ionic radius than it does actually have.

Lead can assume many different geometries when forming complexes and this flexibility means that many ligands can bond to the central metal atom in many ways. Due to the fact that lead is on the borderline between hard and soft metals, it can bond to both hard and soft donor atoms to form complexes.[14]

1.2.3 Some Previous Work Done on Lead

Lead complexes can be classified as either *holodirected* or *hemidirected*. The former refers to a complex where the ligands are distributed equally around the metal centre, and the latter refers to a complex where there is a notable void in the coordination sphere. The most common coordination numbers for Pb(II) are 4 and 6.[15] It is found that the most *holodirected* Pb(II) complexes occur when there is a low coordination number between 2 and 5. The *hemidirected* complexes are more common for the higher coordination numbers such as 9 and 10. The intermediate coordination numbers 6 to 8 give a mix of both *holodirected* and *hemidirected* complexes.[15]

As stated above, lead is a borderline metal in the HSAB theory classification. This allows it to bond to both hard and soft donor ligands. Examples of lead complexes where the Pb(II) ion bonds to carbon, nitrogen, phosphorous, oxygen, sulphur, selenium, and various combinations of the above atoms are reported in the literature. Lead is also used in the complexation to macrocyclic ligands as lead can adopt many coordination numbers as well as geometries. This allows for the use of many different-sized macrocycles to be complexed to the metal ion.[14]

The metal ion of interest in this project is in the +2 oxidation state, i.e. Pb^{2+}. There are several papers that report Pb^{2+} complexes with stereochemically active lone pairs. The following is a brief overview of some work done on Pb(II) complexes with N or O donors and only serves to give a general overview of lead complexes.

A paper by Lyczko *et al.* [16] focused on the synthesis and characterisation of four lead tropolonato complexes, one of which has the metal ion in the +4 oxidation state. All syntheses were done below a pH of 1.0 to avoid producing dimeric complexes. The coordination number of the Pb^{2+} complexes ranges from five to eight. The only Pb^{4+} complex reported is eight-coordinate. Each complex was characterised by UV-vis spectroscopy and NMR. Each of the lead complexes obtained showed an apparently vacant site in its coordination sphere which was attributed to the stereochemically active $6s^2$ lone electron pair on the Pb^{2+} metal ion. The crystal structure of the Pb^{4+} complex was not determined.

Lead complexes of similar ligands were reported by Fan and Zhu.[17] The ligands used by these authors replaced the cyclohexenyl rings with aromatic counterparts. Three of the four reported complexes seemed to have a stereochemically active lone electron pair on the Pb^{2+} ion. This was evidenced by the vacant coordination site in the coordination polyhedron, which was attributed to the lone pair. Further, the M-X bonds, where X = O, N, were shorter than expected on the opposing side of the vacant coordination site. Bonds adjacent to the lone pair became rather longer than expected. They postulated that the coordination environment around the lead atom was defined by three properties: the stereochemical activity of the lone pair of electrons on the lead ion, the lead-oxygen interactions, and the π-π stacking interactions between the various ligand layers.

Yet another paper focused on several rare three-coordinate lead complexes.[18] These complexes were produced by complexing a lead halide salt with a bulky ligand. The geometry around the metal atom was pyramidal. This geometry was attributed to the stereochemically active lone pair of electrons in the Pb^{2+} ion which, it was postulated, occupied the fourth coordination site.

There has been considerable research done at the University of the Witwatersrand concerning the use of chelating agents in heavy metal poisoning.[9,19] One such study has used one of the ligands used in this project.[9] The thesis "*Electrochemical Studies of Metal-Ligand Equilibria Involving Chelating Ligands*" focused on the determination of stability constants of several ligands, including N,N'-bis(2-hydroxycyclohexyl)ethylenediamine, Cy_2-en, Figure 1.4. The ligands can be put into two groups, namely those with hydroxycyclohexyl rings and those with hydroxycyclopentyl rings. The metal ions used in the study were Pb^{2+} and Cd^{2+}. The ligands with the larger rings formed more stable ML complexes than their 5-membered equivalents. They also formed ML_2 complexes whilst only one ML_2 complex was reported for the hydroxycyclopentyl ligands. The ML_2 species was the minor species in the solution as compared to the ML complexes.

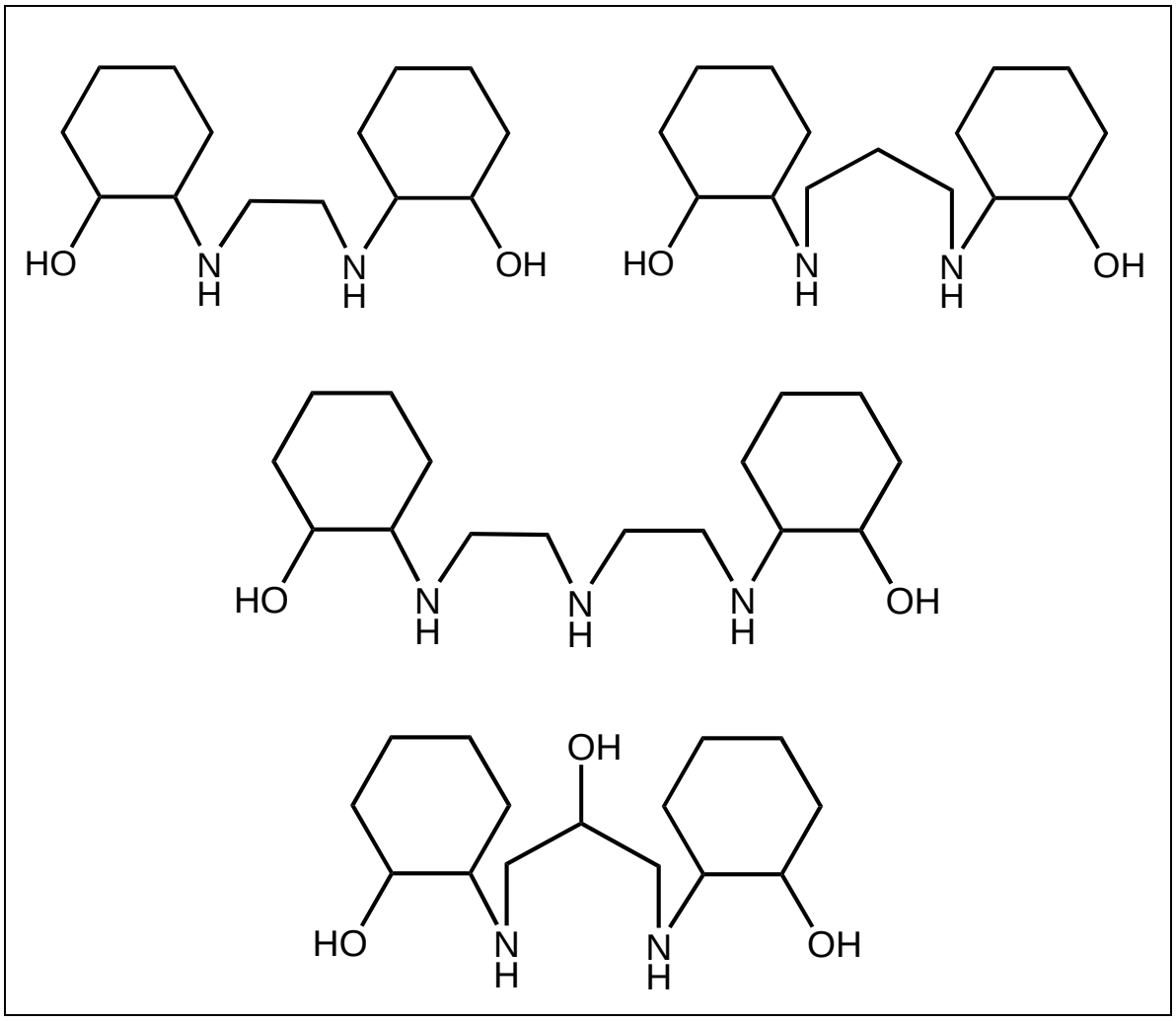


Figure 1.4: The four ligands synthesised in the study: Cy_2-en, Cy_2-tn, Cy_2-dien and Cy_2-Otn

1.3 The Element Cadmium

1.3.1 General Historical Overview

Cadmium is most frequently found as a sulphide or oxide salt in zinc ores. That is also the most common source of cadmium metal. In order for the zinc to be of acceptable purity, the impurities such as cadmium must be removed. This is done by heating the zinc sulphide ores in the presence of oxygen. The cadmium reacts with the oxygen to form cadmium oxide, CdO, and this fine powder is collected at the furnace exit.

It is also possible to obtain the cadmium from the zinc ores by electrolysis. This is the less common process for the extraction of cadmium.[20]

There are several commercial uses for cadmium. The most common use is as a coating for metals. Cadmium is a good protector for metals in alkaline solutions as well as marine environments. It is also used in pigments. There are several commercially available colours that are based on cadmium salts such as cadmium oxide with colours ranging from yellow to maroon. It is also becoming more common to use cadmium in the production of PVC and other plastics. It has been shown that when a cadmium salt of a fatty acid is added to these plastics, the plastic becomes more resistant to radiation and oxygen.[20] Cadmium is also very frequently found in batteries. These cadmium-nickel batteries are slowly but surely being phased out and replaced by metal hydride batteries.

Cadmium is a very toxic cumulative poison. It is a part of our daily diet and in the doses taken daily, not poisonous. But if one is exposed to a cadmium source that can enter the body, such as cadmium vapours, the effects can be very dire. The symptoms of such exposure range from metal fume fever to pneumonitis and death. The primary point of accumulation of cadmium is in the kidney and liver. As time progresses, the level of cadmium in the liver drops and the level in the kidney increases.[20] There is a well documented outbreak of cadmium intoxication in Japan after World War II. There was a strong increase in the mining activity in the area of the Jinzu River. As the cadmium concentration in the river water increased, the number of people living along the river who suffered from Itai-Itai, loosely translated as 'ouch-ouch' as their symptoms were pain during movement, disease increased. Once the source of the contamination was discovered and removed, the number of new cases dropped. The effects of the illness are permanent and not reversible.

1.3.2 The Chemistry of Cadmium

There are only two possible oxidation states for cadmium, +1 and +2. The +2 oxidation state is by far the more common. Cadmium has five stable isotopes, namely ^{108}Cd, ^{110}Cd, ^{111}Cd, ^{112}Cd, and ^{114}Cd with natural abundances of 0.89%, 12.49%, 12.80%,

24.13%, and 28.73% respectively. The remaining 20.96% is made up of isotopes of varying half-lives of over 10^{15} years.[13]

The atom, in its neutral state, has only two valence electrons available for bonding. The 4d electron shell is completely filled and as such not available for bonding. Due to the fact that single electrons are very reactive, it is immediately apparent that the +2 oxidation state is the favoured one. In this oxidation state both $5s^2$ electrons have been removed and the ion has reached a stable electron configuration.

Due to the above electron configuration system, it is anticipated that there will not be a stereochemically active lone pair of electrons on the cadmium ion as is anticipated for the lead ion. This will significantly alter the chemistry as well as the geometry of any complexes formed.

Cadmium is classified as a borderline metal, i.e. it is neither hard nor soft, and as such can bond to both hard and soft ligand donors. The ligand donors in this research project are O- and N-donors, hard donors.

1.3.3 Some Previous Work Done on Cadmium

A short review of some recent work on cadmium complexes is given below.

The thesis "*Electrochemical Studies of Metal-Ligand Equilibria Involving Chelating Ligands*" focused on the determination of stability constants of several ligands, including Cy_2-en with cadmium.[9] The Cd-Cy_2-en complex system had log β values of between 6.15 and 6.70 for the formation of the ML complex and between 9.35 and 9.63 for the formation of the ML_2 complex.

In a further study done at this University,[19] the focus was on the chelating ability of several macrocyclic ligands. Molecular Mechanics (MM) calculations were performed to find the most suitable chelating ligand as a drug in the treatment of cadmium intoxication. It was found that ligands with amine nitrogen atoms have a marked selectivity for cadmium.

The cadmium complexes of TEA, a simple precursor ligand to Cy_2-en, were many and varied. The denticity of the TEA ligand can vary as well as the geometric arrangement around the cadmium ion. This poses the question as to whether or not there

is any variation in the coordination of the desired ligands for this research. One expects the amine nitrogen atoms to be coplanar with the alcoholic oxygen atoms taking up either equatorial positions, if they are available, otherwise they will occupy the axial positions.

Naiini *et al.*[21] focused their efforts on synthesising ML_2 complexes and analysing them by X-ray diffraction, IR spectroscopy, NMR and FAB mass spectrometry. The IR spectra clearly indicated the formation of the complexes. A crystal structure for a cadmium complex was presented. The cadmium cation coordinated to two TEA ligands forming a sandwich complex. The cation was eight-coordinate which is not a normal coordination number for cadmium.

Cadmium and mercury complexes of the form $[M(TEA)_2](sac)_2$, where sac = saccharinate anion, were presented by Andac *et al.*[22] Both complexes were seven-coordinate with a monocapped trigonal prismatic geometry. As was clear from the coordination number, one TEA ligand was tetradentate and the other ligand tridentate. The cadmium complexed to the nitrogen atoms in both ligands, but to only two oxygen atoms for the tetradentate ligand.

An additional cadmium complex that exhibited the same coordination number as the aforementioned saccharinate complex was presented by Uçar *et al.*[23] The complex was of the type ML_2^{2+}. The complex formed a supramolecular structure with the metal being seven-coordinate. Again, one TEA group was tetradentate, coordinating to the metal ion via its amine nitrogen and its three oxygen atoms. The other was tridentate and coordinated to the metal ion via its amine nitrogen and two oxygen atoms affording the complex a capped trigonal prismatic geometry.

1.4 The Element Nickel

1.4.1 General Historical Overview

Nickel is a very common metal in use. It is commonly referred to as a coin metal, i.e. it is one of the metals that are used in the manufacture of money. The five cent coin in the United States, for example, was made of pure nickel.

Nickel is also found in many alloys in industrial and commercial applications. It is found in stainless steel and magnets, for example. It is also used in electroplating and as a dye to make green glass. It also has a common use in laboratories in the form of Raney nickel, a catalyst in hydrogenation reactions.

The most common form of nickel poisoning is nickel dermatitis, a condition in which the skin becomes raw and scratchy upon contact with a nickel compound. The far more dangerous and rare case of nickel intoxication by inhalation is almost exclusively caused by the inhalation of nickel carbonyl, $Ni(CO)_4$, a toxic substance that boils at 43 °C. The result is an increased susceptibility to cancer of the lungs and nasal passage. If the gas is inhaled, the person may feel a tightening of the chest as well as becoming dizzy and suffer from headaches.

1.4.2 The Chemistry of Nickel

There are several oxidation states for nickel, namely -1, 0, +1, +2, +3, and +4.[24] The most common of these is the oxidation state +2. Nickel also has several isotopes. There are five stable isotopes, namely ^{58}Ni, ^{60}Ni, ^{61}Ni, ^{62}Ni, and ^{64}Ni with natural abundances of 68.08%, 26.22%, 1.14%, 3.63%, and 0.93% respectively. The remaining isotopes have short half lives, most commonly less than a second.[13]

In its neutral state, nickel is a metal that has ten valence electrons. The two $4s^2$ electrons are the easiest to donate for bonding, leading to the most common oxidation state of +2. The oxidation state +3 arises from the loss of the above s electrons as well as one of the $3d^8$ electrons. The other oxidation states are very rare, with only a few reported cases of such nickel compounds. Some of these compounds have only been proven to exist using absorption spectroscopy.[24]

Nickel is also known to adopt several coordination geometries. The three coordination geometries that are the most common are the six-coordinate octahedral geometry as well as the four-coordinate square planar and tetrahedral geometries. The four-coordinate molecules are most frequently found to be red or yellow in colour, whilst the six-coordinate molecules are most commonly blue or green.

1.4.3 Some Previous Work Done on Nickel

There are no reported crystal structures that contain TEA complexed to a nickel atom. There are several examples of nickel complexes with ethylenediamine, $NH_2(CH_2)_2NH_2$, though. The number of coordinated ethylenediamine, or en, ligands ranges from one to three. The coordination geometry is octahedral for most of these cases but there are also examples where the geometry is square planar.

McDougall *et al*.[25] reported the synthesis and study of an octahedral mono-substituted nickel complex with en. The paper focused on the N-M-N bond angle upon complexation. The di-substituted nickel complexes with en were reported in the *cis* form by Shiu *et al*.[26] and the *trans* form by Li *et al*.[27] in brief structure reports. The tri-substituted complex was given by Feng *et al*.[28] The only four-coordinate complex reported was the square planar bis(ethylenediamine)nickel(II) dinitrate.[29]

1.5 The Element Zinc

1.5.1 General Historical Overview

Zinc is one of the most frequently used metals in the world. It is used to galvanise metals to prevent their corrosion, it is a major component in many alloys such as brass and nickel silver. It is also used as a coinage metal, functions as a sacrificial anode on ships and boats to prevent marine corrosion, is used as a paint, and zinc is used in sunscreens, vitamin supplements, and skin creams. There are many more uses for zinc but the above-mentioned ones are the most common. As is apparent from the list, zinc is a metal that humanity has a great deal of contact with. In low doses, below 12 mg per day, the metal is good for the body but longer exposure to increased zinc levels can lead to a failure of the kidneys as the metal interferes with the haemoglobin that has been converted to bilirubin. The bilirubin builds up in the liver as the liver cannot cope with the vast amounts of this material produced. The result is that the person suffers from a lack of oxygenated blood and appears anaemic as well as having a yellow skin colour due to the build-up of bile in the liver.

1.5.2 The Chemistry of Zinc

There is only one oxidation state for zinc, namely +2. The metal has 4 stable isotopes, ^{64}Zn, ^{66}Zn, ^{67}Zn, and ^{68}Zn. The respective natural abundances are 48.6%, 27.9%, 4.1%, and 18.8%.[13] The remaining 0.6% is made up of the less stable isotopes.

Zinc is mainly mined in China, Australia, and Peru. It is obtained via extractive metallurgy. The most common ores containing zinc are sphalerite (zinc sulphide), smithsonite (zinc carbonate), hemimorphite (zinc silicate), and franklinite (a zinc spinel).

In its neutral state, zinc has a fully filled d-electron valence shell as well as a filled s electron shell. This makes the metal stable and less reactive to air, as its use as a protective coating for metals proves. When the metal is charged, the two $4s^2$ electrons are lost to form the +2 charged ion. This oxidation state is also stable as the d-shell electrons are all paired and the shell is filled. This clearly indicates that there is no stereochemically active lone pair on the charged ion.

1.5.3 Some Previous Work Done on Zinc

The 2005 dissertation by Uwamariya[9] described the behaviour of several metal complexes in solution. One of the metals used was zinc. The values for the stability constants are given in Table 1.3.

Vallee and Auld[30] presented a most interesting paper on the role of zinc in enzymes and proteins. They noted that zinc showed almost equal preferences for nitrogen and oxygen donors when compared to sulfur donors.

Notni *et al*.[31] presented 24 zinc complexes with nitrogen macrocycles and thiolate counterions. Of these 24 complexes, the crystal structures of 20 were presented. The average bond length for the Zn-N bonds was between 2.037(2) and 2.076(2) Å. The zinc complexed readily to the nitrogen donors on the macrocyclic ligands as well as one thiolate ion only. In almost all of the reported structures, the zinc ion sat above the cavity of the ligand, irrespective of the size of the macrocycle. If the macrocycle contained less than 11 atoms in its ring, the zinc did not form a complex with it but rather bonded to the thiolate ion.

Berreau *et al*.[32] investigated nitrogen/sulfur donor ligands complexed to zinc. The two complexes were distinctly different. The one formed a dimeric complex with bridging oxygen atoms on water molecules. The second complex was a monomer and surrounded by the pendant arms of the ligand. The only difference in the synthetic pathway was the addition of potassium hydroxide to the first solution that went on to form the dimer.

Naiini *et al*.[21] presented a simple and direct method for the synthesis of zinc complexes with TEA. This is a method that was investigated during the course of the research project.

1.6 X-Ray Diffraction

The study of solid state structures is frequently performed by X-ray crystallography. This is the study of crystals by the measurement of their refractive properties when bombarded with X-rays. This bombardment leads to the electrons in the molecule being disturbed and absorbing certain wavelengths, whilst the rest of the X-ray beam is diffracted. This emission of electrons is monitored and the resulting data is analysed to obtain the crystal structure.

The incoming radiation of the X-rays is scattered by the crystal in a very distinct manner and only at certain wavelengths. The number of electrons in each atoms affects the degree to which scattering occurs and the resultant term, known as the scattering factor, helps to determine the identity of each atom during the process of interpreting the diffraction data. This relationship between the incoming radiation and the emitted radiation is given by Bragg's Law. Figure 1.5 shows the relationship between the incoming and outgoing radiation.

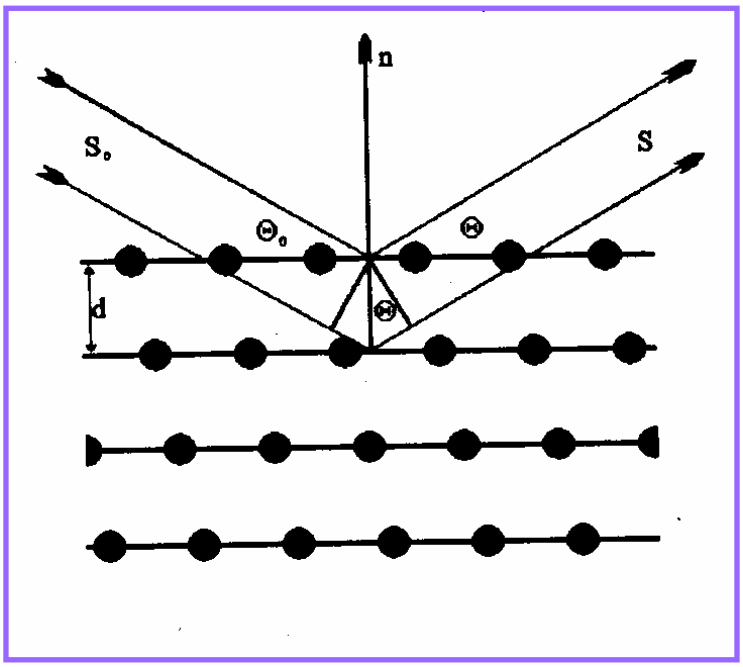


Figure 1.5: The Bragg scattering angles

Bragg's Law:

$$d = \frac{n \times \lambda}{2 \times \sin\theta} \qquad \textbf{(4)}$$

From these values, the d-spacings can be calculated. The data generated by this equation are then further manipulated to give distinct intensities and widths. These allow the crystallographer to determine the nature and position of the atom that lead to that particular peak.

The prerequisite for the success of this operation is that the crystal is well-ordered and has a definite arrangement in two or three dimensions.

In crystallographic terms the crystal is defined as being made up of repeating simple building blocks. This building block is called the unit cell. The unit cell contains the lattice points. These are points that are uniformly distributed in all three dimensions. A diagrammatic representation is given in Figure 1.6.

The combination of the structural motif and the lattice make up the crystal structure. This crystal structure is determined by its unit cell, its symmetry, and its fractional coordinates.

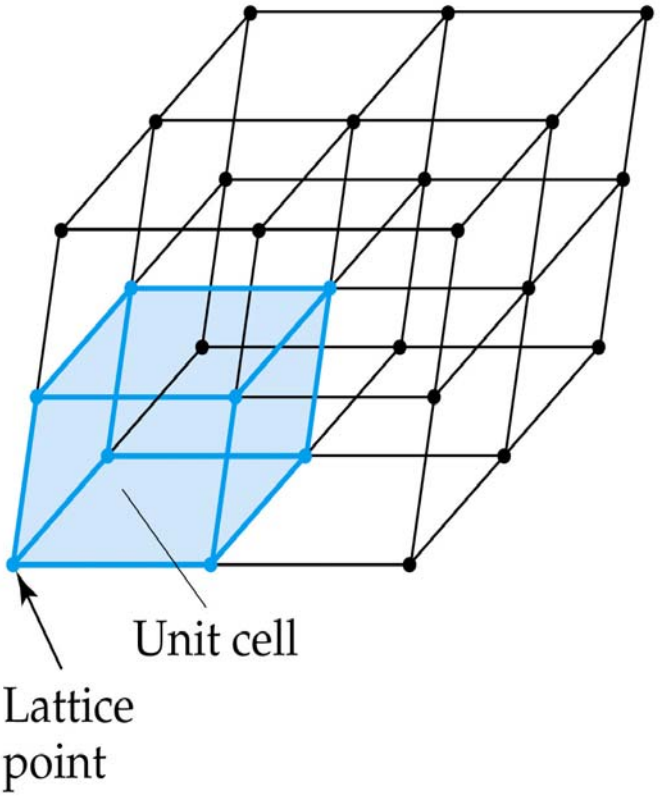


Figure 1.6: Representation of the unit cell and lattice points

The unit cell has six values associated with it: the length, height, and width of the unit cell, and the three angles within the unit cell. They are given by a, b, c, and α, β, γ respectively. The different arrangements are given different names and summarised in Figure 1.7.

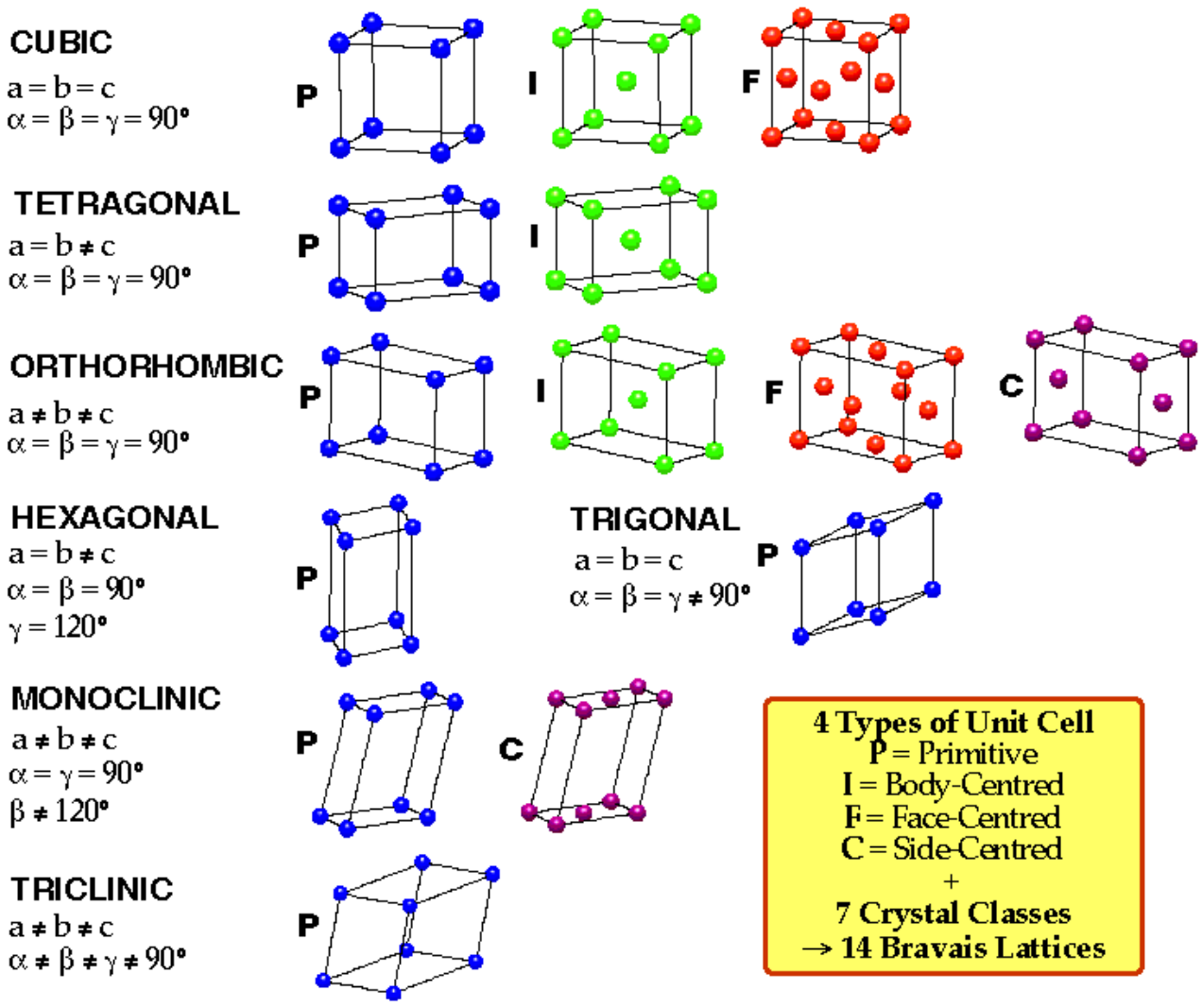


Figure 1.7: The various unit cell types

1.7 Molecular Modelling

1.7.1 General Overview

Quantum theory is a model of mechanics that has replaced the classical Newtonian mechanics model at the atomic as well as the subatomic level.[33] This theory was developed in the early twentieth century to account for the gross deviations that

appeared between the systems predicted by classical mechanics and the experimentally observed systems.

Quantum theory proposes that the energy in the system is only present in unit packages (also known as quanta) with discrete values. These units of energy also explain the dual wave and particle nature of light.

Several mathematical models have been developed to predict quantum mechanical properties. Two notable models are: the matrix mechanics formulation developed by Werner Heisenberg and the wave mechanics formulation developed by Erwin Schrödinger. These two sets were then incorporated into one coherent mechanical model by Paul Dirac. This is the most commonly used formulation.[34]

The Schrödinger model is summarized by two equations, namely the time-dependent Schrödinger equation and the time-independent Schrödinger equation. The general form of these equations is:

$$\hat{H}\Psi = E\Psi \qquad \textbf{(5)}$$

In the equation Ψ is the wave function of the molecule, $\hat{H}$ is the Hamiltonian, and E is the energy of the molecule. The Hamiltonian operator is an expression that combines the coordinates and momenta of a system as one function.

The equation is nigh to impossible to solve for a molecule with more than two electrons. Consequently, several approximations must be made in order to solve or rather approximate the wave function and hence the energy of a molecule. The first of these approximations is the Born-Oppenheimer approximation:

$$\hat{H} = K_N + K_e + V_{NN} + V_{Ne} + V_{ee} \qquad \textbf{(6)}$$

The Hamiltonian operator is given by the sum of the kinetic-energy operators for the nuclei and the electrons, K_N and K_e, and the potential energies of the repulsions between the nuclei V_{NN}, the potential energy of the attractions between electrons and nuclei V_{Ne}, and the potential energy of the repulsions between the electrons V_{ee}.

The above equations are used in quantum mechanical calculations. In molecular mechanics calculations, the simpler mechanical model, the electrons of the molecules are ignored and only the interactions of the nuclei are considered.

In the most simple mechanics force field, the four components that contribute to the inter- and intra-molecular forces in the system can be described by simple equations. The four factors that are considered are the change of bond lengths and angles from a described reference value, the rotation of bonds to give various torsions, and finally the interactions of the non-bonded atoms with one another. The result is a formula that has the form, **(7)** below:

$$\nu(\mathrm{r}^{\mathrm{N}}) = \sum_{bonds} \frac{k_i}{2}(l_i - l_{i,0})^2 + \sum_{angles} \frac{k_i}{2}(\theta_i - \theta_{i,0})^2 + \sum_{torsions} \frac{V_n}{2}(1+\cos(n\omega - \gamma)) + \sum_{i=1}^{N}\sum_{j=i+1}^{N}\left(4\varepsilon_{ij}\left[\left(\frac{\sigma_{ij}}{r_{ij}}\right)^{12} - \left(\frac{\sigma_{ij}}{r_{ij}}\right)^{6}\right] + \frac{q_i p_i}{4\varepsilon_0 r_{ij}}\right) \quad \textbf{(7)}$$

The terms define the potential energy of N particles with respect to their positions (r). The four terms in the equation model the bond length contribution, the bond angle contribution, the torsion angle contribution, and the non-bonded interaction contribution to the potential energy of the molecule. Each of the contributions will be discussed in more detail below.

The bond length contribution focuses on the deviation of the bond length, l_i, from the reference value, $l_{i,0}$. The most simple and most frequently used equation to estimate this deviation is Hooke's law:

$$\nu(l) = \sum_{bonds} \frac{k_i}{2}(l_i - l_{i,0})^2 \quad \textbf{(8)}$$

The formula indicates that the potential energy of the bonds, *v(l)*, is proportional to the square of the difference between the reference bond length and the actual bond length. The stretching constant, k_i, is unique for each type of atom.

It is acceptable to use Hooke's law to estimate the bond stretching contribution as the bonds do not tend to deviate significantly from their reference value as a great deal of energy is required to do so.

More detailed forms of the equation can also be used, incorporating Taylor series expansions but they require a great deal more calculation power and do not significantly change the result.

The angle bending contribution is also calculated by Hooke's law:

$$v(\theta) = \sum_{angles} \frac{k_i}{2}(\theta_i - \theta_{i,0})^2 \quad \textbf{(9)}$$

The formula indicates that the potential energy of the angles, *v(l)*, is proportional to the square of the difference between the reference bond angle, $\theta_{i,0}$, and the actual bond length, θ_i.

Again, Hooke's law is an appropriate approximation to the potential energy as the bond angles can vary a great deal but the associated energy penalty is low and the bending constants, k_i, are proportionally less than those in the bonding term. It is also possible to express the angle contribution by expanding the term as in the bond contribution.

The torsion contribution, $v(\omega)$, is expressed by a cosine series expansion:

$$v(\omega) = \sum_{torsions} \frac{V_n}{2}(1 + \cos(n\omega - \gamma)) \quad \textbf{(10)}$$

The torsion angle is ω. V_n gives a qualitative indication as to the height of the barrier that must be overcome to move from one conformation to another. γ is the phase factor. It indicates when the minimum value for the torsion angle is obtained.

The fourth term in the equation to determine the potential energy of a molecule describes the non-bonded interaction contributions. This term is made up of two parts, namely the electrostatic contribution and the van der Waals contribution. The van der Waals contribution is generally expressed using the Lennard-Jones 12-6 potential, the first part of the term:

$$v(r) = \sum_{i=1}^{N} \sum_{j=i+1}^{N} \left(4\varepsilon_{ij} \left[\left(\frac{\sigma_{ij}}{r_{ij}} \right)^{12} - \left(\frac{\sigma_{ij}}{r_{ij}} \right)^{6} \right] \right) \qquad \textbf{(11)}$$

The two adjustable parameters in the equation are the collision parameter, σ, and the well depth, ε. The distance between the two atoms, i and j, studied is r_{ij}.

The electrostatic contribution is expressed using the Coulomb potential, the second part of the term:

$$v(r) = \sum_{i=1}^{N} \sum_{j=i+1}^{N} \left(\frac{q_i p_i}{4\varepsilon_0 r_{ij}} \right) \qquad \textbf{(12)}$$

The electrostatic contribution describes the unequal distribution of attractive forces in the molecule. The charges on the two atoms are q and p. The distance between the two is r. The permittivity of a vacuum is ε_o.

1.7.2 Models

To perform molecular mechanics calculations, a force field must first be set up. This is a model that contains all of the values for the parameters in the equation 3. The force field must contain the reference bond length values, $l_{i,0}$, and the stretching constant, k. The values differ for each element as well as the different hybridisation types and bonding substituents for an element. The reference bond angle values, $\theta_{i,0}$, and the bending constants, k, also differ for each element as well as for the same element but with different environments. For the torsion section of the equation, it must contain the value of V_n which gives an estimation of the height of the barrier that must be overcome to

move from one conformation to another and the phase factor, γ. For the electrostatic contribution, the collision parameter, σ, and the well depth, ε, must be specified for each element. The van der Waals potential equation requires that the permittivity of a vacuum, ε_o, be specified.

The final aspect of molecular modelling that must be taken into account is the concept of atom types. An atom type is specified as the classification of an atom. Every atom can have different bonding environments and hybridisations. Each of these factors gives rise to a different chemical environment and as a consequence, the choice and variety of atom types on a force field predispose it toward certain types or classes of molecules.

One of the more common force fields to be used is the one set up by Kollman[35] and co-workers called AMBER, an acronym for Assisted Model Building and Energy Refinement. It was published in 1984. It was designed to perform molecular simulations for nucleic acids as well as proteins. The parameters are obtained from microwave, neutron diffraction, NMR studies, and crystal packing. It is still commonly in use today. The disadvantage of the model is that it works only for organic molecules. Inorganic molecules can only be poorly modelled using this force field. The force field has to be substantially altered by the manual addition of further parameters to describe the metals. This process is time-consuming and the altered force field works only for the narrow range of metal bonds that are specified in the new force field.

Kollman and co-workers[36] have since developed a newer and more inclusive force field called GAFF, the General Amber Force Field. It can handle organic and pharmaceutical molecules that contain C, H, N, O, S, P, and halogen moieties as well as nucleic acids and proteins. This force field can also adapt rather well to metal complexes once the additional parameters for the metals are added.

1.8 Hydrogen Bonds and Close Contacts

There are several types of bonded and non-bonded interactions that involve hydrogen atoms. Several types are outlined below.

1.8.1 Bonded Interactions

The simplest type of bonded interaction between two hydrogen atoms is the bond in H_2. But hydrogen can also bond to other ions. In a metal hydride bond, M-H, the hydrogen atoms assumes a negative charge in response to the positive charge on the metal ion. If, however, the hydrogen forms a bond to a non-metal, then the hydrogen atom will assume a positive charge whilst the bonded atom is negatively charged.

1.8.2 Non-Bonded Interactions

The most common and well-known type of non-bonded interaction is the hydrogen bond. This is a strong non-bonded interaction between a proton and strongly electronegative atoms such as N, O, or F. The bond may be formed intramolecularly or intermolecularly. A very particular case of a hydrogen bond is the low-barrier hydrogen bond. In such a bond, the separation between the donor atom and the acceptor atom of the hydrogen bond are so close that the proton is free to move between the two atoms. This is a common feature in enzymes.

A hydrogen-hydrogen bond, H-H bond, is defined as an interaction of the form X-H···H-Y, where X and Y are both moderately electronegative, and both of the hydrogen atoms are either neutral or have a small charge that may be of opposite sign. Several papers have been published debating the stabilising nature of these interactions.[37-39]

A further non-bonded interaction is the dihydrogen bond. This interaction is of the form M-H···H-X, where M is either a metal or the element boron, and X is an electronegative atom. The two hydrogen atoms must be of opposite sign. In the broadest sense this interaction may be regarded as a hydrogen bond. A good paper that gives a general overview of the definitions of hydrogen-hydrogen bonds and dihydrogen bonds is by Hernández-Trujillo and Matta.[37]

1.9 Objectives and Scope of the Research Project

During the course of the project, the four ligands, N,N'-bis(2-hydroxycyclohexyl)ethylenediamine, Cy_2-en, N,N'-bis(2-hydroxycyclohexyl)-1,3-propanediamine, Cy_2-tn, N,N'-bis(2-hydroxycyclohexyl)diethylenetriamine, Cy_2-dien, and 2,2'-[(hydroxypropane-1,3-diyl)diimino]dicyclohexanol, Cy_2-Otn, in Figure 1.4 are synthesised and attempts made at crystallising them. The final ligand in the project is commercially available and was used without further purification, N,N'-bis(2-hydroxyethyl)ethylenediamine, BHEEN, Figure 1.8. These ligands are then complexed with lead, cadmium, nickel, and zinc. Attempts are made to grow crystals of these complexes and study them by XRD analysis. The structures obtained from XRD analysis are then used to determine the non-bonding interactions between the hydrogen atoms on the cyclohexenyl rings with the hydrogen atoms on the bridging carbons. These interactions are referred to as hydrogen-hydrogen bonds.[37] This type of interaction is not a bond per say but an attractive interaction between the two protons. These can only be determined by the analysis of the solid state structure. The size and orientation of the cavity formed by the ligand can also help to explain the solution behaviour. This property will also be investigated using MM in an attempt to find the ideal metal ion to fit into the cavity of the ligands.

A comparison is also made between the complexes of Cy_2-en and BHEEN, its acyclic analogue, in order to explain the difference in observed log *K* values as given in Table 1.3. Borderline Lewis acids and bases, in particular, are strongly affected by the nature of their coordinating ligands and an increase in the electron-donating ability of the nitrogen moieties and oxygen moieties when fewer carbon groups are present, changes the complexation properties of the acceptor Lewis acids.

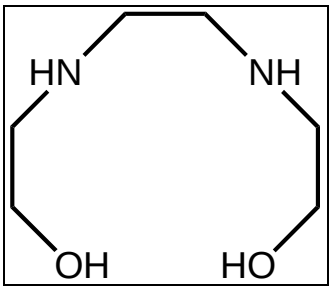


Figure 1.8: The ligand BHEEN

The complexes of interest are synthesised and attempts made at crystallising them. If crystals form, their molecular structure was determined from X-ray diffraction data. The complexes are also characterised by NMR, mass spectrometry, and infra-red spectroscopic methods to confirm their structures and purity.

1.10 References

(1) Jones, C. J.; Thornback, J. R. *Medicinal Applications of Coordination Chemistry*; First ed.; The Royal Society of Chemistry, 2007.

(2) Pearson, R. G. *J. Am. Chem. Soc.* **1963**, *85*, 3533-3539.

(3) Parr, R. G.; Pearson, R. G. *J. Am. Chem. Soc.* **1983**, *105*, 7512-7516.

(4) Pearson, R. G. *Chemical Hardness*; Wiley-VCH: Weinheim, 1997.

(5) Huheey, J. E.; Keiter, E. A.; Keiter, R. L. *Inorganic Chemistry: Principles of Structure and Reactivity*; Fourth ed.; Harper Collins: New York, 1993.

(6) Bell, C. F. *Principles and applications of metal chelation*; Oxford University Press: Oxford, 1977.

(7) Gordon, G. F. *EDTA and Chelation Therapy: History and Mechanisms of Action, an Update*; Gordon, G. F., http://www.gordonresearch.com/articles_oral_chelation/edtachel.html; 10-02-2008

(8) Emsley, J. *The Elements of Murder - A History of Poison*; Oxford University Press: Oxford, 2005.

(9) Uwamariya, V. Master of Science Dissertation, University of the Witwatersrand, 2005.

(10) Hancock, R. D.; De Sousa, A. S.; Walton, G. B.; Reibenspies, J. H. *Inorg. Chem.* **2007**, *46*, 4749-4757.

(11) Warren, C. *Brush with Death - A Social History of Lead Poisoning*; The Johns Hopkins University Press: Baltimore, 2000.

(12) Bryson, B. *A Short History of Nearly Everything*; 1st ed.; Broadway Books: New York, 2003.

(13) Parrington, J. R.; Knox, H. D.; Breneman, S. L.; Baum, E. M.; Feiner, F. *Nuclides and Isotopes Chart of the Nuclides*; 15 ed.; GE Nuclear Energy Lockheed Martin, 1996.

(14) Parr, J. *Polyhedron* **1997**, *16*, 551-566.

(15) Shimoni-Livny, L.; Glusker, J. P.; Bock, C. W. *Inorg. Chem.* **1998**, *37*, 1853-1867.

(16) Lyczko, K.; Starosta, W.; Persson, I. *Inorg. Chem.* **2007**, *46*, 4402-4410.

(17) Fan, S.-R.; Zhu, L.-G. *Inorg. Chem.* **2007**, *46*, 6785-6793.

(18) Chen, M.; Fulton, J. R.; Hitchcock, P. B.; Johnstone, N. C.; Lappert, M. F.; Protchenko, A. V. *Dalton Trans.* **2007**, 2770-2778.

(19) Casimiro, E. M. Doctor of Philosophy, University of the Witwatersrand, 2000.

(20) Webb, M. *The Chemistry, biochemistry, and biology of cadmium*; Elsevier/North-Holland Biomedical Press sole distributors for the U.S.A. and Canada, Elsevier North-Holland: New York, New York, 1979.

(21) Naiini, A. A.; Young, V.; Verkade, J. G. *Polyhedron* **1995**, *14*, 393-400.
(22) Andac, O.; Topcu, Y.; Yilmaz, V. T.; Guven, K. *Acta Crystallogr. Sect. C* **2001**, *C57*, 1381-1384.
(23) Uçar, I.; Yesilel, O. Z.; Bulut, A.; Icbudak, H.; Ölmez, H.; Kazak, C. *Acta Crystallogr. Sect. C* **2004**, *C60*, m392-m394.
(24) Lancaster, J. R. *The Bioinorganic Chemistry of Nickel*; VCH: New York, 1988.
(25) McDougall, G. J.; Hancock, R. D. *J. C. S. Dalton* **1979**, 654-659.
(26) Shiu, K.-B.; Yen, C.-H.; Liao, F.-L.; Wang, S.-L. *Acta Cryst. Sect. E* **2004**, *E60*, m121-m122.
(27) Li, M.-T.; Wang, C.-G.; Wu, Y.; Fu, X.-C. *Acta Cryst. Sect. E* **2005**, *E61*, m1613-m1615.
(28) Feng, H.; Tu, B.; Li, Y. Q.; Lü, Y. P.; Jin, Z.-M. *Acta Cryst. Sect. E* **2006**, *E62*, m1405-m1407.
(29) Krause Bauer, J. A.; Edison, S. E.; Baldwin, M. J. *Acta Cryst. Sect. E* **2005**, *E61*, m82-m84.
(30) Vallee, B. L.; Auld, D. S. *Biochemistry* **1990**, *29*, 5647-5659.
(31) Notni, J.; Görls, H.; Anders, E. *Eur. J. Inorg. Chem.* **2006**, 1444-1455.
(32) Berreau, L. M.; Allred, R. A.; Makowska-Grzyska, M. M.; Arif, A. M. *Chem. Commun.* **2000**, 1423-1424.
(33) Dirac, P. *The Principles of Quantum Mechanics*; Oxford University Press, 1981.
(34) Wikipedia *Quantum mechanics*; Wikipedia, 30 March 2008, http://en.wikipedia.org/wiki/Quantum_mechanics; 30-03-2008
(35) Weiner, S. J.; Kollman, P. A.; Case, D. A.; Singh, U. C.; Ghio, C.; Alagona, G.; Profeta, S. J.; Weiner, P. *J. Am. Chem. Soc.* **1984**, *106*, 765-784.
(36) Wang, J.; Wolf, R. M.; Caldwell, J. W.; Kollman, P. A.; Case, D. A. *J. Comput. Chem.* **2004**, *25*, 1157-1174.
(37) Hernández-Trujillo, J.; Matta, C. F. *Struct. Chem.* **2007**, *18*, 849-857.
(38) Damodharan, L.; Pattabhi, V. *Tetrahedron Letters* **2004**, *45*, 9427-9429.
(39) Wojtulewski, S.; Grabowski, S. J. *J. Mol. Struct.* **2003**, *645*, 287-294.

Chapter 2

Materials and Methods

2.1 Materials

The ligands in this study were either synthesised from commercially readily available materials or bought directly. The metal salts were also bought directly as were the solvents. The following is a list containing the sources from which all of the starting materials were bought. All chemicals were reagent grade and used without further purification.

All Appendices are found on the accompanying CD.

Table 2.1: List of Chemicals Used with Suppliers

Chemical Name	Supplier
Ethylenediamine	Merck
Lead monoxide	Aldrich
Ammonium nitrate	SaarChem
Dimethyl formamide	SaarChem
1,3-Diaminopropane	Merck
Cyclohexene oxide	Aldrich
Absolute ethanol	SaarChem

Diethylene triamine	Riedel-de Haën A.-G. Seelze bei Hannover
Lead(II) nitrate	Aldrich
Methanol	SaarChem
Lead(II) chloride	Aldrich
Diethyl ether	SaarChem
Cadmium(II) chloride hydrate	Riedel-de Haën A.-G. Seelze bei Hannover
1,3,-Diamino-2-propanol	Fluka
Zinc chloride	Aldrich
Zinc nitrate	Aldrich
N,N'-bis(2-hydroxyethyl)ethylenediamine	Aldrich
Nickel(II) nitrate	Aldrich
Nickel(II) chloride	Aldrich
Potassium hydroxide	SaarChem
Dimethyl acetamide	Aldrich

2.2 Physical Techniques of Characterisation

2.2.1 Nuclear Magnetic Resonance Spectroscopy (NMR)

Hydrogen (^{1}H) and carbon (^{13}C) nuclear magnetic resonance spectra were recorded on Bruker Avance-300 at 300.13 MHz respectively using standard pulse sequences. The probe temperature for all experiments was 300 ± 1 K. All spectra were recorded in either deuterium oxide (D_2O), deuterated methanol (CD_3OD), or deuterated chloroform ($CDCl_3$) in 5 mm NMR tubes unless otherwise stated. Chemical shifts are reported in parts per million (ppm) relative to the central signal of deuterated chloroform taken at δ 77.00 or deuterated methanol taken at δ 49.00 for the ^{13}C NMR. The ^{1}H NMR chemical shifts are reported as: value (splitting pattern, number of hydrogens, assignment). ^{13}C NMR chemical shifts are reported as: value (assignment). Abbreviations used: s = singlet, d = doublet, t = triplet, q = quartet, m = multiplet.

All NMR data were collected by Richard Mampa and further refined by the author. All NMR data are found in Appendix B.

2.2.2 Infrared Spectroscopy (IR)

Infrared spectra were recorded on a Bruker Vector 22 spectrometer. The absorptions are reported on the wavenumber (cm^{-1}) scale, in the range 400-4000 cm^{-1}. The signals are reported as: value (assignment if possible).

All IR data were collected and analysed by the author. All IR data are found in Appendix C.

2.2.3 Electrospray Ionization (ESI) or Atmospheric Pressure Chemical Ionization (APCI) – Mass Spectrometry

Low-resolution mass spectra were recorded on a VG7-SEQ Double Focussing Mass Spectrometer at 70 eV and 4.5 μA. The polarity was positive, ionisation employed was ESI or APCI, as quoted, with a resolution of 3000, a mass range of 3000 amu (8 kV) and a scan rate of 5 s/decade. The sample was dissolved in methanol and the mobile phase was a 50:50 methanol:water mixture in 0.1% formic acid. Data are quoted as: *m/z* value (relative abundance).

All mass spectrometry data were collected by Martin Brits and analysed by the author. All mass spectrometry data are found in Appendix D.

2.2.4 Single Crystal X-Ray Diffraction (XRD)

Intensity data were collected on a Bruker APEX II CCD area detector diffractometer with graphite monochromated Mo K_α radiation (50kV, 30mA) using the APEX 2 [1] data collection software. The collection method involved ω-scans of width 0.5° and 512x512 bit data frames. Data reduction was carried out using the program *SAINT+* [2] and face indexed absorption corrections were made using the program *XPREP*).[2]

The crystal structure was solved by direct methods using *SHELXTL*.[3] Non-hydrogen atoms were first refined isotropically followed by anisotropic refinement by full matrix least-squares calculations based on F^2 using *SHELXTL*. All hydrogen atoms were first located in the difference map then positioned geometrically and allowed to ride on their respective parent atoms. Hydrogen atoms bonded to nitrogen atoms were located in the difference map, and not positioned geometrically. Diagrams as well as publication material were generated using SHELXTL, PLATON [4] and ORTEP-3.[5]

All XRD data were collected by Dr. Manuel Fernandes and analysed by the author. All XRD data are found in Appendix E.

2.3 Synthesis of the Free Ligands

The ligands were synthesised in the manner as shown below in Figure 2.1. The ligand BHEEN was not synthesised as it is commercially available. It was used directly and without further purification.

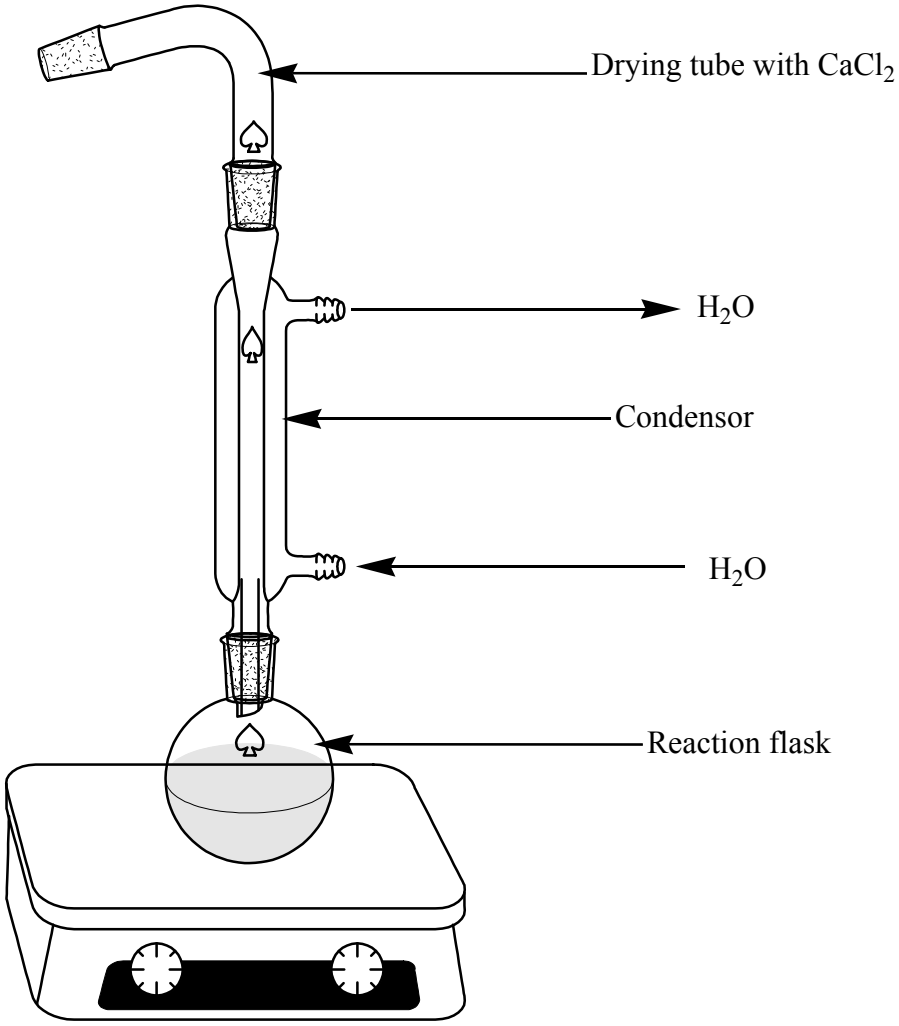


Figure 2.1: General Setup of the Ligand Reactions

2.3.1 Synthesis of Cy_2-en

Ethylenediamine was dissolved in the dry ethanol. To this, cyclohexene oxide was added and the resultant mixture refluxed at 80 ^{o}C for 6 hours with a $CaCl_2$ drying tube attached. The solution was filtered and the ethanolic solution collected and triturated with ice-cold acetone. The resulting white powder was collected and dried.

The reaction was performed several times and the relative masses and volumes of the reagents tabulated below.

Table 2.2: Masses and Volumes Used to Synthesise Cy_2-en

	Ethylenediamine		Cyclohexene oxide		Ethanol
	Mass	Moles	Mass	Moles	Volume
1	2.9589 g	49.234 mmol	14.9094 g	151.91 mmol	100 mL
2	1.3194 g	21.954 mmol	5.3441 g	54.452 mmol	50 mL
3	3.1702 g	52.750 mmol	12.6745 g	129.14 mmol	100 mL

The samples were characterised by NMR, IR, and mass spectrometry.

Sample 1:

The product was obtained in a 73 % yield (9.2445 g).

$\delta_H(D_2O)$ 3.27 (m, 2H, C<u>H</u>OH), 2.81 (m, 4H, C<u>H</u>$_2$NHR), 2.07 (m, 2H, C<u>H</u>NHR), 1.75 (s, 4H, C<u>H</u>$_2$CHOH), 1.58 (br s, 4H, C<u>H</u>$_2$CHNHR), 1.13 (br m, 8H, $CH_2C\underline{H}_2C\underline{H}_2CH_2$)

$\delta_C(CDCl_3)$ 74.93(CHOH), 64.13 (CHNHR), 47.34 (CH_2NHR), 33.76 (CH_2CHOH), 31.60 (CH_2CHNHR), 25.63 ($CH_2CH_2CH_2CH_2$)

ITMS + c APCI: m/z 257.25 (Cy_2-en^+ + 1)

IR (cm^{-1}): 3266 (N-H stretch), 2963 (O-H stretch), 2851 (alkane C-H stretch), 1451 and 1479 (CH_2 bending), 1367 (C-H bending), 1336 (O-H bending), 1251 (C-N stretch), 1219 (C-O stretch), 1195 and 916 (C-C stretch), 841 (N-H bending), 820 (C-H bending)

Sample 2:

The product was obtained in a 45 % yield (2.5061 g).

$\delta_H(D_2O)$ 3.23 (m, 2H, CHOH), 2.55 (m, 2H, CH_2NHR), 2.68 (m, 4H, CHNHR), 2.27 (m, 2H, CHNHR), 1.84 (s, 4H, CH_2CHOH), 1.56 (br s, 4H, CH_2CHNHR), 1.14 (br m, 8H, $CH_2CH_2CH_2CH_2$)

$\delta_C(CDCl_3)$ 75.08(CHOH), 64.16 (CHNHR), 47.57 (CH_2NHR), 33.74 (CH_2CHOH), 31.73 (CH_2CHNHR), 25.70 ($CH_2CH_2CH_2CH_2$)

ITMS + c ESI: m/z 257 (Cy_2-en^+ + 1)

IR (cm^{-1}): 3312 (N-H stretch), 2929 (O-H stretch), 2853 (alkane C-H stretch), 1451 and 1478 (CH_2 bending), 1352 (C-H bending), 1339 (O-H bending), 1244 (C-N stretch), 1196 (C-O stretch), 1169 and 929 (C-C stretch), 841 (N-H bending), 820 (C-H bending)

Sample 3:

The product was obtained in a 71 % yield (9.6431 g).

$\delta_H(D_2O)$ 3.27 (m, 2H, CHOH), 2.79 (m, 2H, CH_2NHR), 2.67 (m, 4H, CHNHR), 2.37 (m, 2H, CHNHR), 1.83 (s, 4H, CH_2CHOH), 1.57 (br s, 4H, CH_2CHNHR), 1.13 (br m, 8H, $CH_2CH_2CH_2CH_2$)

$\delta_C(CDCl_3)$ 74.05 (<u>C</u>HOH), 64.37 (<u>C</u>HNHR), 47.05 (<u>C</u>H_2NHR), 35.29 (<u>C</u>H_2CHOH), 30.99 (<u>C</u>H_2CHNHR), 25.64 ($CH_2\underline{C}H_2\underline{C}H_2CH_2$)

ITMS + c APCI: m/z 257.33 (Cy_2-en$^+$ + 1)

IR (cm^{-1}): 3265 (N-H stretch), 2924 (O-H stretch), 2852 (alkane C-H stretch), 1453 and 1479 (CH_2 bending), 1366 (C-H bending), 1337 (O-H bending), 1237 (C-N stretch), 1195 (C-O stretch), 1147 and 939 (C-C stretch), 841 (N-H bending), 821 (C-H bending)

The solid state structures of the free ligand as well as the protonated ligand were also solved. The solid state structure of the free ligand is tabulated in Table 2.3. The full data can be found in Appendix E in tables E.1 to E.6.

Table 2.3: Crystal Data and Structure Refinement for Cy_2-en

Temperature	293(2) K	
Crystal system	Monoclinic	
Space group	*P* 2_1/c	
Unit cell dimensions	a = 12.281(5) Å	α = 90°.
	b = 8.110(5) Å	β = 102.776(5)°.
	c = 7.123(5) Å	γ = 90°.
Volume	691.9(7) $Å^3$	
Z	1	
Density (calculated)	1.220 Mg/m^3	
Absorption coefficient	0.084 mm^{-1}	

Goodness-of-fit on F^2	1.038
Final R indices [I>2σ(I)]	$R_1 = 0.0584$, $wR_2 = 0.1399$
R indices (all data)	$R_1 = 0.0784$, $wR_2 = 0.1520$

The solid state structure of the protonated ligand is tabulated in Table 2.4. The full data can be found in Appendix E in tables E.7 to E.12.

Table 2.4: Crystal Data and Structure Refinement for the chloride salt of Cy_2-en

Temperature	293(2) K	
Crystal system	Triclinic	
Space group	$P\ \bar{1}$	
Unit cell dimensions	a = 5.8557(3) Å	α = 97.885(3)°.
	b = 6.9089(3) Å	β = 98.174(4)°.
	c = 11.1223(7) Å	γ = 107.415(3)°.
Volume	417.21(4) $Å^3$	
Z	1	
Density (calculated)	1.311 Mg/m^3	
Absorption coefficient	0.393 mm^{-1}	
Goodness-of-fit on F^2	1.306	
Final R indices [I>2σ(I)]	$R_1 = 0.0586$, $wR_2 = 0.1699$	
R indices (all data)	$R_1 = 0.0615$, $wR_2 = 0.1708$	

2.3.2 Synthesis of Cy_2-tn

1,3-Diaminopropane was dissolved in the dry ethanol. The cyclohexene oxide was added to this solution and the resultant mixture refluxed at 80 ^{o}C for 24 hours with a $CaCl_2$ drying tube attached. The solvent was then removed and the resulting oil placed under reduced pressure to leave behind a white powder. This powder was then triturated with ice-cold acetone, filtered and dried.

The reaction was performed twice and the relative masses and volumes of the reagents tabulated below.

Table 2.5: Masses and Volumes Used to Synthesise Cy_2-tn

	1,3-Diaminopropane		Cyclohexene oxide		Ethanol
	Mass	Moles	Mass	Moles	Volume
1	1.7023 g	22.965 mmol	8.7592 g	89.248 mmol	60 mL
2	2.1371 g	28.831 mmol	11.0384 g	112.47 mmol	120 mL

The samples were characterised by NMR, IR, and mass spectrometry.

Sample 1:

The product was obtained in a 78 % yield (4.8589 g).

$\delta_H(D_2O)$ 3.25 (m, 2H, C<u>H</u>OH), 2.63 (m, 2H, C<u>H</u>$_2$NHR), 2.48 (m, 2H, C<u>H</u>$_2$NHR), 2.29 (m, 2H, C<u>H</u>NHR), 1.87 (br d, 4H, C<u>H</u>$_2$CHOH), 1.58 (br m, 6H, C<u>H</u>$_2$CHNHR and C<u>H</u>$_2$CH$_2$NHR), 1.15-0.96 (br m, 8H, CH$_2$C<u>H</u>$_2$C<u>H</u>$_2$CH$_2$)

$\delta_C(CDCl_3)$ 74.32(<u>C</u>HOH), 64.26 (<u>C</u>HNHR), 45.88 and 45.65 (<u>C</u>H$_2$NHR), 34.12 (<u>C</u>H$_2$CHOH), 31.20 (<u>C</u>H$_2$CHNHR), 25.81 (<u>C</u>H$_2$CH$_2$NHR), 25.09 (CH$_2$<u>C</u>H$_2$<u>C</u>H$_2$CH$_2$)

ITMS + c APCI: m/z 271.31 (Cy_2-tn$^+$ + 1), 369.35 (Cy_3-tn$^+$ + 1)

IR(cm^{-1}): 3276 (N-H stretch), 3123 (O-H stretch), 2923 and 2853 (alkane C-H stretch), 1449 (CH_2 bending), 1337 (C-H bending), 1284 (O-H bending), 1201 (C-N stretch), 1109 (C-O stretch), 1078 and 966 (C-C stretch), 888 (N-H bending), 840 (C-H bending)

Sample 2:

The product was obtained in a 86 % yield (6.7166 g).

$\delta_H(D_2O)$ 3.07 (m, 2H, C<u>H</u>OH), 2.44 (m, 2H, C<u>H</u>$_2$NHR), 2.30 (m, 2H, C<u>H</u>$_2$NHR), 2.11 (m, 2H, C<u>H</u>NHR), 1.69 (br d, 4H, C<u>H</u>$_2$CHOH), 1.40 (br m, 6H, C<u>H</u>$_2$CHNHR and C<u>H</u>$_2$CH$_2$NHR), 0.99-0.78 (br m, 8H, CH$_2$C<u>H</u>$_2$C<u>H</u>$_2$CH$_2$)

$\delta_C(CDCl_3)$ 74.02(<u>C</u>HOH), 63.61 (<u>C</u>HNHR), 49.52 and 46.03 (<u>C</u>H$_2$NHR), 33.49 (<u>C</u>H$_2$CHOH), 31.15 (<u>C</u>H$_2$CHNHR), 25.27 (<u>C</u>H$_2$CH$_2$NHR), 24.50 (CH$_2$<u>C</u>H$_2$<u>C</u>H$_2$CH$_2$)

ITMS + c ESI: m/z 271.32 (Cy_2-tn$^+$ + 1), 293.31 (Cy_2-tn + Na^+), 369.40 (Cy_3-tn$^+$ + 1)

IR (cm^{-1}): 3276 (N-H stretch), 3126 (O-H stretch), 2925 and 2854 (alkane C-H stretch), 1448 (CH_2 bending), 1337 (C-H bending), 1285 (O-H bending), 1204 (C-N stretch), 1109 (C-O stretch), 1072 and 956 (C-C stretch), 887 (N-H bending), 840 (C-H bending)

2.3.3 Synthesis of Cy_2-dien

Diethylenetriamine was dissolved in the dry ethanol. The cyclohexene oxide was added to this solution and the resultant mixture refluxed at 80 ^oC for 24 hours with a $CaCl_2$ drying tube attached. The solvent was then removed and the resulting oil placed under reduced pressure to leave behind a white powder. This powder was then triturated with hot acetone, filtered and dried.

The reaction was performed twice and the relative masses and volumes of the reagents tabulated below.

Table 2.6: Masses and Volumes Used to Synthesise Cy_2-dien

	Diethylenetriamine		Cyclohexene oxide		Ethanol
	Mass	Moles	Mass	Moles	Volume
1	1.4456 g	14.012 mmol	4.7599 g	48.499 mmol	40 mL
2	2.2097 g	21.419 mmol	9.5669 g	97.478 mmol	60 mL

The samples were characterised by NMR, IR, and mass spectrometry.

Sample 1:

The product was obtained in a 29 % yield (4.0497 g).

$\delta_H(D_2O)$ 3.25 (m, 2H, C<u>H</u>OH), 2.64 (m, 8H, C<u>H</u>$_2$NHR), 2.30 (m, 2H, C<u>H</u>NHR), 1.87 (br d, 4H, C<u>H</u>$_2$CHOH), 1.59 (br s, 4H, C<u>H</u>$_2$CHNHR), 1.17-0.97 (br m, 8H, $CH_2C\underline{H}_2C\underline{H}_2CH_2$)

$\delta_C(CDCl_3)$ 74.28(<u>C</u>HOH), 63.96 (<u>C</u>HNHR), 49.69 and 46.31 (<u>C</u>H_2NHR), 33.95 (<u>C</u>H_2CHOH), 31.39 (<u>C</u>H_2CHNHR), 25.56 and 24.89 ($CH_2\underline{C}H_2\underline{C}H_2CH_2$)

ITMS + c APCI: m/z 300.34 (Cy_2-dien$^+$ + 1), 398.40 (Cy_3-dien$^+$ + 1)

IR (cm^{-1}): 3248 (N-H stretch), 2919 (O-H stretch), 2853 (alkane C-H stretch), 1498 (CH_2 bending), 1447 (C-H bending), 1338 (O-H bending), 1261 (C-N stretch), 1202 (C-O stretch), 1133 and 911 (C-C stretch), 844 (N-H bending), 821 (C-H bending)

Sample 2:

The product was obtained in a 36 % yield (2.331 g).

$\delta_H(D_2O)$ 3.07 (m, 2H, C<u>H</u>OH), 2.51 (m, 8H, C<u>H</u>$_2$NHR), 2.10 (m, 2H, C<u>H</u>NHR), 1.69 (br d, 4H, C<u>H</u>$_2$CHOH), 1.41 (br s, 4H, C<u>H</u>$_2$CHNHR), 0.99-0.78 (br m, 8H, $CH_2C\underline{H}_2C\underline{H}_2CH_2$)

$\delta_C(CDCl_3)$ 73.85(<u>C</u>HOH), 63.71 (<u>C</u>HNHR), 45.20 and 45.09 (<u>C</u>H_2NHR), 33.42 (<u>C</u>H_2CHOH), 30.72 (<u>C</u>H_2CHNHR), 25.27 and 24.45 ($CH_2\underline{C}H_2\underline{C}H_2CH_2$)

ITMS + c ESI: m/z 300.38 (Cy_2-dien$^+$ + 1), 322.34 (Cy_2-dien + Na^+), ~400 (Cy_3-dien$^+$ + 1), 420.44 (Cy_3-dien + Na^+)

IR (cm^{-1}): 3249 (N-H stretch), 2920 (O-H stretch), 2853 (alkane C-H stretch), 1497 (CH_2 bending), 1448 (C-H bending), 1338 (O-H bending), 1261 (C-N stretch), 1200 (C-O stretch), 1131 and 910 (C-C stretch), 844 (N-H bending), 820 (C-H bending)

2.3.4 Synthesis of Cy_2-Otn

1,3-diamino-2-propanol was dissolved in the dry ethanol. To this was added the cyclohexene oxide and the resultant mixture left to stir at room temperature for 24 hours with a $CaCl_2$ drying tube attached. The solution was then left to evaporate slowly when an oil formed that solidified upon standing to form a white powder. This powder was then triturated with ice-cold acetone, filtered and dried.

The reaction was performed three times and the relative masses and volumes of the reagents tabulated below.

Table 2.7: Masses and Volumes Used to Synthesise Cy_2-Otn

	1,3-Diamino-2-propanol		Cyclohexene oxide		Ethanol
	Mass	Moles	Mass	Moles	Volume
1	0.5585 g	6.197 mmol	1.4502 g	14.78 mmol	30 mL
2	2.0261 g	22.48 mmol	5.4913 g	55.951 mmol	50 mL
3	1.0599 g	11.761 mmol	2.8724 g	29.267 mmol	60 mL

The samples were characterised by NMR, IR, and mass spectrometry.

Sample 1:

The product was obtained in a 39 % yield (0.6532 g).

$\delta_H(D_2O)$ 3.82 (m, 1H, $CH_2C\underline{H}OH$), 3.27 (m, 2H, $C\underline{H}OH$), 2.83-2.41 (m, 4H, $C\underline{H_2}NHR$), 2.25 (m, 2H, $C\underline{H}NHR$), 1.99 (br d, 4H, $C\underline{H_2}CHOH$), 1.71 (br d, 4H, $C\underline{H_2}CHNHR$), 1.25-0.83 (br m, 8H, $CH_2C\underline{H_2}C\underline{H_2}CH_2$)

$\delta_C(CDCl_3)$ 73.51(bridging $\underline{C}HOH$), 63.94 ($\underline{C}HNHR$), 50.71 ($\underline{C}H_2NHR$), 33.82 ($\underline{C}H_2CHOH$), 30.40 ($\underline{C}H_2CHNHR$), 24.74 and 24.53 ($CH_2\underline{C}H_2\underline{C}H_2CH_2$), the cyclic $\underline{C}HOH$ is obscured by the solvent peak

ITMS + c APCI: m/z 287.34 (Cy_2-Otn^+ + 1)

IR(cm^{-1}): 3283 (N-H stretch), 3117 (O-H stretch), 2923 and 2853 (alkane C-H stretch), 1448 (CH_2 bending), 1338 (C-H bending), 1220 (O-H bending), 1166 (C-N stretch), 1120 (C-O stretch), 1074 and 963 (C-C stretch), 907 (N-H bending), 841 (C-H bending)

Sample 2:

The product was obtained in an 18 % yield (1.1549 g).

$\delta_H(D_2O)$ 3.73 (m, 1H, $CH_2C\underline{H}OH$), 3.23 (m, 2H, $C\underline{H}OH$), 2.70-2.57 (m, 4H, $C\underline{H_2}NHR$), 2.28 (m, 2H, $C\underline{H}NHR$), 1.82 (br d, 4H, $C\underline{H_2}CHOH$), 1.57 (br d, 4H, $C\underline{H_2}CHNHR$), 1.13-0.92 (br m, 8H, $CH_2C\underline{H_2}C\underline{H_2}CH_2$)

$\delta_C(CDCl_3)$ 73.35($\underline{C}HOH$), 63.26 ($\underline{C}HNHR$), 51.12 and 50.89 ($\underline{C}H_2NHR$), 34.22 ($\underline{C}H_2CHOH$), 30.24 ($\underline{C}H_2CHNHR$), 24.97 and 24.67 ($CH_2\underline{C}H_2\underline{C}H_2CH_2$), the cyclic $\underline{C}HOH$ is obscured by the solvent peak

ITMS + c APCI: m/z 287.35 (Cy_2-Otn^+ + 1)

IR(cm^{-1}): 3282 (N-H stretch), 3119 (O-H stretch), 2924 and 2853 (alkane C-H stretch), 1440 (CH_2 bending), 1338 (C-H bending), 1220 (O-H bending), 1166 (C-N stretch), 1119 (C-O stretch), 1073 and 962 (C-C stretch), 907 (N-H bending), 841 (C-H bending)

Sample3:

The product was obtained in a 10 % yield (0.5103 g).

$\delta_H(D_2O)$ 6.34 (m, 1H, $CH_2C\underline{H}OH$), 5.85 (m, 2H, $C\underline{H}OH$), 5.31-5.18 (m, 4H, $C\underline{H}_2NHR$), 4.89 (m, 2H, $C\underline{H}NHR$), 4.41 (br d, 4H, $C\underline{H}_2CHOH$), 4.16 (br d, 4H, $C\underline{H}_2CHNHR$), 3.74-3.51 (br m, 8H, $CH_2C\underline{H}_2C\underline{H}_2CH_2$)

$\delta_C(CDCl_3)$ 74.45 ($\underline{C}HOH$), 63.61 ($\underline{C}HNHR$), 52.68 and 51.62 ($\underline{C}H_2NHR$), 34.46 ($\underline{C}H_2CHOH$), 30.81 ($\underline{C}H_2CHNHR$), 25.69 and 25.57 ($CH_2\underline{C}H_2\underline{C}H_2CH_2$), the cyclic $\underline{C}HOH$ is obscured by the solvent peak

ITMS + c ESI: m/z 287.32 (Cy_2-Otn$^+$ + 1)

IR(cm^{-1}): 3282 (N-H stretch), 3113 (O-H stretch), 2923 and 2853 (alkane C-H stretch), 1440 (CH_2 bending), 1338 (C-H bending), 1221 (O-H bending), 1166 (C-N stretch), 1120 (C-O stretch), 1078 and 964 (C-C stretch), 907 (N-H bending), 842 (C-H bending)

The solid state structure of the free ligand was solved and tabulated in Table 2.8. The full data can be found in Appendix E in tables E.13 to E.18.

Table 2.8: Crystal Data and Structure Refinement for Cy_2-Otn

Temperature	293(2) K	
Crystal system	Triclinic	
Space group	$P\ \bar{1}$	
Unit cell dimensions	a = 10.0830(2) Å	α = 104.5330(10)°.
	b = 10.6966(3) Å	β = 104.7020(10)°.
	c = 16.6006(4) Å	γ = 90.5310(10)°.

Volume	1671.31(7) $Å^3$
Z	2
Density (calculated)	1.174 Mg/m^3
Absorption coefficient	0.083 mm^{-1}
Goodness-of-fit on F^2	1.002
Final R indices [I>2σ(I)]	$R_1 = 0.0504$, $wR_2 = 0.1196$
R indices (all data)	$R_1 = 0.0868$, $wR_2 = 0.1338$

2.4 Synthesis of the Lead Complexes

Due to the ease with which Cy_2-en could be produced, it was used as the initial ligand for complexations until a successful complexation method was found. This method was then applied to the other ligands.

2.4.1 Synthesis of the Cy_2-en/Pb(II) complex

Several methods were employed to obtain the lead complex. The unsuccessful methods are listed first.

Method 1:

Lead monoxide, PbO, (1.1257 g, 5.043 mmol) was placed in a round-bottomed flask along with 0.8586 g (10.73 mmol) of ammonium nitrate and 2.5905 g (10.104 mmol) Cy_2-en.

Then 10 mL dry DMF was added. The resultant mixture was refluxed at 100 ^{o}C for 20 hours. The solution was then left to cool to room temperature and then left to evaporate slowly. At first the ligand precipitated out. This product was filtered off and the remaining solution left to evaporate to dryness. The resulting tar-like black oil was then washed with acetone and each washing filtered. The initial filtrate was merely degraded DMF but as the solution cleared the final product, an imidazolinium salt (Figure 6.5), was obtained. The crystals formed were clear and brick-like. The crystals had to be kept moist or else they shattered.

The product was obtained in an 11 % yield (0.2980 g).

$\delta_H(D_2O)$ 7.87 (s, 1H, NHC<u>H</u>NH_2^+), 3.69 (m, 4H, C<u>H</u>$_2$NHR), 3.34 (m, 2H, C<u>H</u>OH), 3.13 (m, 2H, C<u>H</u>NHR), 2.71 and 2.56 (degraded DMF residues), 1.76 and 1.67 (m, 4H, C<u>H</u>$_2$CHOH), 1.45 (br s, 4H, C<u>H</u>$_2$CHNHR), 1.27-0.99 (br m, 8H, CH_2C<u>H</u>$_2C$<u>H</u>$_2CH_2$)

$\delta_C(CD_3OD)$ 155.23 (NHR<u>C</u>HNHR), 60.76(<u>C</u>HOH), 55.43 (<u>C</u>HNHR), 47.34 (<u>C</u>H$_2$NHR), 33.76 (<u>C</u>H$_2$CHOH), 31.60 (<u>C</u>H$_2$CHNHR), 25.63 (CH_2<u>C</u>H$_2$<u>C</u>H$_2CH_2$)

ITMS + c APCI: m/z 267.29 (imidazolinium ion + 1, as described in Chapter 6)

IR (cm^{-1}): 3415 (N-H stretch), 2939 (O-H stretch), 2856 (alkane C-H stretch), 1644 (C=N bond), 1455 (CH_2 bending), 1412 (C-H bending), 1362 (O-H bending), 1268 (C-N stretch), 1229 (C-O stretch), 1133 and 952 (C-C stretch), 846 (N-H bending), 824 (C-H bending)

Method 2:

Lead nitrate (0.1247 g, 0.3765 mmol) was dissolved in 0.75 mL of water. To that was added a solution of Cy_2-en (0.0897 g, 0.350 mmol) dissolved in 1.00 mL water and 2.00 mL ethanol. This solution was initially heated to dissolve the ligand. The resultant mixture was heated to 55 ^{o}C and left to stir for 2 hours. The solution was decanted and refrigerated. Crystals formed almost immediately which were the free ligand. The solution was decanted and left to evaporate slowly at room temperature when a powder precipitated out of solution which was a mixture of the lead salt as well as the Cy_2-en.

ITMS + c APCI: m/z 257.24 (Cy_2-en$^+$ + 1)

Method 3:

Lead(II) chloride (0.1049 g, 0.3772 mmol) was dissolved in 1.25 mL water. This solution was heated to 55°C. In the meantime, Cy_2-en (0.0801 g 0.312 mmol) was dissolved in a mixture of 1.00 mL water and 2.00 mL methanol. This solution was added to the lead solution. This mixture was then left to stir at 55°C for 2 hours. The solution was decanted and refrigerated. The resulting crystals formed were of the protonated ligand with a chloride counter-ion. The crystal structure of this salt was determined and described in Chapter 4.1.1.

The product was obtained in a 50 % yield (0.0453 g).

$\delta_H(D_2O)$ 3.40 (m, 2H, C<u>H</u>OH), 3.17 (m, 4H, C<u>H$_2$</u>NHR), 2.69 (m, 2H, C<u>H</u>NHR), 1.89 (d, 4H, C<u>H$_2$</u>CHOH), 1.63 (br s, 4H, C<u>H$_2$</u>CHNHR), 1.16 (br m, 8H, $CH_2C\underline{H_2}C\underline{H_2}CH_2$)

ITMS + c APCI: m/z 257.26 (Cy_2-en$^+$ + 1)

Method 4:

Lead carbonate (0.31047 g, 0.4006 mmol) was dissolved in 1.75 mL water and heated to 55 °C. To that was added a solution of Cy_2-en (0.0858 g, 0.335 mmol) dissolved in 2.00 mL ethanol. The resultant mixture was again heated to 55 °C and left to stir for 2 hours. The solution was filtered and refrigerated. The filtrate contained the free ligand.

ITMS + c APCI: m/z 257.27 (M^+ + 1 of the ligand)

Method 5:

The method that led to successful formation of the desired complex is described below.

Lead monoxide, 0.4502 g (2.017 mmol), and 0.3254 g (4.065 mmol) ammonium nitrate, NH_4NO_3, were dissolved in 20mL DMF and 0.9931 g (3.873 mmol) Cy_2-en was added to this solution. This solution was left to reflux at 160 °C for 90 minutes upon dissolution of the lead monoxide (~10 min). The solution was left to cool to room temperature when crystals formed.

These first crystals were the free ligand. The solution was filtered. The remaining solution was then left to evaporate slowly (approx. 2 months). Crystals were then found in the solution. They were washed with acetone to give the desired product.

Initially, 0.2149 g of ligand was recovered. Then the desired product was collected in a 30 % yield (0.3499 g).

ITMS + c APCI: m/z 257.31 (Cy_2-en^+ + 1), 588.28 (M^+ + 1 of complex [$Pb(Cy_2$-$en)(NO_3)_2$])

IR (cm^{-1}): 3368 (O-H stretch), 2935 (N-H stretch), 2860 (alkane C-H stretch), 1638 (CH_2 bending), 1446 (C-H bending), 1319 (O-H bending), 1285 (C-N stretch), 1202 (C-O stretch), 1133 and 916 (C-C stretch), 845 (N-H bending), 824 (C-H bending), 718 and 698 (Pb-N stretch), 608 (Pb-N bending)

The solid state structure of the Cy_2-en/Pb complex is described in Table 2.9. The full data can be found in Appendix E in tables E.25 to E.30.

Table 2.9: Crystal Data and Structure Refinement for Cy_2-en/Pb Complex

Temperature	273(2) K	
Crystal system	Monoclinic	
Space group	$P\ 2_1$	
Unit cell dimensions	a = 9.0573(2) Å	α = 90°.
	b = 9.7265(2) Å	β = 107.4940(10)°.
	c = 11.4533(2) Å	γ = 90°.
Volume	962.32(3) $Å^3$	
Z	2	

Density (calculated)	2.021 Mg/m^3
Absorption coefficient	8.815 mm^{-1}
Goodness-of-fit on F^2	1.013
Final R indices [I>2σ(I)]	$R_1 = 0.0196$, $wR_2 = 0.0441$
R indices (all data)	$R_1 = 0.0212$, $wR_2 = 0.0444$

2.4.2 Attempted synthesis of the Cy_2-tn/Pb(II) complex

Lead monoxide, 0.2667 g (1.195 mmol), and 0.1880 g (2.349 mmol) ammonium nitrate, NH_4NO_3, were dissolved in 15mL DMF and 0.6283 g (2.323 mmol) Cy_2-tn was added. This solution was left to reflux at 160 ^oC for 2 hours upon dissolution of the lead monoxide (~15 min). The ligand struggled to go into solution. The solution was left to cool to room temperature when crystals formed. These first crystals were the free ligand. The solution was filtered. The remaining solution was then left to evaporate slowly (approx. 2 months). The powder that formed was washed with acetone and found to be the free ligand.

The ligand was initially regenerated (0.0096 g) followed by a further 0.0127 g of the ligand.

ITMS + c APCI: m/z 271.32 (Cy_2-tn^+ + 1)

IR (cm^{-1}): 3350 (N-H stretch), 2931 (O-H stretch), 2859 (alkane C-H stretch), 1737 (CH_2 bending), 1654 (C-H bending), 1353 (O-H bending), 1091 (C-N stretch), 1043 (C-O stretch), 827 (N-H bending), 777 (C-H bending)

2.4.3 Synthesis of the Cy_2-dien/Pb(II) complex

Lean monoxide, 0.4682 g (2.098 mmol), and 0.1750 g (2.186 mmol) ammonium nitrate, NH_4NO_3, were dissolved in 15mL DMF and to this solution 0.6250 g (2.087 mmol) Cy_2-dien was added. This solution was left to reflux at 160 ^oC for 1.5 hours upon dissolution of the lead monoxide (~20 min). The ligand did not dissolve at room temperature but dissolved once the solution was heated above 100 ˚C. The solution was left to cool to room temperature when crystals formed. These first crystals were the free ligand. The solution was filtered. The remaining solution was then left to evaporate slowly (approx. 2 months). The powder that formed was washed with acetone. This powder was insoluble in acetone, water, DMF, dioxane, isopropanol and IR analysis indicated that a complex had formed. The powder was redissolved in dilute HNO_3.

The ligand was initially regenerated (0.0153 g) followed by 0.0214 g of the insoluble, desired product.

ITMS + c APCI: m/z 300 (Cy_2-dien$^+$ + 1)

IR (cm^{-1}): 3265 (O-H stretch), 3082 (N-H stretch), 2852 (alkane C-H stretch), 1675 (CH_2 bending), 1465 (C-H bending), 1337 (O-H bending), 1310 (C-N stretch), 1195 (C-O stretch), 1115 and 917 (C-C stretch), 841 (N-H bending), 821 (C-H bending), 794 and 682 (Pb-N stretch)

2.4.4 Synthesis of the Cy_2-Otn/Pb(II) complex

Lead monoxide, 0.1539 g (0.6895 mmol), and 0.1128 g (1.409 mmol) ammonium nitrate, NH_4NO_3, were dissolved in 10mL DMF, and to this solution 0.1969 g (0.6875 mmol) Cy_2-Otn was added. This solution was heated to 50 ^oC for and left to stir for 1 hour. The solution was then cooled to room temperature and left to stir for a further 24 hours. The solution was filtered. The remaining solution was then left to evaporate slowly (approx. 2 months). The powder that formed was washed with acetone. Attempts were made to recrystallise the powder from DMF,

water, methanol, and ethanol. Although crystals formed in the solutions, none were of sufficient quality to yield a useable diffraction data set.

The desired product was collected (0.0108 g).

IR (cm^{-1}): 3547 (O-H stretch), 2931 (N-H stretch), 2859 (alkane C-H stretch), 1738 (CH_2 bending), 1392 (C-H bending, O-H bending, C-N stretch, C-O stretch), 1083 and 1047 (C-C stretch), 845 (N-H bending), 755 (C-H bending), 695 and 682 (Pb-N stretch), 610 (Pb-N bending)

2.4.5 Synthesis of the BHEEN/Pb(II) complex

Lead(II) nitrate (1.1766 g, 3.5525 mmol) was dissolved in 90 mL of water. To this was added 0.4900 g BHEEN (3.306 mmol). The solution was left to stir at room temperature for 24 hours, filtered and the remaining solution left to evaporate slowly. The initial crystals that formed were analysed and found to be a complex of lead with BHEEN. No further product formed when the solution evaporated. Attempts were made to recrystallise the sample from water, methanol, and ethanol but no crystals of suitable XRD quality could be obtained.

The complex collected weighed 0.9870 g.

ITMS + c APCI: m/z 148.17 ($BHEEN^+$ + 1), 237.26 ($PbCl^+$), 282.41 ($Pb(NO_3)(OH)$), 371.18 ($[Pb(BHEEN)](OH)^+$), 445.15 ($[Pb(BHEEN)](Cl)(NO_3)^+$), 462.03 ($[Pb(BHEEN)](NO_3)_2^+$), 519.04 ($[Pb(BHEEN)_2](OH)^+$), 536.09 ($[Pb(BHEEN)_2Cl_2]$ + 1)

IR (cm^{-1}): 3532 (O-H stretch), 2945 (N-H stretch), 2887 (alkane C-H stretch), 1736 (CH_2 bending), 1380 (O-H bending, C-N stretch, C-O stretch), 1043 and 894 (C-C stretch), 849 (N-H bending), 777 (C-H bending), 680 (Pb-N stretch), 616 (Pb-N bending)

2.5 Synthesis of the Cadmium Complexes

2.5.1 Synthesis of the Cy_2-en/Cd(II) complex

Cadmium chloride hydrate, $CdCl_2 \cdot 2.5H_2O$, (0.2347 g, 1.028 mmol) were dissolved in 10mL water. To this was added 0.5395 g (2.104 mmol) Cy_2-en. This solution was left to reflux at 90 ^oC for 24 hours. The solution was filtered and washed with ether to remove the free ligand from the product. Most of the remaining solution was then removed to produce a second product. This was the desired product. This powder was then redissolved in methanol and brought to the boil. The temperature was then slowly reduced in 5 ^oC steps and crystals of suitable quality were obtained.

The ligand was initially regenerated (0.2377 g) followed by 0.1683 g of the desired product in an 18 % yield.

ITMS + c APCI: m/z 257.27 (Cy_2-en^+ + 1)

IR (cm^{-1}): 3357 (O-H stretch), 2934 (N-H stretch), 2862 (alkane C-H stretch), 1449 (C-H bending), 1396 (O-H bending), 1210 (C-O stretch), 1137 and 938 (C-C stretch), 891 (N-H bending), 840 (C-H bending), 718 (Cd-N stretch)

The solid state structure of the Cy_2-en/Cd complex is described in Table 2.10.

Table 2.10: Crystal Data and Structure Refinement for Cy_2-en/Cd Complex

Temperature	223(2) K	
Crystal system	Triclinic	
Space group	$P\ \bar{1}$	
Unit cell dimensions	a = 7.6698(7) Å	α = 75.694(4)°.
	b = 11.0270(10) Å	β = 80.960(4)°.
	c = 12.4807(13) Å	γ = 81.170(4)°.
Volume	1002.84(17) $Å^3$	
Z	2	
Density (calculated)	1.549 Mg/m^3	
Absorption coefficient	1.369 mm^{-1}	
Goodness-of-fit on F^2	1.068	
Final R indices [I>2σ(I)]	R_1 = 0.0280, wR_2 = 0.0697	
R indices (all data)	R_1 = 0.0304, wR_2 = 0.0713	

2.5.2 Synthesis of the Cy_2-tn/Cd(II) complex

Cadmium chloride hydrate, $CdCl_2 \cdot 2.5H_2O$, (0.5922 g, 2.593 mmol) was dissolved in 20 mL water. To this was added 0.5864 g (2.169 mmol) Cy_2-tn. This solution was left to reflux at 90 ^oC for 48 hours. The solution was filtered and washed with ether to remove the free ligand from the product. Most of the remaining solution was then removed. No further product was

obtained. This powder was then redissolved in methanol and brought to boil. The temperature was then slowly reduced in 5 ^{o}C steps. No crystals were obtained.

ITMS + c APCI: m/z 271.35 (Cy_2-tn $^{+}$ + 1)

ITMS + c ESI: m/z 271.34 (Cy_2-tn $^{+}$ + 1)

IR(cm^{-1}): 3310 (O-H stretch), 3255 (N-H stretch), 2936 and 2860 (alkane C-H stretch), 1451 (CH_2 bending), 1334 (C-H bending), 1287 (O-H bending), 1209 (C-N stretch), 1098 (C-O stretch), 1050 and 968 (C-C stretch), 878 (N-H bending), 844 (C-H bending), 716 and 618 (Cd-N stretch), 559 (Cd-N bending)

2.5.3 Attempted synthesis of the Cy_2-dien/Cd(II) complex

Cadmium chloride hydrate, $CdCl_2 \cdot 2.5H_2O$, (0.2059 g, 0.9015 mmol) were dissolved in 12 mL water. To this was added 0.2100 g (0.7013 mmol) Cy_2-dien. This solution was left to reflux at 90 ^{o}C for 48 hours. The solution was filtered and washed with ether to remove the free ligand from the product. Most of the remaining solution was then removed. No further product was obtained. The filtered powder was then redissolved in methanol and brought to boil. The temperature was then slowly reduced in 5 ^{o}C steps. No crystals were obtained.

ITMS + c APCI: m/z 300.39 (Cy_2-dien $^{+}$ + 1)

IR (cm^{-1}): 3249 (O-H stretch), 2920 (N-H stretch), 2853 (alkane C-H stretch), 1497 (CH_2 bending), 1449 (C-H bending), 1338 (O-H bending), 1262 (C-N stretch), 1200 (C-O stretch), 1131 and 910 (C-C stretch), 844 (N-H bending), 821 (C-H bending)

2.5.4 Synthesis of the Cy_2-Otn/Cd(II) complex

Cadmium chloride hydrate, $CdCl_2 \cdot 2.5H_2O$, (0.2220 g, 0.9720 mmol) was dissolved in 10 mL water. To this was added 0.1015 g (0.3544 mmol) 2,2'-[(hydroxypropane-1,3-diyl)diimino]dicyclohexanol. This solution was left to stir at room temperature for 24 hours. The solution was then set aside and left to stand for a further 24 hours. The solution was then filtered and washed with ether to remove the free ligand from the product. Most of the remaining solution was then removed to produce a second product. This was the desired product. This powder was then redissolved in methanol and brought to boil. The temperature was then slowly reduced in 5 ^oC steps but no crystals of suitable quality were obtained.

The ligand was initially regenerated (0.0986 g) followed by 0.1384 g of the desired product.

ITMS + c APCI: m/z 287.35 (M^+ + 1 free ligand), 435.27 ([Cd(Cy_2-Otn)]Cl^+)

IR (cm^{-1}): 3355 (O-H stretch), 2937 (N-H stretch), 2861 (alkane C-H stretch), 1450 (C-H bending), 1403 (O-H bending), 1230 (C-O stretch), 1133 and 930 (C-C stretch), 889 (N-H bending), 847 (C-H bending), 782 (Cd-N stretch)

2.5.5 Synthesis of the BHEEN/Cd(II) complex

Cadmium chloride hydrate, $CdCl_2 \cdot 2.5H_2O$, (0.7791 g, 3.411 mmol) were dissolved in 10 mL water. To this was added 0.5069 g (3.420 mmol) BHEEN. This solution was left to reflux at 80 ^oC for 24 hours. The solution was filtered and washed with ether to remove the free ligand from the product. Most of the remaining solution was then removed to produce a second product. This was the desired product. This powder was then redissolved in methanol and brought to boil. The temperature was then slowly reduced in 5 ^oC steps and crystals of suitable quality were obtained.

The ligand was initially regenerated (0.0872 g) followed by 0.5631 g of the desired product in an 41 % yield.

ITMS + c ESI: m/z 149.22 ($BHEEN^+$ + 1), 253.17 to 259.13 ($[Cd(BHEEN)]^+$ +1), 295.11 to 299.10 ($[Cd(BHEEN)Cl]^+$ +1), 321.17 to 323.21 ($[Cd(BHEEN)Cl_2]^+$ +1), 514.16 to 519.13 ($[Cd(BHEEN)]_2^+$ +1), 555.11 ($[Cd(BHEEN)]_2Cl^+$ +1), 591.07 to 595.06 ($[Cd(BHEEN)Cl]_2^+$ +1), 627.01 ($[Cd(BHEEN)Cl]_2Cl^+$ +1), ~665 ($[Cd(BHEEN)Cl_2]_2^+$ +1)

IR (cm^{-1}): 3370 (O-H stretch), 2931 (N-H stretch), 2881 (alkane C-H stretch), 1447 (C-H bending), 1380 (O-H bending), 1235 (C-O stretch), 1151 and 940 (C-C stretch), 865 (N-H bending), 840 (C-H bending), 675 (Cd-N stretch)

The solid state structure of the Cy_2-en/Cd complex is described in Table 2.11.

Table 2.11: Crystal Data and Structure Refinement for BHEEN/Cd Complex

Temperature	173(2) K	
Crystal system	Orthorhombic	
Space group	*P* b c a	
Unit cell dimensions	a = 11.0918(3) Å	α = 90°
	b = 12.4205(3) Å	β = 90°
	c = 15.9911(4) Å	γ = 90°
Volume	2203.03(10)) $Å^3$	
Z	4	
Density (calculated)	1.999 Mg/m^3	
Absorption coefficient	2.440 mm^{-1}	
Goodness-of-fit on F^2	0.956	
Final R indices [I>2σ(I)]	R_1 = 0.0222, wR_2 = 0.0498	
R indices (all data)	R_1 = 0.0301, wR_2 = 0.0521	

2.6 Synthesis of Nickel Complexes

2.6.1 Synthesis of the Cy_2-en/Ni(II) complex

Bright green nickel(II) chloride hexahydrate (0.2342 g, 0.9853 mmol) was dissolved in 4 mL water. To this was added a solution of potassium hydroxide (0.0948 g, 1.69 mmol) in 1 mL water. The ligand, Cy_2-en (0.5037 g, 1.965 mmol), was dissolved in 20 mL water. The solution containing the two salts was then stirred in an ice bath for 20 minutes. The ligand was then added drop wise and the containers washed to ensure complete transfer of the ligand. This solution was then left to stir at room temperature for 72 hours, filtered and set aside to evaporate slowly. The product formed was a bright blue, amorphous gel that would not solidify. This gel was then reheated in water to boiling and left to reflux for 24 hours. The same gel was regenerated upon filtration and slow evaporation.

The product was found to have a weight of 0.8742 g. The yield could not be calculated as the formula of the product was unknown.

ITMS + c APCI: m/z 116.26 (Cy-en$^+$ + Na^+, net +2 charge), 159.29 (Cy-en$^+$ + 1), 233.33 (Cy-enNa^+), 257.34 (Cy_2-en$^+$ +1), 349.29 ([Ni(Cy_2-en)]Cl^+), 373.25 ([Ni_2(Cy_2-en)$^+$), 451.44 ([Ni_2(Cy_2-en)]Cl_2^+), 497.45 ([Ni_3(Cy_2-en)]Cl_2^+), 569.39 ([Ni(Cy_2-en)]$_2^+$), 663.39 ([Ni(Cy_2-en)]$_2$$Cl^+$)

IR (cm^{-1}): 3164 (N-H stretch), 2931 (O-H stretch), 2858 (alkane C-H stretch), 1449 (C-H bending), 1343 (O-H bending), 1241 (C-O stretch), 1199 and 947 (C-C stretch), 878 (N-H bending), 846 (C-H bending), 643 (Ni-N stretch)

2.6.2 Synthesis of the Cy_2-Otn/Ni(II) complex

Bright green nickel(II) chloride hexahydrate (0.1670 g, 0.7026 mmol) was dissolved in 10 mL water. To this was added a solution of potassium hydroxide (0.0893 g, 1.59 mmol) in 10 mL water. The ligand, Cy_2-Otn (0.1002 g, 0.3499 mmol), was dissolved in 20 mL water. The solution containing the two salts was then stirred in an ice bath for 30 minutes. The ligand was then added drop wise. This solution was then initially left to stir in the ice bath for 90 minutes and the for a further 22 hours at room temperature, filtered and set aside to evaporate slowly. The solution changed colour from an orange brown to a royal blue during the course of the first week. Upon evaporation product formed that was a bright blue, amorphous gel that would not solidify. This gel was then reheated in water to boiling and left to reflux for 24 hours. The same gel was regenerated upon filtration and slow evaporation.

The product was found to have a weight of 0.0951 g. The yield could not be calculated as the formula of the product was unknown.

ITMS + c APCI: m/z 116.28 (Cy-OtnNa$^+$), 189.38 (Cy-Otn$^+$ + 1), 287.37 (Cy_2-Otn$^+$ +1), 343.29 ([Ni(Cy_2-Otn)]$^+$), 403.12 ([Ni_2(Cy_2-Otn)]$^+$), 462.01 ([Ni_3(Cy_2-Otn)]$^+$), 536.12 ([Ni_3(Cy_2-Otn)]Cl_2^+), 685.44 ([Ni(Cy_2-en)]$_2^+$)

IR (cm^{-1}): 3117 (N-H stretch), 2932 (O-H stretch), 2858 (alkane C-H stretch), 1449 (C-H bending), 1341 (O-H bending), 1206 (C-O stretch), 1162 and 921 (C-C stretch), 844 (C-H bending), 618 (Ni-N stretch)

2.6.3 Synthesis of the BHEEN/Ni(II) complex

Bright green nickel(II) chloride hexahydrate (0.8138 g, 3.424 mmol) was dissolved in 10 mL water. To this was added a solution of potassium hydroxide (0.1847 g, 3.292 mmol) in 5 mL water. The ligand, BHEEN (1.0006 g, 6.7512 mmol), was dissolved in 10 mL water. The solution containing the two salts was then stirred in an ice bath for 20 minutes. The ligand was

then added drop wise and led to an immediate colour change to a bright purple. This solution was then initially left to stir in the ice bath for 2 hours, filtered and set aside to evaporate slowly. The solution changed colour from the aforementioned purple to a dark blue during the course of the stirring. Upon evaporation product formed that was a blue, amorphous gel that would not solidify. This gel was then reheated in water to boiling and left to reflux for 24 hours. The same gel was regenerated upon filtration and slow evaporation.

The product was found to have a weight of 1.0175 g. The yield could not be calculated as the formula of the product was unknown.

ITMS + c APCI: m/z 149.28 ($BHEEN^+$ + 1), 205.23 ($[Ni(BHEEN)]^+$), 241.24 ($[Ni(BHEEN)]Cl^+$), 287.42 ($[Ni(BHEEN)_3]Cl_2^{2+}$), 345.22 ($[Na(BHEEN)]_2^+$), 353.37 ($[Ni(BHEEN)_2]^+$), 389.25 ($[Ni(BHEEN)_2]Cl^+$), 409.32 ($[Ni(BHEEN)]_2]^+$), 447.27 ($[Ni(BHEEN)]_2Cl^+$), 483.16 ($[Ni(BHEEN)]_2]Cl_2^+$), 505.04 ($[Ni(BHEEN)_3]^+$), 541.12 ($[Ni(BHEEN)]_3Cl^+$), 651.20 ($[Ni(BHEEN)]_4]^+$), 679.09 ($[Ni_4(BHEEN)_3]^+$)

IR (cm^{-1}): 3210 (N-H stretch), 2937 (O-H stretch), 2881 (alkane C-H stretch), 1458 (C-H bending), 1339 (O-H bending), 1249 (C-O stretch), 1157 and 974 (C-C stretch), 855 (C-H bending), 558 (Ni-N stretch)

2.7 Synthesis of Zinc Complexes

2.7.1 Synthesis of the Cy_2-en/Zn(II) complex

Zinc chloride, $ZnCl_2$, (0.7606 g, 5.581 mmol) was added to a solution of 0.2684 g (1.047 mmol) Cy_2-en in 10 mL methanol. This solution was left to stir at room temperature for 21 hours. The solution was filtered and left to evaporate slowly. A powder crashed out that was redissolved in 25 mL water and 50 mL methanol. The resultant solid was too amorphous for XRD purposes. It was redissolved in 100 mL water and refluxed at 100 ˚C for 24 hours. The

solution was filtered and left to evaporate slowly. Again, the crystals formed were not of suitable quality for XRD analyses to be performed.

The product was found to weigh 0.1683 g.

ITMS + c ESI: m/z 257.32 (Cy_2-en^+ + 1), 319.25 to 323.27 ([$Zn(Cy_2$-en)]$^+$), 355.25 ([$Zn(Cy_2$-en)]Cl^+), 379.21 to 384.28 ([$Zn(Cy_2$-en)]NO_3^+), 639.45 ([$Zn(Cy_2$-$en)_2$]NO_3^+), 677.37 ([$Zn(Cy_2$-$en)_2$](NO_3)Cl^+)

IR (cm^{-1}): 3436 (O-H stretch), 2938 (N-H stretch), 2863 (alkane C-H stretch), 1461 (C-H bending), 1360 (O-H bending), 1203 (C-O stretch), 1144 and 938 (C-C stretch), 880 (N-H bending), 834 (C-H bending), 780 (Zn-N stretch), 570 (Zn-N bending)

2.7.2 Synthesis of the Cy_2-Otn/Zn(II) complex

Zinc chloride, $ZnCl_2$, (0.0494 g, 0.362 mmol) was added to a solution of 0.2051 g (0.7161 mmol) Cy_2-Otn in 20 mL water. This solution was left to stir at room temperature for 21 hours. The solution was filtered and left to evaporate slowly. A powder crashed out that was redissolved in 25 ml water. The resultant solid was too amorphous for XRD purposes. It was redissolved in 50 ml water and refluxed at 100 ˚C for 24 hours. The solution was filtered and left to evaporate slowly. Again, the crystals formed were not of suitable quality for XRD analyses to be performed.

The product was found to weigh 0.0964 g.

ITMS + c APCI: m/z 287.30 (Cy_2-Otn^+ + 1), 409.12 ([$Zn_2(Cy_2$-Otn)]$^+$), 513.28 ([$Zn_2(Cy_2$-Otn)]Cl_3^+), 741.06 ([$Zn(Cy_2$-$en)_2$](NO_3)Cl^+)

IR (cm^{-1}): 3197 (O-H stretch), 2929 (N-H stretch), 2857 (alkane C-H stretch), 1449 (C-H bending), 1356 (O-H bending), 1199 (C-O stretch), 1047 and 923 (C-C stretch), 892 (N-H bending), 846 (C-H bending), 787 (Zn-N stretch), 571 (Zn-N bending)

2.7.3 Synthesis of the BHEEN/Zn(II) complex

Zinc chloride, $ZnCl_2$, (0.2306 g, 1.692 mmol) was added to a solution of 0.5094 g (3.437 mmol) BHEEN in 20 mL water. This solution was left to stir at room temperature for 21 hours. The solution was filtered and left to evaporate slowly. A powder crashed out that was redissolved in 25 ml water and refluxed at 100 ˚C for 24 hours. The solution was filtered and left to evaporate slowly. The crystals formed were of suitable quality for XRD analyses to be performed.

The product was found to weigh 0.3680 g.

ITMS + c APCI: m/z 149.23 (BHEEN $^+$ + 1), 367.56 ($[Zn(BHEEN)_2]^+$), 395.22 ($[Zn(BHEEN)_2]Cl^+$), 439.65 ($[Zn(BHEEN)_2]Cl_2^+$), 461.28 ($[Zn(BHEEN)_2]Cl_3^+$)

IR (cm^{-1}): 3250 (O-H stretch), 3163 (N-H stretch), 2874 (alkane C-H stretch), 1447 (C-H bending), 1329 (O-H bending), 1194 (C-O stretch), 1054 and 937 (C-C stretch), 887 (N-H bending), 822 (C-H bending), 789 (Zn-N stretch), 576 (Zn-N bending)

The solid state structure of the BHEEN/Zn(II) complex is described in Table 2.12. The full data can be found in Appendix E in tables E.22 to E.28.

Table 2.12: Crystal Data and Structure Refinement for BHEEN/Zn Complex

Temperature	173(2) K	
Crystal system	Monoclinic	
Space group	*P* 2_1/c	
Unit cell dimensions	a = 15.3169(2) Å	a = 90°.
	b = 8.98000(10) Å	b = 105.2260(10)°.
	c = 14.3231(2) Å	g = 90°.
Volume	1900.93(4) $Å^3$	
Z	4	
Density (calculated)	1.512 Mg/m^3	
Absorption coefficient	1.596 mm^{-1}	
Goodness-of-fit on F^2	1.042	
Final R indices [I>2σ(I)]	R_1 = 0.0211, wR_2 = 0.0546	
R indices (all data)	R_1 = 0.0247, wR_2 = 0.0556	

2.8 References

(1) Bruker; 2.0-1. ed.; Bruker AXS Inc.: Madison, Wisconsin, USA, 2005.

(2) Bruker; 6.0. (includes XPREP and SADABS) ed.; Bruker AXS Inc.: Madison, Wisconsin, USA, 2005.

(3) Bruker; 5.1 (includes XS, XL, XP, XSHELL) ed.; Bruker AXS Inc.: Madison, Wisconsin, USA, 1999.

(4) Spek, A. L. *J. Appl. Cryst.* **2003**, *36*, 7-13.

(5) Farrugia, L. J. *J. Appl. Cryst.* **1997**, *30*, 565.

Chapter 3

Molecular Mechanics

Over the last thirty years there has been a marked increase in the amount of work done on molecular mechanics or MM. This can be attributed to the increase in computing power as well as its affordability. It has been found that MM is a useful method for the structure analysis of inorganic molecules as the sheer number of papers published in this area suggests. There have been studies done on metalloproteins,[1] cobalt corrinoids,[2,3] metalloporphyrins,[3] and lead complexes[4] to name but a few.

In this project attempts were made to use molecular mechanics to reproduce the XRD structure of three of the species. All structures where the average bond lengths had a difference of less than 0.01 Å and a difference of less than 3.0˚ for the average bond angles were assumed to be good reproductions of the original XRD structure.

All data pertaining to the MM work done are given in Appendix A.

3.1 Modelling of the Free Ligands

3.1.1 MM Calculations on Cy_2-en

The coordinates obtained from the crystal structure of the free ligand, Cy_2-en, were copied into the AMBER module of HyperChem.[5] Before starting MM calculations, the atoms in the molecule had to be assigned charges. The first method that was used was the semi-empirical method PM3, a method useful for organic molecules. Once all of these parameters had been set, a single point calculation was performed. In order to compare the free ligand to the complex, it was decided to also perform the above semi-empirical calculation using ZINDO/1 as a method rather than PM3. ZINDO/1 is useful for compounds containing metals. The same parameters as for the PM3 calculation were kept. Some of the charges are tabulated in Table 3.1.

Table 3.1: Charges on Cy_2-en Calculated by Semi-empirical Methods Using PM3 and ZINDO/1

Atom	PM3 charge	ZINDO/1 charge
Secondary amine nitrogen, NH	-0.319	-0.746
Secondary amine nitrogen, NH	-0.319	-0.746
Alcohol group, OH	-0.407	-0.796
Alcohol group, OH	-0.407	-0.796
Carbon on ethylene bridge bonded to amine, CH_2	0.007	-0.133
Carbon on ethylene bridge bonded to amine, CH_2	0.006	-0.133
Carbon on ring bonded to amine, CH	0.077	0.002
Carbon on ring bonded to amine, CH	0.076	0.002
Carbon on ring bonded to alcohol, CH	0.151	0.185
Carbon on ring bonded to alcohol, CH	0.151	0.185

Upon inspection of the data, it was decided that the charges calculated by ZINDO/1 were the better choice because intuitively the charges reflected the distribution of partial charges within the molecule more closely and, in particular, the charges on the nitrogen and oxygen atoms.

Using the molecule with the charges as calculated by ZINDO/1, the effectiveness of setting the dielectric constant, *K*, for the MM calculations to that of water was investigated. The value was altered to 2, 5, 10, and 50 to ascertain if any changes in bond lengths and angles occurred. Once the desired dielectric constant had been set, the molecule was submitted for a MM geometry optimisation. The bond lengths and angles of each molecule were then measured and the average calculated. This average was then compared to the equivalent average of the XRD structure. No notable differences were observed. The averages are given in Table 3.2. The dielectric constant was added to simulate the presence of solvent molecules around the molecule being studied. This was done to simulate the effect of having a condensed phase acting on the electrostatic interactions of the molecule being studied.

Table 3.2: Average Bond Lengths and Angles of Cy_2-en Calculated Using Different Dielectric Constants

Bond Length (Å) or Angle (˚)	$K = 76$	$K = 50$	$K = 10$	$K = 5$	$K = 2$
C—C	1.545	1.545	1.545	1.545	1.545
C—N	1.480	1.480	1.480	1.480	1.479
C—O	1.432	1.432	1.432	1.432	1.431
C—C—C	111.2	111.2	111.2	111.2	111.1
C—C—N	110.2	110.2	110.1	110.1	110.1
C—C—O	109.3	109.3	109.3	109.3	109.3
C—N—C	114.5	114.5	114.5	114.5	114.5

As the tabulated data clearly indicates, there was no significant difference in the bond lengths and angles with the use of the different dielectric constants. Hence, a dielectric constant of $K = 76$ was chosen for all calculations in all ligands and complexes from then on.

The next step in the attempt to reproduce the XRD structure was to use molecular dynamics to find the different energy minima of Cy_2-en, and to find if one of them indeed corresponded to the XRD structure. The method used was simulated annealing. A detailed account of the procedure is given in Appendix A. The resulting structures were saved and MM calculations performed to find the total energy of the molecule. These values were then compared to the energy of the XRD structure. These values are given in Table 3.3. It became clear that the structure had many local minima and many of them were in the energy region of the XRD structure. Some of the structures were also at significantly higher energy values than the XRD structure, by as much as 10 kcal mol^{-1}.

The simulated annealing structures were also compared to the XRD structures with respect to their bond lengths and angles. All of the average bond lengths differed by less than 0.01 Å when compared to the XRD structure. The bond angles were also all less than 3.0˚. This indicated that the various structures that had been predicted by HyperChem were good approximations of the initial XRD structure.

Table 3.3: Energies of Cy_2-en after Simulated Annealing Runs with Various Run Times Compared to the Energy of the XRD Structure

Run Time	Energy [kcal mol^{-1}]
XRD structure	16.745
5 ps	18.583
10 ps	18.560
15 ps	19.605
20 ps	26.816
25 ps	18.011
30 ps	22.309
35 ps	18.552
40 ps	16.954
45 ps	18.492
50 ps	22.579
55 ps	18.560
60 ps	17.920
65 ps	16.779
70 ps	18.436
75 ps	17.078
80 ps	23.868
85 ps	16.727
90 ps	17.853
95 ps	25.510
100 ps	17.357

The various structures that were obtained during the simulated annealing runs were then superimposed onto the XRD structure to verify that the modelling software had indeed managed to predict the actual structure. The best approximation is given in Figure 3.1. The best approximation is defined as the structure that has the best overlay with the original structure. This is not necessarily the lowest energy structure.

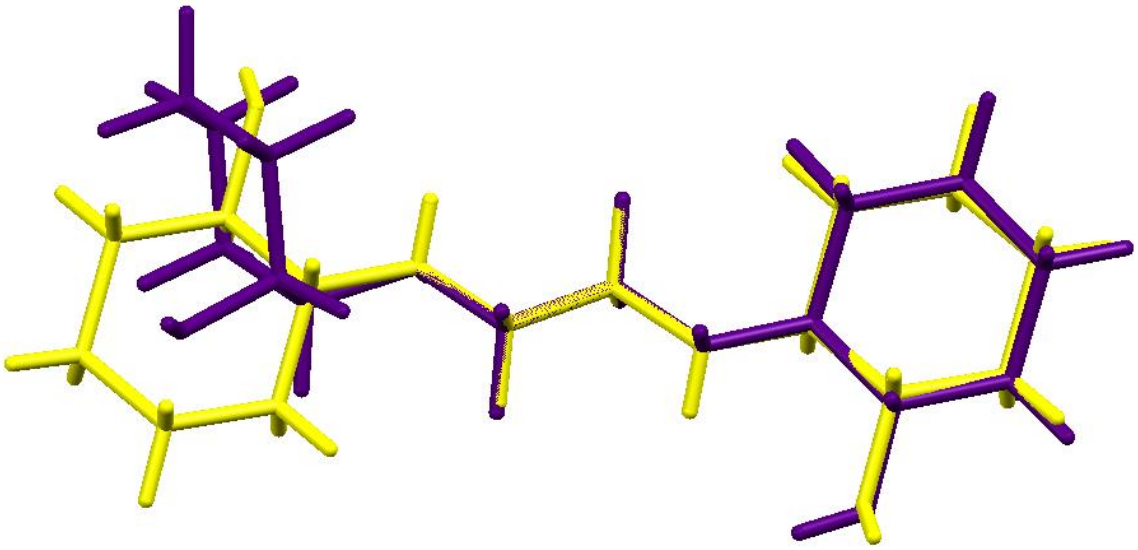


Figure 3.1: Superimposed images of the XRD structure (Yellow) of Cy_2-en and the lowest energy structure predicted by MM methods (Purple)

The figure clearly indicated that all but one of the rings could be superimposed upon the XRD structure. The ring was rotated through 180˚ with both alcoholic oxygen groups on the same side. The XRD structure assumed a geometry that optimised the number of hydrogen-hydrogen, or H-H, bonds. These nonbonded interactions were not considered by the MM program used and so the stabilising effect of these interactions could not be factored into the geometry of the molecule.

3.1.2 MM Calculations on Cy_2-Otn

The crystal structure of the free ligand, Cy_2-Otn, was copied into the molecular mechanics program HyperChem. The same parameters as for Cy_2-en were selected and the atom types assigned. To confirm that the ZINDO/1 method was also superior to the PM3 method for this ligand, the same single point calculations were performed as previously described. The resultant charges are given in Table A.1.

As before, the ZINDO/1 method intuitively gave the better approximation of the partial charges on the atoms. It was used in the further calculations.

Simulated annealing runs were then performed using the same heating and cooling times, as well as the same run times as for Cy_2-en. The energies calculated after these runs were compared to the value of the XRD structure. The resultant values are tabulated in Table A.2.

The simulated annealing structures were also compared to the XRD structures with respect to their bond lengths and angles. All of the average bond lengths differed by less than 0.01 Å when compared to the XRD structure. The bond angles were also all less than 3.0˚. This indicated that the various structures that had been predicted by HyperChem were good approximations of the initial XRD structure.

The various structures obtained were then overlaid with the XRD structure to determine if the fit was indeed ideal. The best overlay is given in Figure 3.2.

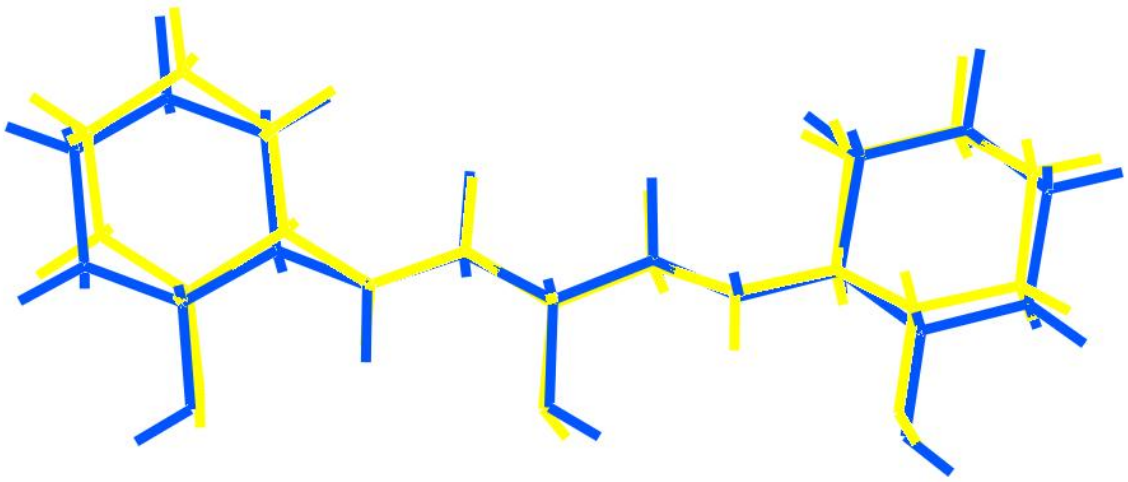


Figure 3.2: Superimposed images of the XRD structure (Yellow) of Cy_2-Otn and the lowest energy structure predicted by MM methods (Blue)

The two images were indeed a very good fit. The degree of superimposability was far greater than that of the ligand Cy_2-en, as indicated in Figure 3.1. The resultant conclusion was that MM with the Generalised AMBER force field (GAFF) could indeed predict the structure of this amino alcohol. The XRD structure indicated that there were many H-H bonds in the molecule (Figure 4.19) as well as close contacts between the alcoholic oxygens and adjacent amine hydrogens (Figure 4.20). All of these stabilising interactions were optimised by a planar arrangement of the molecule. This pattern was not reflected by the MM calculations as none of the above interactions were considered.

3.1.3 MM Calculations on BHEEN

The crystal structure of the protonated BHEEN nitrate salt was copied into the molecular mechanics program HyperChem. The same parameters as for Cy_2-en were selected, with the exception of the total charge of the system which was set to +1, and the atom types assigned. To confirm that the ZINDO/1 method was also superior to the PM3 method for this ligand, the same single point calculations were performed as previously described. The resultant charges are given in Table A.3.

As in both prior cases, the ZINDO/1 method gave the better approximation of the partial charges on the atoms. It was used in the remaining calculations for BHEEN.

Simulated annealing runs were then performed using the same heating and cooling times, as well as the same run times as for Cy_2-en and Cy_2-Otn. The energies calculated after these runs were then compared to the value of the XRD structure. The resultant values are tabulated in Table A.4.

Again, the simulated annealing structures were also compared to the XRD structures with respect to their bond lengths and angles. Each of the average bond lengths differed by less than 0.01 Å when compared to the XRD structure. The bond angles were also all less than 3.0˚. This indicated that the various structures that had been predicted by HyperChem were good approximations of the initial XRD structure, Figure 3.3. Again, the presence of close contacts within the molecule most likely caused the deviations observed.

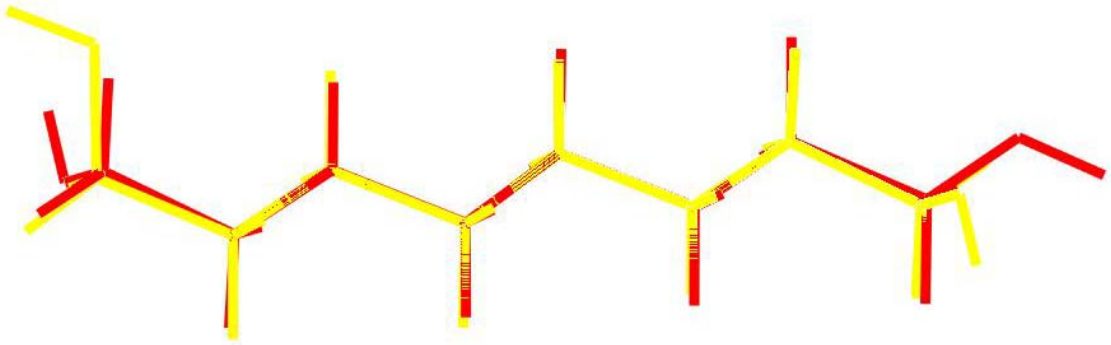


Figure 3.3: Superimposed images of the XRD structure (Yellow) of BHEEN and the lowest energy structure predicted by MM methods (Red)

The MM calculations on the three ligands clearly indicated that GAFF was a good MM force field to use for the amino alcohols of the type studied. The force field did not have to be modified in any way to fulfil the criteria for a good prediction as outlined at the beginning of the chapter. This is also a good sign as it implies that the same force field can be used further for the prediction of a cadmium complex of Cy_2-en.

It must be noted though that the calculations are all performed using gas phase calculations and the consequence is that there is a good chance that some of the soft parameters, such as the torsions, are not reproduced. This can be seen in Figure 3.1 for Cy_2-en. The discrepancy between the predicted and the observed structures can be explained when looking at the crystal packing of the species. In the XRD structure, the two alcoholic oxygen groups are pointed away from one another because this enables them to form hydrogen bonds to neighbouring molecules. If both of the alcohols had been on the same side of the ethylene bridge, then there would have been only one available site for hydrogen bonding in place of the two that are observed if the one cyclohexenyl ring is rotated through 180˚. Furthermore, the presence of H-H bonds as well as close contacts between the alcoholic oxygen atoms and the amine hydrogens add stability to the molecule. These interactions are not taken into account in the MM force field.

3.2 Modelling of the Cadmium Complex of Cy_2-en

As no parameters for the calculation of cadmium complexes existed, it was decided to begin the MM work by assuming a "points on a sphere model". It is derived from VSEPR theory in that it strives to give the optimal bond angles and torsions by assigning no energetic penalty to them, i.e. these angles are allowed to do as they wish.[6] The coordination sphere of a metal ion is then controlled by the non-bonded 1,3-interactions between ligands. In such a case there are certain geometries that lead to a minimum amount of steric repulsion: a linear arrangement for two domains, an equilateral triangular arrangement for three domains, a tetrahedral arrangement for four domains, a trigonal bipyramidal arrangement for five domains, and an octahedral arrangement for six domains.[6]

The lowest energy structure of the ligand Cy_2-en was chosen and the metal cadmium(II) added. The ligand was manipulated so that it resembled the actual crystal structure that had been determined. Two chloride ions were bonded to the cadmium ion as well. The charges on the complex were calculated using ZINDO/1 only as PM3 was designed for organic molecules only.

The atom types were then assigned to the atoms in the molecule. The GAFF force field did not contain any parameters for cadmium and so they had to be defined manually and added to the force field prior to the assignment of atom types. The five parameters that had to be set were the atom type for cadmium in the +2 oxidation state, the bond length parameters, the bond angle parameters, the nonbonded interaction parameters, and the torsion parameters.

To do this, the runfiles of GAFF had to be modified. This file had already been modified to contain other metal atoms and saved as WitsGAFF. The six files that were edited were WitsGAFFtyp.txt for the atom type, WitsGAFFben.txt for the bond angles, WitsGAFFimp.txt for the improper torsion angles, WitsGAFFndb.txt for the nonbonded interactions, WitsGAFFstr.txt for the bond angles, and WitsGAFFtor.txt for the torsions. All data and files henceforth referred to are found in Appendix A.

The first file that was edited was WitsGAFFtyp.txt. The cadmium atom had to be added as an atom type. The file contained, in its first row, the definition of each column.

The first column described the atom type. In the case of the cadmium(II) ion, the type cd2 was chosen to indicate the fact that it was cadmium in the +2 oxidation state. The following column described the atomic mass of each atom type specified. The atomic mass of cadmium was set at 112.41. The reference was set as the initials of the person editing the program and the particular date. The resultant file was saved.

The next items added were the bond lengths. These were obtained by searching the Cambridge Structural Database, CSD, and manipulating the resultant structures in the statistical software VISTA[7], given in Table 3.4. All of the histograms generated by the software are in Appendix A.

Table 3.4: Average Bond Lengths Found in the CSD and Sorted by VISTA

Bond length	Type of bond length specified	Mean (Å)	Standard deviation, σ, (Å)	Value used (Å)	Figure in Appendix
Cd(II)—O	Cd(II)—O(H)(C)	2.447	± 0.130	discarded	A.1
	Cd(II)—O(C)	2.440	± 0.115	2.440	A.2
Cd(II)—N	Cd(II)—N(H)(C)(C)	2.390	± 0.063	2.390	A.3
Cd(II)—Cl	Cd(II)—Cl	2.605	± 0.058	2.605	A.4

The final bond length, the Cd(II)—Cl bond length, posed some problems. The search criterion was set to Cd(II)—Cl and the CSD found 11 matches. There was no clear average from the histogram that was generated by VISTA as there was no statistically significant normal distribution but rather a scattering of values. The average bond length calculated by the software was 2.605 Å. This was the value taken as a starting point.

Once these values had been determined, the WitsGAFFstr.txt file was opened and edited. The values for the stretching constants had to be determined as well. Initially the MM2 for field developed by Allinger was consulted to ascertain if any cadmium parameters had been specified in that force field but that was not the case. The values of other similar metal bonds were then looked at in the WitsGAFF force field. It was noted

that the stretching constant for the Cu(II)—N as well as Ni(II)—N bonds was set to 300.0 kcal mol^{-1} $Å^{-2}$. This value was then adopted for the Cd(II)—N bond length as well. The Cu(II)—O bond and Ni(II)—O bond stretching constants were found to have a value of 150.0 kcal mol^{-1} $Å^{-2}$ and that value was then used for the stretching constant for the Cd(II)—O bond length. There were no additional data available for metal-chloride bonds, and a value of 150.0 kcal mol^{-1} $Å^{-2}$ was chosen as a starting point for that stretching constant. All values for Cu(II) come from as yet unpublished work on Cu(II) complexes with amine ligands.

The WitsGAFFstr.txt file was set up so that the first two columns indicated the two atom types between which there was a bond, the third column gave the stretching constant, and the fourth column gave the equilibrium bond length of that bond. The final column gave the reference.

The next step was to find the bond angles that had to be defined. The same method as for the bond lengths was employed. All bond angles with cadmium as the central atom were searched for in the CSD.

The first bond angle that was investigated was the (R)(R)(H)N—Cd—N(H)(R)(R) bond angle. The CSD gave 68 hits with an average of 108˚ ± 33˚. The same bond angle was then searched for in the CSD without the hydrogen atoms present. The resulting 98 matches gave an average angle of 103˚ ± 32˚. It was then decided to search the CSD for the specific case of a N—Cd(II)—N bond where the two nitrogen atoms were connected via an ethylene bridge. This was the most accurate description of the complex and the result was an average bond angle of 74˚ ± 3˚. This search was more reflective of the actual complex and so the average bond angle for N—Cd(II)—N was chosen to be 74.0˚.

The following bond angle to investigate was the (R)(H)N—Cd—O(H)(R) angle. The initial search of the CSD yielded few useable results. The two R groups were then modified to be bonded so as to form a five-membered chelate ring, the search yielded 17 hits. The average bond angle calculated by VISTA from this data was 70˚ ± 2˚. The initial value of the N—Cd(II)—O bond angle was then selected to be 70.0˚.

The Cl—Cd(II)—Cl bond angle gave eight matches in the CSD. The average of those bonds was 113˚ ± 38˚. The histogram was very unclear as there was a gathering of bonds in the region of 80˚ to 100˚ and then again from 165˚ to 180˚. This clearly implied

that the average calculated by VISTA was not useful and it was decided to use 90.0˚ as a starting value for the Cl—Cd(II)—Cl bond angle.

The Cl—Cd(II)—O(H)(R) angle was then checked in the CSD. The single match gave a clustering of values between 80˚ and 90˚ as well as one additional value around 175˚. Again, due to the general lack of a clear preference value, a general starting value of 90.0˚ was selected.

The final bond angle with a central cadmium atom that had to be determined was the Cl—Cd(II)—N(H)(R) angle. The CSD gave yet another unclear histogram. There was clustering of values at certain values of between 104˚ and 105˚ as well as at 106˚. The lack of a clear average resulted in the choice of a starting value of 90.0˚ for that angle.

The final step for those angles was to add the bending constants for the bonds. There was no clear data to use as an equivalent and so it was decided to begin with bending constant values of 0.00 kcal mol^{-1} deg^{-2} for all of the five abovementioned angles.

The last four bond angles were derived from modified GAFF parameters. The first of these was the Cd(II)—N—C bond angle. This bond angle was chosen to have exactly the same parameters as the c3—n3—c3 bond angle. The Cd(II)—O—C bond angle settings were taken from the GAFF c3—os—c3 bond angle. The Cd(II)—N—H bond angle was given the same values as the c3—n3—hn bond angle. The Cd(II)—O—H bond angle derived its data from the c3—oh—ho data. It must be noted that these values are gross a approximations and intended only as starting values to aid in getting an idea of the modelling.

The WitsGAFFben.txt file was set up so that the first three columns indicated the three atom types between which there was a bond angle, the fourth column gave the bending constant, and the fifth column gave the equilibrium bond angle. The final column gave the reference.

The next parameter file that was edited was WitsGAFFnbd.txt. The data for the cadmium(II) ion was derived by plotting the nonbonded parameters for all metals found in the MM2 force field. The force field contained the following entries. Table 3.5.

Table 3.5: Nonbonded Parameters for All Metals Found in the MM2 Force Field

TYPE	RSTAR	EPS	REMARKS
ge	2.4000	0.2000	"Allinger, MM2 (1991)"
sn	2.5500	0.2700	"Allinger, MM2 (1991)"
pb	2.7000	0.3400	"Allinger, MM2 (1991)"
se	2.2500	0.2760	"Allinger, MM2 (1991)"
te	2.4000	0.3680	"Allinger, MM2 (1991)"
mg	2.2000	0.0150	"Allinger, MM2 (1991)"
fe2	2.2000	0.0200	"Allinger, MM2 (1991)"
fe3	2.2000	0.0200	"Allinger, MM2 (1991)"
ni2	2.2000	0.0200	"Allinger, MM2 (1991)"
ni3	2.2000	0.0200	"Allinger, MM2 (1991)"
co2	2.2000	0.0200	"Allinger, MM2 (1991)"
co3	2.2000	0.0200	"Allinger, MM2 (1991)"

The various third ionisation energies of the metals were then looked up in the *Handbook of Chemistry & Physics*.[8] The resultant values are given in Table 3.6.

Table 3.6: Third Ionisation Energies of Selected Metals Found in the MM2 Force Field

Element	Third Ionisation Energies [eV]
Germanium (ge)	34.21
Tin (sn)	30.49
Lead (pb)	32.92
Selenium (se)	32
Tellurium (te)	31
Magnesium (mg)	80
Iron(II) (fe2)	30.6
Iron(III) (fe3)	56.8
Nickel(II) (ni2)	35.16
Copper(II) (co2)	33.49
Copper(III) (co3)	83.1
Cadmium(II)	37.47

The radii values were then plotted against the value of epsilon, listed as EPS in Table 3.4, the value of the well depth for each atom. The well depth is defined as the value of the local minimum in the potential energy. The resulting plot was then edited to contain a straight line graph. From this graph, the value of r* was calculated for cadmium(II). The graph containing all metals was given in Figure 3.4.

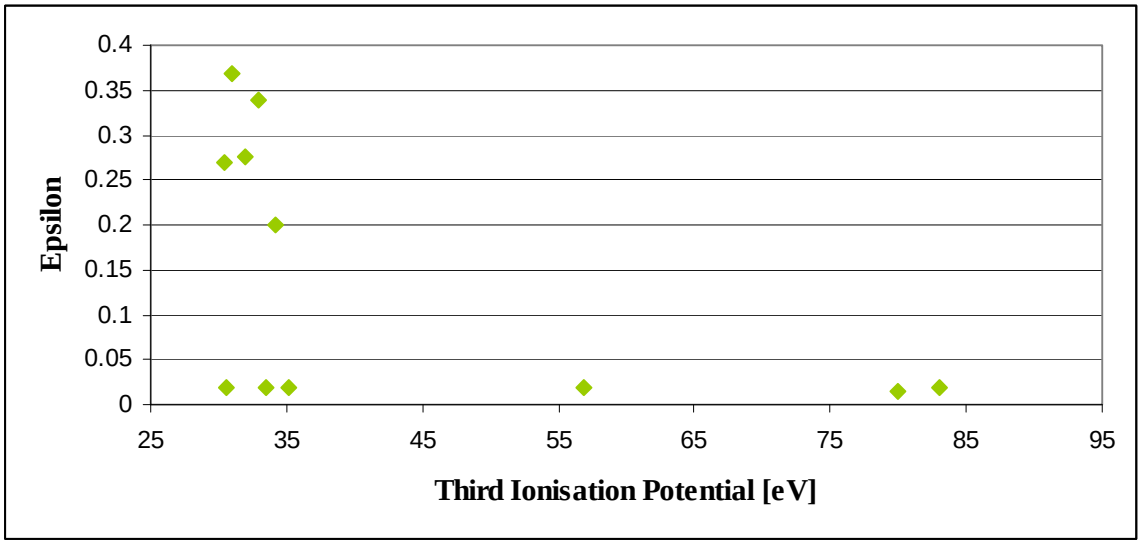


Figure 3.4: Plot of epsilon versus the third ionisation energy for all metals listed in the MM2 force field

The graph clearly indicated that there were outliers. It was then decided to remove all of the points that had been assigned the epsilon value of 0.0200. This was done as the value 0.0200 was the generic value assigned to the atoms in the force field. This value was in no way refined, and so could be easily ignored. The new graph, Figure 3.5, gave a much better estimate of the value of epsilon for cadmium(II).

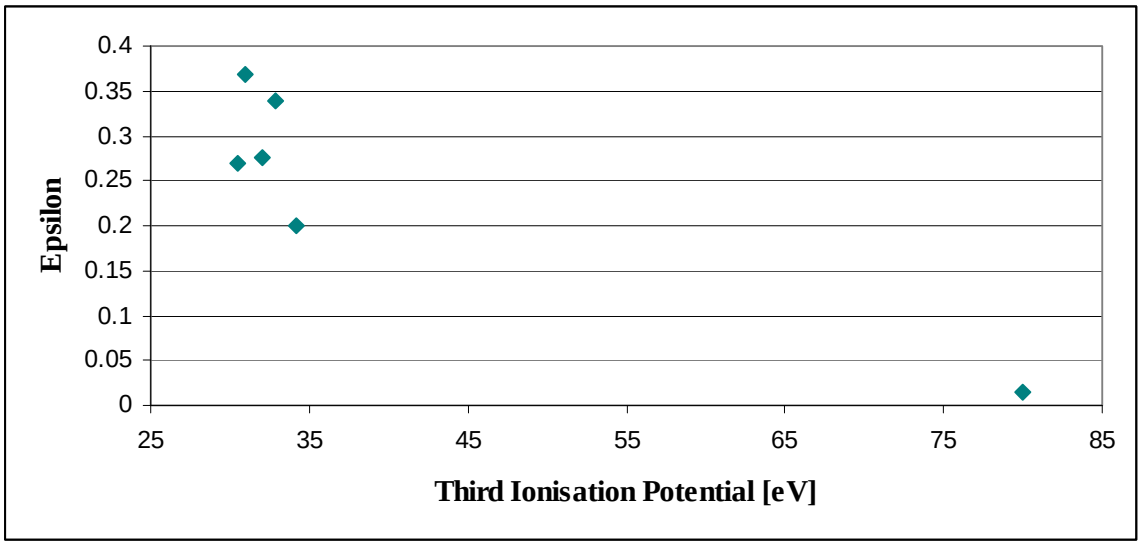


Figure 3.5: Plot of epsilon versus the third ionisation energy for all metals listed in the MM2 force field not having an epsilon value of 0.0200

It then also became clear that the value for magnesium was an outlier. The value of epsilon calculated was 0.26. This value was also removed to give the final graph, Figure 3.6, from which the value of epsilon for cadmium(II) was calculated. The calculated value of epsilon for cadmium(II) was found to be 0.17.

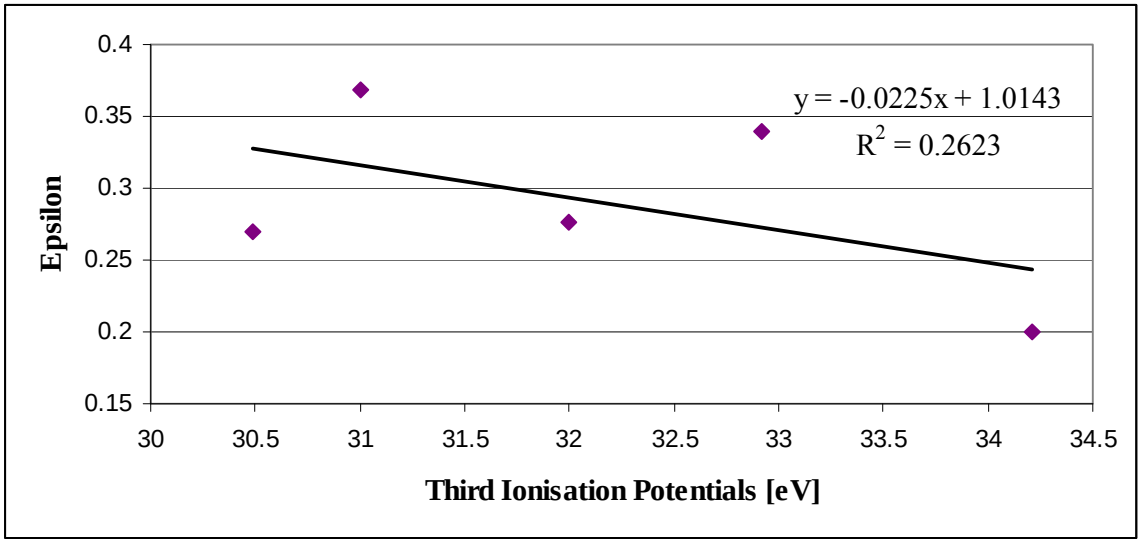


Figure 3.6: Plot of epsilon versus the third ionisation energy for selected metals listed in the MM2 force field

It was decided to use the value of 0.26 for epsilon as the value for magnesium was not in reality an outlier. The ionisation energy of that metal was only that high because the third ionisation potential required removing an electron from an inner shell. The file was edited so that the atom type in column one was specified by the ionic radius in column two and the value of epsilon in column three.

The next file to edit was the WitsGAFFtor.txt file. This file defined the various torsion angles for each interaction. Due to the fact that there were no data to fall back on to use as a starting point it was decided to add the following to the runfile. The first four columns describe the order of the atoms between which the torsion angle is to be calculated. If one sets ** as the atom type, the implication was that it could be any atom type at all. The next number indicated the number of terms, 1 here. The next column gave the value of $0.5V_n$, set to 0.00. This value set the barrier height to rotation. The next two columns gave the value of θ, 180.0˚, and the period, 1. This was the most general possible starting point for the modelling.

The final editing had to be done on the WitsGAFFimp.txt file, the file that specified the improper torsions. These torsions are defined as torsion angles where three of the four atoms are bonded to the one central atom. In this study, cadmium was selected as the central atom. As with the torsion file, the most general case was selected. Only the cadmium atom type was specified and $0.5V_n$ set to 0.00. The value of θ was set to 180.0˚ and the period set to 2.00.

HyperChem was reopened and the atom types assigned. It must be noted that the Parameter set had to be reselected and recompiled. This ensured that the new parameters were indeed being used. The nest step was to run several simulated annealing processes to ascertain if the chosen parameters were useful. The same conditions and run times as for the ligands was selected. The resulting energies are given in Table A.11.

The average bond lengths and angles were then calculated. The data indicated that certain parameters had been good choices but others still had to be improved upon. The average C—C, C—N, and C—O bond lengths were acceptable. The N—Cd bond length was, on average, 0.042 Å too long. The average bond lengths in the XRD structure had an uncertainty factor of ± 0.002 Å and this did not cover the observed deviation. The same pattern was observed for the O—Cd and Cd—Cl bond lengths.

They were, on average, 0.060 Å and 0.115 Å too long, respectively. As was noted when the parameters were set, the choice of values for the stretching constants had been somewhat arbitrary. It was clear from the fact that the bonds were too long that the values assigned to the stretching constants were too small. It was thus decided to alter the values of the stretching constants from 300.0 to 320.0 kcal mol^{-1} $Å^{-2}$ for the cd2—n3 atom type bond from 150.0 to 175.0 kcal mol^{-1} $Å^{-2}$ for the cd2—oh atom type bond, and from 150.0 to 200.0 kcal mol^{-1} $Å^{-2}$ for the cd2—cl atom type bond. It must be noted that the initial value for the Cd—Cl bond had been a guess and as such it was not surprising to see that that bond had the greatest deviation from the actual structure.

The C—C—C, C—C—N, C—C—O, C—N—C, and C—O—Cd bond angles were within the acceptable range. The C—N—Cd bond angle was 3.8˚ smaller than the average of the XRD structure. This was also acceptable three of the four bond angles in the XRD structure matched the range given by the MM calculations but one of the XRD-determined bond angles was much larger, thus eschewing the average bond angle values. The values were thus in an acceptable range. The O—Cd—N, N—Cd—Cl, and O—Cd—Cl bond angles were not uniformly distributed at all. There was no region where there was a concentration of values. The deviations ranged from 3.9˚ to 84.4˚. The parameters for these bond angles all had a bending constant of 0.00 kcal mol^{-1} deg^{-2}. Obviously this was not the best choice. Initially, these values were not changed.

A second simulated annealing process was then started by using the five lowest energy states from the first annealing run. Each of these five structures was submitted to three annealing processes. The run started at 0 K and heated to 800 K over 10 ps, and then the sample was left at a run time of 5, 10, or 100 ps. The structure was then cooled to 0 K over 20 ps. The resulting energies were then calculated, Table A.12.

The average bond lengths and angles were then calculated. The data indicated that the changes made to the bond length parameters had made a negligible change to the bond lengths. This clearly indicated that the choice of the points on a sphere model did not work for the cadmium complexes. If the initial structure of the complex was not known, there was no chance whatsoever, using the given parameters, to accurately predict the structure of that complex. The only manner in which to attain a feasible prediction might be to perform density functional theory (DFT) calculations. These are quantum

mechanical calculations and not MM calculations. Some work in this area has already been done. A very early study of amino- and pyridyl-containing cadmium(II) complexes were modelled using by Mel'nikov and Pletnev using a force field based on the Gillespie-Kepert model.[9] Meloxicam, an anti-inflammatory drug, has also been investigated using DFT calculations to predict the IR and Raman spectra and compare them to the actual spectra.[10] A further DFT study was done on dimetallocenes of the type MM'$(C_5H_5)_2$ where M could be cadmium.[11] Cadmium-metallothionein was also studied using DFT calculations.[12] All of the papers mentioned above focused on cadmium complexes and show that DFT calculations are indeed a plausible and viable means to better study the cadmium complexes of amino alcohols.

It was then decided to use the XRD structure as a starting point for the MM calculations and to define further atom types. The XRD structure was analysed and shown to have, essentially, a square pyramidal structure with the two coordinated nitrogen atoms, one chloride ion, and the coordinated oxygen atom defining the plane. The cadmium atom sits above the plane defined by these four atoms. The final chloride ion was in an axial position.

The two chloride ions bonded to the cadmium atom were redefined as clx and cly, the one axial and the other equatorial, respectively. The two coordinated nitrogen atoms were also relabelled as n3x and n3y, with n3x being the nitrogen atom in a *cis* arrangement to the coordinated oxygen atom and a *trans* arrangement to the equatorial chlorine atom, Figure 3.7.

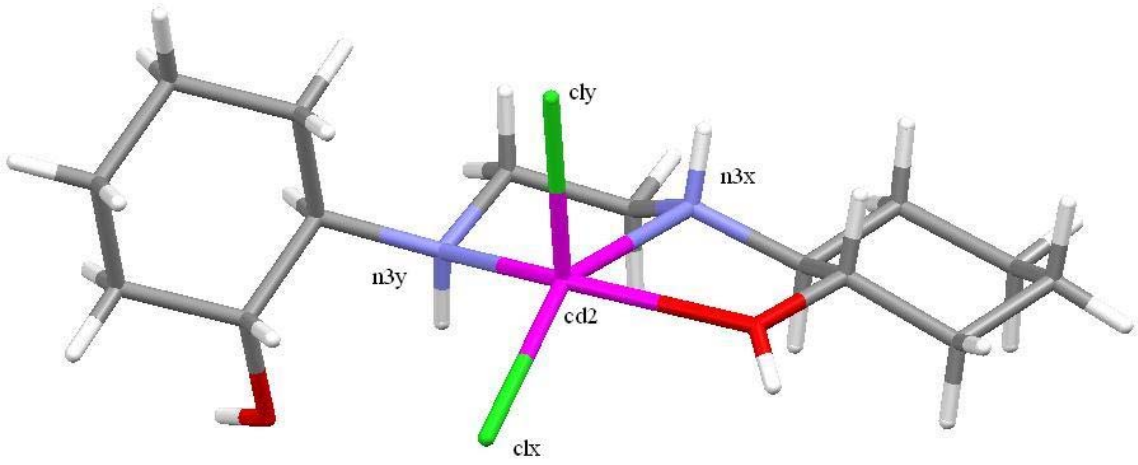


Figure 3.7: Atom labelling scheme for the MM calculations with selected atom types specified

The atom type was set so as to have the identical settings as the original atom type, i.e. clx and cly were the same as cl, and n3x and n3y were the same as n3.

The bond lengths also had to be modified so as to accommodate the new atom types, Table A.13. Again, the same settings were used for the clx and cly atoms as for the cl atom, and the n3 settings were used for the n3x and n3y atoms. This led to six new bonds being defined, namely the clx—cd2, cly—cd2, n3x—cd2, n3y—cd2, n3x—hn, and n3y—hn bonds.

The bond angles were then determined, Table A.14. The initial settings were set so that the geometry described by the complex was a perfectly square pyramidal one, i.e. the equatorial angles were set at 90˚ for *cis* atoms and 180˚ for *trans* atoms. All axial angles were set at 180˚. The next step was to then set the stretching constants. Arbitrary values from the nickel complexes were initially adopted. The remaining bond angles were then defined using the previously determined values as shown in Table A.15.

The nonbonded interactions were then altered to accommodate the four new atom types, Table A.16. The values used for n3x and n3y were those for n3, and the values used for clx and cly were the same as those for cl.

All torsion angles were then defined and $0.5V_n$ set to 0.00, Table A.17. In other words, the same settings as for the points on a sphere model were kept implying that all torsion penalties involving the metal ion were set to zero.

The new parameter sets were the saved and the parameter sets recompiled in HyperChem. The XRD structure was then opened and the new atoms types assigned. The structure was then energy minimised. The resultant structure was then compared to the XRD structure to see if the initial estimates made were acceptable. The Cd—Cl bond was too large, by 0.117 Å. The bond angles that were not within the 3˚ allowed for an acceptable structure were the C—N—Cd bond which was 6.4˚ to small, the C—O—Cd bond angle that was 10.2˚ too small, and the O—Cd—N bond angle that was 12.6˚ too large. It was then determined that the bond angles would be altered first so as to minimise the errors brought forward by those entities. The angles were then inspected on the XRD structure and the averages calculated for each type of bond angle. These average values were then few into the parameter file for the bond stretching, Table A.18. The bond lengths were kept constant. The parameter set was then recompiled and a second energy minimisation performed using the XRD structure as the starting point.

The result was that the only bond length that was too long was the Cd—Cl bond which was 0.116 Å too long, on average. The C—N—Cd bond angle changed from being 6.4˚ too small to being within the 3˚ tolerance. The C—O—Cd bond angle improved slightly but was still too small by 9.5˚ and the O—Cd—N was still too large at 10.0˚. The O—Cd—Cl bond angle, which had been fine after the first geometry optimisation, was suddenly out by 44.4˚. It was then decided to return the C—N—Cd angle to its original value of 109.9˚. The Cd—Cl bond length was altered to have an increased stretching constant of 225.0 kcal mol^{-2} $Å^{-2}$ and the equilibrium bond length was set to 2.605 Å from 2.610 Å. The files were then saved, HyperChem reset and a third geometry optimisation performed.

The calculation showed that the Cd—Cl bond length had improved but was still 0.111Å too large. The C—N—Cd bond length was within the accepted range for bond angles if the standard deviation of the XRD structure was taken into account. The bond angles had improved slightly. The C—O—Cd bond angle was still 9.5˚ too small, the O—Cd—N bond angle was 10.4˚ too large, and the O—Cd—Cl bond angle 6.6˚ too

small. The parameter files were then again edited by changing the stretching constant for the Cd—Cl bond length from 225.0 to 250.0 kcal mol^{-2} $Å^{-2}$ and the equilibrium bond length from 2.605 Å to 2.590 Å. The oh—cd2—cly bond angle was also changed from 95.0˚ to 90.0˚. The fourth geometry optimisation was then done.

The result was that all bond angles were now below the 3.0˚ threshold for acceptable values. The bond lengths still did not all give acceptable values. The N—Cd bond length was 0.038 Å too long, the O—Cd bond length was 0.049 Å too long, and the Cd—Cl bond length was 0.096 Å too long. The parameter file was then edited so that the setting for the N—Cd bond length was set to have a smaller stretching constant of 300.0 kcal mol^{-2} $Å^{-2}$. The O—Cd bond stretching constant was changed from 175.0 to 150.0 kcal mol^{-2} $Å^{-2}$. The Cd—Cl bond length was altered from 2.590 Å to 2.500 Å. The fifth geometry optimisation was then done.

The result was that the Cd—Cl bond length was now within the accepted bond length range. The N—Cd and O—Cd bond angles had improved but were still not acceptable. The stretching constant for the N—Cd bond length was then changed from 300.0 to 275.0 kcal mol^{-2} $Å^{-2}$, and the O—Cd stretching constant was changed from 150.0 to 125.0 kcal mol^{-2} $Å^{-2}$ and a sixth geometry optimisation done.

The N—Cd and O—Cd bond lengths were still not acceptable. It was then decided to alter the equilibrium bond lengths of these two bonds. The N—Cd bond length value was changed from 2.390 Å to 2.380 Å, and the O—Cd bond length was changed from 2.440 Å to 2.400 Å. The seventh, and final, geometry optimisation was then performed.

The XRD structure was now acceptably reproduced by the molecular modelling program, Figure 3.8.

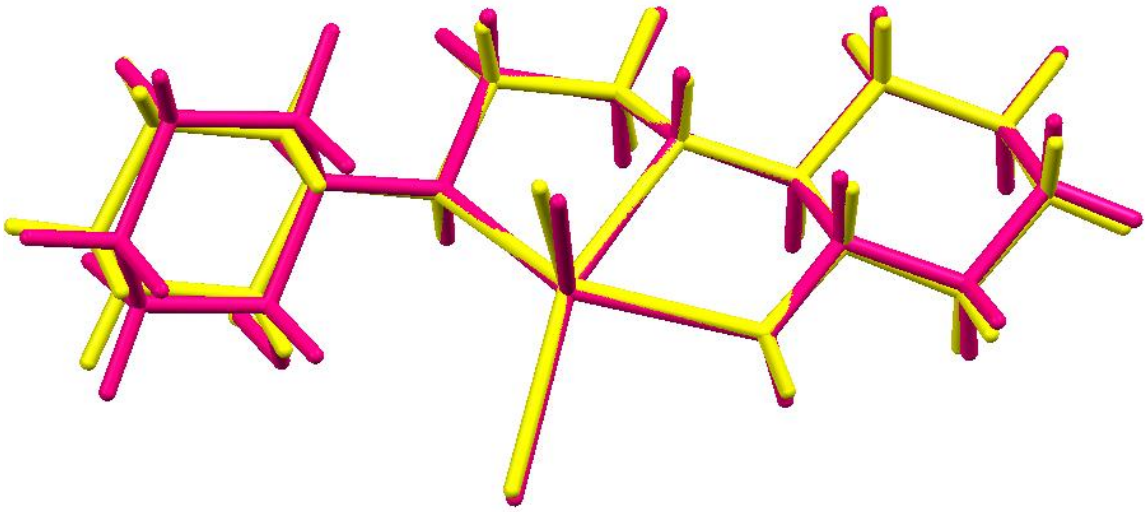


Figure 3.8: Superimposed images of the XRD structure (Yellow) of the Cy_2-en/Cd complex and the lowest energy structure predicted by MM methods (Blue)

The nature of the close contacts between hydrogen atoms was then investigated. This was done as one of the premises of this research project was that the close contacts between the hydrogen atoms on the ring and the hydrogen atoms on the backbone affected the stability of the complex. In our study, a close contact between two hydrogen atoms was defined as being less than the sum of the van der Waal's radii, i.e. less than 2.40 Å.[13] In the best approximation given by the modelling program there were four such close contacts. The same close contacts were observed in the XRD structure.

To investigate the effect of these close contacts, several sets of close contacts were deleted, in turn. The change in the geometry of the complex was then compared to the initial structure. If the parameters that had been set were indeed as good as assumed, the removal of two hydrogen atoms should not significantly change the overall structure. The four sets of close contacts were then removed and the four new structures analysed via geometry optimisation. The geometry optimisations clearly showed that the structure of the complex was not significantly altered in most cases, Figures 3.9 and 3.10.

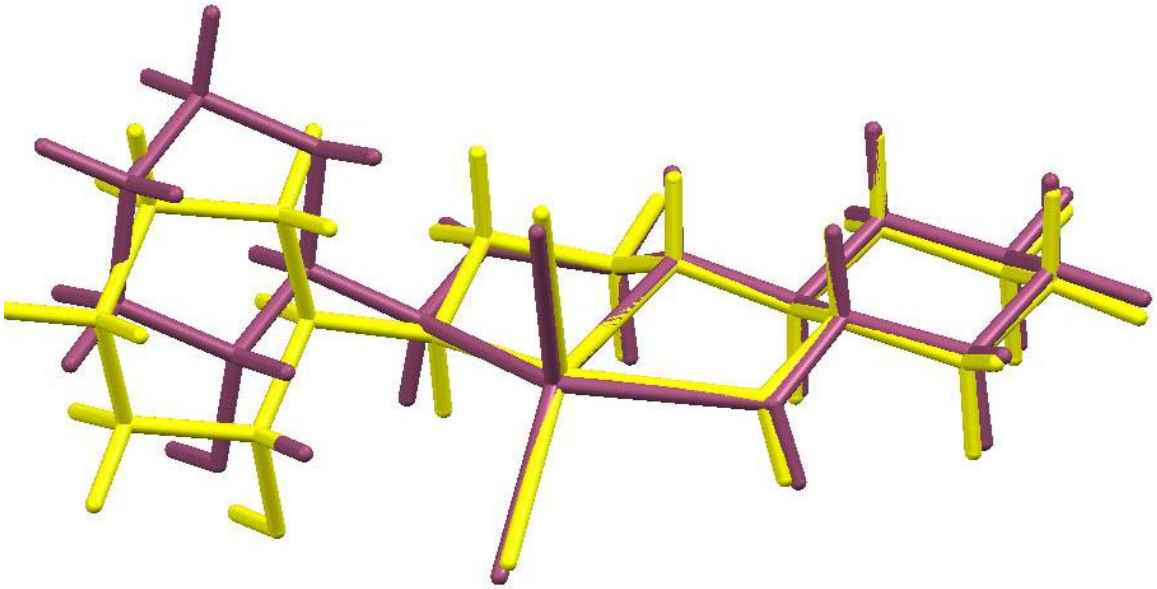


Figure 3.9: Superimposed images of the lowest energy structure predicted by MM methods (Yellow) of the Cy_2-en/Cd Complex and an approximation after removal of one set of close contact hydrogen atoms (Purple)

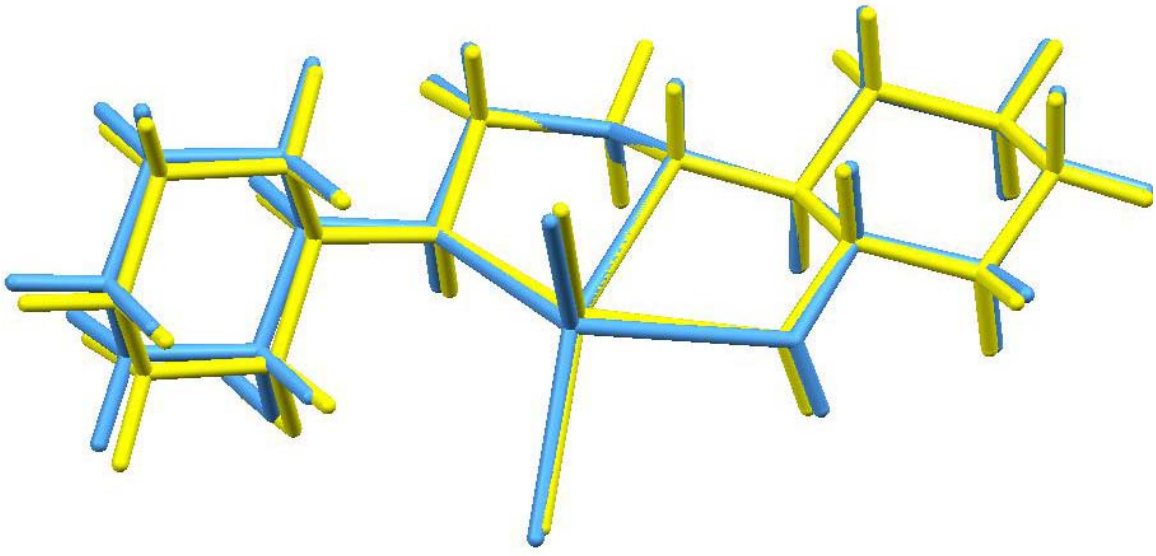


Figure 3.10: Superimposed images of the lowest energy structure predicted by MM methods (Yellow) of the Cy_2-en/Cd Complex and an approximation after removal of one set of close contact hydrogen atoms (Blue)

The close contacts are tabulated in Table 3.7. The labelling scheme from the XRD structure was used for all measurements made. The reference values given by the best geometry optimisation (column 2) were similar to the values of the complex when one set of close contacts was removed. The same could be said of the values for the bond angles around the metal ion, Table 3.8. The bond lengths, Table 3.9, did show a larger deviation though. The N—Cd bond lengths changed from around 2.376 Å to around 2.584 Å. The O—Cd bond length changed from 2.391 Å to 2.576 Å. Clearly, the removal of hydrogen atoms that formed close contacts did affect the complex. The values indicate that the removal of the hydrogen atoms led to a move of the cadmium ion out of the cavity, i.e. the complex became less stable. Although the conclusions reached clearly supported the initial assumption made at the beginning of this research project that the hydrogen close contacts played a role in the formation of the complex as well as the stability of the complex once formed, the fact that the force field did not contain a parameter for this interaction made no connection between the assumption and the conclusion possible.

Table 3.7: Hydrogen Close Contacts Found in the XRD Structure and the Corresponding Values from the Geometry Optimisations as well as the Removal of Several Close Contact Hydrogen Atoms

Close contact	XRD	G.O. Result	H5A, H7A removed	H8B, H10B removed	H6A, H7B removed	H8A, H9A removed
H10B - H9A	2.341 Å	2.507 Å	2.502 Å		2.500 Å	
H10B - H8B	2.381 Å	2.238 Å	2.243 Å		2.252 Å	2.225 Å
H9A - H8A	2.371 Å	2.385 Å	2.336 Å	2.410 Å	2.381 Å	
H8A - H7B	2.362 Å	2.547 Å	2.610 Å	2.462 Å		
H8B - H7A	2.359 Å	2.528 Å			2.423 Å	2.557 Å
H8B - H7B	2.333 Å	2.521 Å	2.410 Å			2.404 Å
H7A - H5A	2.270 Å	2.180 Å		2.159 Å	2.196 Å	2.151 Å

H7B - H1N	2.216 Å	2.353 Å	2.411 Å	2.348 Å	2.926 Å	2.940 Å
H7B - H6A	2.308 Å	2.400 Å	2.501 Å	2.471 Å		2.473 Å
H6A - H5A	2.348 Å	2.501 Å		2.504 Å		2.506 Å

Table 3.8: Selected Bond Angles in the XRD Structure and the Corresponding Values from the Geometry Optimisations as well as the Removal of Several Close Contact Hydrogen Atoms

Bond Angle	XRD	G.O. Result	H5A, H7A removed	H8B, H10B removed	H6A, H7B removed	H8A, H9A removed
Cl2 - Cd1 - O2	94.79˚	89.75˚	89.09˚	90.39˚	89.92˚	91.46˚
Cl2 - Cd1 - N2	96.02˚	94.85˚	96.80˚	95.73˚	95.96˚	95.18˚
Cl2 - Cd1 - N1	105.93˚	109.42˚	108.86˚	108.89˚	108.20˚	109.53˚
Cl1 - Cd1 - O2	90.16˚	91.07˚	94.45˚	94.24˚	94.42˚	93.49˚
Cl1 - Cd1 - N2	152.96˚	152.71˚	151.49˚	151.96˚	151.91˚	152.28˚
Cl1 - Cd1 - N1	111.03˚	112.79˚	114.60˚	114.84˚	114.94˚	114.26˚
N1 - Cd1 - N2	77.04˚	73.69˚	70.89˚	70.26˚	70.42˚	70.96˚
N1 - Cd1 - O2	144.23˚	142.05˚	138.16˚	136.69˚	137.45˚	136.57˚
N2 - Cd1 - O2	71.97˚	72.26˚	69.63˚	69.49˚	69.62˚	69.59˚

Table 3.9: Selected Bond Lengths in the XRD Structure and the Corresponding Values from the Geometry Optimisations as well as the Removal of Several Close Contact Hydrogen Atoms

Bond Length	XRD	G.O. Result	H5A, H7A removed	H8B, H10B removed	H6A, H7B removed	H8A, H9A removed

Cl1 - Cd1	2.494 Å	2.500 Å	2.499 Å	2.499 Å	2.499 Å	2.499 Å
Cl2 - Cd1	2.495 Å	2.501 Å	2.500 Å	2.500 Å	2.500 Å	2.500 Å
N1 - Cd1	2.362 Å	2.374 Å	2.590 Å	2.588 Å	2.587 Å	2.583 Å
N2 - Cd1	2.334 Å	2.378 Å	2.581 Å	2.578 Å	2.581 Å	2.58 Å
O2 - Cd1	2.382 Å	2.391 Å	2.575 Å	2.581 Å	2.576 Å	2.573 Å

The next step to fully confirm the conclusion that the selected parameters were acceptable for the work done was to find the optimal bond lengths of a metal to the oxygen atom as well as the nitrogen atom in the cavity. This would lead us to find the optimal metal for complex formation with this ligand, looking at size only. The size of the metal calculated would go some way to explaining the observed log *K* values for this ligand.

To do this, the values of the Cd—N and Cd—O stretching constants were kept constant at 275.0 kcal mol^{-2} $Å^{-2}$ and 125.0 kcal mol^{-2} $Å^{-2}$ respectively. The values of the bond lengths were varied from 2.00 Å to 2.60 Å for each bond in turn and the resultant energy of the complex calculated, Table A.32. The resultant three-dimensional graph is given in Figure 3.11. All three-dimensional data were plotted using Matlab.[14]

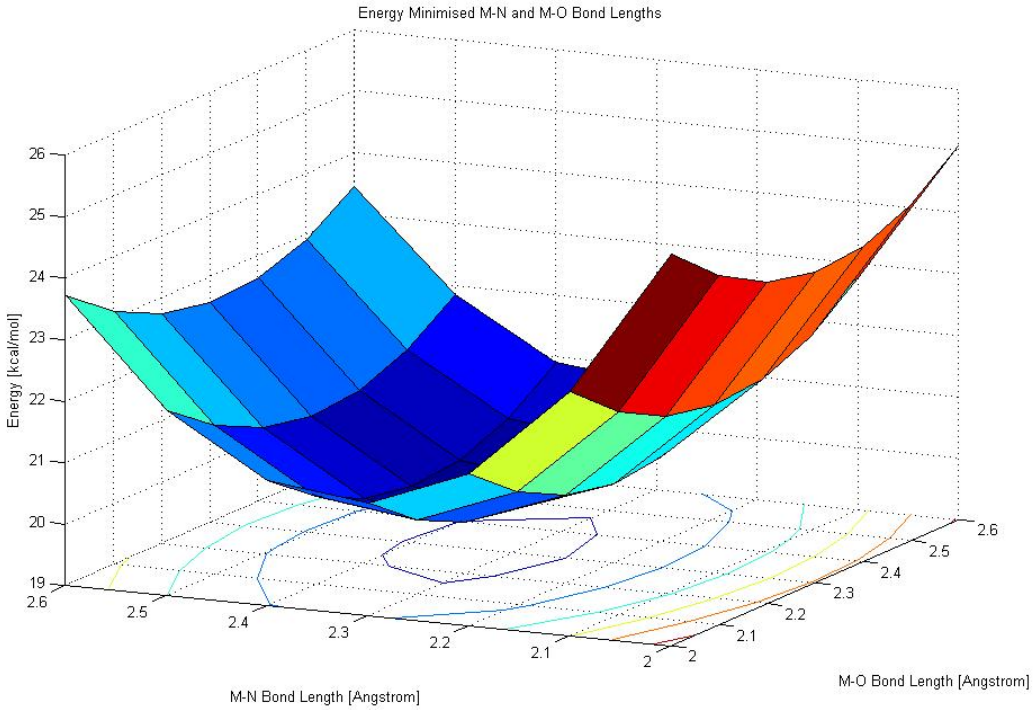


Figure 3.11: The three-dimensional plot of the energy minimised M—N and M—O bond lengths with their respective energy values

The graph indicated that the desired minimum value did indeed lie in the range of 2.00 Å to 2.60 Å for both bond lengths. The surface generated by the plotted points was too rough to fit a curve to it. Two methods to interpolate and so smooth the data were then used. The first was to use a cubic polynomial to fit the data, Figure 3.12. A cubic polynomial is a function of degree three that fits a bicubic surface through existing data points. The value of an interpolated point is a combination of the values of the sixteen closest points. This method is piecewise bicubic, and produces a much smoother surface than bilinear interpolation.[14] At each of the boundaries between the measured points, the derivates of the two surfaces must be the same to ensure a continuous and smooth interpolation. This method can only be used in a two-dimensional problem. The second method was to use the cubic spline method, Figure 3.13. A cubic spline is a spline that is a particular function redefined at each point in a smoothing process. A spline can be used for any degree of a polynomial but as the degree increases the accuracy of the spline decreases. A two-dimensional problem is still well-approximated by a cubic spline. The

polynomial used in each step must be continuous over that range and the first and second derivates of that polynomial must also be continuous over that range. Due to the fact that the data used in this graphing problem were continuous and relatively uniform, there was no notable preference when either method was used. The three graphs were overlayed to confirm that the smoothing had indeed worked, Figure 3.14. In all of the graphs, a contour plot was added to the graph to indicate the approximate convergence area for the minimum values of the bond lengths.

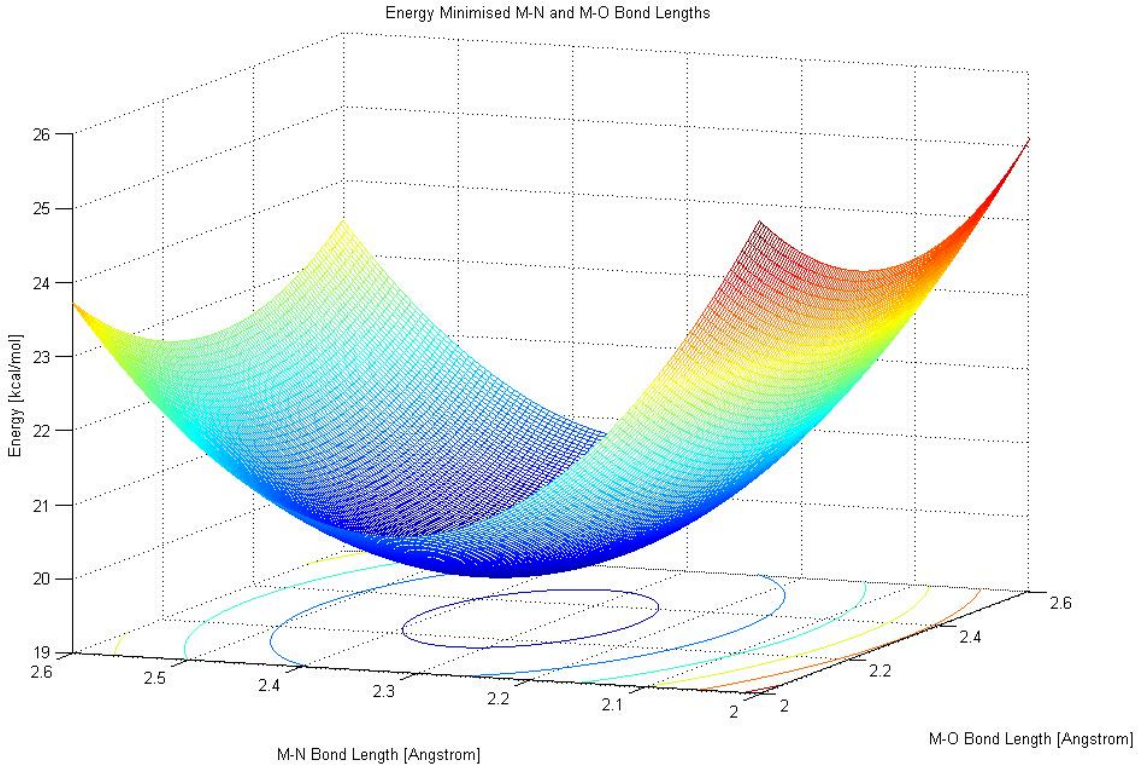


Figure 3.12: The three-dimensional plot of the energy minimised M—N and M—O bond lengths with their respective energy values using a cubic polynomial to interpolate and smooth the data

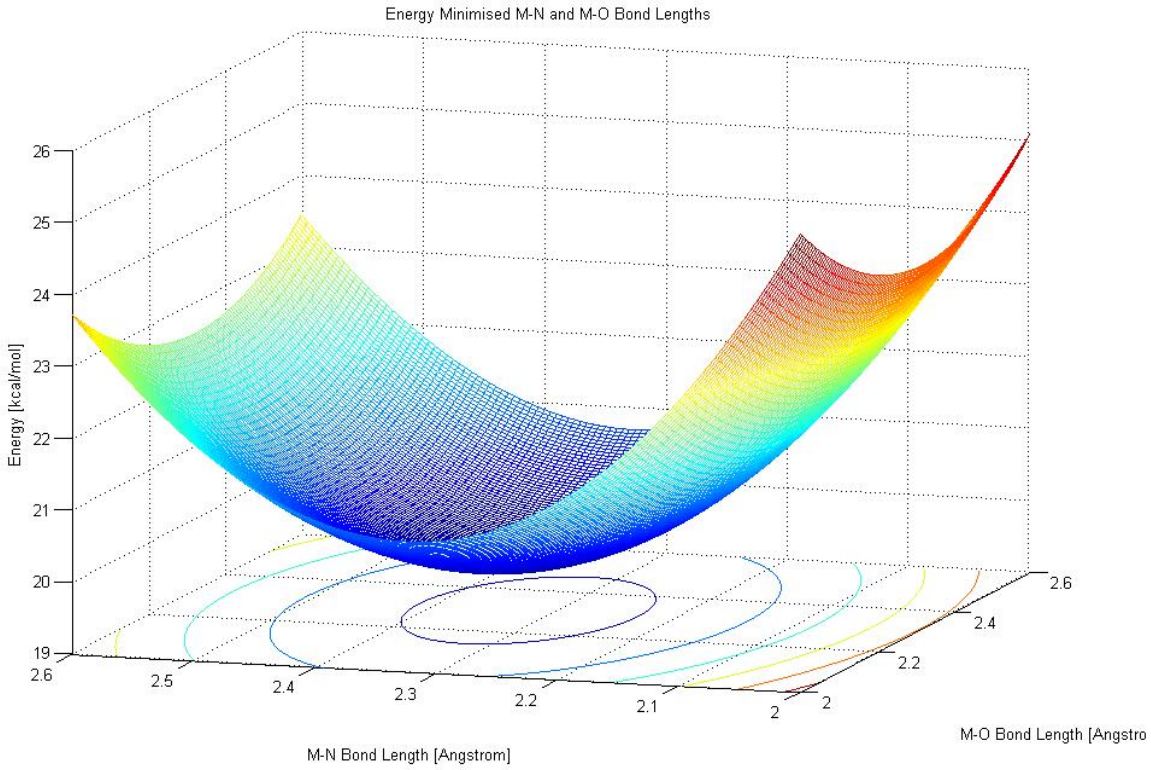


Figure 3.13: The three-dimensional plot of the energy minimised M—N and M—O bond lengths with their respective energy values using a cubic spline to interpolate and smooth the data

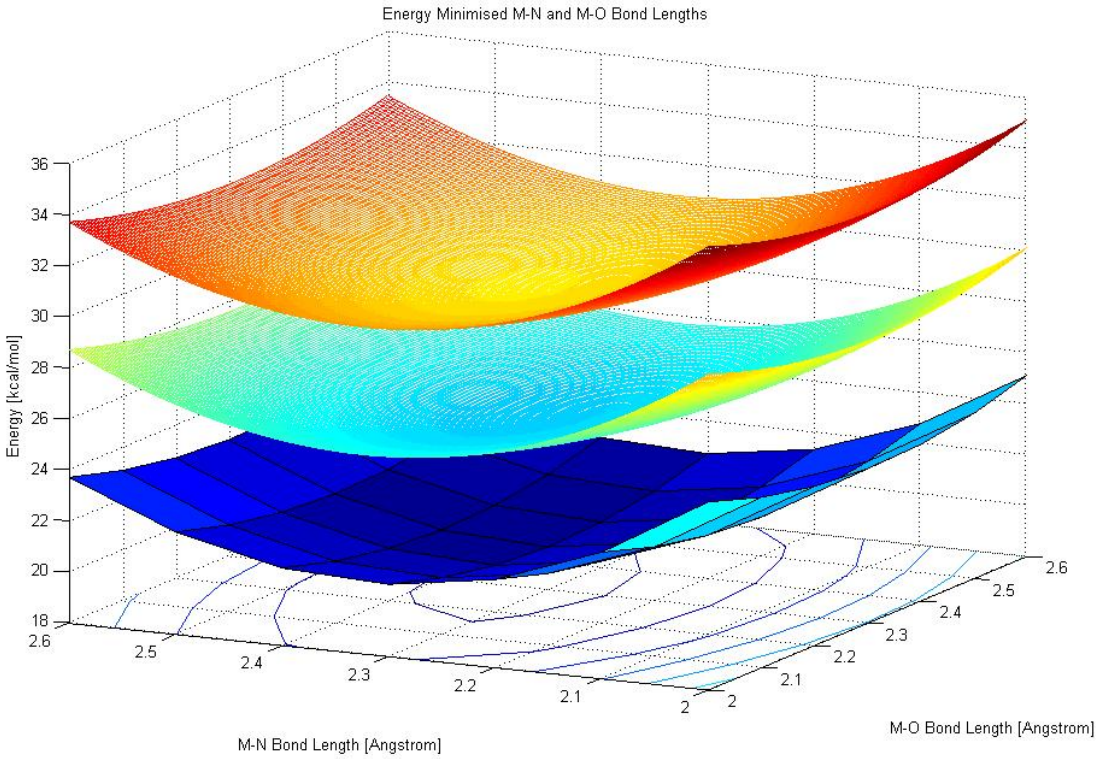


Figure 3.14: The three-dimensional plots of the energy minimised M—N and M—O bond lengths with their respective energy values, unaltered (bottom), using a cubic spline to interpolate and smooth the data (centre), using a cubic polynomial to interpolate and smooth the data (top)

The data was then analysed in a stepwise manner and the minimum value of the energy was found to be 19.67 kcal mol^{-1} for both methods. The corresponding M—N and M—O bond lengths were calculated to be 2.32 Å and 2.31 Å, respectively. The average bond lengths for the four metals of interest in this study were 2.534 Å for the Pb—N bond, 2.353 Å for the Cd—N bond, 2.116 Å for the Zn—N bond and 2.071 Å for the Ni—N bond, when the values were obtained from the CSD.[7] The values differed when taken from Allen's paper on bond lengths: 2.318 Å for the Cd—N bond, 2.143 Å for the Zn—N bond and 2.097 Å for the Ni—N bond.[15] The M—O bonds were also different for the two given references: 2.622 Å for the Pb—O bond, 2.407 Å for the Cd—O bond, 2.150 Å for the Zn—O bond, and 2.106 Å for the Ni—O bond in Vista,[7] and 2.283 Å for

the Cd—O bond, 2.268 Å for the Zn—O bond, and 2.087 Å for the Ni—O bond in Allen's paper.[15]

The best fit for the cavity calculated above was found to be the metal cadmium. This was not surprising as the force field parameters used had been optimised for cadmium. Other metals that may also work were found to be molybdenum and iron(II). The values calculated also clearly showed why the complex formation with lead was not that easy, the bond lengths are not optimal to fit the cavity if the geometry of the cavity were retained.

3.3 Conclusions

The Generalised AMBER force field (GAFF) was able to reproduce the free ligands in an acceptable manner. The same could not be said of the cadmium complex with Cy_2-en. The GAFF force field could not adequately predict the structure of the complex if a 'points-on-a-sphere' model was used. If the force field was altered so that exact values of the bond lengths, bond angles, and torsions were used, the force field did give a good estimate. The general conclusion from this work was that the GAFF force field could not predict the geometry of the desired cadmium complex in any manner. If such a model were to be developed, it would have to be calculated from *ab initio* methods and employ DFT (density functional theory). Molecular mechanics is not a viable option at this time. But the model, as such, did indicate the type of metal that would be useful to fit into the cavity created by the ligand upon complexation. The metal was found to be cadmium, an unsurprising result, as the force field had been optimised using particular cadmium parameters.

This clearly paves the way for further work on the cadmium complexes of amino alcohols. Further XRD structures of cadmium complexes with similar ligands are known and reported in this dissertation. It would be interesting to investigate the suitability of the current cadmium parameters for these different ligands.

3.4 References

(1) Deeth, R. J. *Chem. Commun.* **2006**, 2551-2553.

(2) Marques, H. M.; Brown, K. L. *Coord. Chem. Rev.* **1999**, 127-153.

(3) Marques, H. M.; Brown, K. L. *Coord. Chem. Rev.* **2002**, *225*, 123-158.

(4) Chen, M.; Fulton, J. R.; Hitchcock, P. B.; Johnstone, N. C.; Lappert, M. F.; Protchenko, A. V. *Dalton Trans.* **2007**, 2770-2778.

(5) HyperChem; 7.03 ed.; Inc., H., Ed. Gainsville, Fl., 2004.

(6) Gillespie, R. J. *Chem. Soc. Rev.* **1992**, 59-69.

(7) Allen, F. H. *Acta Cryst. Sect. B* **2002**, *B58*, 380-388.

(8) *Handbook of Chemistry & Physics*; 51 ed.; The Chemical Rubber Co.: Ohio, 1970.

(9) Mel'nikov, V. L.; Pletnev, I. V. *Russ. Chem. Bull.* **1997**, *46*, 1221-1227.

(10) Defazio, S.; Cini, R. *J. Chem. Soc., Dalton Trans.* **2002**, 1888-1897.

(11) Philpott, M. R.; Kawazoe, Y. *Chem. Phys.* **2007**, *333*, 201-207.

(12) Yalovega, G.; Smolentsev, G.; Soldatov, A.; Chan, J.; Stillman, M. *Nucl. Instr. Meth. Phys. Res.* **2007**, *575*, 162-164.

(13) Bondi, A. J. *Phys. Chem.* **1964**, *68*, 441-451.

(14) Matlab; Version 6.5 ed.; Works, T. M., Ed. 2002.

(15) Orpen, A. G.; Brammer, L.; Allen, F. H.; Kennard, O.; Watson, D. G. *J. Chem. Soc., Dalton Trans.* **1989**, S1-S83.

Chapter 4

Results and Discussion

All analytical data are given in detail in Chapter 2 Materials and Methods.

It should be noted that all discussions referring to hydrogen atoms are based on XRD data only. XRD cannot place hydrogen atoms from the experimental data as the method measures the diffraction of electrons. In the present compounds, all hydrogen atoms are positively charged meaning that they have no electrons. Thus all hydrogen atoms are placed according to a general best-fit formula meaning all hydrogen positions are calculated from ideal geometries and not placed experimentally. That can only be done by neutron diffraction. All crystals obtained during the course of the research were too small to be analysed by this technique. Furthermore, the actual positions of the hydrogen atoms may be vastly different from the geometrically palced ones. Again, this can only be verified by neutron diffraction.

4.1 Synthesis and Characterisation of the Free Ligands

4.1.1 Synthesis of Cy_2-en

The synthesis was performed using a method previously described by De Sousa and Hancock.[1] Two of the three yields obtained were above 70 % whilst the third yield was low at 45 %. This was attributed to not having left the reaction to run long enough. The reaction could have been left to reflux for more than the recommended 6 hours as there was no risk of the cyclohexene reacting more than twice with the starting amine to give the desired product.

All of the analytical data clearly indicated that the reaction had been successful and that the sample was clean. NMR data are given in Figures B.1 to B.6, the IR data are in Figures C.1 to C.3, and the MS data in Figures D.1 to D.3. The crystal data information is given in the Experimental section under Table 2.3 as well as in Appendix E (Figure E.1, Tables E.1 to E.6).

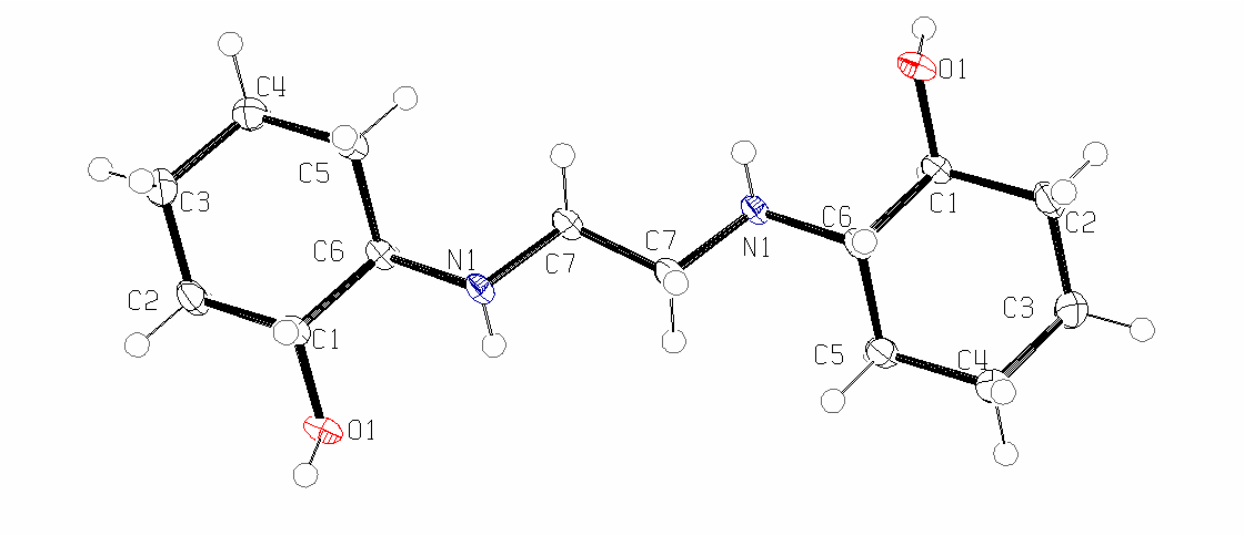


Figure 4.1: The molecular structure of Cy_2-en, showing the atom-labelling scheme and 50% probability displacement ellipsoids

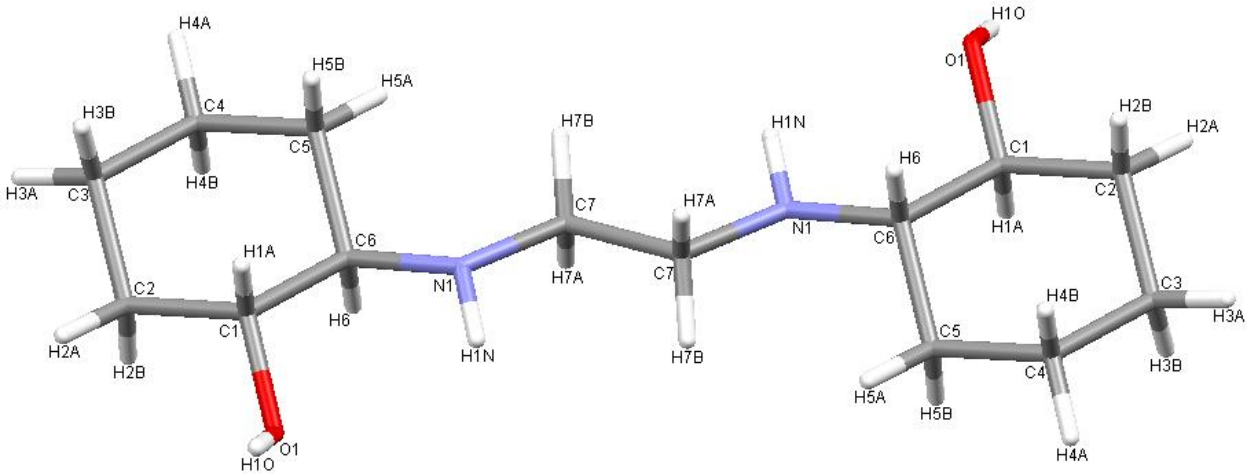


Figure 4.2: The molecular structure of Cy_2-en with its labelling scheme (hydrogen atoms included)

The relative steroechemistry of the molecule is of interest as the adjoining atoms C6 and C1 adopt the same stereochemistry. The set of atoms on the left of the molecule in Figure 4.2 adopt a *R,R* configuration whilst the equivalent atoms on the right of the molecule adopt an *S,S* configuration. This pattern is repeated for all molecules within the unit cell. This pattern leading to the formation of only the *meso* form has been previously reported[2,3] It is not clear as to why the sole product of the reaction is so particular in its arrangement.

The molecule formed an effectively planar crystal. The two cyclohexenyl rings are both in the chair conformation and coplanar. The two alcoholic oxygen moieties are on opposite sides of the molecule and hydrogen bond to two further molecules via the amines. By adopting this geometry, the number of hydrogen bonds is optimised as each oxygen atom hydrogen bonds to an amine nitrogen on a different molecule, Figure 4.3. This implies that there is not a great deal of pre-organisation of the ligand for complexation in the solid state. The observed is only one of an infinite number of arrangements that the molecule can adopt in solution and so it is highly likely that there will be many conformations that lead to an arrangement that is ideal for complexation. This also allows for several conformations in which dimeric or even polymeric complexes can form. The ideal geometry for complexation would be a cavity formed by the two amine nitrogens and the two alcoholic oxygen atoms, i.e. the oxygen moieties would have to be on the same side of the ethylene bridge.

The molecule has four hydrogen bonds to four different molecules, two above it, and two below, Figure 4.3. These hydrogen bonds extend in all three dimensions. Due to the staggered arrangement of the molecules in adjoining layers, the hydrogen bonds formed between the molecules in two layers is such that the donor alcohol group hydrogen bonds to the acceptor amine nitrogen group. On each molecule there are two such bonds to two different molecules. In each case, the two molecules involved in the hydrogen bond are almost at right angles to one another ensuring that a suitably large angle exists for the hydrogen bonds.

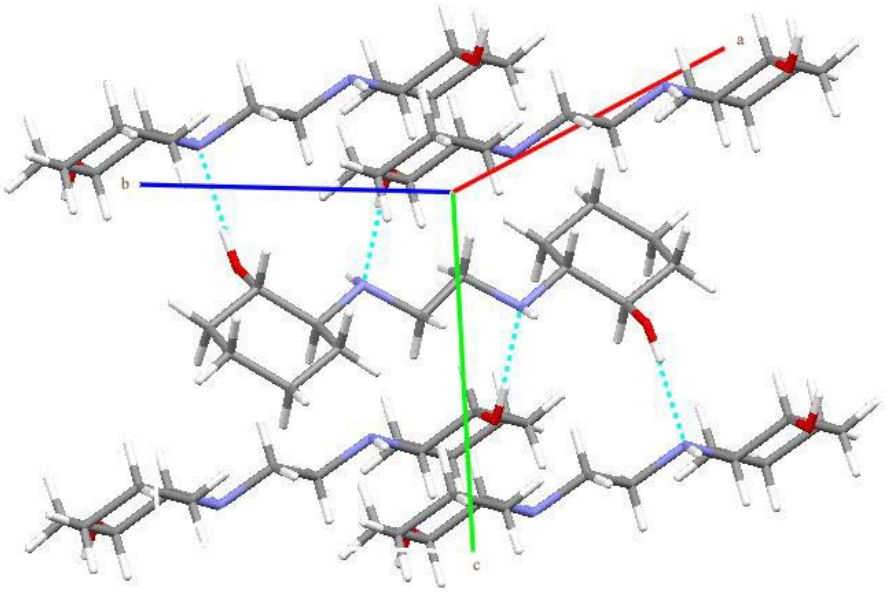


Figure 4.3: Hydrogen-bonding network of Cy_2-en indicating the four hydrogen bonds emanating from the central Cy_2-en molecule to four further molecules (two above and two below)

Cy_2-en forms alternating layers of transposed molecules. Each layer is shifted so that the cyclohexenyl rings are not directly atop one another, Figure 4.4. This allows the oxygen atoms to form the strongest possible hydrogen bonds to the nitrogen atoms, Figure 4.5.

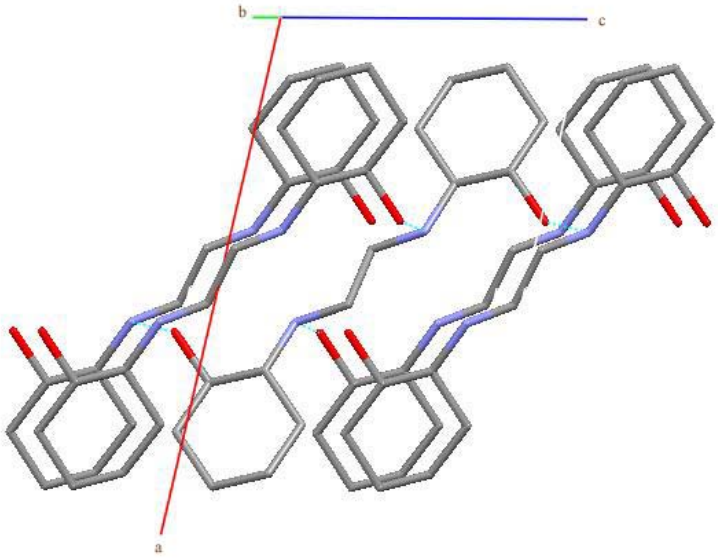


Figure 4.4: Crystal packing of Cy_2-en viewed along the *b*-axis (H atoms omitted for clarity)

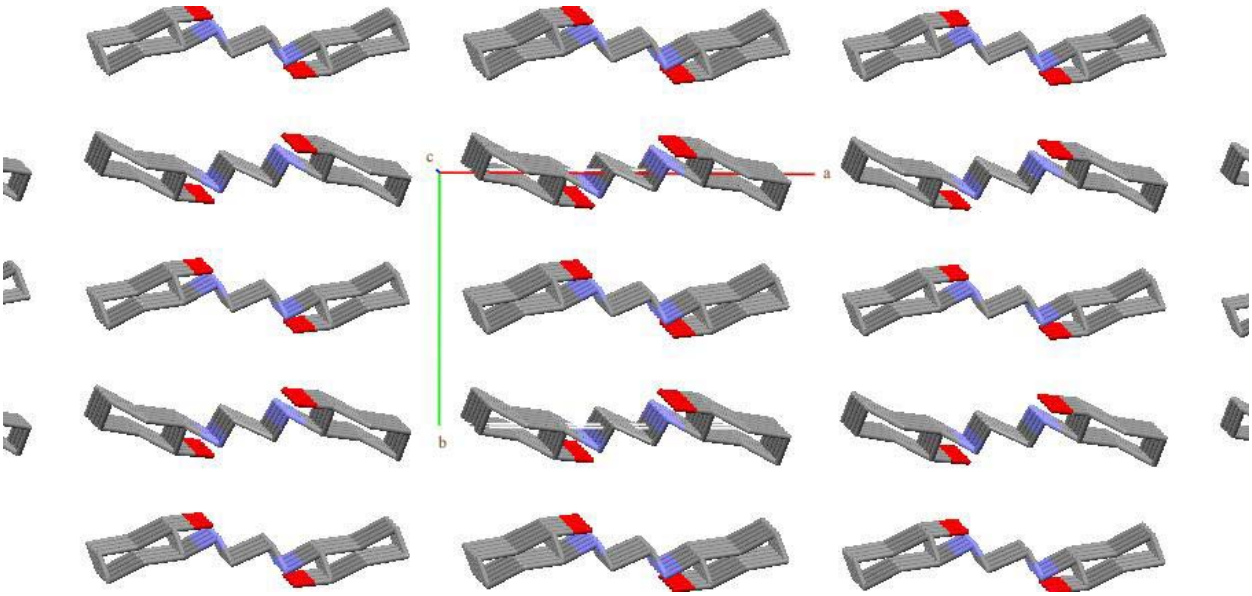


Figure 4.5: The 2D packing arrangement of Cy_2-en viewed along the *c*-axis (H atoms omitted for clarity)

It was initially hypothesised that the hydrogen atoms on the ring interacted with the hydrogen atoms on the ethylene bridge during complexation reactions. The distance between each of these atoms was then measured and all of the distances that were less than the sum of the van der Waal radii (2 x 1.20 Å = 2.40 Å) were noted and these interactions found to vary from 2.187 Å to 2.204 Å, Figure 4.6. A list of the relevant hydrogen-hydrogen bonds, henceforth referred to as H-H bonds, found in the ligand is given in Table 4.1.

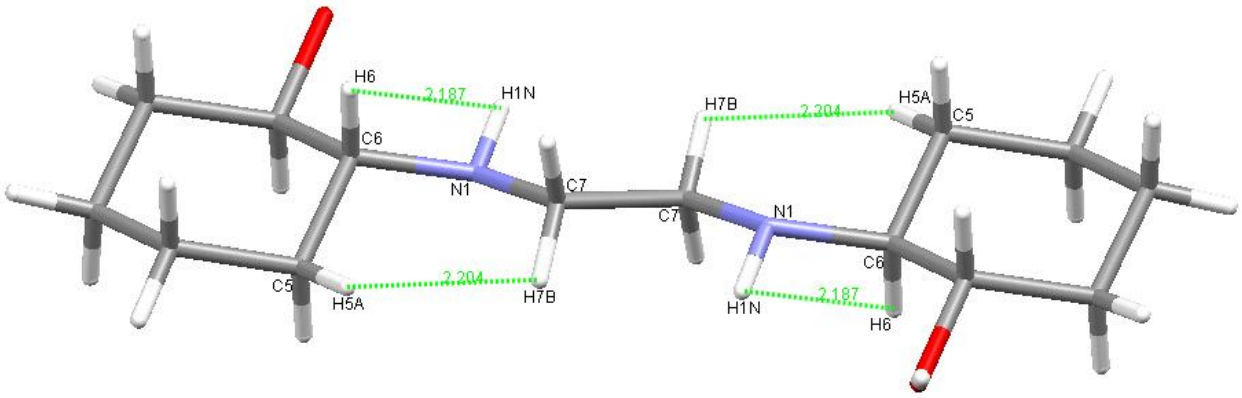


Figure 4.6: The H-H bonds in Cy_2-en

At this point it is important to note that there is some room for debate as to the exact X-H bond lengths. The average bond length assigned to a N-H bond of the type X_2-N-H is 1.033 Å if analysed by neutron diffraction.[4] The equivalent bond length is set at 0.830 Å for XRD analyses. The other X-H bonds in the molecules are similarly set at shorter values. It is possible to extend the bond lengths using other software but it must be noted that the initial assignment of the hydrogen atoms is already an approximation and the values selected for the XRD data are the result of many approximations. Thus, any extension of the bond lengths would merely involve an increase of the starting approximations. It is still a viable possibility but this course of action was not chosen for this work.

The N-H···H-C interactions are also referred to as H-H bonds as they conform to the criteria set for the definition of such bonds. That is to say, the two hydrogen atoms are of not too dissimilar charge and they are both bonded to atoms that are not particularly electronegatively charged. This definition is supported by the point charge calculations performed on Cy_2-en as described in Chapter 3. The point charges are calculated to be +0.037 and +0.048 for the N-H and C-H protons respectively if a PM3 force field is used; the values change to +0.165 and +0.022 respectively if the ZINDO/1 force field is used. In contrast, the Bader charges, the charges calculated using an atoms in molecules approach, are calculated to be +0.368 and -0.047 respectively using a 6-31G(d,p) basis set in a X3LYP DFT calculation. If the Bader charges are used as the accepted charges, then it becomes a viable option to term the close contact between the two hydrogen atoms a dihydrogen bond. A dihydrogen bond is defined as a non-bonded interaction between two hydrogen atoms, one of which carries a partial positive charge and the other a partial negative charge. The atoms to which these hydrogen atoms are bonded must also carry partial charges of opposite sign to the charge on the hydrogen. Due to the uncertainty of the exact charges on the protons in question, it was decided to refer to these bonds as H-H bonds.

Table 4.1: H-H Bonds for the Ligand Cy_2-en

Atom 1	Atom 2	H-H Bond Distance (Å)	X-H-H Bond Angles (˚), where X denotes a donor atom
H6	H1N	2.187	60.11 and 66.67
H5A	H7B	2.204	111.80 and 107.93

The H-H bond for H6 and H1N has angles of 60.11˚ and 66.67˚. The two angles are measured from the carbon C6 and the nitrogen atom N1 respectively. The two H-H bond angles for the H5A and H7B protons is between 111.80˚ and 107.93˚ when measured from C5 and C7 respectively. The angles for several other H-H bonds involving protons on carbon atoms were

measured by Damodharan and Pattabhi[5] and found to lie between 90˚ and 150˚. The observed values are thus within these ranges.

The torsion angles for the rings indicated no flattening of the cyclohexenyl ring unlike in the structure reported by De Sousa and Fernandes.[3]

The most interesting close contact was the one between the alcoholic oxygen atom O1 and the amine hydrogen H1N, Figure 4.7. This interaction is not defined as a hydrogen bond as the angle between the acceptor and donor atoms is too obtuse at 103.72˚. A hydrogen bond is commonly accepted as having and angle above 120˚ at the very least. The distance between the two is significantly less than the sum of their van der Waals radii. The oxygen group has a van der Waals radius of 1.52 Å and hydrogen 1.20 Å. The distance between the two atoms is 2.485 Å which is less than the sum of their radii at 2.72 Å. Clearly this attractive interaction significantly affects the packing behaviour of the molecule in that the two alcoholic groups are on opposite sides of the molecule so as to link to the amine hydrogens. It is noted in a paper by Damodharan and Pattabhi[5] that dihydrogen bonds and H-H bonds are most commonly found in centrosymmetric space groups.

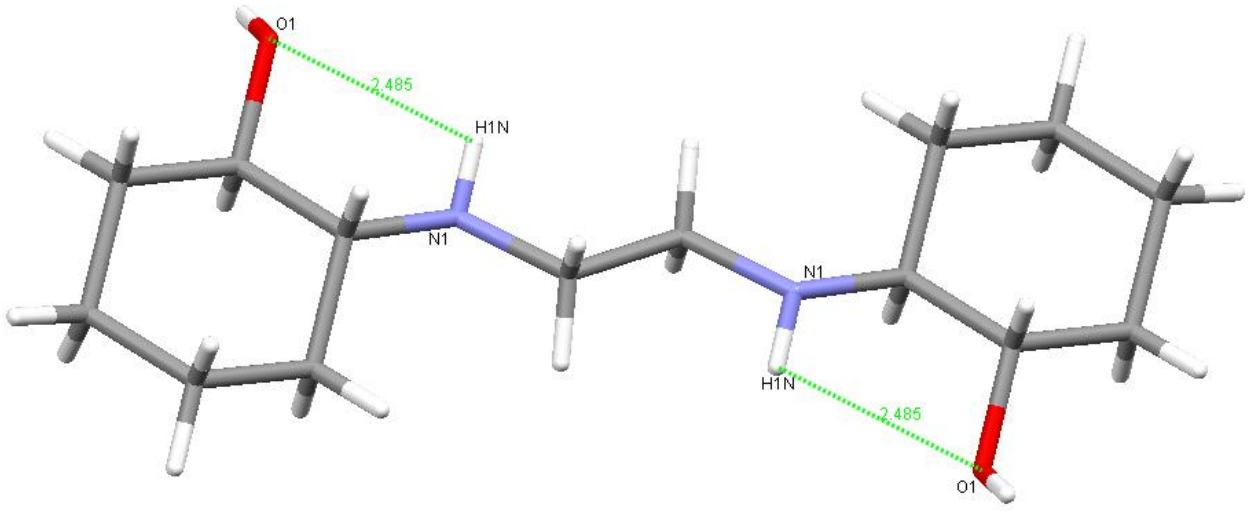


Figure 4.7: The close contact distance between the alcohol oxygen and the amine hydrogen in Cy_2-en

The ligand was then analysed by AIM (atoms in molecules) theory by Pradeep R. Varadwaj.[6] The Cy_2-en molecule was analysed in the gas phase by doing DFT calculations using an 6-31G(d,p) basis set. AIM is a theory proposed by Bader that defines chemical bonding between all atoms according to the electronic charge density of these atoms in relation to one another.[7] The interactions are then evaluated to find the paths of maximum electron density between the two atoms, called a bond path. Along this bond path, there is a point at which the electron density is at a minimum, called the bond critical point or bcp. If the bond paths interact to form a ring, then the point in the ring at which all of the electron densities interact so that they have zero magnitude is called the ring critical point or rcp. The resultant diagram indicating the bond critical points (bcp's, red points) as well as the ring critical points (rcp's, yellow points) is given in Figure 4.8. The more centred this point is within the ring, the more thermodynamically stable the ring. If an rcp overlaps with a bcp, then the bond path involving the bcp is broken in order to overcome the destabilising interaction that this overlapping event brings with it. This molecule has two rcp's that are optimal (in the cyclohexenyl rings) and two that are weak (involving the H-H bonds).

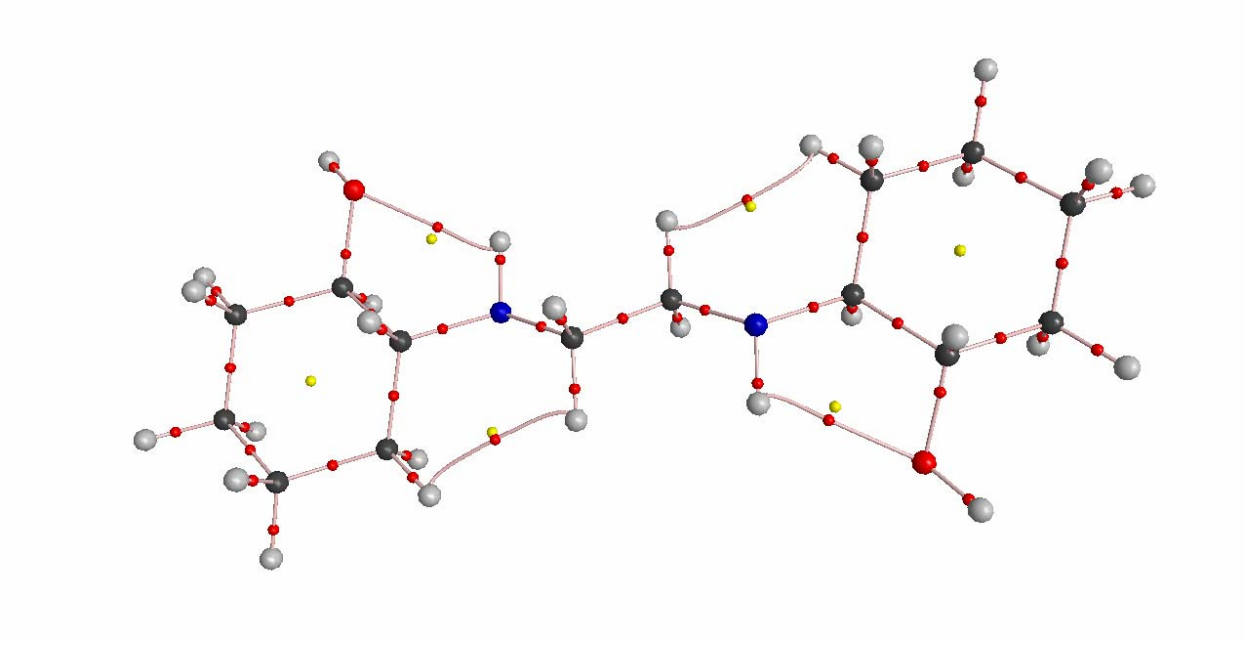


Figure 4.8: The AIM analysis of Cy_2-en in the gas phase[6]

The interesting point to note is that AIM theory detects the interactions of interest in the molecule, namely the H-H bond between the two hydrogen atoms on the carbon atoms as well as the close contact between the amine hydrogen and the oxygen atom. The default setting in the software was chosen as a cut-off for bond paths, namely that the interaction had to be above 0.5 kcal mol^{-1}.

It is of interest to note that the molecular graph depicts six ring systems rather than the two that are expected in the molecular structure. The two cyclohexenyl rings are stable as is demonstrated by the central location of the respective rcp in the centre of the ring. The general statement made by AIM is that the more central the rcp the more stable is the observed ring. The ring formed by the interaction of the amine hydrogen and the oxygen atom is not as stable. The bcp of that bond path is in close proximity to the rcp of the ring. This implies that the ring is not that stable and that the bond path that is approached by the bcp is the one that is the weakest. In the observed structure, that is the aforementioned close contact. This is not surprising as all of the other bond paths involved in the ring are known to be actual bonds. The same pattern is observed for the ring formed by the H-H bond. In this ring, the rcp and bcp are even closer together than the previous example. This indicates that the H-H bond is even weaker than the aforementioned close contact.

The next structure that was analysed was the equivalent protonated Cy_2-en chloride salt, Figure 4.10. Full XRD data is given in Figure E.2 and Tables E.7 to E.12 in Appendix E.

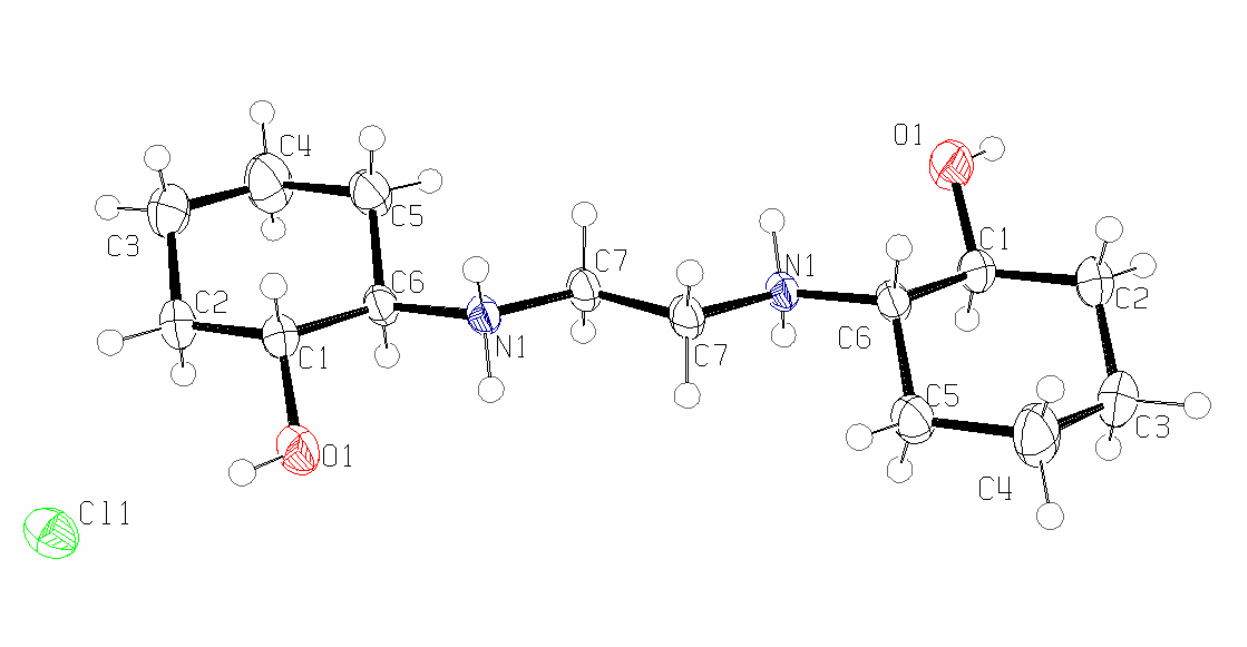


Figure 4.9: The molecular structure of the chloride salt of Cy_2-en, showing the labelling scheme and 50% probability displacement ellipsoids

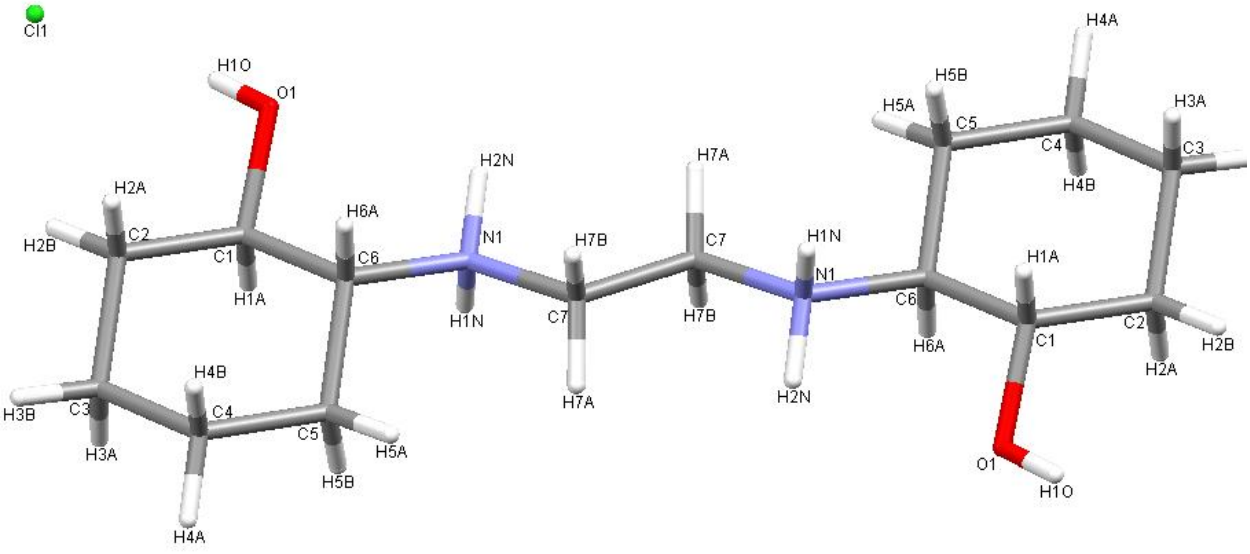


Figure 4.10: The molecular structure of the chloride salt of Cy_2-en with its labelling scheme (hydrogen atoms included)

The relative stereochemistry of the protonated molecule is the same as the free ligand, i.e. the adjoining atoms C6 and C1 adopt the same configuration. The set of atoms on the left of the molecule in Figure 4.8 adopt a *R,R* configuration whilst the equivalent atoms on the right of the molecule adopt an *S,S* configuration. This pattern is repeated for all molecules in the unit cell.

The space group changed from $P\ 2_1/c$ to $P\ \bar{1}$. The same spatial arrangement was adopted as previously described for the free ligand. The bond lengths and angles are within the accepted ranges. The torsion angles are also all as expected. The 2-dimensional arrangement of the molecules is also maintained, Figure 4.11.

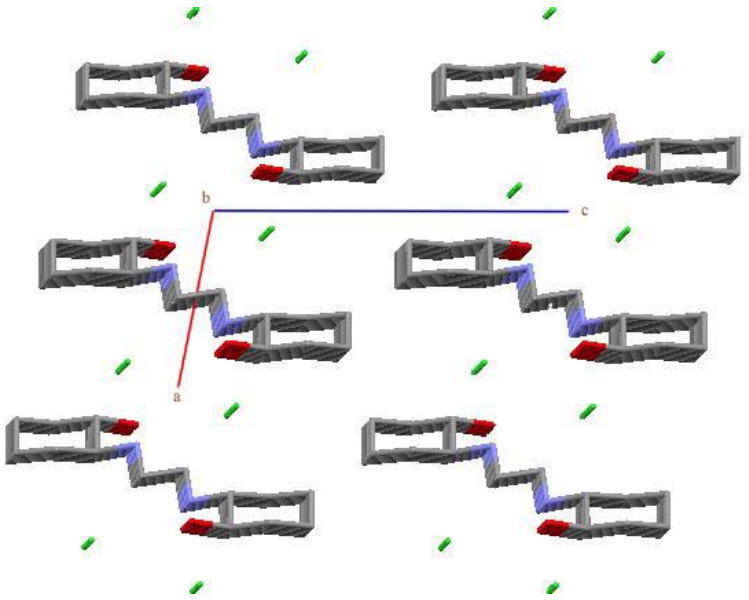


Figure 4.11: The 2D packing arrangement of the Cy_2-en chloride salt viewed along the *b*-axis (H atoms omitted for clarity)

The hydrogen bonding network is strongly affected by the addition of the chloride counter ion. There is no longer hydrogen bonding between the alcoholic oxygen atoms and the amine nitrogens. All hydrogen bonds are to the chloride ion via either the oxygen atom or the nitrogen atom, Figure 4.12. Each of the molecules forms a linked chained to the molecules

above and below it via two hydrogen bonds in each case. The two molecules effectively form a ring via the hydrogen bonds to the shared chloride ions.

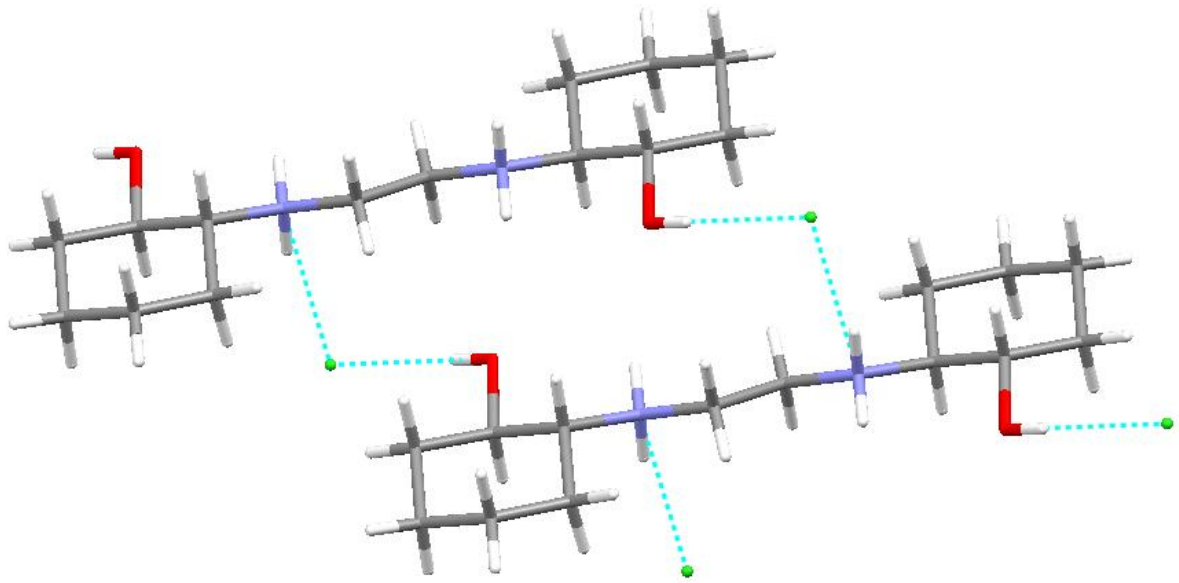


Figure 4.12: Hydrogen-bonding network of the Cy_2-en chloride salt

The hydrogen-hydrogen bond, as described for the free ligand, is found to be longer for the salt than the neutral ligand. The average distance increases from 2.204 Å to 2.220 Å, Figure 4.13. This is can be attributed to the fact that the ligand in its protonated form is more planar or to the uncertainty in the bond lengths from the XRD structure. In an effort to verify the planarity hypothesis, a plane was drawn through the four atoms on the ethylene bridge and the two structures compared, Figures 4.14 and 4.15.

If a plane is drawn through the six members of the cyclohexenyl ring, each of the rings adopts a parallel arrangement that is at an angle of 28.0(2)˚ to the plane through the bridging atoms in the free ligand. The same pattern is observed for the protonated ligand with the two rings inclined at an angle of 29.2(4)˚ to the plane.

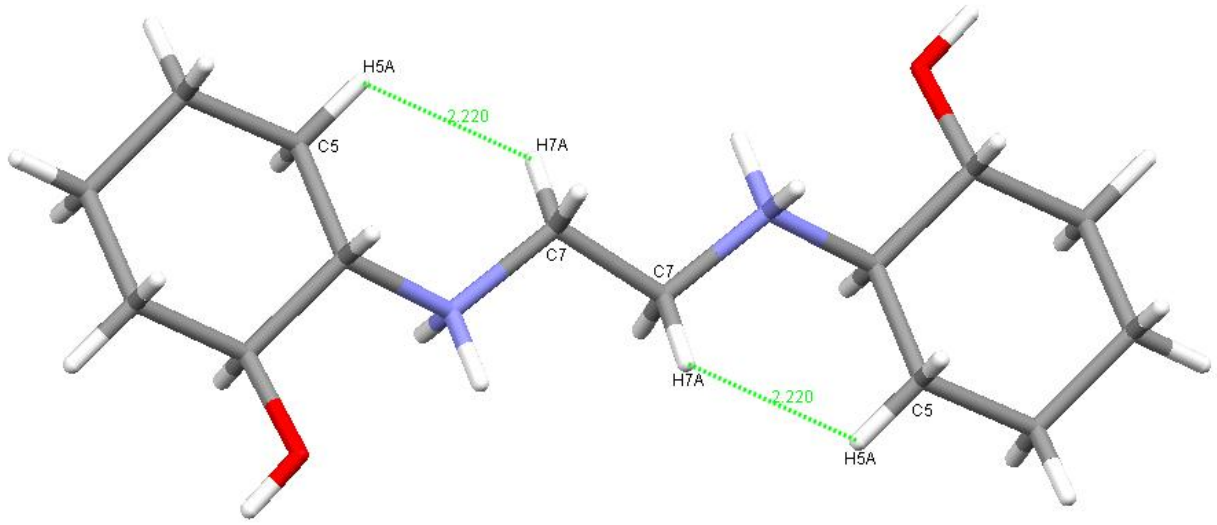


Figure 4.13: The H-H bonds in the chloride salt of Cy_2-en

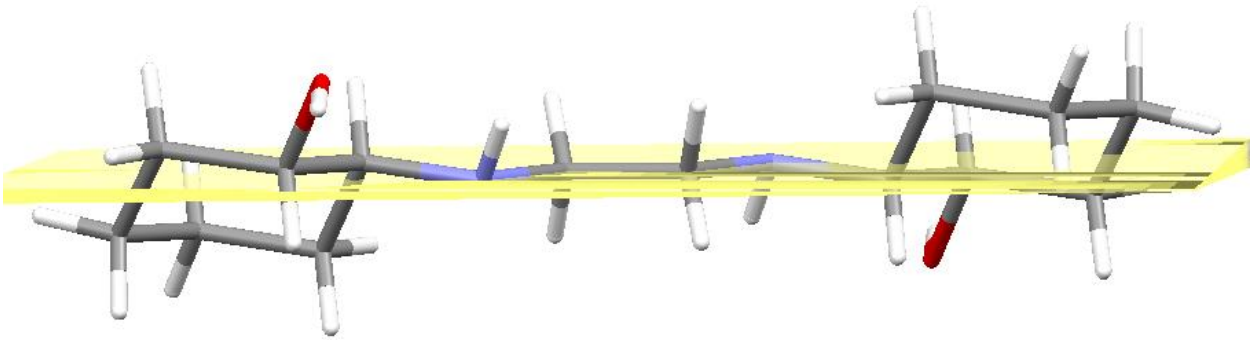


Figure 4.14: The plane defined by the four elements in the ethylene bridge in Cy_2-en

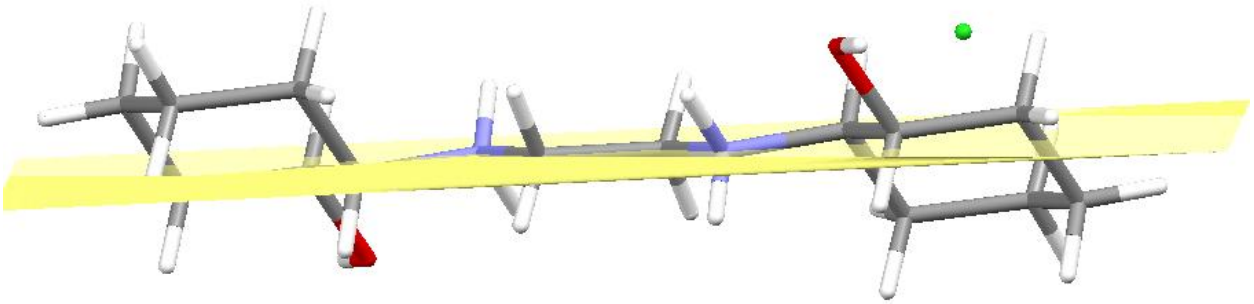


Figure 4.15: The plane defined by the four elements in the ethylene bridge in the Cy_2-en chloride salt

The deviation of equivalent atoms from the mean plane is similar in both structures. The general conclusion is that the ligand in its neutral form is not significantly different to the salt.

The close contact involving the hydrogen atom on the amine and the oxygen group in the alcohol was then examined, Figure 4.16. The distance between the two atoms remains less than the sum of their van der Waals radii. Again, these close contacts are of an attractive nature and most likely have a strong effect on the packing of the molecule so that these attractive forces are optimised. The protonation of the ligand does not affect the crystallisation in a centrosymmetric space group.

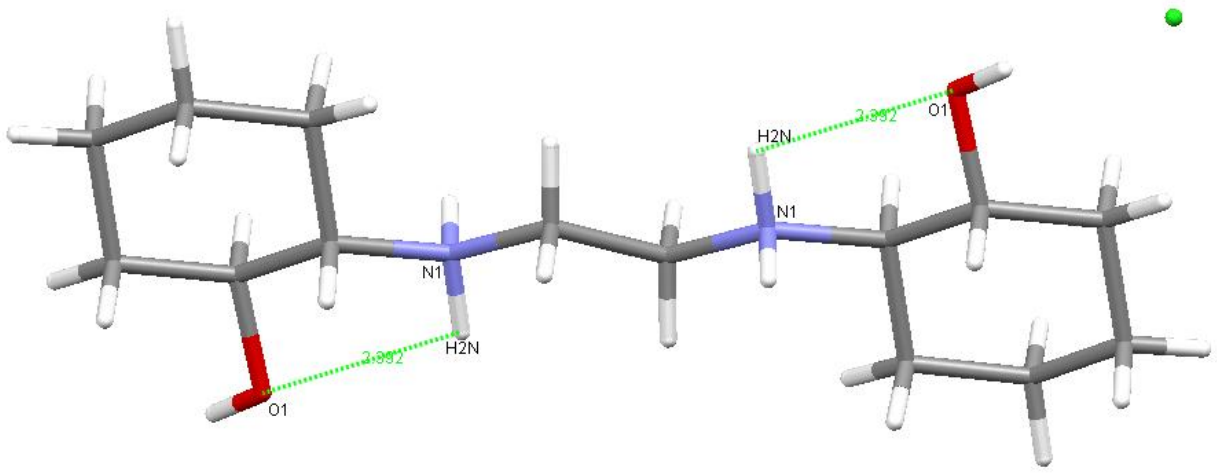


Figure 4.16: The close contact distances between the alcohol oxygen and an amine hydrogen in the chloride salt of Cy_2-en

4.1.2 Synthesis of Cy_2-tn

The same methodology as described for the synthesis of Cy_2-en was used to synthesise the ligand Cy_2-tn. The two reactions produced good yields above 75 %.

No crystals could be obtained of this ligand by slow evaporation of the ligand in water, methanol, or ethanol. The product of each of these evaporations was a fine white powder. No crystal structure was determined but the NMR (Figures B7 to B.10), IR (Figures C.4 and C.5), and MS data (Figures D.4 and D.5) clearly indicated that the desired product had been formed. The ^{1}H NMR had the required number of peaks with the corresponding integrations. These values corresponded to the values reported by De Sousa and Hancock.[1] The same conclusion was reached when the ^{13}C NMR data was analysed. The IR data clearly indicated the presence of OH and NH bands at wavenumbers of 3123 cm^{-1} and 3276 cm^{-1} respectively, but the absence of an epoxide O-C band. At the same time, the MS data gave clear spectra with a strong peak at an m/z value of 271. This corresponded to a Cy_2-tnH^+ molecular ion molecule.

4.1.3 Synthesis of Cy_2-dien

The same methodology as described for the syntheses of Cy_2-en as well as Cy_2-tn was used to synthesise the ligand Cy_2-dien. The two reactions performed gave poor yields of below 40 %. This was attributed to the fact that a far smaller amine to epoxide ratio (1:2.5) was used to the prior two reactions (1:5). This was done so as to avoid a concentration of epoxide that would lead to a tri-substituted product rather than a di-substituted product. Leaving the reaction to run for longer would also have led to this problem arising. Again, no crystals could be obtained that were of XRD quality (only powders were obtained) and so the NMR (Figures B.11 to B.14), IR (Figures C.6 and C.7), and MS data (Figures D.6 and D.7) were carefully analysed to confirm that the desired product had indeed been formed. The MS spectra also gave peaks for the tri-substituted ligand, Cy_3-dienH^+, at an m/z value of 398. There was no evidence of this tri-substituted product in the NMR spectra. This indicated that the product was only present in a very low concentration, and so not visible above the baseline. The IR data could not assist in determining which of the two assumptions was correct. To avoid this product, a lower amine to epoxide ratio should be used or the reaction time should be decreased.

4.1.4 Synthesis of Cy_2-Otn

The method that was used to synthesise the previous ligands could not be used directly as the starting amine for this synthesis, 1,3-diamino-2-propanol, was temperature sensitive. The amine was reacted with the epoxide in ethanol at room temperature for 24 hours. The reaction gave poor yields of between 10 and 39 %. It was noted that the best yield was obtained when the amine sample had been newly opened but as time progressed, the yields decreased. Ultimately, the reaction produced a carbamate of the starting aminoporpanol rather than the required amino alcohol (See Chapter 6 for a discussion of the carbamate).

NMR (Figures B.15 to B.20), IR (Figures C.8 to C.10), MS (Figures D.8 to D.10), and XRD analyses were performed and indicated that the desired product had indeed been formed in

good purity. The crystal data for Cy_2-Otn are given in the Experimental section under Table 2.8 with the full data available in Tables E.13 to E.18.

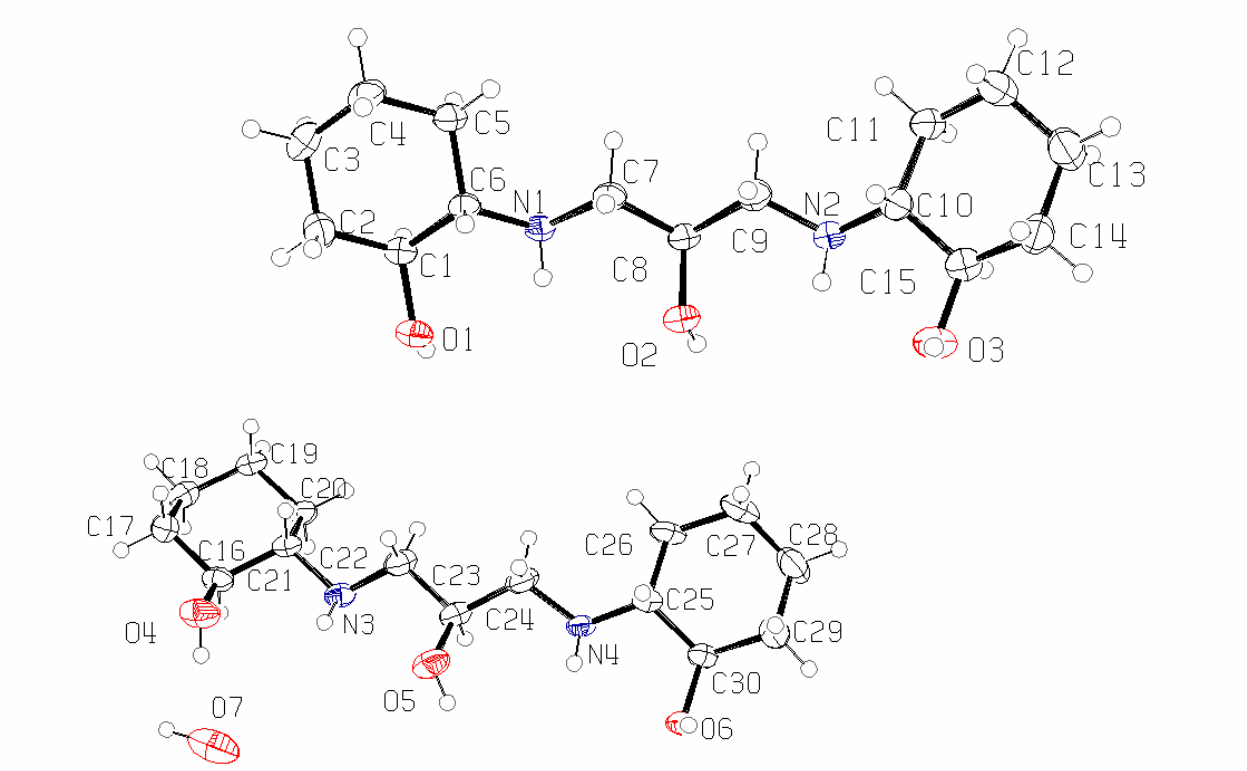


Figure 4.17: The molecular structure of Cy_2-Otn, showing the atom-labelling scheme and 50% probability displacement ellipsoids

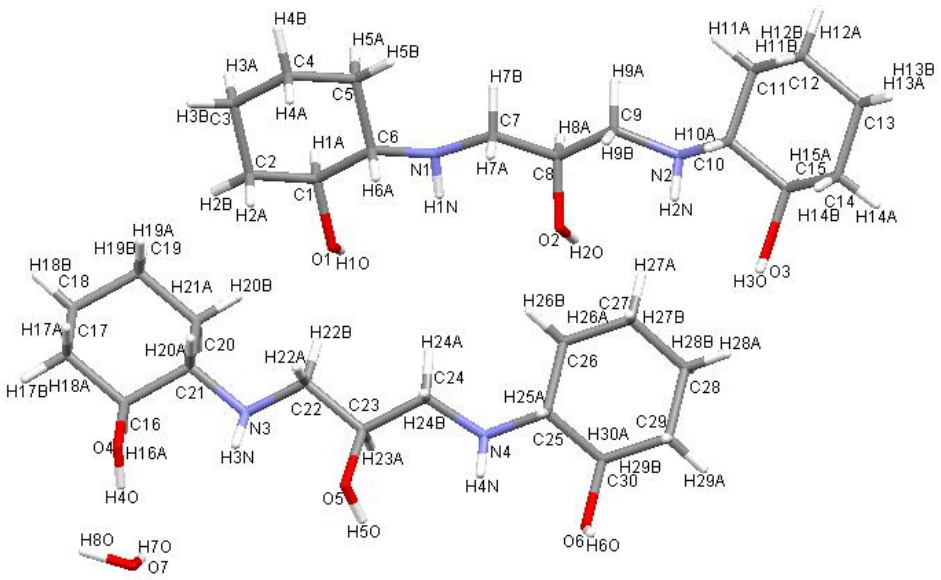


Figure 4.18: The molecular structure of Cy_2-Otn with its labelling scheme (hydrogen atoms included)

Both of the molecules adopt the same type of chirality in that each pair of chiral carbon atoms is either *R* or *S*, i.e. the each molecule has an *S,S,R,R* configuration. The molecule has two molecules in its asymmetric unit each with a planar arrangement.

In both molecules, the two cyclohexenyl rings were on the same side of the plane formed by the five atoms in the propyl bridge, Figure 4.19. If a plane is drawn through the bridging atoms in either molecule, then the two planes are at an angle of 27.92˚ to one another, Figure 4.19. The first of the molecules in the asymmetric unit (containing the carbon atoms C1 to C15 as well as the amine nitrogens N1 and N2) has an r.m.s. fit of 0.0505 Å for the plane through its bridging group. The cyclohexenyl ring with atoms C1 to C6 is inclined at 22.49(8)˚ to this plane whilst the second cyclohexenyl ring is inclined to the same plane at an angle of 49.11(8)˚. The r.m.s. fit indicates that the atoms on the bridge between the two cyclohexenyl rings are quite planar.

The second molecule in the asymmetric unit (the carbon atoms C16 to C30 and the amine nitrogens N3and N4) has a larger r.m.s. for the plane through its bridging atoms, at 0.1079 Å. The atoms are not quite as planar as the abovementioned ones but the r.m.s. still indicates that

there is a good deal of planarity. The cyclohexenyl ring with atoms C16 to C21 is inclined at 63.5(1)˚ to the plane defined by the bridging atoms. The second cyclohexenyl ring is inclined at 29.5(1)˚ to the same plane. The rings on the second molecule are hence inclined at a greater angle than the first molecule. This is most likely due to the presence of the water molecule in the closer vicinity of the second molecule.

In both molecules the rings adopted a chair conformation. The two alcoholic oxygen moieties are on the same side of the molecule and form hydrogen bonds to the water molecule, further alcoholic oxygen moieties, and one of the amine nitrogens, Figure 4.20. This arrangement allows for the maximum number of hydrogen bonds to be formed between the various molecules within the unit cell.

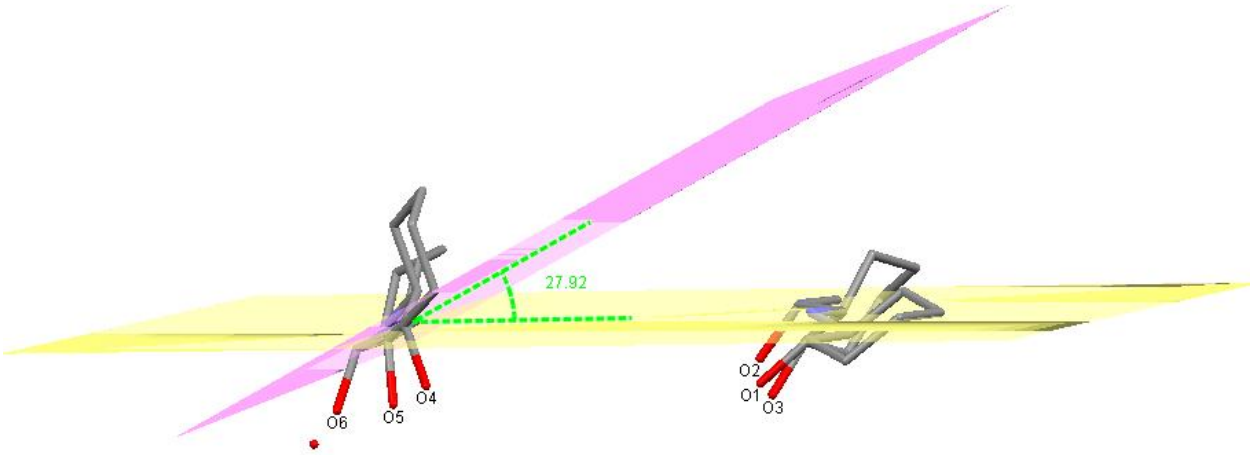


Figure 4.19: The planes defined by the five elements in the propyl bridge in each of the two Cy_2-Otn molecules in the asymmetric unit (hydrogen atoms omitted for clarity)

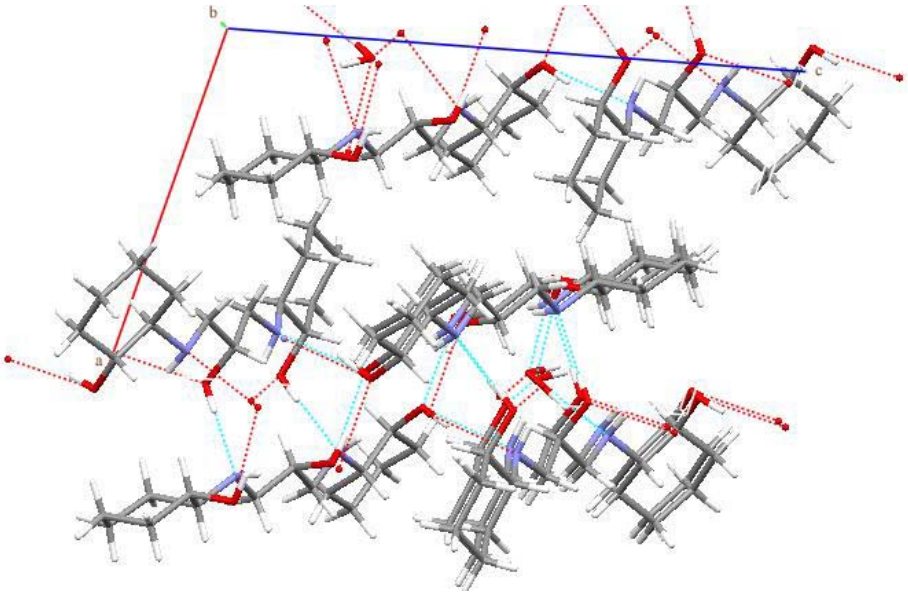


Figure 4.20: Hydrogen-bonding network of Cy_2-Otn, viewed along the *b*-axis

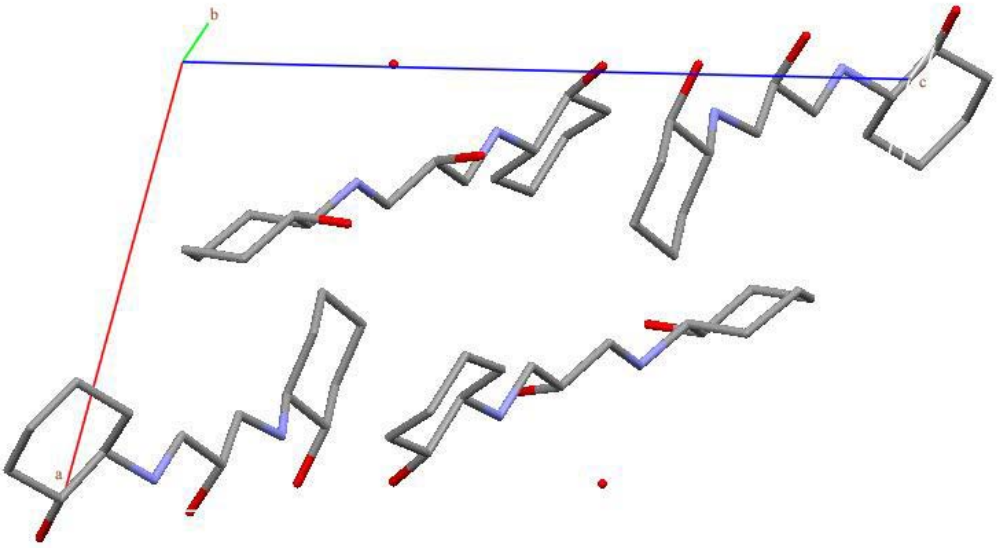


Figure 4.21: Crystal packing of Cy_2-Otn, viewed along the *b*-axis (hydrogen atoms omitted for clarity)

Cy_2-Otn forms alternating layers of transposed molecules that have been rotated through 90˚ to one another. The transposition of the molecule by half a molecule length leads to the cyclohexenyl rings not overlapping but rather interacting via hydrogen bonds with the alcohol group on the propyl bridge.

As with the Cy_2-en molecule, it was of interest to monitor the interaction of the hydrogen atoms on the ring with those on the bridge, and to see if there was a change in the distances once a complex had been formed with the ligand. The H-H bonds and their angles are tabulated in Table 4.2. and shown in Figure 4.22. Again, there was a great deal of contact between the hydrogen atoms on the cyclohexenyl rings and the hydrogen atoms in the bridging atoms.

Table 4.2: H-H Bonds for the Ligand Cy_2-Otn

Atom 1	Atom 2	H-H Bond Distance (Å)	X-H-H Bond Angle (˚), where X denotes a donor atom
H5B	H7B	2.312	104.44 and 109.63
H6A	H7A	2.339	95.87 and 90.65
H7A	H9B	2.362	95.70 and 88.56
H9B	H10A	2.136	98.77 and 97.05
H20B	H22B	2.234	117.59 and 115.76
H21A	H22A	2.315	88.05 and 97.19
H22B	H24A	2.345	96.88 and 90.89
H26B	H24A	2.248	108.16 and 108.84

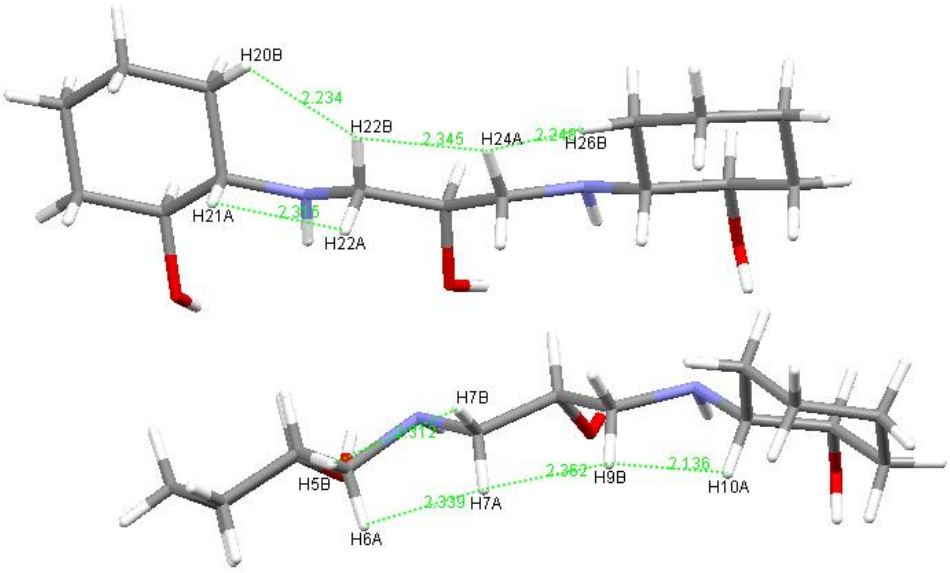


Figure 4.22: The H-H bonds Cy_2-Otn

All of the H-H bonds are within the ranges of previously reported examples.[5] The preferential range is found to be 90˚ to 150˚. Only two readings are below 90˚ but they are close enough not to merit further discussion.

The molecule has further close contacts that are of interest, Figure 4.23. As in the structures of Cy_2-en reported, the oxygen atoms on the cyclohexenyl rings have strong attractive interactions with the hydrogen atoms on the amine groups. In addition to these interactions, the alcoholic oxygen on the propyl bridge also interacts very closely with the amine hydrogen on one side.

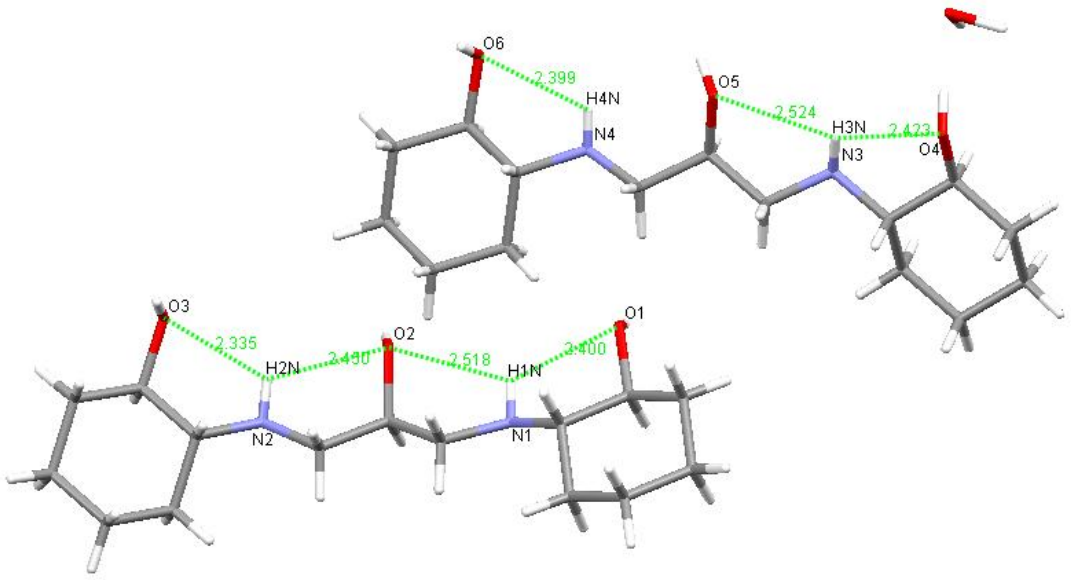


Figure 4.23: Close contacts involving hydrogen and non-hydrogen atoms in Cy_2-Otn

4.1.5 Crystallisation of BHEEN

In an attempted complexation reaction of BHEEN with the lead salt PbO and ammonium nitrate, crystals of the nitrate salt of BHEEN were obtained that yielded an XRD structure of the nitrate salt of the ligand, Figure 4.25. All crystallographic data are given in Tables E.19 to E.24.

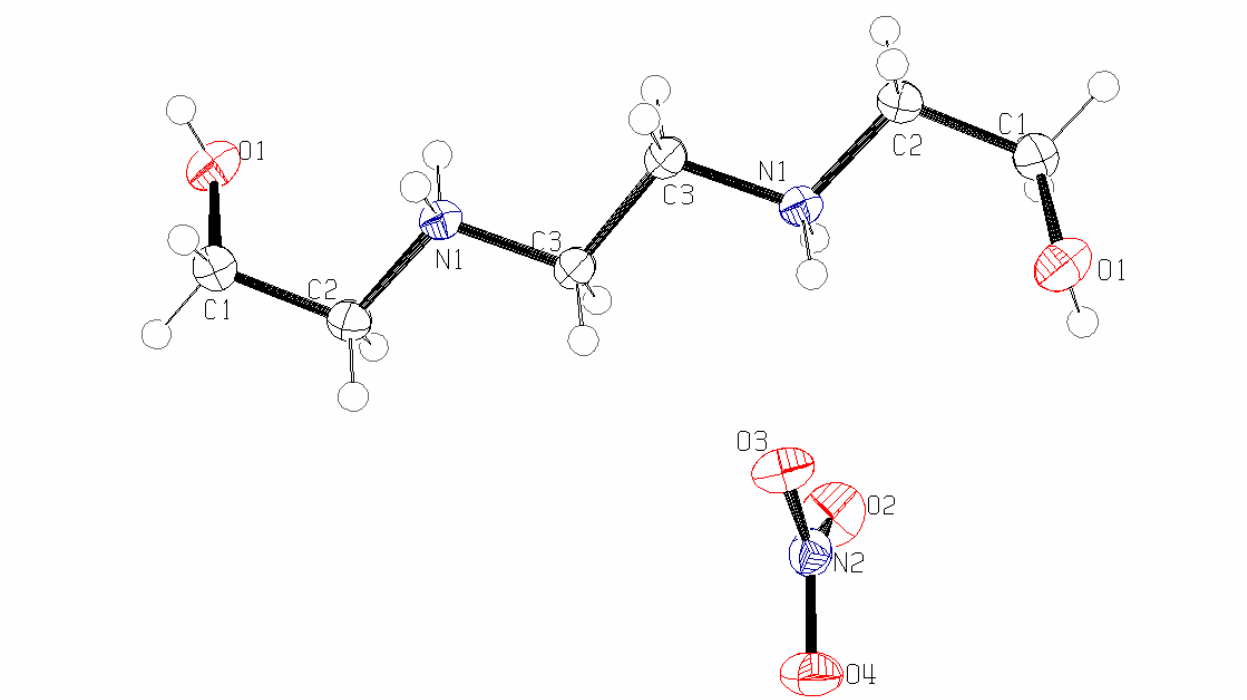


Figure 4.24: The molecular structure of the nitrate salt of BHEEN, showing the atom-labelling scheme and 50% probability displacement ellipsoids

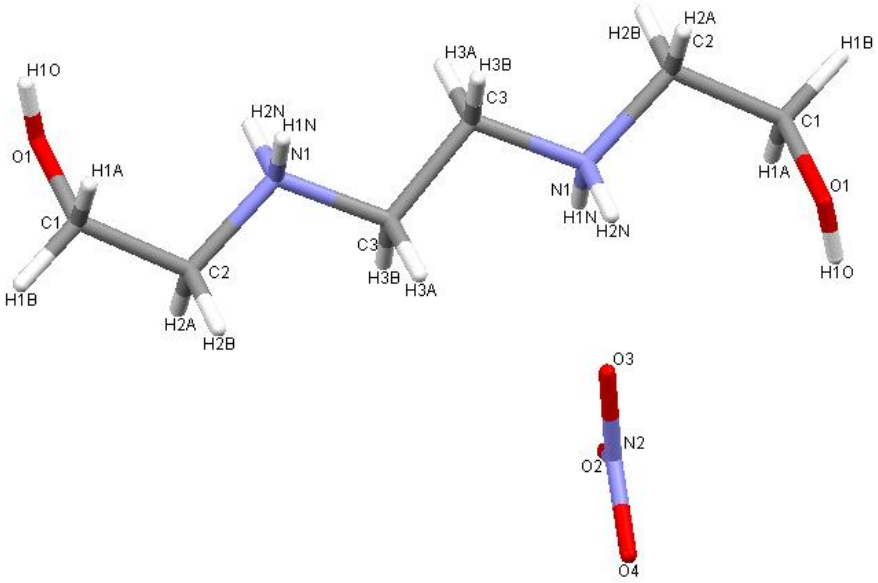


Figure 4.25: The molecular structure of Cy_2-Otn with its labelling scheme (hydrogen atoms included)

The molecule is completely planar, Figure 4.26. The two alcoholic oxygen moieties are on opposite sides of the molecule to minimise any steric interactions. The hydrogen bonding network is interesting in that all hydrogen bonds exist between the BHEEN molecule and the nitrate ions surrounding it. No hydrogen bonds are formed between BHEEN molecules in different layers, Figure 4.27. This leads to the hydrogen bonds extending in only two dimensions. The hydrogen bonds are all short (well below 2.87 Å) and have angles above 165°. These bonds are very strong and significantly affect the packing arrangement of the molecules within the unit cell. The nitrate ions effectively shield individual BHEEN cations from interacting with one another.

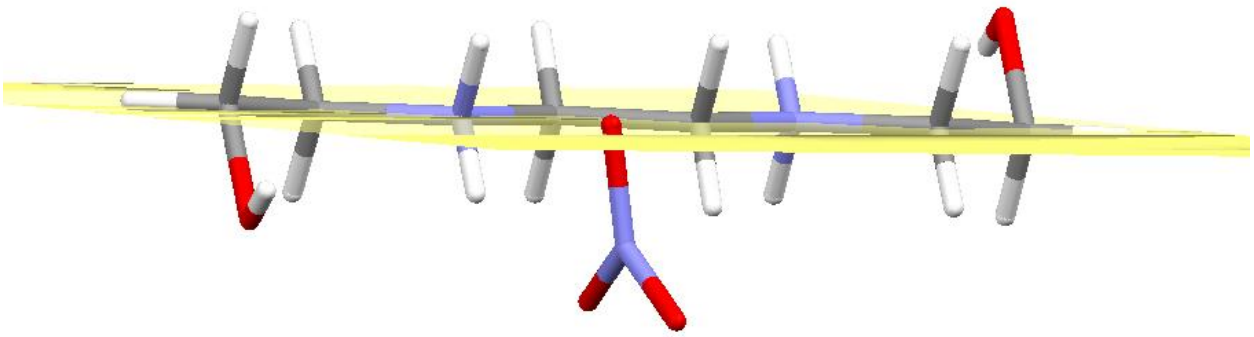


Figure 4.26: The plane defined by the two amine nitrogen atoms and the two carbon atoms in their midst in the nitrate salt of BHEEN

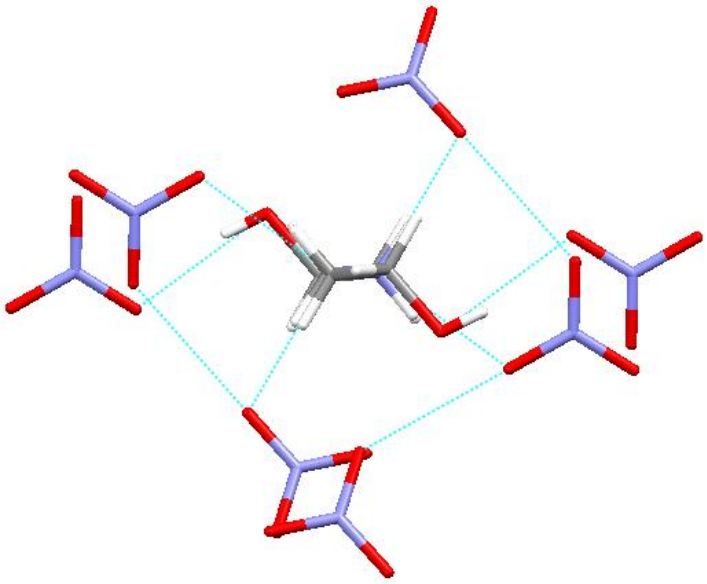


Figure 4.27: Hydrogen-bonding network of the nitrate salt of BHEEN

The ligands arrange themselves in a herringbone-type structure, Figure 4.28. This allows the particular type of hydrogen bonding observed in this structure to be optimised.

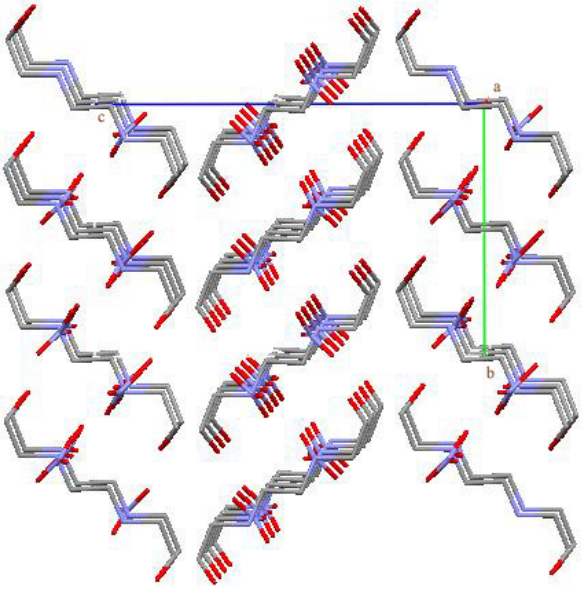


Figure 4.28: The 2D packing arrangement of the nitrate salt of BHEEN (H atoms omitted for clarity) showing the herring-bone type arrangement of the molecules

There are no H-H bonds between the hydrogen atoms on the central ethylene group and the two ethylene groups on either side. There are, however, a great deal of close contacts that involve hydrogen atoms interacting with non-hydrogen atoms such as oxygen and nitrogen, Figure 4.29. These close contacts are summarised in Table 4.3.

Table 4.3: Close Contacts for the Nitrate Salt of BHEEN

Atom 1	Atom 2	Close Contact Distance (Å)
H1N	H3A	2.307
H2N	H3B	2.316
H2N	O1	2.518
H2N	O3	2.031
H3A	O3	2.494

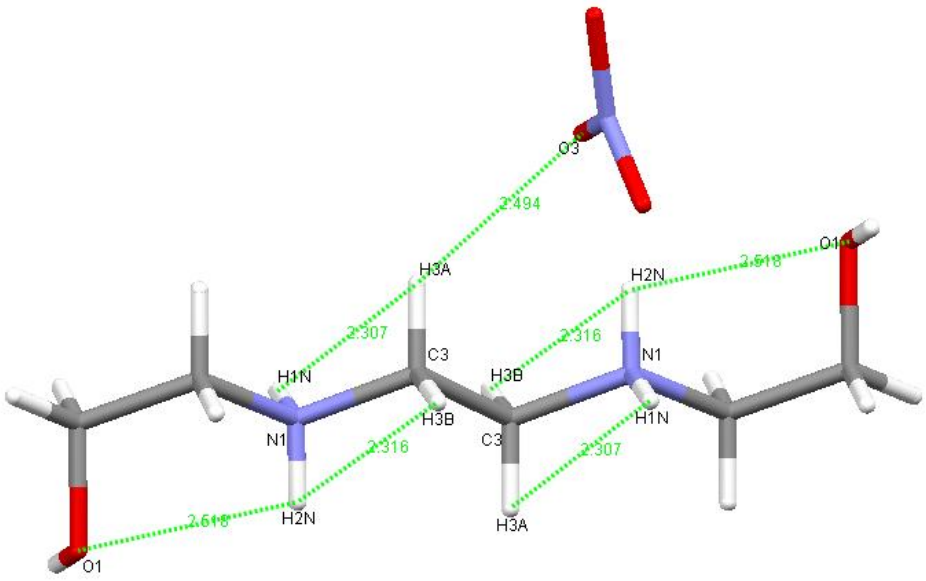


Figure 4.29: Close contacts involving hydrogen and non-hydrogen atoms in BHEEN

Each of the amine hydrogens is involved in an attractive interaction with an oxygen atom. These interactions are all attractive and strongly affect the manner in which the BHEEN molecule packs.

4.1.6 Comparison of the Ligands

The synthetic route to obtain the three ligands, Cy_2-en, Cy_2-tn, and Cy_2-dien, is the same but produced very different yields for the three ligands. This can be attributed to the nature and size of the starting amine. The increase in the number of carbons on the amine decreases the solubility of the amine in polar solvents and affects the degree to which the amine interacts with the polar epoxide. The ligand Cy_2-Otn gives low yields due to the nature of the starting amine; it is readily reacts with the carbon dioxide in the atmosphere. This was only discovered once the starting amine had been opened and the sample not stored under an inert atmosphere. It is advisable to henceforth store the starting amine under nitrogen or argon between 4 and 8 ˚C. The temperatures are the ones advised by the manufacturer, Sigma-Aldrich.

The solid state structures of Cy_2-en and Cy_2-Otn are similar. Both the ligands are almost planar with the cyclohexenyl rings bisecting the planes. The cyclohexenyl rings do adopt different geometries though; the alcoholic oxygen groups face away from one another in Cy_2-en but in Cy_2-Otn they are on the same side of the molecule. In either case, this arrangement is adopted to maximise the number of hydrogen bonds that can be formed between the various molecules. Both molecules also have H-H bonds between atoms on the ring and atoms on the carbon bridge.

When the BHEEN molecule is compared to Cy_2-en, it becomes apparent that the addition of the cyclohexenyl rings does not aid in pre-organisation of the ligand for complexation. Neither BHEEN nor Cy_2-en show pre-organisation for complexation. The solid state structures hence do not explain the complexation behaviour observed for these ligands.[8] The change in log *K* values on going from BHEEN (denoted DHEEN in the diagram) complexes to Cy_2-en complexes, with this change being denoted by $\Delta\log K_1$, indicates that the latter forms the more

stable complexes with the metal ions studied, Figure 4.30. This may be attributed to the addition of the cyclohexenyl rings, or perhaps lends credence to the assumption made that the hydrogen-hydrogen close contacts between the hydrogens on the ring and on the bridge affect the complex stability. This conclusion can of course only be verified when the solid state structures of many more complexes are determined and their neutron and XRD structures compared. Further thermodynamic data would also have to be gathered to fully verify the results.

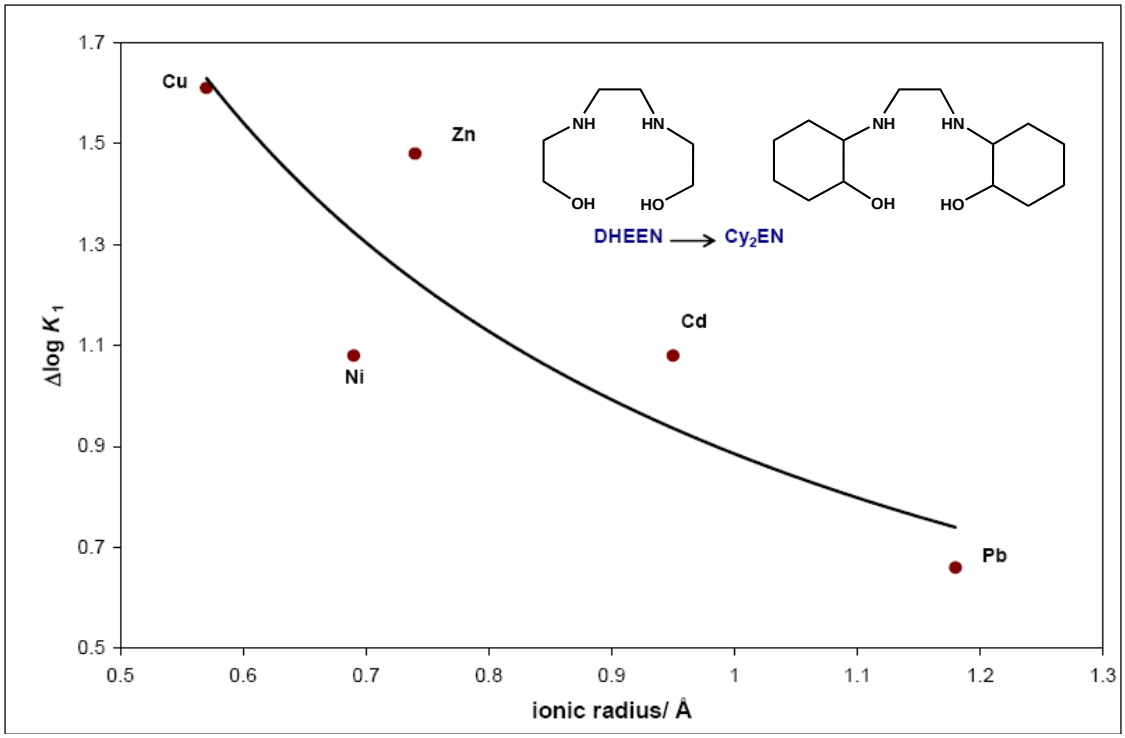


Figure 4.30: Plot of change in complex stability relating to metal ion size when passing from BHEEN (or DHEEN) to Cy_2-en.[8]

The close contacts involving the amine nitrogens and the alcoholic oxygens are a commonality amongst all of the structures. These strong attractive interactions strongly affect the manner in which the molecules pack in the unit cell. In all cases, the molecule is rotated in such a manner that the alcoholic oxygen groups are on the same side of the molecule as the closer amine hydrogens.

4.2 Synthesis and Characterisation of the Lead Complexes

Several methods were used to find an ideal method to form the desired complexes. Cy_2-en was used as the ligand of choice for these reactions as it was a readily available starting material. Due to the insoluble nature of the lead complexes, once formed, no NMR analyses could be conducted.

4.2.1 Synthesis of the Cy_2-en/Pb Complex

The first method used, as described in Chapter 2, was a method described by Sienkiewicz and Kokozay[9] which they used to synthesise several lead(II) complexes with TEA. It was decided to leave the reaction to run for longer than the stipulated 2 hours as TEA is an oil and Cy_2-en is a solid. It took considerably longer for the Cy_2-en to dissolve in the DMF than TEA. Furthermore, the reaction temperature was lowered to 100 ˚C rather than the 160 ˚C described in the literature. This was done as the available oil baths became unstable above a temperature of 140 ˚C.

Once the reaction had been completed, it was observed that the solution had changed from a clear colour to a murky brown. This was attributed to the degradation of the DMF. The black, tar-like substance that remained behind was washed repeatedly with acetone until clear, brick-like crystals formed. They were not a lead complex but rather an imidazolinium salt. This imidazolinium salt is described in detail in Chapter 6.

The next method used involved the use of water as a solvent and lead(II) nitrate as the metal salt. It was hoped that this would avert the degradation problem encountered in the first reaction. TEA had previously been reacted with lead(II) under such conditions to form a complex.[10] No reaction took place and the sole product collected was the free ligand.

The above method using water was then modified and a third reaction performed using a lead(II) chloride salt instead of a nitrate salt. Again, the sole product obtained was the ligand,

but in this case the ligand was collected in the form of a chloride salt and its structure analysed by XRD.

The same method was then used for a fourth reaction. A lead(II) carbonate salt was used in place of the nitrate or chloride salt. Only the free ligand was recovered.

The synthetic route that led to the successful complexation of lead(II) with Cy_2-en was a modification of the first method used. It was decided that the reaction be done as indicated in the literature with the exception of the addition of the isopropanol. The isopropanol was initially added so as to separate the unreacted starting material from the complex. Cy_2-en was too sparingly soluble in isopropanol for the addition of the alcohol to be viable.

The complex was analysed by MS (Figure D.15) and FTIR spectroscopy (Figure C.14). None of the MS methods used, in particular APCI and ESI, were gentle enough for the complex to survive the initial ionisation process. Hence the MS data indicated that only the ligand was present. This finding was contradicted by the XRD analysis as well as the IR spectrum which indicated a metal-nitrogen bond. The general region for a metal-nitrogen bond is in the region of 600 to 500 cm^{-1}.[11] Two peaks in the IR spectrum were used as markers to determine whether or not a complex had formed: (i) the appearance of a new band in the 600 cm^{-1} region indicated a metal-nitrogen bond, and (ii) the shift of the N-H stretch band. When the complex forms, the NH groups are normally bonded to the central metal ion and the result is that the N-H bonds are weakened. This weakening of the bond was evident in the shift of the band by up to 200 cm^{-1} to a lower wavenumber. The NH band was found at a value of around 3280 cm^{-1} for the free ligand but that band shifted to a value of 2935 cm^{-1} for the complex. The Pb-N stretching and bending bands also appeared between 700 and 600 cm^{-1}.

The XRD structure of this complex was determined. It showed the chemical formula to be $[Pb(Cy_2\text{-en})(NO_3)](NO_3)$. The structure is given in Figure 4.32. The R-factor of 1.96% is very low and implies that the crystal used is of good quality and the resultant data set well interpreted.

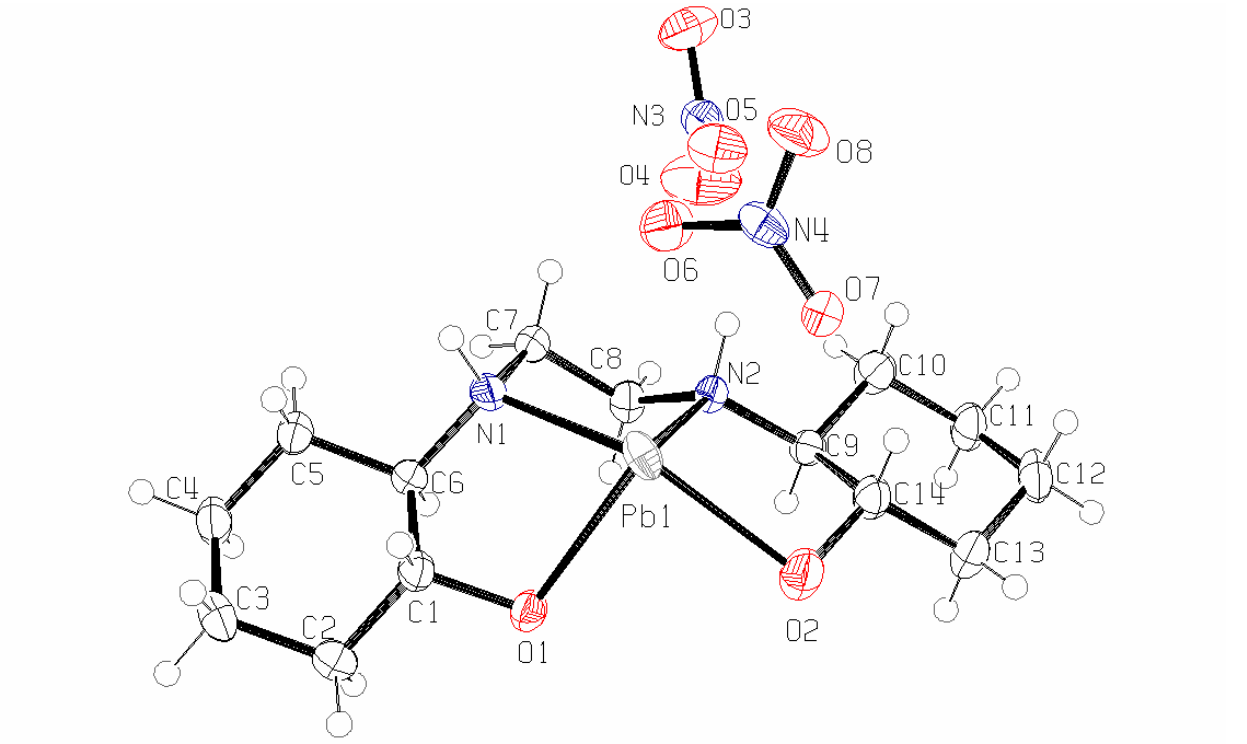


Figure 4.31: The molecular structure of the lead(II) complex of Cy_2-en, showing the atom-labelling scheme and 50% probability displacement ellipsoids

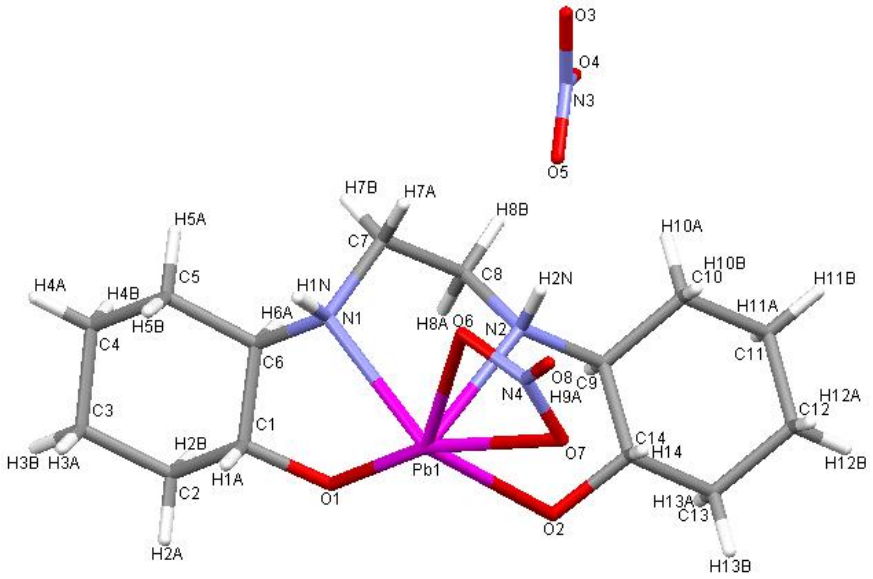


Figure 4.32: The molecular structure of the lead(II) complex of Cy_2-en with its labelling scheme (hydrogen atoms included)

The complex ligand retains its *R,R,S,S* chirality upon complexation. It must be noted that the hydrogen atoms on the two alcohol groups could not be placed. This may be the result of one of two possibilities: (1) an inability by the solving software to account for the hydrogen atoms, or (2) the lead ion is now in the +4 oxidation state. The latter of the two is unlikely as there is evidence of a stereochemically active lone lair of electrons on the metal ion. This is only possible if the lead is in the +2 oxidation state. The structure clearly indicates that the lead(II) ion assumes a distorted six coordinate geometry. A seventh coordination site seems vacant and can be attributed to a stereochemically active lone pair of electrons on the lead(II) ion.[12] According to Shimoni-Livny *et al.*[12] the above complex would be classified as having a hemidirected lead(II) metal ion, i.e. the lone pair is stereochemically active. This was not unexpected as the authors found that hard ligand donors, such as the ones found in the ligand Cy_2-en, favour this arrangement. The holodirected geometry clearly supports the behaviour shown in solution. Lead complexes with certain ligands tend to be more stable than expected when one plots the relative selectivities of the free ligands and the complexes formed by them with various metal ions.[8] Due to the stereochemically active lone pair, the lead(II) ion appears to have a smaller ionic radius than if the lone pair of electrons were inactive. Several such examples have previously been reported in the literature[10,13,14] although no quantitative values for this phenomenon were given.

This phenomenon would explain why the lead(II) complexes of Cy_2-en are more stable than expected in solution. Upon complexation Cy_2-en forms five-membered chelate rings with the metal ion. The ideal M-N bond lengths for complexes with en and tn are given in Figure 4.33.[15,16] These values are derived from MM work done to determine the conformation that would be required for the electrons on nitrogen donor atoms to interact in the most efficient manner with the electron-poor metal ion.



Figure 4.33: The ideal bond lengths for chelate rings with en and tn respectively[15,16]

The average bond length for a Pb(II)-N bond is found to be 2.62(11) Å.[12] Thus, if the effective ionic radius of the lead(II) ion decreases , the stability of the complex would increase as the value of the Pb(II)-N bond tends toward the ideal value of 2.5 Å. This decrease in radius is caused by the stereochemically active lone pair of electrons on the lead(II) ion.

The complex formation changes the arrangement of the four donor atoms in the ligand, Figure 4.34. The molecule is no longer planar and the lead(II) ion does not occupy the cavity formed by the ligand but rather sits 1.394 Å above the plane defined by the four ligand donor atoms. The r.m.s fit of these four atoms to the plane is calculated to be 0.2341 Å. The coordinated nitrate ion is inclined at an angle of 42.02(8)˚ to this plane, whilst the plane defined by the atoms O1, O6, and O7 is found to be at an angle of 39.28(9)˚ to the plane defined by the four ligand donor atoms.

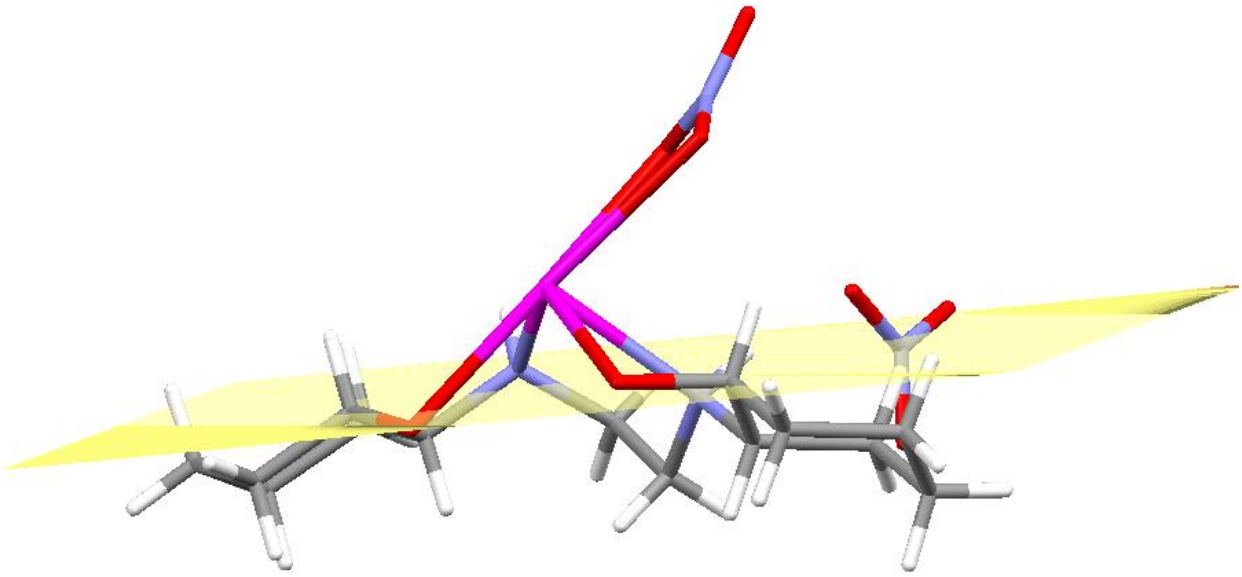


Figure 4.34: The plane defined by the four donor moieties in the ligand Cy_2-en upon complexation to lead(II)

The complex was then analysed to see if there was any evidence of a stereochemically active lone pair of electrons. It is noted that one side of the complex has vacant coordination sites, Figure 4.35, and all of the remaining coordination sites are on the opposite side of the plane

defined by the two coordinated oxygen moieties on the nitrate ion and one of the alcoholic oxygen moieties on the ligand. In this arrangement the lead(II) ion is bisected by the plane.

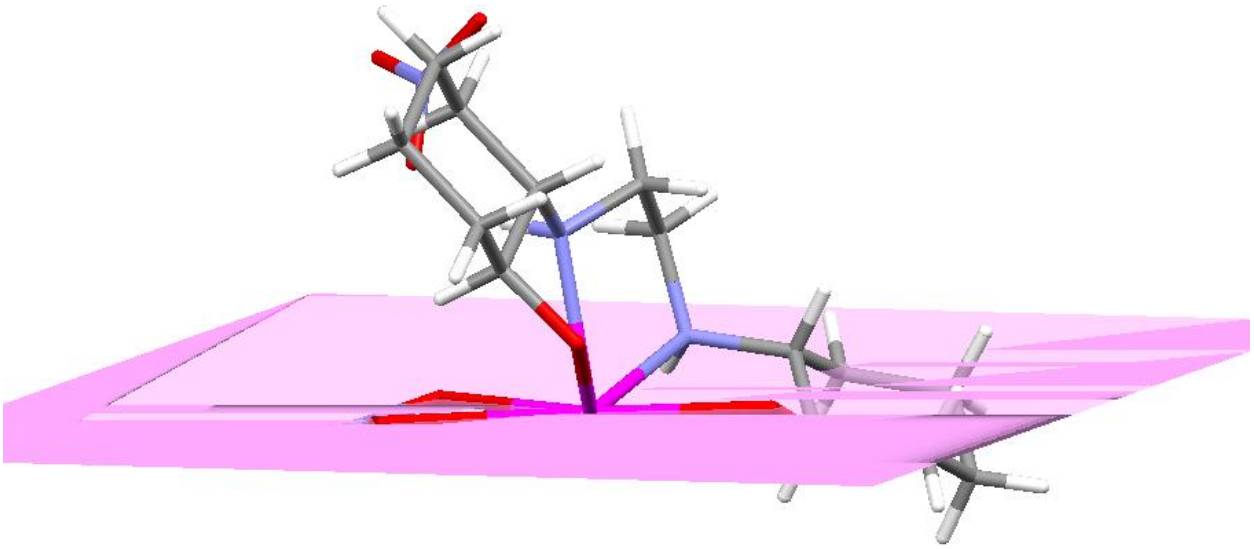


Figure 4.35: The plane defined by the two coordinated oxygen moieties on the nitrate ion and one of the alcoholic oxygen moieties on the ligand Cy_2-en upon complexation to lead(II)

The hydrogen bonding network of the complex extends in one dimension only, Figure 4.36. There is a strong interaction between the nitrate oxygen atoms and the alcohol groups on the complex. Although the hydrogen atoms on these alcohols have not been placed, there seems to be a non-bonded interaction between the atoms. This possible hydrogen bonding arrangement leads to the packing occurring in such a way that the cyclohexenyl rings of the complex overlap in the separate layers as do the metal complex ions, Figure 4.37 and 4.38.

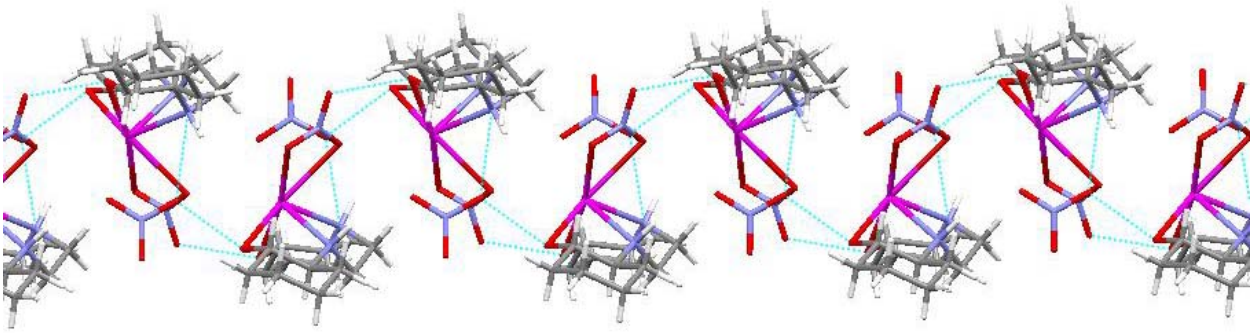


Figure 4.36: The possible hydrogen-bonding network of the complex of lead(II) with Cy_2-en

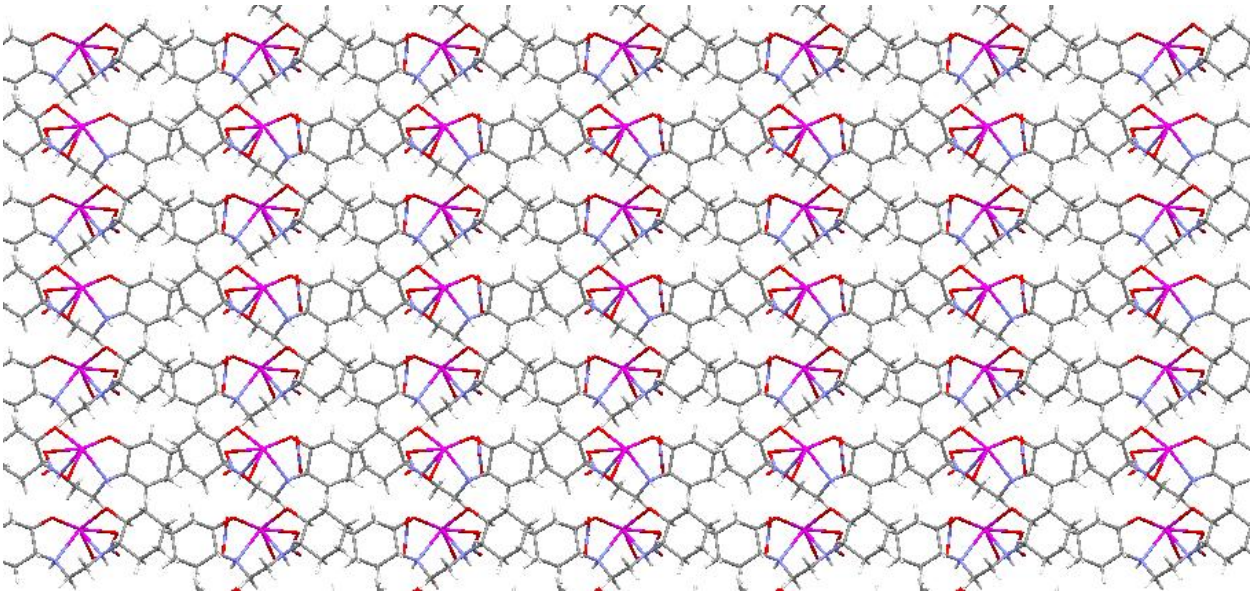


Figure 4.37: The layered arrangement of the complex of lead(II) with Cy_2-en showing the parallel arrangement of the cyclohexenyl rings as well as the metal ions in layers

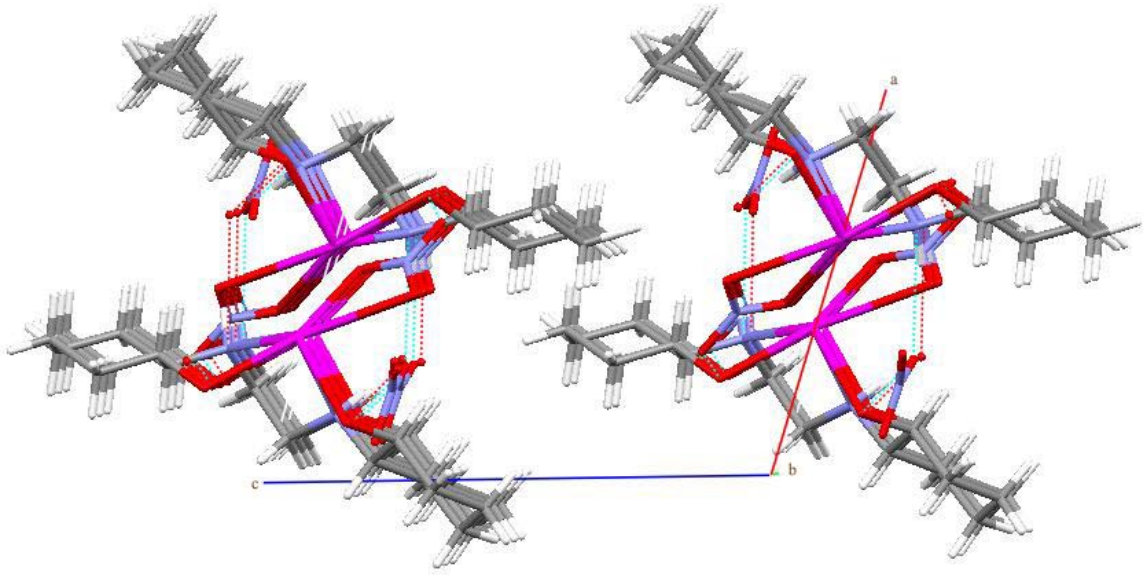


Figure 4.38: The packing of the lead(II) complex with Cy_2-en viewed along the *b*-axis

The number of H-H bonds remain the same when the free ligand and the complex are compared, Table 4.4. The figure depicting these distances is Figure 4.39.

Table 4.4: H-H Bonds for the Lead(II) Complex of Cy_2-en

Atom 1	Atom 2	H-H Bond Distance (Å)	X-H-H Bond Angle (˚), where X denotes a donor atom
H8A	H9A	2.338	98.53 and 85.66
H2N	H10B	2.314	84.20 and 104.33
H6A	H7B	2.285	88.75 and 91.27
H1N	H5B	2.278	84.87 and 104.60

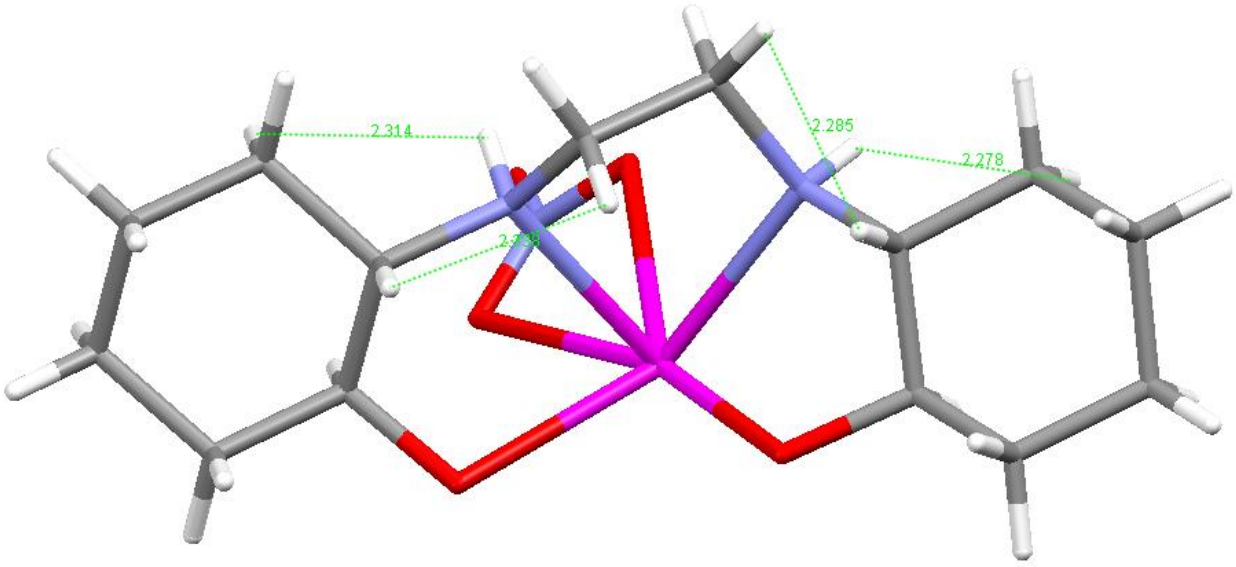


Figure 4.39: The H-H close contacts of selected hydrogen atoms in the lead(II) complex of Cy_2-en

The nature of the H-H bonds changes once the complex has formed. All of the H-H bonds in the complex are between atoms where there has been no H-H bond in the free ligand. The average distance for the H-H bonds in the free ligand was 2.204 Å. The average distance for the complex is 2.304 Å. Thus, the H-H bond distances have increased upon complexation. It will be further investigated if the change in these interactions affects complex stability.

4.2.2 Attempted Synthesis of the Cy_2-tn/Pb Complex

The synthetic route was the same as the one that led to the successful synthesis and characterisation of the lead(II) complex of Cy_2-en. A product did form, but if proved insoluble in acetone, water, DMF, dioxane, and isopropanol, as well as mixtures of the above solvents. It was found that the complex did dissolve in dilute nitric acid but in the process the complex broke apart and the free ligand was regenerated. It was therefore not possible to determine the solid state structure of the complex.

The IR and the MS data could not provide evidence of the formation of the complex. The IR spectrum showed no shifts in the N-H stretch band and there was no evidence of a Pb-N band in the 600 cm^{-1} region. The MS spectrum indicated only a peak for the free ligand with no evidence whatsoever of any lead in the sample. This directly contradicted the observed changes in the solubility of the product collected as the change in solubility was attributed to a complex formation.

A possible explanation for these contradicting results would be that the product used for the analyses contained a far larger amount of the ligand than the complex and as such the observed peaks, in particular in the IR spectrum, were of the ligand and the complex peaks were overshadowed by these peaks. As stated at the start of the chapter, due to insolubility of the complex in the available NMR solvents no NMR's could be run to confirm the formation of the complex.

4.2.3 Synthesis of the Cy_2-dien/Pb Complex

The complex was synthesised as described for the complexation of lead(II) with Cy_2-en. As described in the synthesis of the lead(II) complex with Cy_2-tn, the lead(II) complex of Cy_2-dien also proved insoluble in all solvents tested. The sole solvent that seemed to dissolve the complex was dilute nitric acid, and this led to the regeneration of the free ligand. The product could not be crystallised in any manner and thus no solid state structure could be determined.

The IR data did indicate the formation of the complex as the N-H peak had shifted from a value of 3248 cm^{-1} to 3265 cm^{-1}, and a new band for the Pb-N stretch at 682 cm^{-1} had appeared in the spectrum. The MS data did not support this conclusion as all that was found was a peak for the free ligand. This was not surprising as the MS data had not been useful for any of the previous samples studied. No NMR investigation was undertaken due to solubility issues described previously.

4.2.4 Synthesis of the Cy_2-Otn/Pb Complex

As with the other lead complexes, the same method was used that had led to the successful synthesis of the Cy_2-en complex. Due to the instability of the starting amine, the ligand was handled with care and not subjected to high temperatures. The solution was only heated to 50 ˚C for one hour and then cooled to room temperature. The product obtained was recrystallised from several different solvents and crystals obtained. These crystals were of too poor a quality to use for diffraction purposes.[i]

The IR data indicated that the desired complex was formed. This was confirmed by the shift of the N-H band as well as the appearance of Pb-N stretch bands at wavenumbers of 695 and 682 cm^{-1}, whilst the Pb-N bending band appeared at a wavenumber of 610 cm^{-1}.

4.2.5 Synthesis of the BHEEN/Pb Complex

The synthetic route that led to a successful complexation of lead(II) with BHEEN was modified from the initial procedure by leaving the reaction to proceed at room temperature. Unlike some of the previous samples, this lead(II) complex was soluble in water, methanol, and ethanol (although only sparingly). The sample was redissolved in these solvents and attempts were made to grow crystals of XRD quality but these attempts proved unsuccessful.

The IR data clearly indicated that the lead(II) complex had been formed when the N-H peak shifting from 3267 cm^{-1} to 2945 cm^{-1}, and the Pb-N stretch band at 680 cm^{-1} as well as the Pb-N bending peak at 619 cm^{-1} were observed. The MS data also supported this conclusion as the data showed both a mono-substituted and a di-substituted species. No conclusion as to the nature of the actual complex could be made as it was unclear as to whether the mono- or di-substituted species was present, or if the product was a mixture of both. NMR's of the samples

[i] Unfortunately at the time of the submission deadline mass spectra for this compound were not yet available.

were prepared but because less than 1 mg of the product went into solution, data collection was not possible.

4.2.6 Comparison of the Lead Complexes

Only one of the five attempted complexations of the ligands with lead yielded crystals that were of suitable quality to run XRD experiments. Due to solubility issues with the other four complexes, all attempts at recrystallisations failed.

The analyses performed on the complexes yielded mixed results. Whilst the IR data clearly indicated complex formation (if it occurred), the MS data failed to detect the lead complex ions in all but one case. Further analytical methods must be investigated as indicators of lead complexations.

No structural features of the complexes, apart from the lead(II) complex of Cy_2-en, could be determined as there was insufficient data to do so.

4.3 Synthesis and Characterisation of the Cadmium Complexes

No NMR's could be run on any of samples as the cadmium complexes made were too sparingly soluble in the available NMR solvents.

4.3.1 Synthesis of the Cy_2-en/Cd Complex

The method described by Naiini and co-workers[17] led to a successful synthesis of the desired complex of cadmium(II) with Cy_2-en. The complex is a monomeric species with two chloride ions as ligands.

MS data (Figure D.19) were collected but the data failed to indicate the formation of the desired complex. The IR data (Figure C.19), on the other hand, indicate that the reaction has been successful and this finding is supported by the change in physical properties of the product when compared to the starting materials. Crystals that were suitable for XRD analysis were obtained and the resultant structure determined, Figure 4.41.

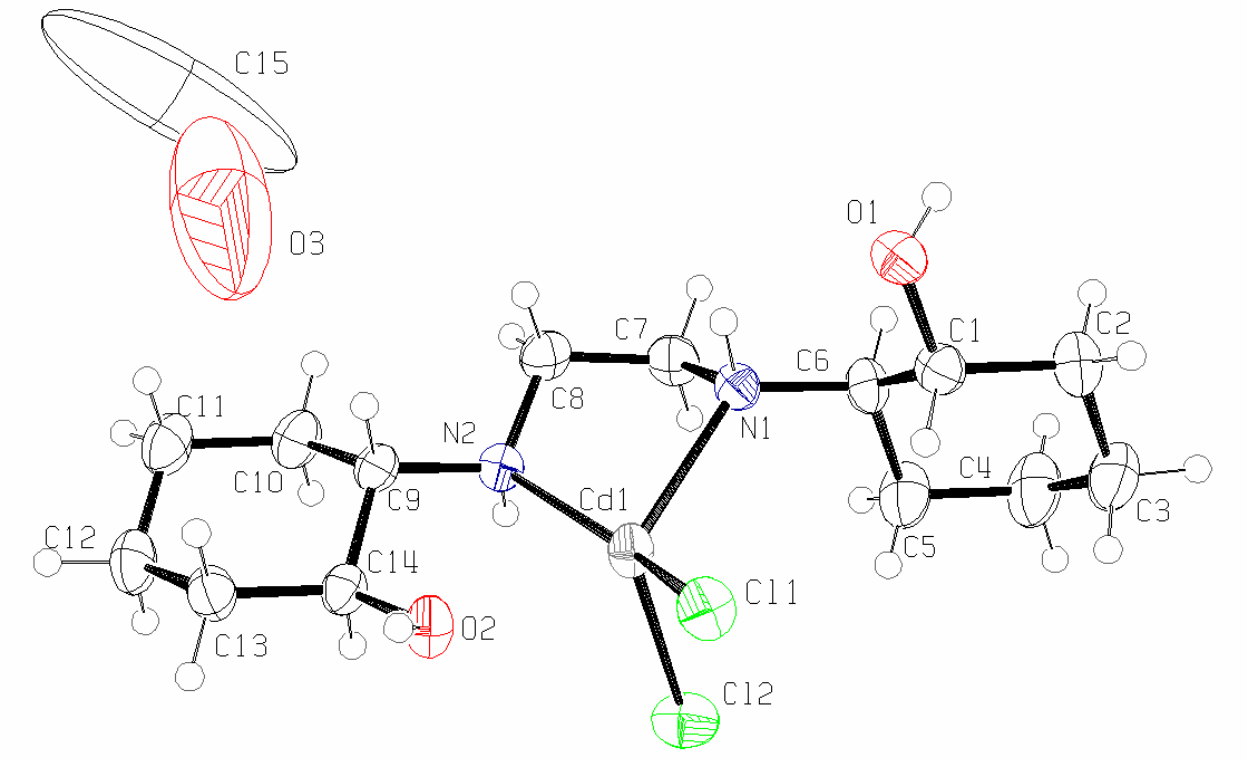


Figure 4.40: The molecular structure of the cadmium(II) complex of Cy_2-en, showing the atom-labelling scheme and 50% probability displacement ellipsoids

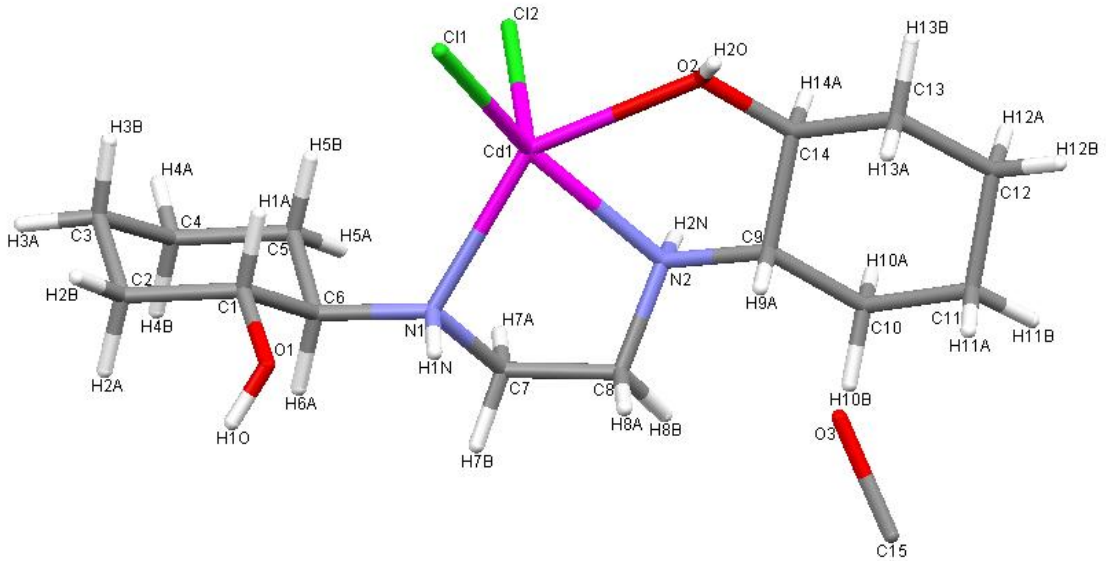


Figure 4.41: The molecular structure of the cadmium(II) complex of Cy_2-en with its labelling scheme (hydrogen atoms included)

The compound has a methanol molecule included in the crystal lattice. Due to the disordered nature of the methanol the hydrogen atoms on the solvent molecule cannot be placed.

The structure has a clearly defined square pyramidal structure with one of the chloride ions, the one bonded oxygen atom and both of the nitrogen atoms defining a plane with an r.m.s. of 0.3059 Å, Figure 4.42. The cadmium ion is located 0.487 Å above this plane.

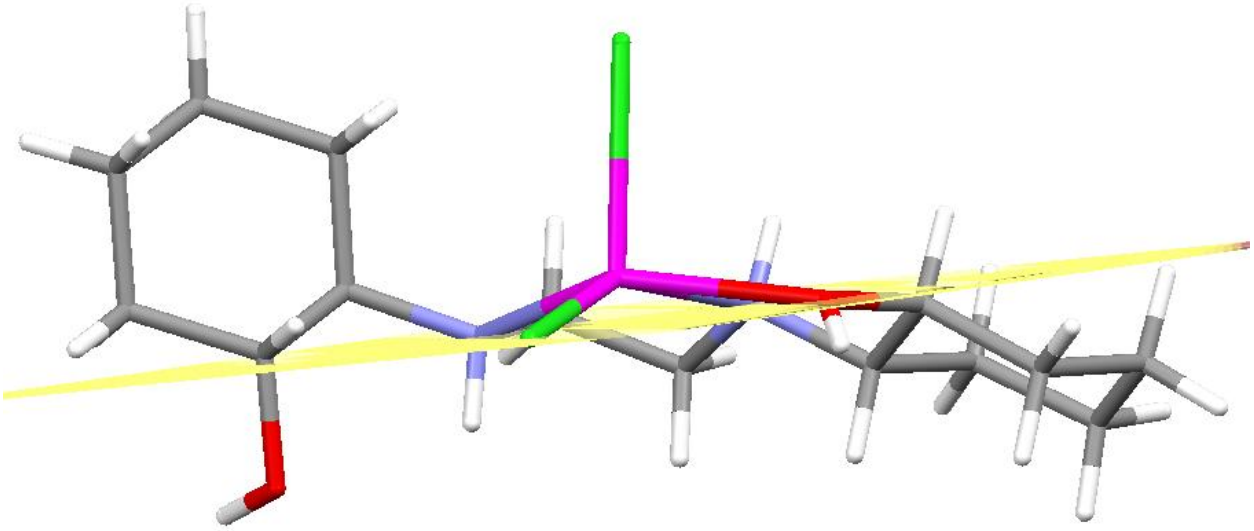


Figure 4.42: The plane defined by the two nitrogen atoms, the one coordinated oxygen atom, and one of the chloride ions in the cadmium(II) complex of Cy_2-en

Only one of the alcohol groups is coordinated to the metal ion. The Cd-O bond length is 2.384 Å, while the non-bonded Cd-O distance is 4.341 Å. Each cyclohexenyl ring is perpendicular to the other in the complex. This arrangement of the rings leads to the one alcoholic oxygen atom being too far away from the cadmium ion to form a bond with it.

As indicated in Figure 4.33, the ideal M-N bond length for a five-membered chelate ring with an ethylene bridge is calculated to be 2.5 Å. The observed M-N bond lengths for this complex are 2.362 Å and 2.335 Å. In the literature, the average value for this bond length is found to be 2.283 Å by Allen[18] and the statistical average of all such bonds in the CSD is found

to be 2.407 Å. The measured bond lengths are thus longer than both of the averages but still less than the ideal value for a five-membered chelate ring.

The hydrogen bonding network of the cadmium(II) complex of Cy_2-en is limited to an interaction between two complex molecules, Figure 4.43. The hydrogen bonding pattern formed is interesting as it forms between two centrosymmetrically related complex molecules.

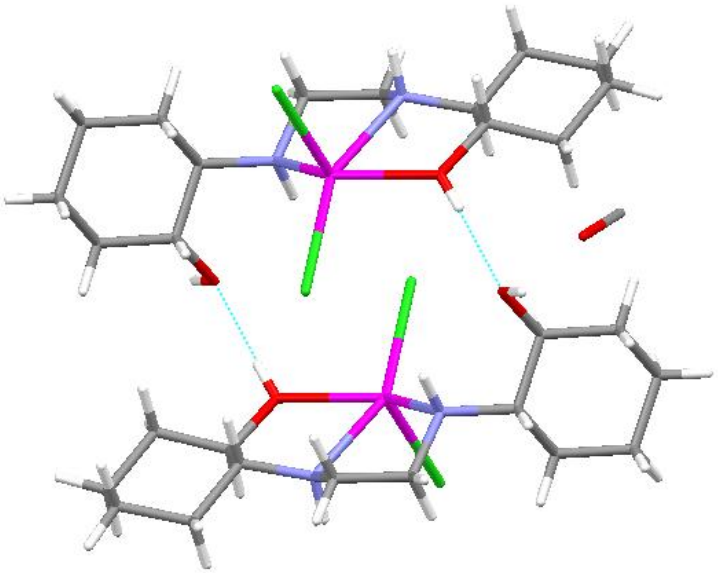


Figure 4.43: The hydrogen-bonding network of the cadmium(II) complex of Cy_2-en

Each unit cell contains two complex molecules, Figure 4.44. The molecules are arranged in such a manner that the cyclohexenyl rings face one another and the complex metal centres are at opposite ends of the unit cell, Figure 4.45.

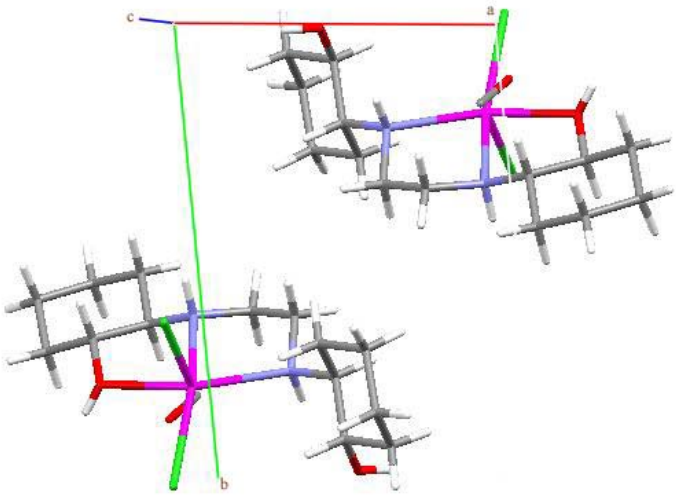


Figure 4.44: The packing of the cadmium(II) complex of Cy_2-en viewed along the *c*-axis

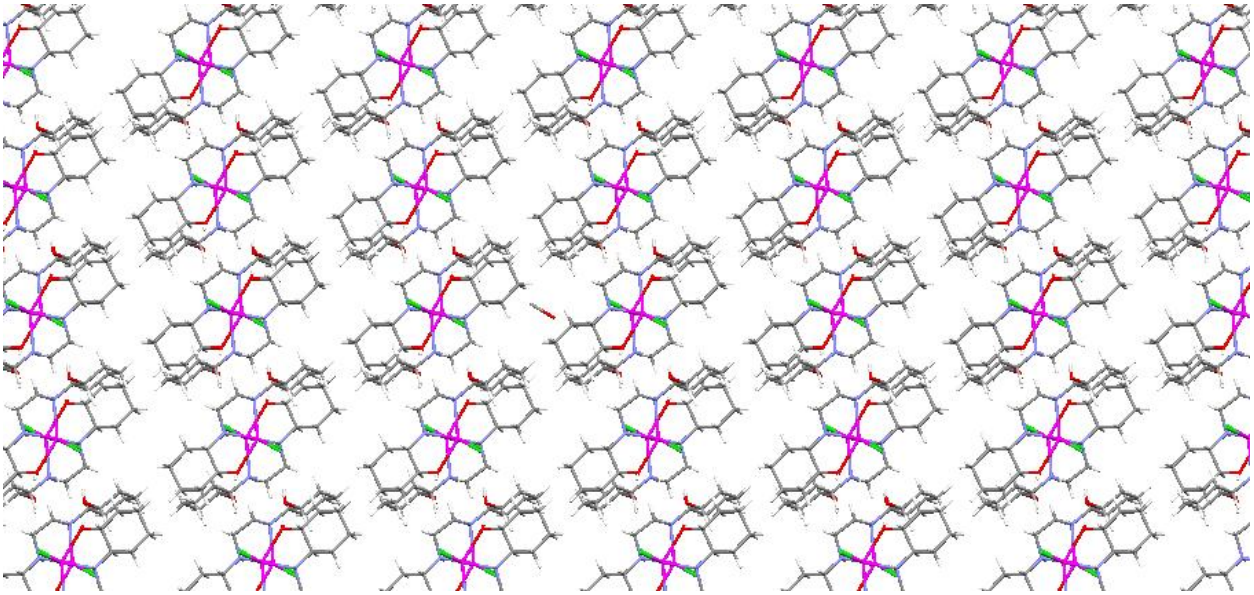


Figure 4.45: The layered arrangement of the complex of cadmium(II) with Cy_2-en showing the parallel arrangement of the cyclohexenyl rings as well as the metal ion centres

The number of H-H bonds remains constant upon complexation when the number of bonds in the free ligand and the complex are compared, Table 4.5. The diagrammatic representation of these H-H bonds is given in Figure 4.46.

Table 4.5: H-H Bonds for the Cadmium(II) Complex of Cy_2-en

Atom 1	Atom 2	H-H Bond Distance (Å)	X-H-H Bond Angle (˚), where X denotes a donor atom
H5A	H7A	2.270	115.97 and 115.42
H6A	H7B	2.308	90.87 and 97.30
H8A	H9A	2.371	92.31 and 93.96
H8B	H10B	2.381	110.86 and 105.87

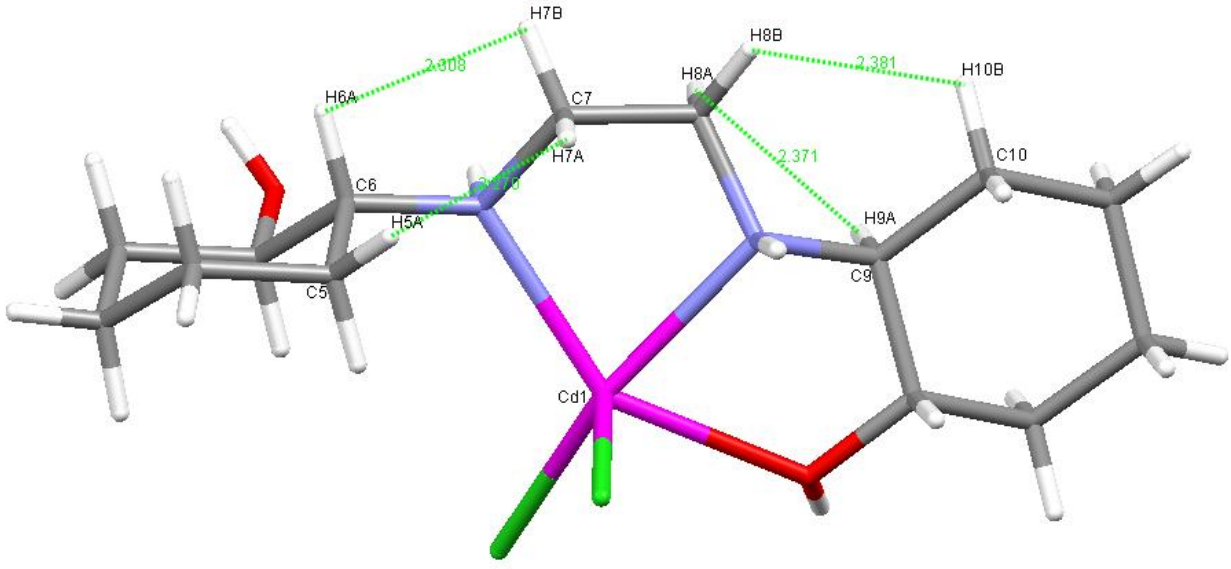


Figure 4.46: The H-H close contacts of selected hydrogen atoms in the cadmium(II) complex of Cy_2-en

The nature of the H-H bonds changes upon complexation. Interestingly, the H-H bond involving an amine hydrogen and a CH is no longer found. The new H-H bonds are all formed between a hydrogen atom on a bridging carbon and a hydrogen on a carbon in the ring. The average distance for the H-H bonds in the free ligand is 2.204 Å. The average distance for the complex is 2.266 Å. The H-H bond distances have increased upon complexation.

The close contacts between the amine hydrogen atoms and the alcoholic oxygens are also examined and found to have altered. The alcoholic oxygen group that coordinated to the cadmium ion no longer has a close interaction with the amine hydrogen but the uncoordinated moiety does, Figure 4.47. Instead, the alcohol now forms hydrogen bonds that are stronger and more energetically favourable to the simple close contacts.

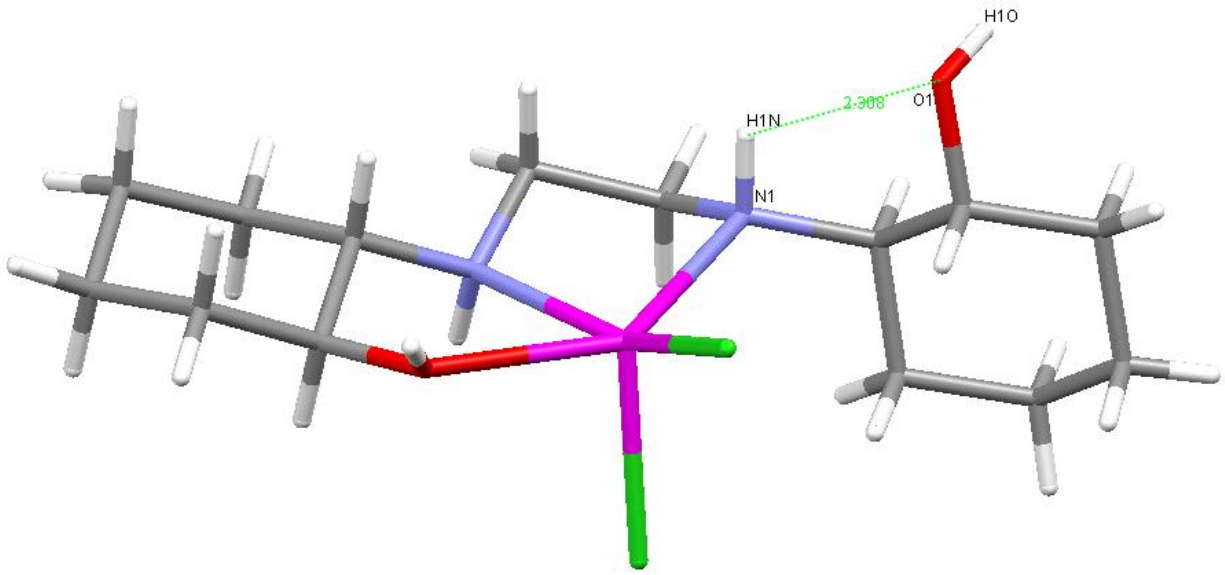


Figure 4.47: Close contacts involving hydrogen and non-hydrogen atoms in the cadmium(II) complex of Cy_2-en

The conclusion is that the H-H bonds as well as the close contacts do indeed affect the coordination behaviour in some small manner. It must also be noted that the H-H close contacts become longer in the complex when compared to the free ligand. Furthermore, the close contacts on the side of the ligand where the oxygen atom does not coordinate to the metal ion are shorter than on the other side. Clearly, the central metal ion affects these interactions by

weakening them as is indicated in the lengthening of the contact lengths if the donor atom (in this case the nitrogen or the oxygen) is coordinated to the metal ion.

4.3.2 Synthesis of the Cy_2-tn/Cd Complex

The same method as described for the synthesis of the cadmium(II) complex of Cy_2-en was used to make the cadmium(II) complex of Cy_2-tn. Several attempts were made to recrystallise the product from methanol but all attempts were unsuccessful and only a polycrystalline powder was obtained.

The IR data (Figure C.20) indicated that the desired complex had been formed but no information as to the exact chemical composition could be made. The NH band shifted from a wavenumber of 3276 cm^{-1} to a value of 3255 cm^{-1}. This conclusion was not supported by the MS data which only indicated a peak for the protonated ligand. This was not surprising as the same MS processes had failed to indicate the formation of the lead(II) complexes. NMR's proved unsuccessful and yielded no useable spectra as the solubility of the complex was too low and no proper signals could be determined above the baseline.

4.3.3 Attempted Synthesis of the Cy_2-dien/Cd Complex

The same method was used to make this complex. The product obtained was the free ligand. No evidence of complex formation could be found in either the IR or MS data. The reaction was performed twice with the same result.

About half of the starting ligand was regenerated leading to the assumption that the product formed was a monomeric species. No analytical data could be generated to substantiate this assumption.

4.3.4 Synthesis of the Cy_2-Otn/Cd Complex

The method used to form the cadmium(II) complex of Cy_2-Otn was similar to the process used thus far with the sole modification that the reaction was performed at room temperature due to the thermal instability of the starting ligand. Several attempts were made to recrystallise the complex from methanol but the process proved unsuccessful. Only the powder precipitated.

The analytical data, both IR and MS, indicated that the product had formed. The regeneration of approximately half the ligand starting material as well as the MS data indicated that the product was most likely a monomeric species.

4.3.5 Synthesis of the BHEEN/Cd Complex

The identical method as described for the synthesis of the cadmium(II) complex of Cy_2-en was used. Both IR (Figure C.23) and MS data (Figure D.24) clearly indicate complex formation. The MS data also shows a range of various fragments of the complex as well as the isotopic distribution of cadmium. The complex forms a dimer, as shown in Figure 4.49.

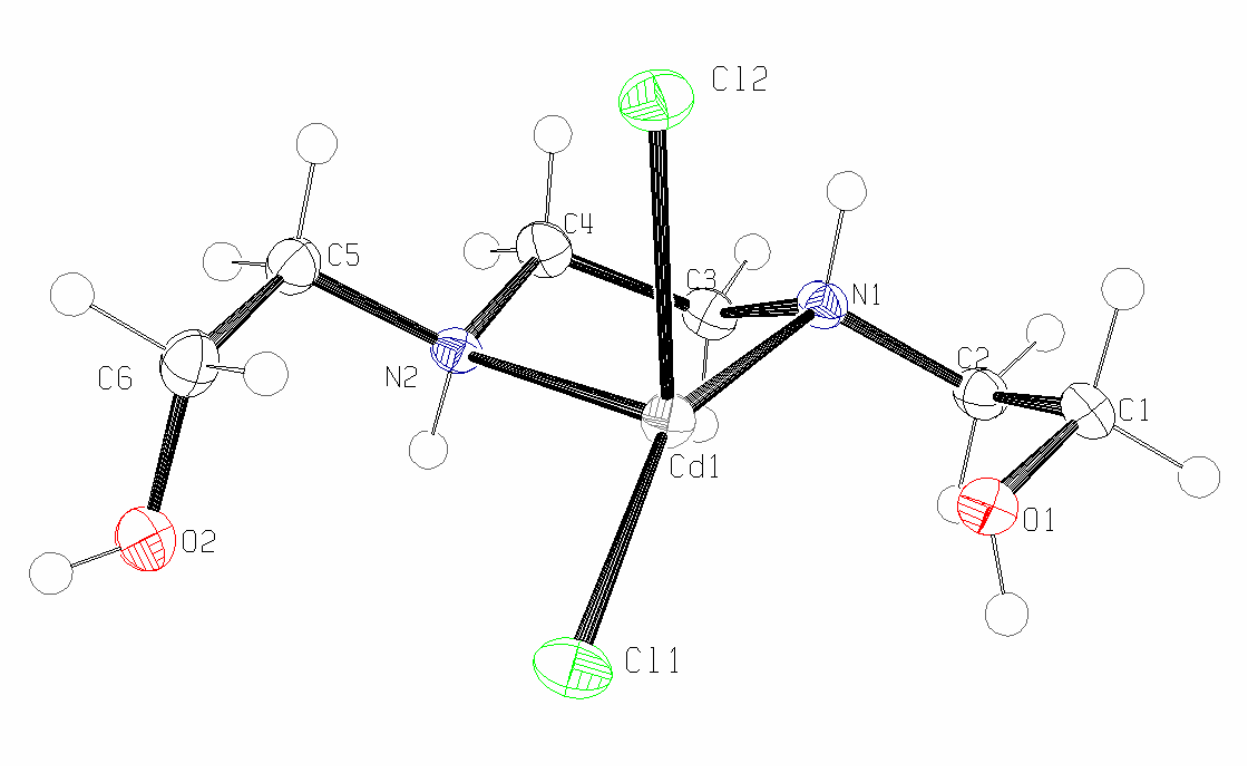


Figure 4.48: The molecular structure of the cadmium(II) complex of BHEEN, showing the atom-labelling scheme and 50% probability displacement ellipsoids

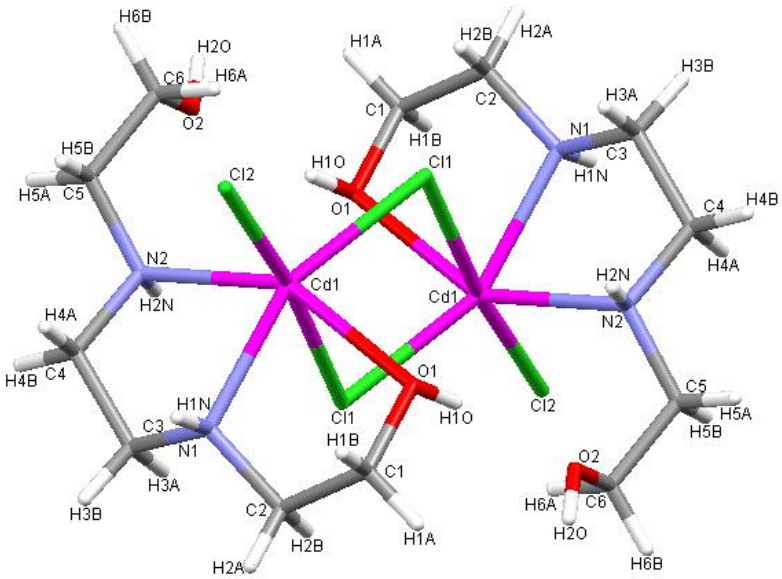


Figure 4.49: The molecular structure of the cadmium(II) complex of BHEEN with its labelling scheme (hydrogen atoms included)

No solvent molecules are present in the unit cell. The given solution assumes that each of the cadmium ions has a distorted octahedral geometry.

A plane is plotted through the two amine nitrogen atoms, the one coordinated alcoholic oxygen atom, and the co-planar chloride ion, Figure 4.50. The cadmium ion is located 0.341 Å above the plane defined by these atoms.

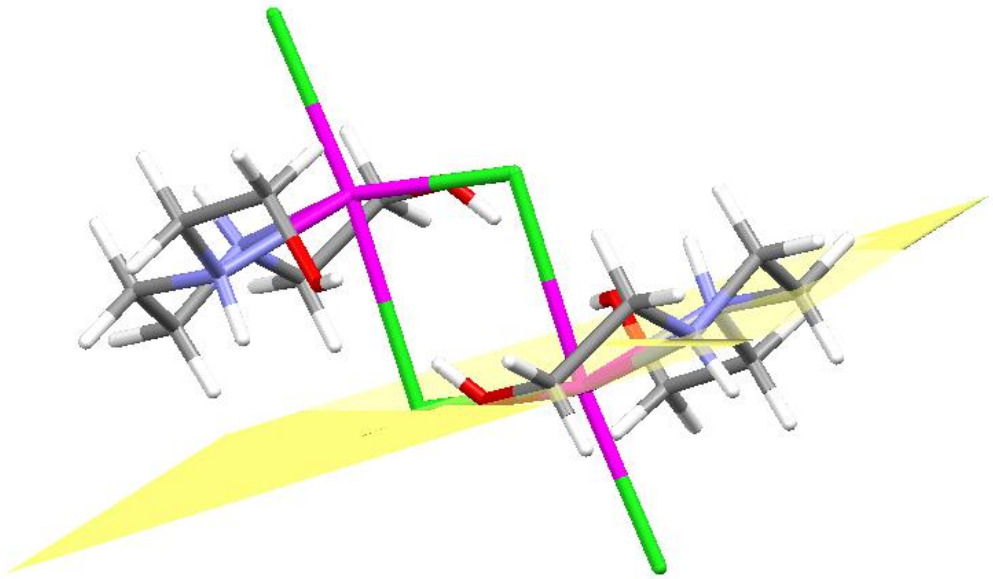


Figure 4.50: The plane defined by the two nitrogen atoms, the one coordinated oxygen atom, and one of the chloride ions in the cadmium(II) complex of BHEEN

Again, only one of the oxygen moieties on the ligand forms a bond to the central metal ion. The Cd-O bond length is 2.403 Å long whilst the distance between the cadmium(II) ion and the nonbonded oxygen atom is 4.010 Å, which is clearly too long for a bond.

The average M-N bond length calculated for this complex is 2.324 Å. This is less than the ideal bond length of 2.5 Å indicated in Figure 4.33.

The complex molecule has both intra- and intermolecular hydrogen bonds, Figure 4.51. The intermolecular hydrogen bonds are formed between the non-bonded alcoholic oxygen atoms and the chloride ions on co-planar molecules.

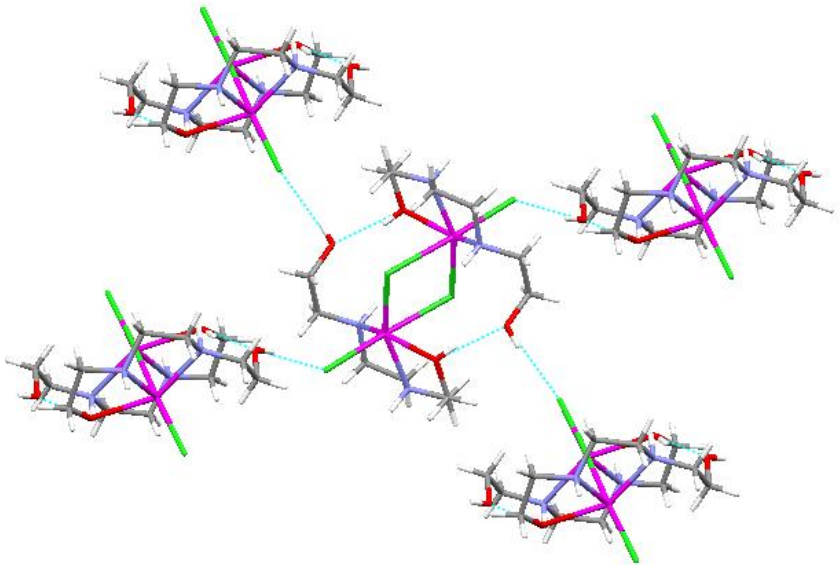


Figure 4.51: The hydrogen-bonding network of the cadmium(II) complex of BHEEN

If viewed along the *a*-axis, the molecules arrange themselves so that two layers form, Figure 4.52. One layer contains the bulk of the molecule, whilst the second contains only the side-arm of the molecule containing the nonbonded oxygen atom.

If the molecule is viewed along the *c*-axis, the interwoven nature of the molecule can be seen, Figure 4.53.

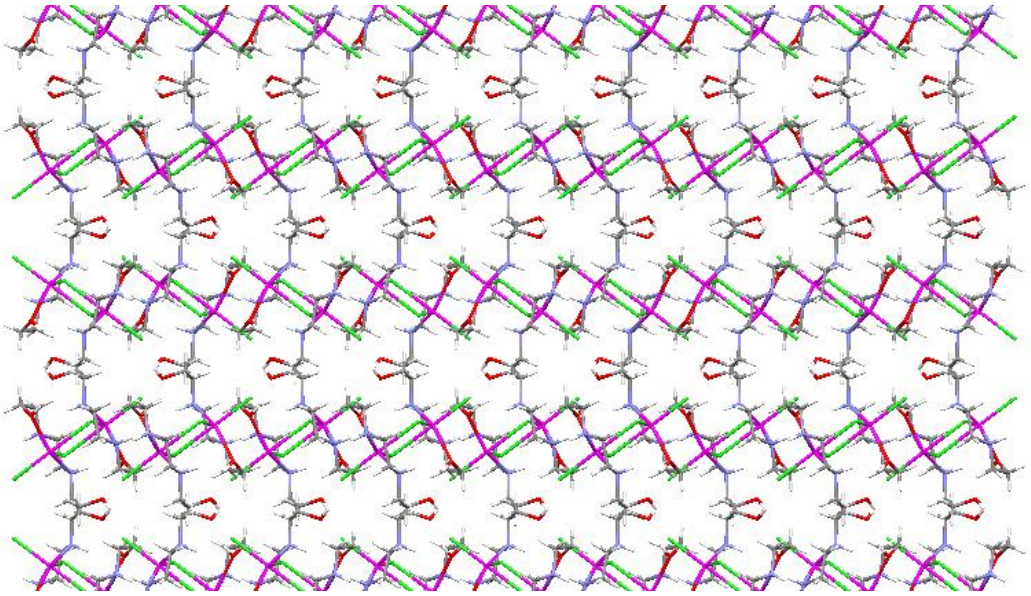


Figure 4.52: The layered arrangement of the complex of cadmium(II) with BHEEN showing the parallel arrangement of the two layers

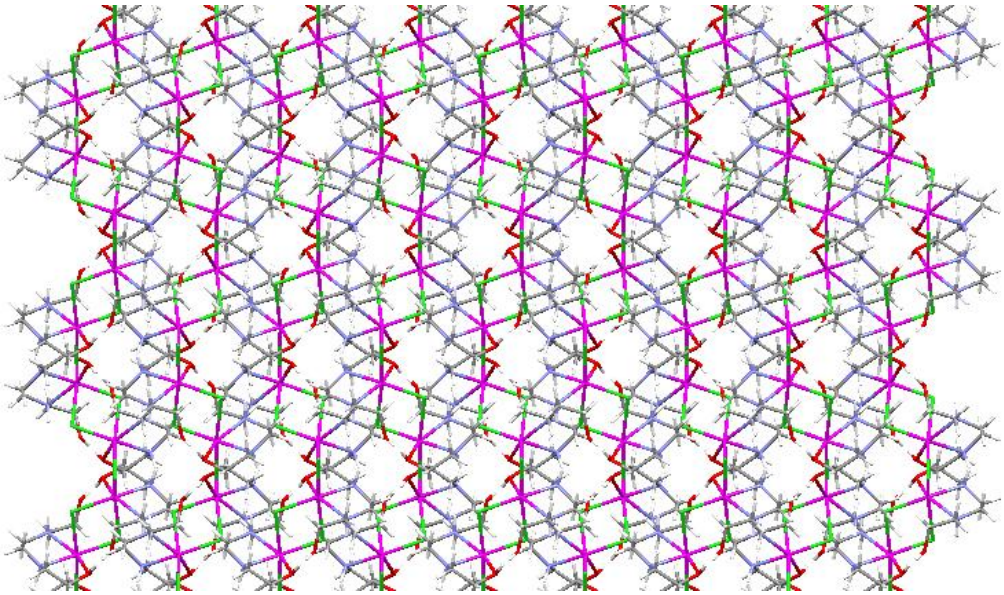


Figure 4.53: The helical arrangement of the complex of cadmium(II) with BHEEN

The H-H bonds in the complex are then investigated. Although the ligand used contains no cyclohexenyl rings, it was of interest to compare the H-H bond distances of the ligands to ascertain if the H-H bonds affect the complexation behaviour. The H-H bonds found in the molecule are tabulated in Table 4.6 and indicated in Figure 4.54. The average length of the H-H bonds in the cadmium(II) complex is 2.347 Å.

Table 4.6: H-H Bonds for the Cadmium(II) Complex of BHEEN

Atom 1	Atom 2	H-H Bond Distance (Å)	X-H-H Bond Angle (˚), where X denotes a donor atom
H2B	H3A	2.392	92.70 and 93.07
H4A	H5B	2.302	93.16 and 94.53

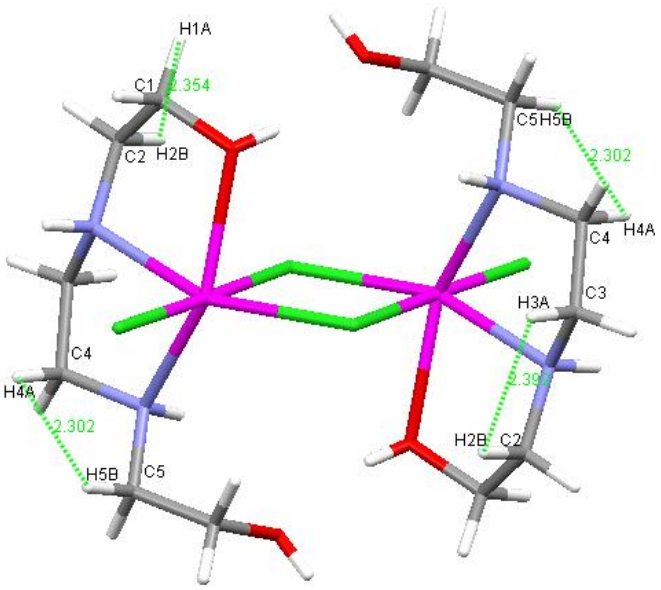


Figure 4.54: The H-H close contacts of selected hydrogen atoms in the cadmium(II) complex of BHEEN

The close contacts involving the amine hydrogens and the alcoholic oxygens as described for the free ligand are no longer present. This is because the molecule has rearranged itself so that the two atoms are no longer on the same side of the ligand.

4.3.6. Comparison of the Cadmium Complexes

Two of the five cadmium(II) complexes synthesised gave crystals of suitable quality to obtain XRD data. The first structure is that of cadmium(II) with Cy_2-en. The complex is a five-coordinate monomeric complex with two amine nitrogen atoms, one alcoholic oxygen, and two chloride ions coordinating to the central metal ion. The second alcoholic oxygen is not coordinated. The complex of cadmium(II) with BHEEN is a dimer with each metal six-coordinate with two amine nitrogens, one alcoholic oxygen, and one chloride and two bridging chlorides forming bonds with each metal. In each of the two complexes, the donor atoms of the ligand adopt a coplanar arrangement and when a plane is drawn through these points as well as the one coplanar chloride ion, the metal ion is located less than 0.5 Å above this plane.

The addition of the cyclohexenyl rings to the ligand changes the complexation behaviour as indicated by the log *K* data. This observation does not contradict the hypothesis that the H-H bonds between hydrogen atoms on the ring and ones on the backbone affect the complexation behaviour of the ligands. Furthermore, the average H-H bonds measured for the Cy_2-en complex (2.266 Å) are shorter than those measured for the equivalent BHEEN complex (2.347 Å). Each of the H-H bonds occurs when the hydrogen atoms are in an eclipsed arrangement. The H-H bonds are attractive in nature and as such stabilise the structure although their energetic contribution is small (approximately 2-7 kcal mol^{-1}).[19] The close contacts involving non-hydrogen atoms also contribute to the stabilisation of the complexes. The Cy_2-en complex has four H-H bonds and one close contact whilst the BHEEN complex has two H-H bonds and two close contacts. It is not known if any of the other interactions in the molecule destabilise or stabilise the structures further.

The hydrogen bonding networks of the two complexes possess some similarities. Each of the complexes contains intermolecular hydrogen bonds that form a ring between two molecules. This is the only type of bonding available in the Cy_2-en complex but the BHEEN complex has further hydrogen bonds extending in two dimensions.

The Cy_2-en complex has a clear differentiation between organic and inorganic layers in the packing arrangement. This is not the case for the BHEEN complex. This complex has a clearly interwoven arrangement. This may be explained by the hydrogen bonding networks. The more interlinked complex has more hydrogen bonds between many molecules whilst the more separated packing arrangement consists of a complex with limited hydrogen bonding that only exists between two isolated molecules.

The addition of the cyclohexenyl rings strongly affects the geometric arrangement of the complex in the solid state. The complex is in constant motion in solution and so the observed geometry is merely one of many arrangements found in solution.

No conclusions as to the bonding properties of the other complexes can be made as there is no direct indication of the structure as well as the nature of the complexes.

4.4 Synthesis and Characterisation of the Nickel Complexes

No NMR data was included in the dissertation as all samples prepared were found to be a complex mixture of polymeric species and the significant overlapping of peaks yielded no useable data whatsoever. From the state, as well as the colour of the products obtained, it appears unlikely that the product is nickel(II) hydroxide as nickel(II) hydroxide is a green, crystalline solid.

4.4.1 Synthesis of the Cy_2-en/Ni Complex

The synthetic route chosen was the same as the one described by de Sousa *et al.*[2] for the synthesis of an equivalent copper(II) complex. The heating process after evaporation was done to ascertain if heating led to crystallisation. This was not the case.

The reaction gives an almost immediate indication that a complex forms. The initial reaction mixture, before the addition of the ligand, is a bright green. As the ligand is added an almost instantaneous colour change to blue occurs. The literature reports that such a colour would imply the formation of a four-coordinate tetrahedral complex.[20] But at the same time, it is also found that polymeric species have the same colour.[20]

All that the IR can state is that the reaction has indeed occurred. The N-H stretch band shifts from 3266 cm^{-1} to 3164 cm^{-1} whilst there is little change in the values for the O-H stretch band (at 2931 cm^{-1} from 2923 cm^{-1}). This is indicative of complex formation, if this data is compared to the previous lead(II) and cadmium(II) complexes formed. The MS data indicates that the product formed may be polymeric as there is a wealth of peaks with a vast range of M:L ratios. This would explain why a gel formed that would not solidify.

The general conclusion that was drawn from all of the data was that the product formed was of a polymeric nature and could not be separated into smaller units by heating.

4.4.2 Synthesis of the Cy_2-Otn/Ni Complex

The same procedure as detailed above was used to synthesise this nickel(II) complex. The colour change from green to blue is considerably slower for this reaction, taking about seven days. The initial colour of the solution is a brownish orange that then turns to pink, then purple, and finally blue. The colour change can be attributed to a change of the geometry around the nickel(II) ion. The colours from yellow to red are associated with a four-coordinate, square planar arrangement around the nickel(II) ion. The purple and blue tones indicate a tetrahedral, four-coordinate geometry, or an octahedral environment.[20]

The MS data indicates many different metal:ligand ratios, again implying that the end product is most likely a polymeric species. The observed gel-formation underlines this conclusion.

4.4.3 Synthesis of the BHEEN/Ni Complex

The same synthetic procedure as described for the previous two reactions was used. The sample turns purple at the start of the reaction but then quickly turns blue. Thus, either the product is a tetrahedral four-coordinate complex, or the product is a mixture of polymeric species. The latter is assumed to be the case. The product is a gel that would not solidify.

MS data also implies that the product is of a polymeric nature as many different ratios for the ligands and metals are found, ranging from a simple 1:1 ratio to a 4:3 ratio.

4.4.4 Comparison of the Nickel Complexes

All three of the nickel(II) complexes synthesised show clear signs of being polymeric in nature. No further structural features could be determined.

4.5 Synthesis and Characterisation of the Zinc Complexes

4.5.1 Synthesis of the Cy_2-en/Zn Complex

The same method as was described for the synthesis of the nickel(II) complexes was used to make the zinc complexes. The product obtained is an off-yellow, plate-like crystal that does not diffract. Several attempts were made to recrystallise the sample but to no avail. Due to the misplacement of a decimal place, an excess of the metal was used in the synthesis.

The IR and MS data indicate that the zinc complex is formed. Further, the MS data indicates that both a nitrate and a chloride counter-ion are present. It is not clear how the nitrate has been collected during the course of the reaction. It is therefore concluded that the nitrate is most probably a contaminant, most likely the syringe containing the sample was not properly cleaned prior to use. The data does not imply that the species formed is polymeric but rather that it is a monomer with a chloride counter-ion.

4.5.2 Synthesis of the Cy_2-Otn/Zn Complex

The same method was used to make this zinc(II) complex. The product forms a plate-like crystal that twinned and do not diffract well enough to yield a useable data set. Several attempts were made to recrystallise the sample but this does not affect the quality of the crystals.

The IR data indicates that a zinc complex has been formed. The MS data supports this conclusion. It is not clear though if the product formed is monomeric or dimeric.

4.5.3 Synthesis of the BHEEN/Zn Complex

The reaction was performed as described previously and the crude product redissolved in water and refluxed for 24 hours. This solution was then left to evaporate slowly when crystals formed. These crystals are analysed by XRD and the structure shown in Figure 4.56 is calculated from the data.

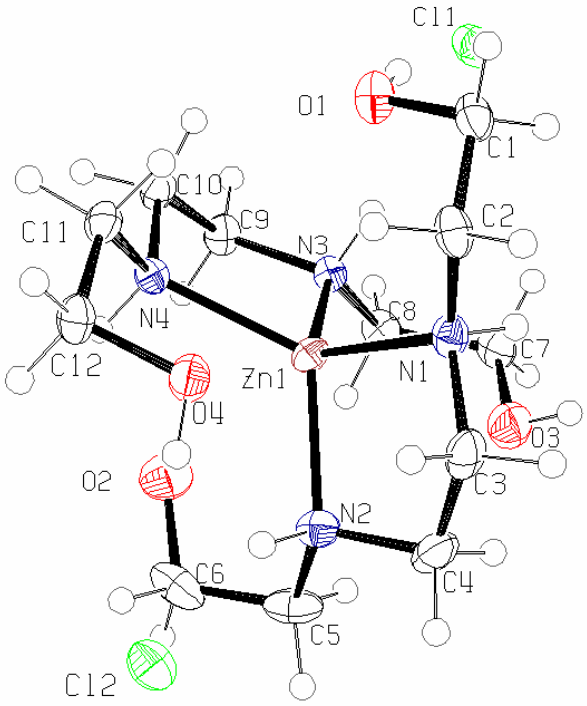


Figure 4.55: The molecular structure of the zinc(II) complex of BHEEN, showing the atom-labelling scheme and 50% probability displacement ellipsoids

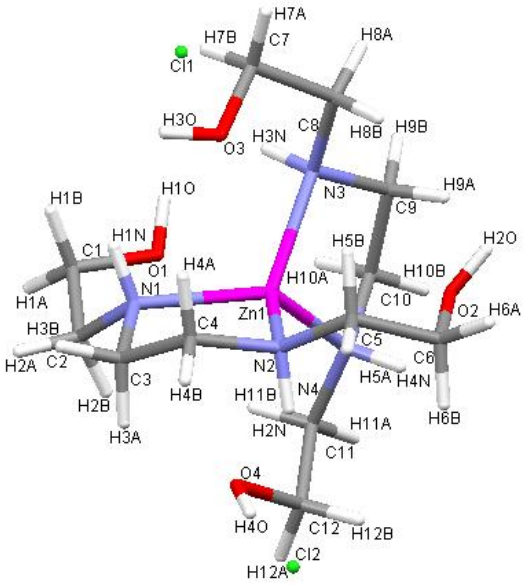


Figure 4.56: The molecular structure of the zinc(II) complex of BHEEN with its labelling scheme (hydrogen atoms included)

The complex formed is of the form ML_2 with two chloride counter-ions. A second attempt at producing the ML complex, by reacting a 1:1 Zn:L mixture, afforded only a polycrystalline material.

No solvent molecules are found in the unit cell. The central zinc(II) ion is four-coordinate with a distorted tetrahedral geometry. All four of the available alcoholic oxygen moieties are too far removed from the zinc(II) ion to form bonds. The exact Zn-O distances involving the pendent hydroxyl ethyl groups are 2.076 Å, 2.856 Å, 3.043 Å, and 3.126 Å. The two BHEEN ligand molecules are perpendicular to one another and hence two planes can be drawn through them, Figure 4.57.

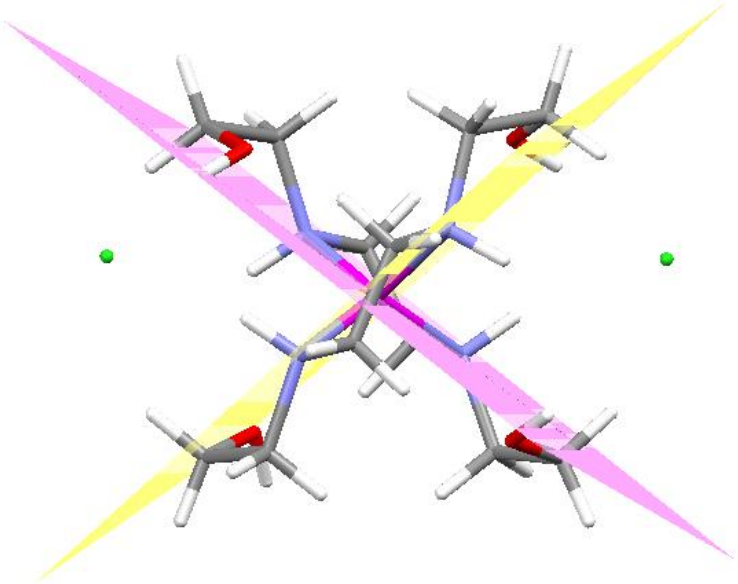


Figure 4.57: The two planes each defined by two nitrogen atoms as well as the central zinc(II) ion in the zinc(II) complex of BHEEN

The molecule has both intra- and intermolecular hydrogen bonds, Figure 4.58. The intermolecular hydrogen bonds are formed between a non-bonded hydroxyl group of a molecule and the amine nitrogen on an adjacent BHEEN molecule.

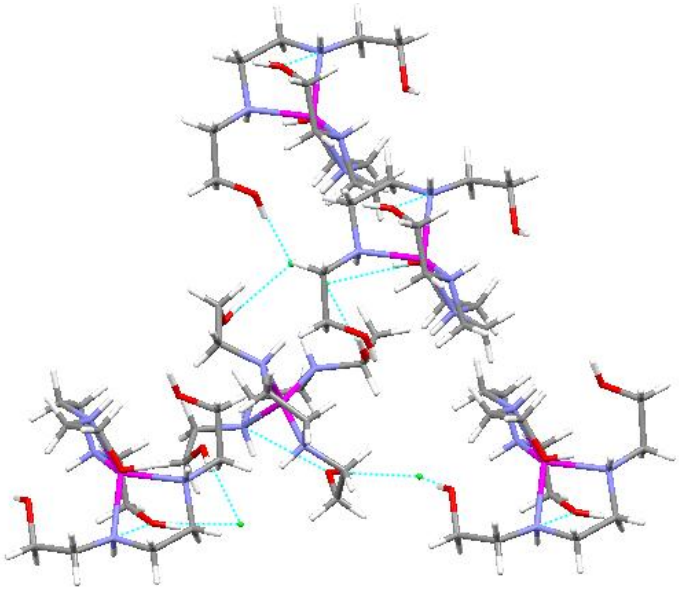


Figure 4.58: The hydrogen-bonding network of the zinc(II) complex of BHEEN

Further hydrogen bonds are between oxygen atoms and the two chloride ions in the complex. The hydrogen bonding network extends infinitely in two dimensions only, Figure 4.59.

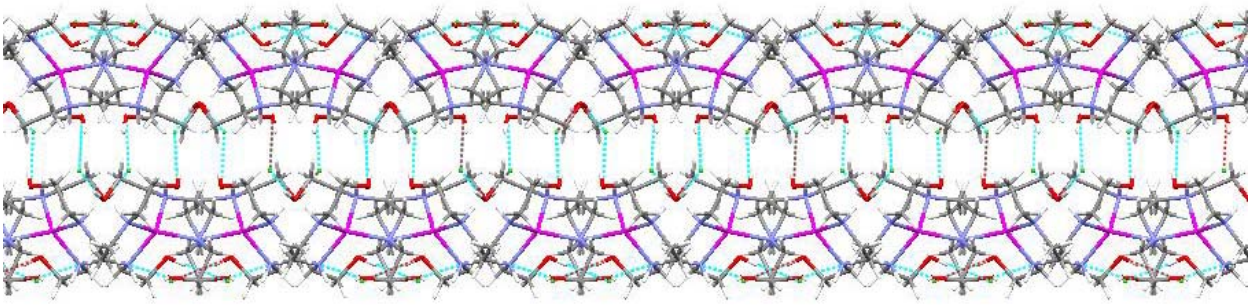


Figure 4.59: The two dimensional hydrogen bonding network of the zinc(II) complex of BHEEN viewed along the *c*-axis

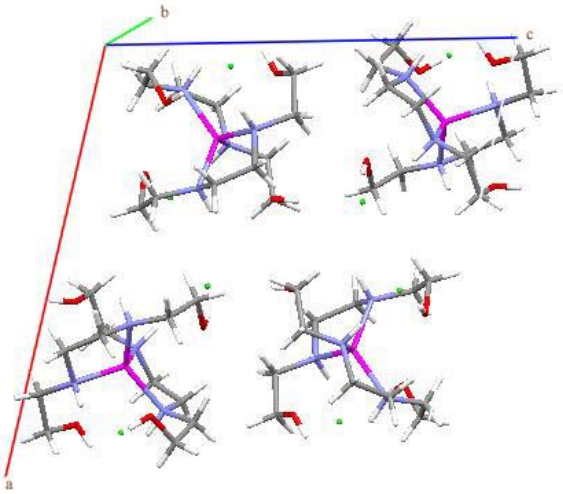


Figure 4.60: The packing arrangement of the zinc(II) complex of BHEEN

The molecules arrange themselves so that two complex molecules interact with one another to form the two-dimensional chains observed for the hydrogen bonding. These layers are clearly separated from one another.

The number of H-H bonds changes from four to three, Figure 4.61 and Table 4.7. Each of these bonds is between an amine hydrogen and an alcoholic hydrogen. This type of H-H bond is not seen in the free ligand.

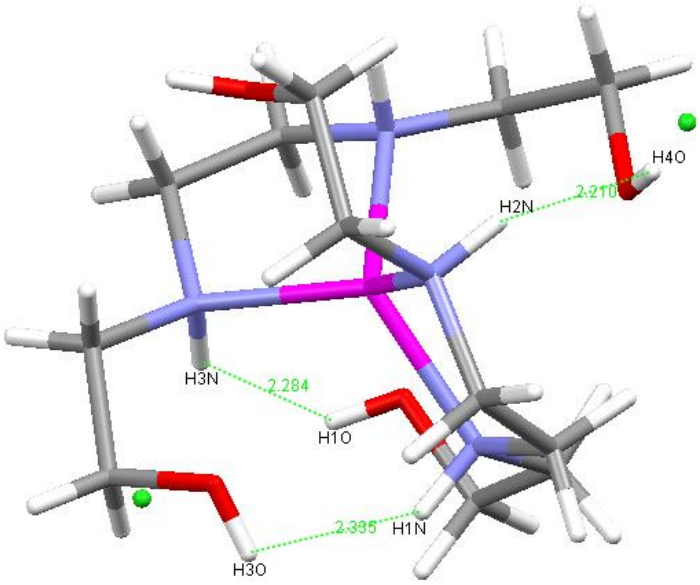


Figure 4.61: The H-H close contacts of selected hydrogen atoms in the zinc(II) complex of BHEEN

Table 4.7: H-H Bonds for the Zinc(II) Complex of BHEEN

Atom 1	Atom 2	H-H Bond Distance (Å)	X-H-H Bond Angle (˚), where X denotes a donor atom
H1N	H3O	2.335	104.64 and 134.05
H2N	H4O	2.210	105.02 and 138.75
H3N	H1O	2.284	139.90 and 105.25

Further interactions within the molecule are also noted, Figure 4.62. The number of close contacts has increased from two to six. Thus, the number of H-H bonds as well as close contacts has increased when the complex is compared to the uncoordinated ligand.

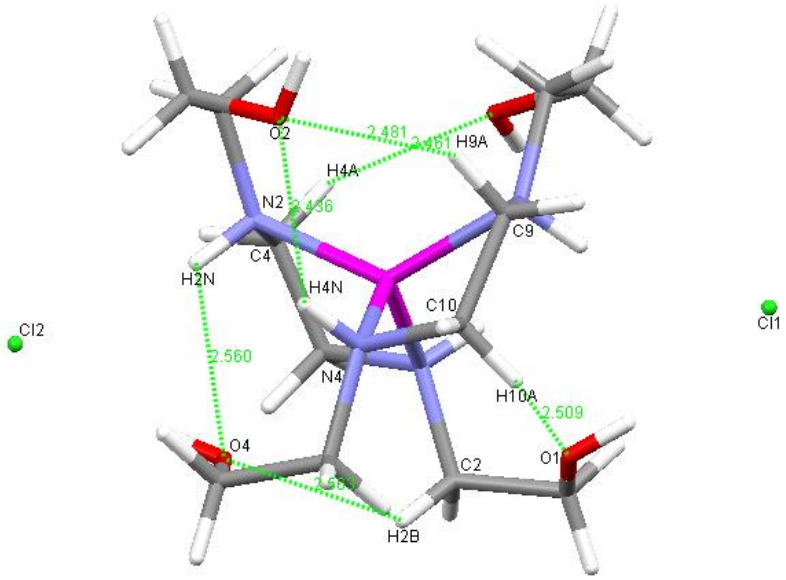


Figure 4.62: Close contacts involving hydrogen and non-hydrogen atoms in the zinc(II) complex of BHEEN

4.5.4 Comparison of the Zinc Complexes

The reactions all yielded crystals. The only issue with the first two ligand complexes (Cy_2-en and Cy_2-Otn) was that the crystals did not diffract sufficiently to yield a dataset of acceptable quality. The zinc(II) complex of BHEEN did diffract. This complex had a solid state structure that was significantly different to the previously reported structures. In all of the structures reported in the CSD involving complexation of BHEEN, there were no reports of a complex where only the amine nitrogen atoms bonded to the metal ion. At least one of the alcoholic oxygens formed a bond as well. This was not the case for the zinc(II) complex. It is unclear as to why this happened.

4.6 Comparison of all Solid State Structures of the Complexes

Two complexes with Cy_2-en as the ligand gave crystals of suitable quality that were then analysed by XRD and the solid state structures determined. The first of these complexes was a lead(II) complex. This complex involved a stereochemically active lone pair of electrons on the lead(II) ion. Furthermore, the metal ion accepted all four of the donor atoms of the ligand in addition to two chloride ions. Although, the structure had a six-coordinate geometry, it was a vacant seventh site that is occupied by the lone pair of electrons.

The next complex studied was that of the cadmium(II) ion. The cadmium(II) only accepted three of the four available donor atoms on the ligand. This was in line with expectations if the analogous ligand BHEEN was studied. The CSD presents several solid state structures that contain BHEEN (codes: EDUYEH, EDUYEH1, HANFUX, HANGAE, IFEJIM, MILMID, NUKJEI, SIXJAK). In almost all of the reported complexes with BHEEN, one of the alcoholic oxygen atoms is not coordinated to the central metal ion. Rather, it is readily available for hydrogen bonding to form a layered arrangement to strengthen the crystal packing.

The lead(II) ion did not sit in the cavity of the ligand but rather sat a distance above it. The cadmium ion was placed within the cavity of the ligand.

Both of the complexes had M-N bond lengths that were longer than the ideal M-N value of 2.5 Å, but neither was far removed from this ideal value although lead approached the value more closely (2.6211 Å). This was surprising as the ideal metal ion calculated in the course for the MM work was cadmium. The ideal bond length values implied that the lead should form the more stable complex but the log *K* values for the complexes of Cy_2-en (Table 1.3) indicated that the opposite was true.

The two complexes share several properties, for example, their increased number of close hydrogen-hydrogen contacts upon complexation. The free ligand was found to have two such close contacts. The complexes were found to have four each. The average close contact distance also decreased upon complexation with the cadmium complex having the shortest contacts.

When the two complexes of BHEEN were compared, it was found that the two

complexes were rather dissimilar. The cadmium(II) complex of BHEEN assumed a rather standard arrangement for BHEEN complexes. Only three of the four donor atoms on the ligand coordinated to the ligand whilst the fourth, an oxygen group, arranged itself in such a manner so as to optimise the hydrogen bonding.

The zinc(II) complex of BHEEN was rather different. Unlike the cadmium complex, this complex only accepted as coordination donors the two amine nitrogen groups. Both of the alcoholic oxygen groups were free to move about and arrange themselves so as to optimise the hydrogen bonding. This was evident from the fact that all of the five hydrogen bonds in the complex involved an oxygen group as either a donor or acceptor atom.

4.7 References

(1) De Sousa, A. S.; Hancock, R. D. *J. Chem. Soc., Chem. Commun.* **1995**, 415-416.

(2) De Sousa, A. S.; Hancock, R. D.; Reibenspies, J. H. *J. Chem. Soc., Dalton Trans.* **1997**, 2831-2835.

(3) De Sousa, A. S.; Fernandes, M. A. *Acta Crystallogr. Sect. E* **2003**, o1872-o1874.

(4) Allen, F. H.; Kennard, O.; Watson, D. G.; Brammer, L.; Orpen, A. G. *J. Chem. Soc., Perkin Trans. II* **1987**, S1-S19.

(5) Damodharan, L.; Pattabhi, V. *Tetrahedron Letters* **2004**, *45*, 9427-9429.

(6) Vasadwaj, P. R. Unpublished work.

(7) Bader, R. F. W. *Atoms in molecules: a quantum theory*; Clarendon Press: Oxford, 2003.

(8) Uwamariya, V. Master of Science Dissertation, University of the Witwatersrand, 2005.

(9) Sienkiewicz, A.; Kokozay, V. *Polyhedron* **1994**, *13*, 1431-1437.

(10) Lyczko, K.; Starosta, W.; Persson, I. *Inorg. Chem.* **2007**, *46*, 4402-4410.

(11) Nakamoto, K. *Infrared And Raman Spectra Of Inorganic And Coordination Compounds*; 4th ed.; J. Wiley: New York, 1986.

(12) Shimoni-Livny, L.; Glusker, J. P.; Bock, C. W. *Inorg. Chem.* **1998**, *37*, 1853-1867.

(13) Fan, S.-R.; Zhu, L.-G. *Inorg. Chem.* **2007**, *46*, 6785-6793.

(14) Chen, M.; Fulton, J. R.; Hitchcock, P. B.; Johnstone, N. C.; Lappert, M. F.; Protchenko, A. V. *Dalton Trans.* **2007**, 2770-2778.

(15) Hancock, R. D. *Progr. Inorg. Chem.* **1989**, *36*, 187.

(16) Hancock, R. D. *Acc. Chem. Res.* **1990**, *23*, 253.

(17) Naiini, A. A.; Young, V.; Verkade, J. G. *Polyhedron* **1995**, *14*, 393-400.

(18) Orpen, A. G.; Brammer, L.; Allen, F. H.; Kennard, O.; Watson, D. G. *J. Chem. Soc., Dalton Trans.* **1989**, S1-S83.

(19) Hernández-Trujillo, J.; Matta, C. F. *Struct. Chem.* **2007**, *18*, 849-857.

(20) Lancaster, J. R. *The Bioinorganic Chemistry of Nickel*; VCH: New York, 1988.

Chapter 5

Conclusions and Future Work

Two of the five ligands synthesised yield crystals of suitable quality to determine their structures by XRD methods. Cy_2-en yielded a structure for the free ligand as well as its chloride salt. Cy_2-Otn was obtained as the free ligand. BHEEN, a commercially available reagent, was isolated and analysed as the nitrate salt. The two ligands containing cyclohexenyl pendant arms possess several H-H bonds between the hydrogen atoms on the rings and the hydrogen atoms on the bridging carbon atoms, whilst BHEEN has no H-H bonds. There are also several non-bonded interactions between the amine hydrogens and the alcoholic oxygens. These interactions are observed in all four crystal structures.

Cy_2-Otn does not crystallise in a centrosymmetric space group and so is an example of a case where the formation of H-H bonds is not predicated by a centre of symmetry in the solid state structure. Hence it appears that the formation of the observed H-H bonds is not merely an artefact of the symmetric requirements of the crystal lattice.

The lead complexes need to be reinvestigated to yield more conclusive data. The one lead(II) complex that yielded an XRD structure, namely the lead(II) complex of Cy_2-en, indicates that the lone pair of electrons on the metal ion is stereochemically active. The analytical methods used are not ideal and work must be done to find an optimal method of analysis. The mass spectrometry methods are the least ideal indicator of complexation as the methods used consistently failed to detect lead(II) complexes, although IR methods as well as XRD experiments indicated that the complex formation was successful. The structure indicates that the H-H bonds that are present in the free ligand no longer exist in the complex, but are replaced by new H-H bonds.

The cadmium(II) complexes were easier to analyse than the lead(II) complexes as the analytical methods, in particular the mass spectrometry methods, were more capable of detecting the cadmium(II) ion than the lead(II) ion. Again, the presence of H-H bonds indicates that the

hypothesis made at the start of the dissertation, namely that these interactions affect the complex stability, has some merit. The hypothesis can only be fully confirmed once an extensive thermodynamic study has been done on the complexes. This data may then indicate if the hypothesis is correct or not.

The nickel(II) complexes must be investigated and a synthetic route found to form an ML complex rather than the polymers that were observed. Spectroscopic studies should also confirm the geometry of the metal ion, i.e. is it four coordinate or six coordinate.

The zinc(II) complexes are of interest as the MS data indicate that the most likely species is the ML_2 complex. The XRD structure of the zinc(II) complex of BHEEN confirms this assumption. Thus far, the ML complex has not been isolated in a crystalline form and a synthetic route to do so needs to be developed. The ML_2 complex indicates extensive H-H bonding as well as close contacts between the amine hydrogens and the alcoholic oxygens.

In order to confirm that the hypothesis made at the start of the dissertation concerning the H-H bonds is correct, the complexes ideally should be analysed by neutron diffraction experiments so that the exact locations of the hydrogen atoms in the structure can be determined, if the crystals are large enough. Once this has been done, the thermodynamic properties can be calculated and related to the observed properties. From these values, an estimate of the strength of the interactions can then be made.

AIM should also be used to further investigate the interactions observed. This quantum mechanics method seems particularly adept at predicting the observed interactions and can calculate the strength of the interactions. These values can then be compared to the values calculated from the thermodynamic data.

Chapter 6

Unexpected Reactions

During the course of the research project several unexpected products were obtained. The structure of the imidazolinium salt 2,2'-bis(2-hydroxycyclohexyl)imidazoline nitrate has not been previously reported. The carbamate (3-ammonio-2-hydroxypropyl)carbamate monohydrate has been previously reported. All NMR, MS, IR, and XRD data is available in Appendices B to E.

6.1 The Imidazolinium Salt 2,2'-Bis(2-hydroxycyclohexyl)imidazoline Nitrate

The imidazolinium salt, 2,2'-bis(2-hydroxycyclohexyl)imidazoline nitrate (**1**), was formed as the product during the attempted synthesis of a lead complex with Cy_2-en, Figure 6.1. The lead complex did not form.

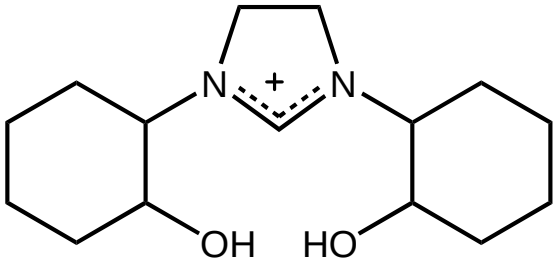


Figure 6.1: The imidazolinium cation produced, 1

An imidazolinium salt is a salt of imidazoline. Imidazoline is a heterocyclic derivative of imidazole, Figure 6.2.

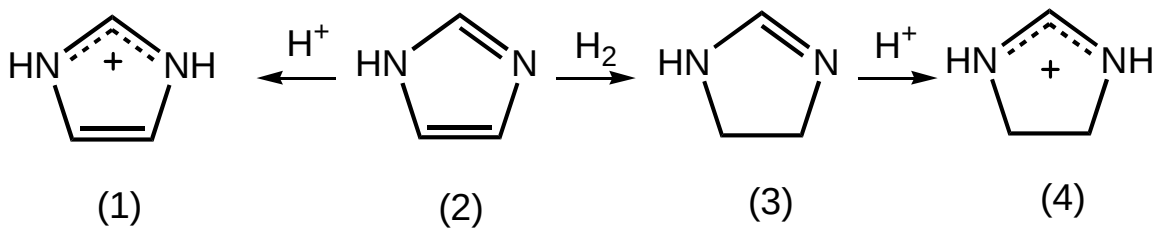


Figure 6.2: Imidazole (2) and its derivatives, the imidazolium cation (1), imidazoline (3), and the imidazolinium cation (4)

Imidazolinium salts are quite frequently found to be ionic liquids.[1] They have properties of interest to scientists as they cannot evaporate, they cannot be inflamed, they work over a very broad temperature range, and they are easy to reclaim or recycle. This makes their synthesis and study of great interest as they may prove to be viable alternatives to the standard solvents in use today. It is because of this characteristic that ionic liquids are commonly mentioned as good candidates for green chemistry.[2] But there has been much debate as to the validity of this claim, as is noted in an editorial in *Green Chemistry* in May 2008.[3]



Figure 6.3: General scheme of imidazolinium cations studied in the literature

Over the last decade a great deal of research has been done on imidazolinium salts of the type shown in Figure 6.3.[2] As ionic liquids, they can be of use as solvents in reactions with medium and strong bases without losing their effectiveness.[4] They are also suitable as solvents or catalysts in asymmetric syntheses.[5] A further use for imidazolinium ionic liquids is their ability to mimic tetrahydrofolate coenzymes.[6] Imidazolinium salts are also very effective as catalysts. There are examples of enantioselective conjugate addition reactions,[7] Diels-Alder reactions,[8] and reactions where the salts act as asymmetric catalysts.[9,10] Further reactions where

they show interesting properties are as chiral shift reagents[11] as well as potential chiral molecular recognition reagents.[12]

The intended product of the reaction of lead monoxide with ammonium nitrate and the ligand N,N'-bis(2-hydroxycyclohexyl)ethylenediamine (Cy_2-en) was a complex of Cy_2-en with lead. The reaction scheme is shown in Figure 6.4. The carbene product 2,2'-bis(2-hydroxycyclohexyl)imidazoline nitrate **1** was formed instead. The low yield of 11 % was attributed to the fact that the DMF degraded during the long reaction time of 20 hours at high temperatures and led to the product having to be washed with acetone at least ten times prior to any product precipitating. The exact mechanism of the reaction is not known as it unclear whether the carbene carbon was donated by the DMF or the acetone. Further experiments were done by replacing the solvent DMF with dimethyl acetamide. The two liquids have similar boiling points. Furthermore, the asymmetric nature of the solvent could give, as a product, an asymmetric product if the solvent was the donor of the carbene carbon. If the acetone had donated the carbene carbon then, irrespective of the solvent, the product would have been the same. This would have been easier to analyse via XRD as well as NMR and have clarified the mechanism. However, the reaction did not yield any product whatsoever and was abandoned. Jurčik[4] used aldehydes such as benzaldehydes as the carbene source whilst trimethylorthoformate was used by Clavier and co-workers.[12]

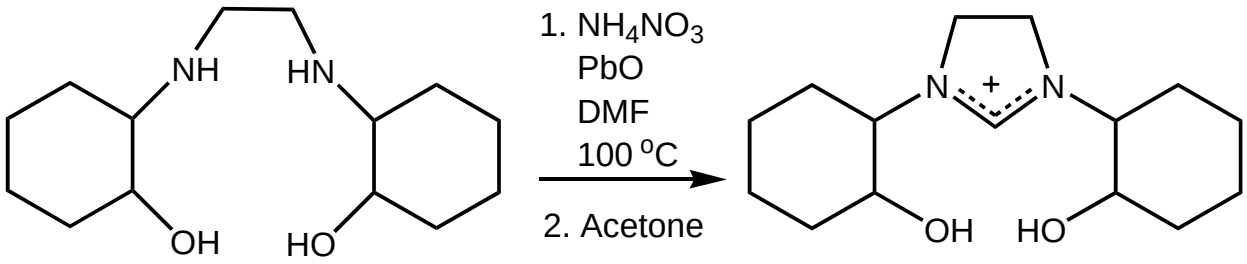


Figure 6.4: Reaction scheme leading to the formation of 1

The structure of **1** was solved by low temperature X-ray diffraction, Figure 6.5. Each amine cation has a closely positioned nitrate anion. Both molecules are generated by symmetry in the orthorhombic and polar space group $C222_1$ with four molecules occupying the unit cell. The two cyclohexenyl rings adopt a perpendicular arrangement presumably so as to minimize steric effects.

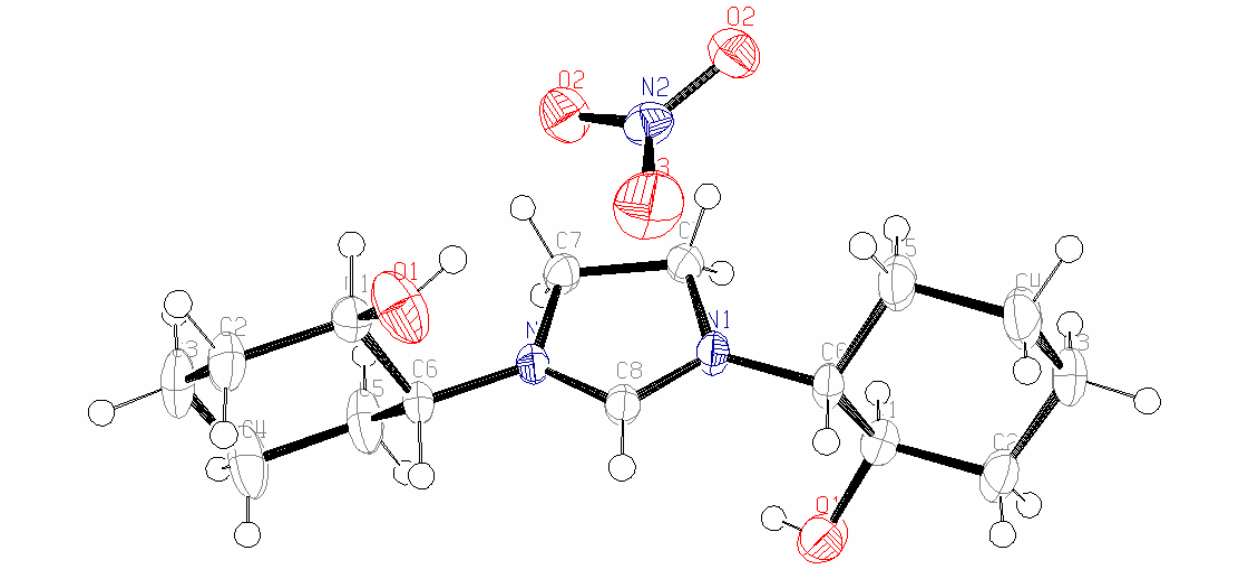


Figure 6.5: The molecular structure of 1, showing the atom-labelling scheme and 50% probability ellipsoids

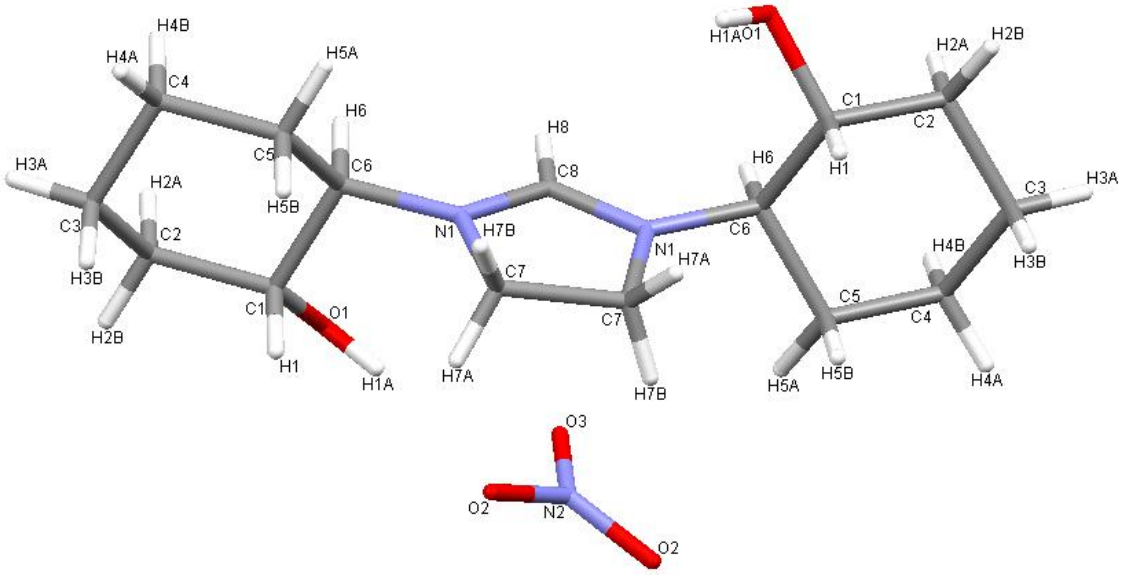


Figure 6.6: The molecular structure of 1 with its labelling scheme (hydrogen atoms included)

The XRD structure was submitted for validation and found to contain several errors that could not be removed, but could be explained. The relevant errors that remained are tabulated in Table 6.1.

Table 6.1: Excerpt from the Validation Window for 1 (Using Platon Validate)

035_ALERT_1_A No _chemical_absolute_configuration info given . ?

432_ALERT_2_B Short Inter X...Y Contact O3 .. C7 .. 2.87 Ang.
432_ALERT_2_B Short Inter X...Y Contact O3 .. C7 .. 2.87 Ang.

032_ALERT_4_C Std. Uncertainty in Flack Parameter too High ... 10.00
033_ALERT_2_C Flack Parameter Value Deviates 2 * su from zero. -10.00
042_ALERT_1_C Calc. and Rep. MoietyFormula Strings Differ .... ?
066_ALERT_1_C Predicted and Reported Transmissions Identical . ?
222_ALERT_3_C Large Non-Solvent H U_{eq}(max)/U_{eq}(min) ... 3.04 Ratio
244_ALERT_4_C Low 'Solvent' U_{eq} as Compared to Neighbors for N2
250_ALERT_2_C Large U3/U1 Ratio for Average $U_{(i,j)}$ Tensor 2.29
764_ALERT_4_C Overcomplete CIF Bond List Detected (Rep/Expd) . 1.15 Ratio
914_ALERT_3_C No Bijvoet Pairs in FCF for Non-centro Structure !

791_ALERT_1_G Confirm the Absolute Configuration of C1 = . R
791_ALERT_1_G Confirm the Absolute Configuration of C6 = . R

The individual errors will be explained. The absolute configuration could not be assigned without reasonable doubt as the space group in which **1** crystallizes is polar and the molecule generated by symmetry. The solution generated by solving the given data indicates an absolute configuration of *R,R* in this case.

There is a very short C-H···O contact of below 2.87 Å. Though short, the close contact is not amongst the shortest reported. The H···O distance is 2.55 Å and the complete C-H···O distance is 3.12 Å, Figure 6.6. An extensive search of all C-H···O contacts in the CSD indicated that it was above the median value of 2.73 Å.[13]

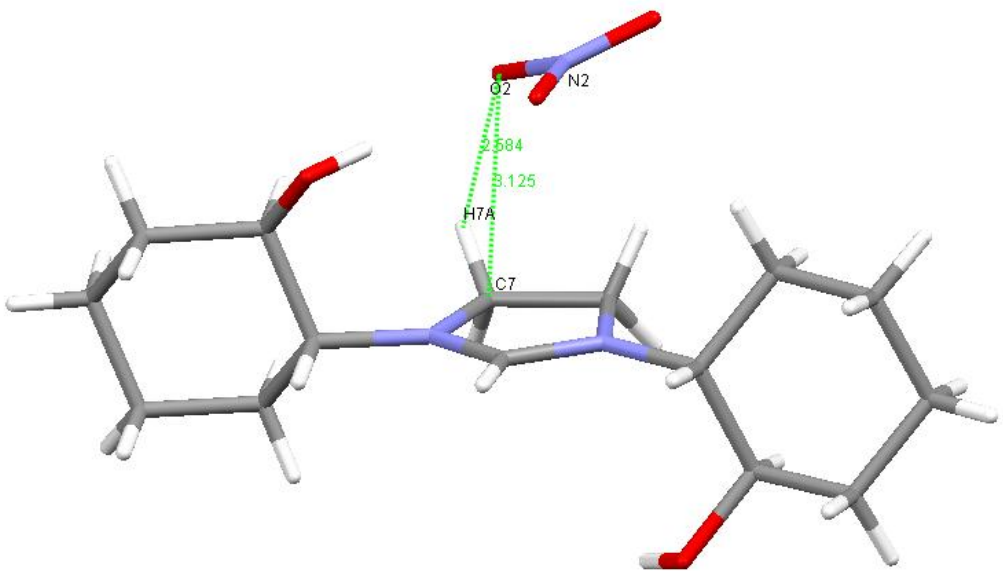


Figure 6.7: The crystal structure of 1 indicating the close contact and its magnitude

The calculated and reported moiety formulas differed as it was not possible to place the single proton on one of the nitrogen atoms due to the fact that the symmetry operation in the molecule would have placed another proton on the second nitrogen atom also. Consequently, the XRD structure appears to look like an imidazoline derivative rather than a salt. This is not the case. The net charge of the entity is zero and this can only be achieved if the negative charge on the nitrate is annulled by a positive charge on the carbene. The proton, in the solid state, was delocalised over the two positions and could not be assigned. Furthermore, if a partial charge were to have been assigned to the nitrogen atoms, then these nitrogen atoms would have been forced from an sp^3 hybridisation to an sp^2 hybridisation and the R-factor increased substantially. The fact that the hydrogen atom could not be placed could also explain the aforementioned short contact. The large non-solvent H error could also be explained by this.

The fact that the U_{eq} for N2 is so small is because the nitrogen atom in question is part of the nitrate ion and so surrounded by three oxygen atoms. These atoms effectively spin around the nitrogen atom using it as an axis and they consequently have much larger ellipsoids.

The overcomplete error arises because only half the molecule is calculated and the rest generated by symmetry. When the bond list is generated, it is possible that the computer program used to solve the XRD structure, in this case SHELXTL,[14] can view some of the bonds that have been symmetry-generated as calculated bonds. Nothing can be done about this.

The structure has hydrogen bonds that extend in only two dimensions, Figure 6.8. The chain formed links the imidazolinium cation to the nitrate anion which, in turn, bonds to the next cation.

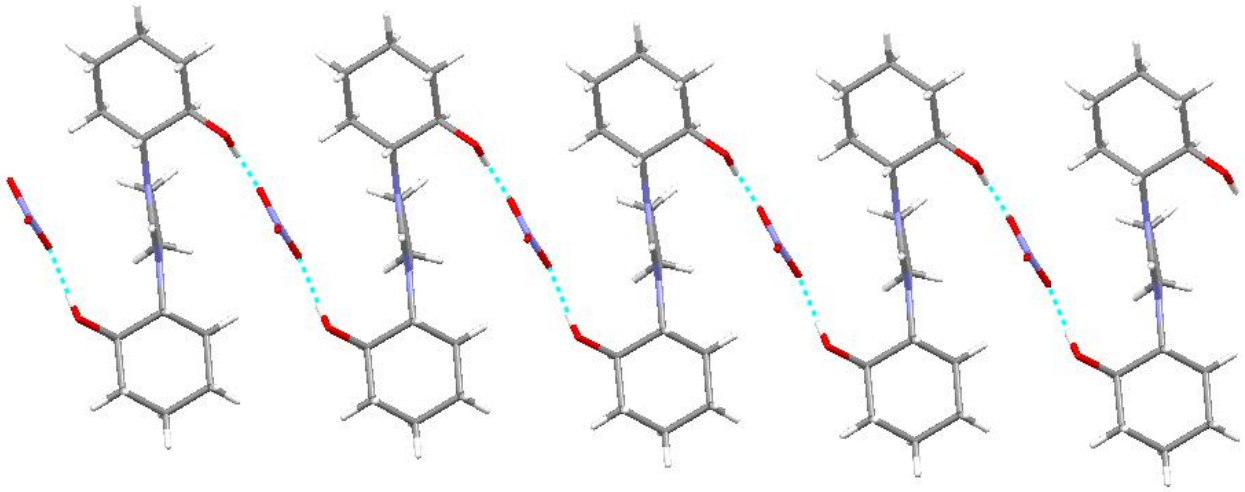


Figure 6.8: The hydrogen-bonding network of 1

The compound **1** is novel in its synthesis and structure. The synthetic route is by no means ideal and if **1** is to be investigated for its potential uses as an ionic liquid, a better and less wasteful, method must be developed. This could be done by reacting Cy_2-en with a carbene source in water as is done by Jurčik and Wilhelm.[4] This may also help to elucidate the mechanism of the reaction. The type of compound is also novel in that it lacks the aromatic character of imidazole-derived structures which have been studied to a far greater extent. Comparative studies of these two types of structures may also help in the understanding of the catalytic properties and ionic liquid properties observed. The synthetic route is also different to the traditional one as it involves a "one-pot" reaction. The disadvantage of this reaction is the low yield of a mere 11% as mentioned above.

Synthesis:

Lead monoxide, PbO, (1.1257 g, 5.043 mmol) was placed in a round-bottomed flask along with 0.8586 g (10.73 mmol) of ammonium nitrate and 2.5905 g (10.104 mmol) Cy_2-en. To this 10 mL dry DMF was added. The resultant mixture was refluxed at 100 ^oC for 20 hours. The solution was left to cool to room temperature and then left to evaporate slowly. At first the ligand, Cy_2-en, precipitated. This product was filtered off and the remaining solution left to evaporate to dryness. The resulting tar-like black amorphous solid was then washed with acetone and each washing filtered. The initial filtrate was merely degraded DMF but as the solution cleared the final product **1** was obtained. The crystals formed were clear and brick-like. The crystals had to be kept moist or else they cracked.

The product weighed 0.2980g, a yield of 11%.

$\delta_H(D_2O)$ 7.87 (s, 1H, NHC<u>H</u>NH_2^+), 3.69 (m, 4H, C<u>H</u>$_2$NHR), 3.34 (m, 2H, C<u>H</u>OH), 3.13 (m, 2H, C<u>H</u>NHR), 2.71 and 2.56 (degraded DMF residues), 1.76 and 1.67 (m, 4H, C<u>H</u>$_2$CHOH), 1.45 (br s, 4H, C<u>H</u>$_2$CHNHR), 1.27-0.99 (br m, 8H, $CH_2C\underline{H}_2C\underline{H}_2CH_2$)

$\delta_C(CD_3OD)$ 155.23 (NHR<u>C</u>HNHR), 60.76(<u>C</u>HOH), 55.43 (<u>C</u>HNHR), 47.34 (<u>C</u>H$_2$NHR), 33.76 (<u>C</u>H$_2$CHOH), 31.60 (<u>C</u>H$_2$CHNHR), 25.63 ($CH_2\underline{C}H_2\underline{C}H_2CH_2$)

ITMS + c APCI: m/z 267.29 (M+1)

IR (cm^{-1}): 3415 (N-H stretch), 2939 (O-H stretch), 2856 (alkane C-H stretch), 1644 (C=N bond), 1455 (CH_2 bending), 1412 (C-H bending), 1362 (O-H bending), 1268 (C-N stretch), 1229 (C-O stretch), 1133 and 952 (C-C stretch), 846 (N-H bending), 824 (C-H bending)

The solid state structure of the imidazolinium salt is described in Table 6.2. The full data can be found in Appendix E in tables E.22 to E.28.

Table 6.2: Crystal data and structure refinement for 1

Temperature	173(2) K	
Crystal system	Orthorhombic	
Space group	C222(1)	
Unit cell dimensions	a = 7.0296(2) Å	α = 90°.
	b = 9.8263(2) Å	β = 90°.
	c = 25.1764(6) Å	γ = 90°.
Volume	1739.06(7) $Å^3$	
Z	4	
Density (calculated)	1.250 Mg/m^3	
Absorption coefficient	0.093 mm^{-1}	
Goodness-of-fit on F^2	1.126	
Final R indices [I>2σ(I)]	R_1 = 0.0580, wR_2 = 0.1784	
R indices (all data)	R_1 = 0.0627, wR_2 = 0.1831	

6.2 The Zwitterion, (3-ammonio-2-hydroxypropyl)carbamate monohydrate

During the course of the work done for this dissertation, an Honours student, Samantha Birtles, attempted to synthesise the ligand Cy_2-Otn. In its place the zwitterion (3-ammonio-2-hydroxypropyl)carbamate monohydrate was the product of a reaction between 1,3-diamino-2-propanol and cyclohexene oxide in the atmosphere.

Zwitterions are molecules that contain both a positive and a negative charge. The most common example of a zwitterion is the amino acid group. It can donate a proton from its carboxylate group to the amine, thereby creating a negatively charged acid group and a positively charged amine group, Figure 6.9.

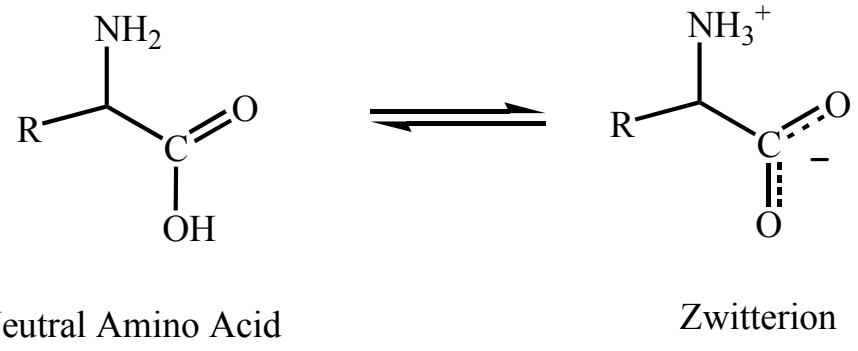


Figure 6.9: The equilibrium between the neutral amino acid and its zwitterion

It is commonly known that all amino acids exist as zwitterions in solution[15] as well as in the solid state.[16] It is also commonly known that not one of these amino acids exists as a zwitterion in the gas phase.[15,16]

The zwitterion in question is (3-ammonio-2-hydroxypropyl)carbamate monohydrate or **2**, Figure 6.10. The same isomer of this compound has previously been reported by Shi *et al.*[17] A carbamate shows some similarities to amino acids in that the positive charge is situated on an amine and the negative charge on a carboxylate.

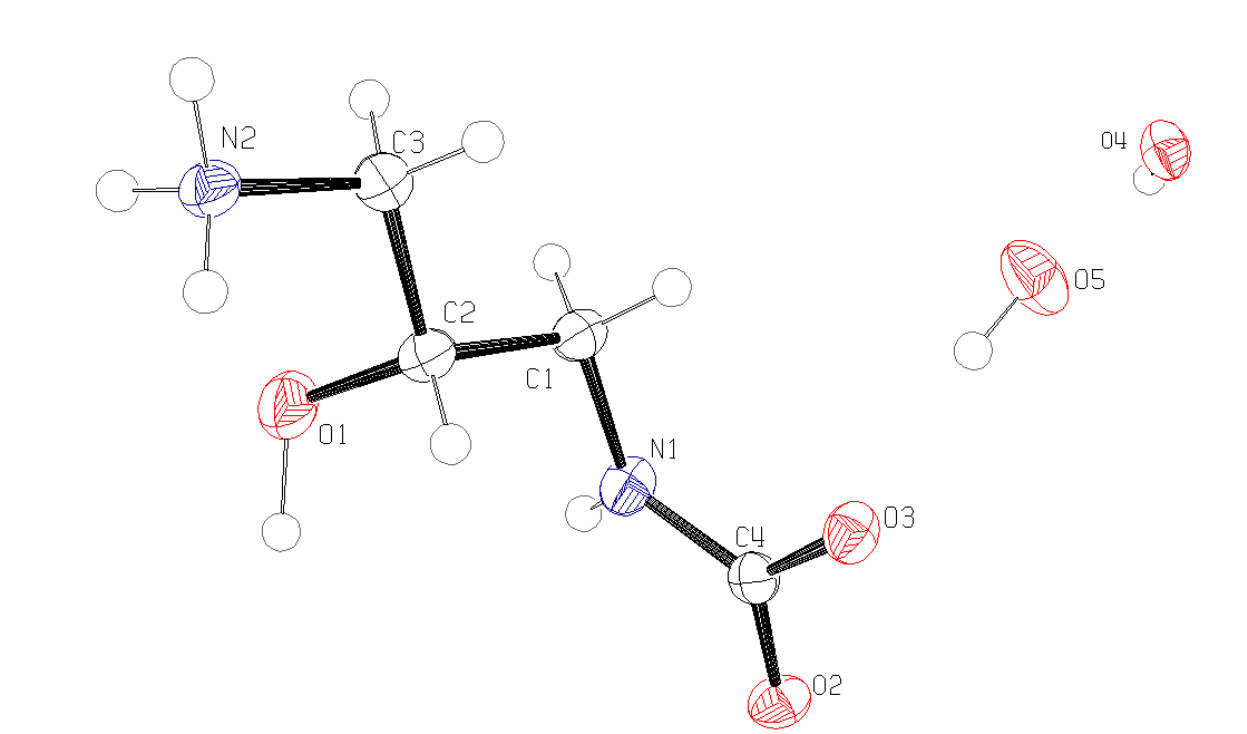


Figure 6.10: The molecular structure of 2, showing the atom-labelling scheme and 50% probability ellipsoids

The zwitterion, Figure 6.11, was not the exclusive product of the reaction. Rather, it was a minor side-product formed during the synthesis of the ligand Cy_2-Otn. The zwitterion was also not immediately formed if a new sample of 1,3-diamino-2-propanol was used. The side-product seemed to occur only once the amine starting material has been left to stand for some time (approximately five months in a refrigerator at 4 to 8˚C). This implied that the starting material may have spontaneously reacted with atmospheric carbon dioxide to form the zwitterion. There was no evidence that the zwitterion product was formed during the reaction as there was no evidence of an amine zwitterion with one cyclohexene oxide ring having substituted onto one of the amine groups. A mixture of these products would have been expected if the zwitterion were formed solely during the reaction as the reaction of the amine with the epoxide was spontaneous at room temperature.

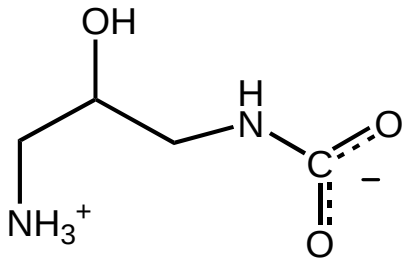


Figure 6.11: The zwitterion, 2, formed during the synthesis of Cy_2-Otn

The zwitterion formed crystals that were of good enough quality to obtain an XRD structure. The unit cell contained four zwitterions as well as four water molecules, Figure 6.12.

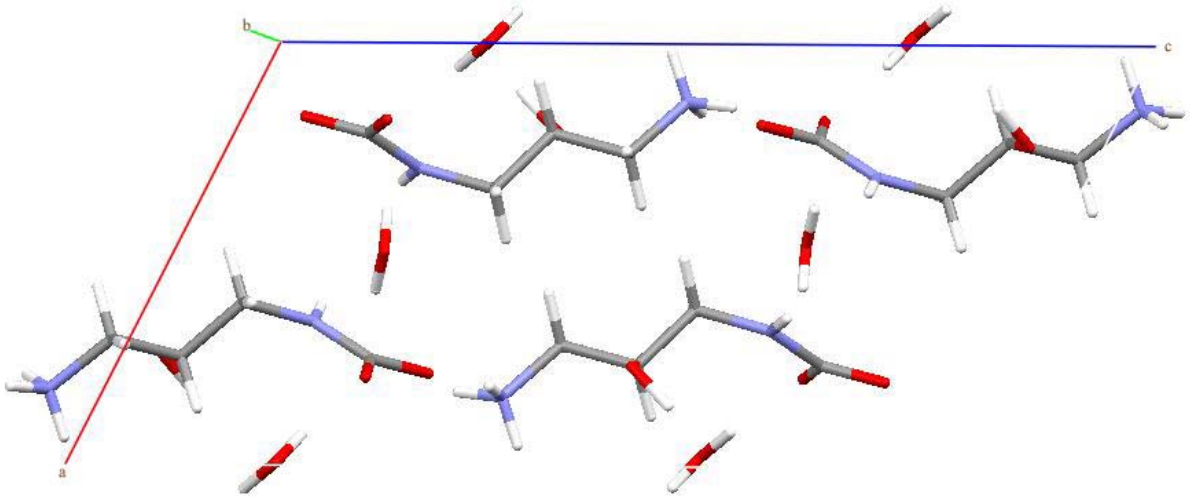


Figure 6.12: The unit cell packing of 2 viewed along the *b*-axis

A 16-membered ring, as reported by Shi *et al.*, was formed,[17] Figure 6.13. The ring was formed through the hydrogen bonding of N – H· · ·O and linked via the O – H· · ·O hydrogen bonds.

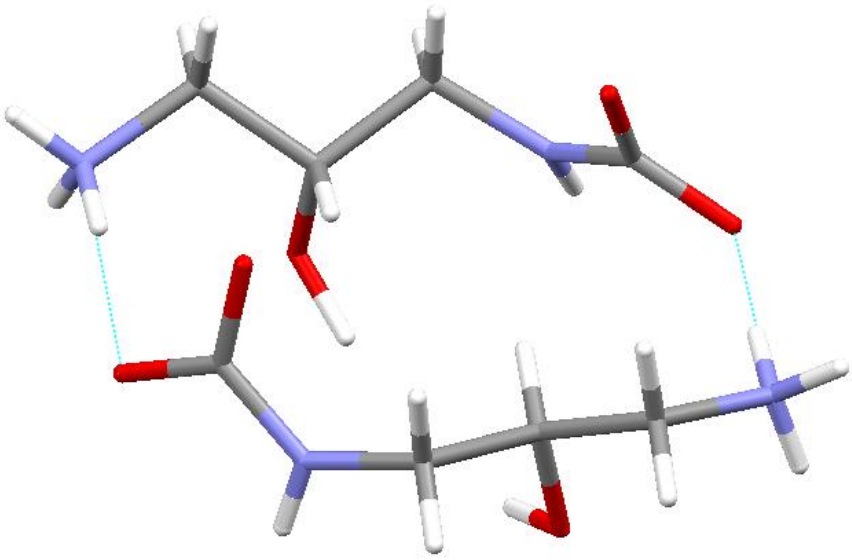


Figure 6.13: The 16-membered ring formed by the hydrogen bonds of two zwitterions

The extended unit cell clearly indicated that the individual zwitterions in the same plane arranged themselves in a head-to-tail fashion so that the negative charge of the one molecule was next to the positive charge of the next molecule, Figure 6.14. The molecules also assumed an anti-parallel arrangement so that the charges balanced one another.

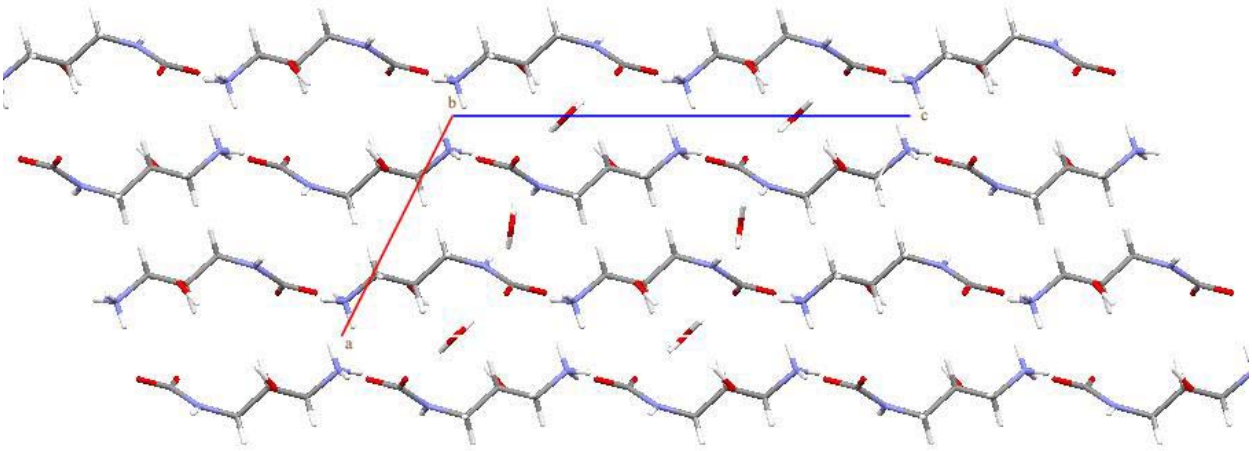


Figure 6.14: The packing arrangement of the zwitterion viewed along the *b*-axis

The zwitterion assumes the same conformation to the previously reported structure.[17]

Synthesis:

1,3-diamino-2-propanol (0.05585g, 6.197mmol) was dissolved in 30 mL dry ethanol. To this was added cyclohexene oxide (1.4502g, 14.78mmol) and the resultant mixture left to stir at room temperature for 24 hours with a $CaCl_2$ drying tube attached. The solution was then left to evaporate slowly in a fume hood when an oil formed that solidified upon standing to form a white powder. This powder was then triturated with ice-cold acetone, filtered and dried.

Yield: 0.0884g (5%)
ITMS + c APCI: m/z 287.31 (Cy_2-Otn + 1)
IR (cm^{-1}): 3282 (N-H stretch), 3150 to 3000 (O-H stretch), 2923 to 2852 (alkane C-H stretch), 1560 ($^-$O-C=O bond), 1439 (CH_2 bend), 1338 (C-H bend), 1220 (C-N stretch), 1166 (O-H bend), 1119 (C-O stretch), 1073 and 963 (C-C stretch), 907 (N-H bend), 841 (C-H bend).

Table 6.3: Crystal Data and Structure Refinement for the Zwitterion

Temperature	293(2) K	
Crystal system	Monoclinic	
Space group	P2/c	
Unit cell dimensions	a = 8.4164(3) Å	α = 90°
	b = 5.9335(2) Å	β = 116.764(2)°
	c = 15.6461(6) Å	γ = 90°
Volume	697.64(4) $Å^3$	
Z	4	
Density (calculated)	1.449 Mg/m^3	
Absorption coefficient	0.128 mm^{-1}	
Goodness-of-fit on F^2	1.027	
Final R indices [I>2σ(I)]	R_1 = 0.0458, wR_2 = 0.1207	
R indices (all data)	R_1 = 0.0682, wR_2 = 0.1296	

6.3 References

(1) Jodry, J. J.; Mikami, K. *Tetrahedron Lett.* **2004**, *45*, 4429-4431.
(2) Bourissou, D.; Guerret, O.; Gabbaï, F. P.; Bertrand, G. *Chem. Rev.* **2000**, *100*, 39-91.
(3) Welton, T. *Green Chem.* **2008**, *10*, 483.
(4) Jurčik, V.; Gilani, M.; Wilhelm, R. *Green Chem.* **2005**, *7*, 844-848.
(5) Cavell, K. J.; Elliott, M. C.; Nielsen, D. J.; Paine, J. S. *Dalton Trans.* **2006**, 4922-4925.
(6) Clemens, N.; Sereda, O.; Wilhelm, R. *Org. Biomol. Chem.* **2006**, *4*, 2285-2290.
(7) Clavier, H.; Coutable, L.; Toupet, L.; Guillemin, J.-C.; Mauduit, M. *J. Organomet. Chem.* **2005**, *690*, 5237-5254.
(8) Howarth, J.; Hanlon, K.; Fayne, D.; McCormac, P. *Tetrahedron Lett.* **1997**, *38*, 3097-3100.
(9) Markowicz, S. W.; Figlus, M.; Leikowski, M.; Karolak-Wojciechowska, J.; Dzierzawska-Majewska, A.; Verpoort, F. *Tetrahedron: Asymmetry* **2006**, *17*, 434-448.
(10) César, V.; Bellemin-Laponnaz, S.; Gade, L. H. *Chem. Soc. Rev.* **2004**, *33*, 619-636.
(11) Jurčik, V.; Gilani, M.; Wilhelm, R. *Eur. J. Org. Chem.* **2006**, 5103-5109.
(12) Clavier, H.; Boulanger, L.; Audic, N.; Toupet, L.; Mauduit, M.; Guillemin, J.-C. *Chem. Commun.* **2004**, 1224-1225.
(13) De Sousa, A. S.; Fernandes, M. A. *Acta Crystallogr. Sect. E* **2003**, o1872-o1874.
(14) Bruker; 5.1 (includes XS, XL, XP, XSHELL) ed.; Bruker AXS Inc.: Madison, Wisconsin, USA, 1999.
(15) Tajkhorshid, E.; Jalkanen, K. J.; Suhai, S. *J. Phys. Chem. B* **1998**, *102*, 5899-5913.
(16) Dunbar, R. C.; Polfer, N. C.; Oomens, J. *J. Am. Chem. Soc.* **2007**, *129*, 14562-14563.
(17) Shi, P.-F.; Xu, T.-T.; Xu, X.-Y.; Niu, S.-R. *Acta Cryst. Sect. E* **2006**, *E62*, o5191-o5193.